NORTHWESTERN UNIVERSITY

Towards High Relaxivity Magnetic Resonance Imaging Contrast Agents for use in Biomaterials

A DISSERTATION

SUBMITTED TO THE GRADUATE SCHOOL
IN PARTIAL FULFILLMENT OF THE REQUIREMENTS

for the degree

DOCTOR OF PHILOSOPHY

Field of Chemistry

by

Steven Richard Bull

EVANSTON, ILLINOIS

June 2007

Abstract

Towards High Relaxivity Magnetic Resonance Imaging Contrast Agents for use in Biomaterials

Steven Richard Bull

High relaxivity contrast agents are of great importance for the advancement of magnetic resonance imaging diagnostics for use in biomaterials. Implanted biomaterials, with the goal of repairing or regenerating lost or damaged need to be tracked noninvasively and temporally. I have completed work using self-assembly as the mechanism to achieve both tissue regenerating materials and their use as a template for noninvasive imaging by MRI.

Attachment of a magnetic resonance contrast agent small molecule to a scaffold that self-assembles into high aspect ratio nanofibers allows for the formation of a high relaxivity contrast agent. I have explored the underlying properties that affect these contrast agents and their efficacy. Elucidation involved the synthesis of multiple peptide amphiphile contrast agents with varying position, linker length, and peptide amphiphile architecture. The most important variables promoting high relaxivity included the positioning of the chelator closer to the middle of the peptide amphiphile and keeping the linker length between the contrast agent and peptide amphiphile as short as possible. These modifications provided relaxivity values ~20 mM^{-1} s^{-1} which are ~7 times greater than the small molecules relaxivity values.

When the peptide amphiphile contrast agents were mixed with other peptide amphiphile nanofiber scaffolds and formed into hydrogels, we were able to obtain homogeneous mixing throughout the gels as measured by MRI. The chosen peptide amphiphile contrast agent had the ability to be mixed with various bioactive peptide amphiphiles for imaging. These experiments

included in vivo monitoring of porcine hearts and it was found that the bioactive gel could be monitored over a two-week period before loss of the signal shedding light on the degradation time of the peptide amphiphile biomaterial in vivo.

Studies were performed on the templation of the peptide amphiphile nanofibers for the eventual use in drug delivery and fate mapping. A molecular dumbbell was synthesized with the properties that would offset the self-assembling properties of the peptide amphiphile monomers. The dumbbell was found to have a profound effect on the nanofiber formation and effectively stopped the high aspect ratio aggregates from forming.

For my family and friends

Acknowledgements

In my years here at Northwestern University I have come to the realization that I have made some incredible friends. I am not sure if it is because all of us here were thrown into the same boat with common threads such as our naivety about graduate school or how we would all change the world through research. About three years into our research we began to realize that the reasons we came to graduate school no longer held the same place in our hearts. We began to see the unromantic view of our time and effort in our endless quest for the currency of academia: papers. About that time we discover that we are not Midas and of the three components that go into papers, time, effort, and luck only one thing is really important. That is luck!

Some of us were luckier than others in our initial picking of groups and that is what the difference in graduate school becomes. You perform for the encouragement of your professor(s). Your hope is to come up with a new idea, and for them to be excited about that idea and give you the resources to pursue it. I was lucky in picking my groups.

After coming to graduate school here at Northwestern, I listened to many professors talk about their work. I found two that I was really interested in and came up with a scheme to become part of both their groups. This entailed a proposal that I wrote combining MRI and biomaterials as well as supramolecular control for the purpose of imaging. Without background in either of these subjects, just my excitement, they accepted me into their groups and allowed me to pursue my own ideas throughout my entire time here. It has been a great ride, challenging and with many failures. But pursuing my own ideas has really been the driving force for me. I

knew if something didn't work, it was my own fault and could not blame the idea on anyone else.

Thomas Meade is the man that has really kept me excited about work and research. I do not think I could have a better advisor. I will go ahead and explain a few of his traits that I think made him such a great advisor. Every time I talked to him, I walked away more motivated than I walked into his office. I have never seen someone more encouraging and trusting than Tom. I would tell him my ideas and I always left his office with the words, "Go get it!" He was accessible whenever I wanted to talk and was a real mentor for any type of problem I presented him with. The most important trait was that I know he would support everyone of my decisions. Even when this entailed a newspaper article against the University's cheating policies and a certain dean. Thank you Tom for everything.

I would like to thank professor Stupp for his support throughout my career here. He has allowed me to pursue my own chemistry and I was able to build my own research the way I thought was best. Thank you Professor Stupp.

Annelise Barron is my committee member who made a great contribution to my work. She is an amazing lady whose enthusiasm for science is unparalleled. She is always able to see how best to fit collaborations with different expertise and is not afraid of trying new things. She always had a willingness to talk with me about my future and science. She was a big part of my Ph.D. at Northwestern and now is off to bigger and better science at Stanford, congratulations. Thank you Annelise for your support.

I must thank my other mentors Professors Richard Silverman and Chad Mirkin. These professors were a large part of my success as well. They helped answer my questions, taught me

about patience, taught me how to sell my work, and helped me look in a different direction when I was stuck.

I would like to thank all my collaborators throughout my Ph.D. Their deeds are too numerous to mention, so their names will have to suffice. Lindsay, Mustafa, Loraine, Ellen, Keith, Rafael, Lesley, Luca, Nathan, Liam, Krista, and Hongzhou. Thank you all.

My friends and family were the most important people to help me throughout graduate school. I must first say that Alisha Taylor, who was my friend and will be my family, is the person that listened to all my problems was a rock for me to lean on when things got tough. I have been incredibly lucky to have her in my corner. We started our friendship in UNC and it grew stronger and stronger by the time we got to graduate school and has become most important person in my life and will be my wife. I have made great friends in graduate school, no better than Ben Messmore, Jovan Giaimo, Mike Ahrens, Rickles Kelley, Emily Weiss, Nathan Fry, Dave Ballweg, Neeraj Saraiya, Luca Frullano, and Liam Palmer. These friends have been an endless source of support whenever I have needed them. I have spent my Ph.D. learning from them all in everyway from stock discussions to learning about life skills. Thank you all for everything.

Finally, I must thank my family and especially my parents for their support throughout my life. They have given me more than I deserved and I am very grateful for their encouragement even though they don't exactly know why I have chosen consulting instead of a career in Chemistry! They have been by my side and sometimes behind me with a stick to keep me in going forward. To Todd and Lara who have always challenged me academically to go to as far as possible. Missy, who has shown me what real creativity and living life to the fullest is. Diana, who showed me courage beyond belief with her decisions throughout life and school. My

family is the most amazing set of people that I have ever met, and I am truly blessed to have them a part of my life.

Table of Contents

List of Figures

List of Schemes

List of Tables

List of Abbreviations

TMV	tobacco mosaic virus
RNA	ribonucleic acid
MRI	magnetic resonance imaging
PA	peptide amphiphile
PEG	poly ethylene glycol
OPE	oligo phenyleneethynylenes
OP	oligo phenylene
TLC	thin-layer chromatography
NMR	nuclear magnetic resonance
MALDI-TOF	matrix assisted laser desorption ionization time of flight
DCM	dichloromethane
TMSA	trimethylsilyl acetylene
HPLC	high performance liquid chromatography
PACA	peptide amphiphile contrast agent
TBAF	Tetrabutyl ammonium fluoride
DOTA	1,4,7,10-tetraazacyclododecane-1,4,7,10 tetraacetic acid
Mtt	4-methyl trityl
ICP	inductively coupled plasma
MS	mass spectrometry
PMMA	poly(methyl methacrylate)
PLLA	poly (L-lactic acid)
PLGA	poly (L-lactic-co-glycolic acid)
τ_R	rotational correlation time
MRA	magnetic resonance angigraphy
MHz	megahertz
mM	millimolar
nm	nanometer
C	Celsius
h	hour
s	second
Hex	hexane
DCM	dichloromethane
DMF	*N,N*-dimethylformamide
DTPA	diethylenetriaminepentaacetic acid
TFA	trifluoroacetic acid
MR	magnetic resonance
MRI	magnetic resonance imaging
PARACEST	paramagnetic chemical exchange saturation transfer

mL	milliliter
J	NMR coupling constant
d	doublet
bm	broad multiplet
m	multiplet
T_1	longitudinal nuclear relaxation time
T_2	transverse nuclear relaxation time
τ_m	water residency lifetime
s	singlet
t	triplet
MWC	molecular weight cutoff
ECM	extracellular matrix
EDT	1,2-ethanedithiol
DTT	dithiothreitol
TMS	trimethylsilyl
bs	broad singlet

Chapter One

Introduction

Adapted from:

Meade, T. J.; Taylor, A. K.; Bull, S. R.; "New magnetic resonance contrast agents as biochemical reporters."

Current Opinion in Neurobiology **2003**, 13 (5), 597-602.

1 Introduction and Background

1.1 Introduction to Magnetic Resonance Imaging

Magnetic Resonance Imaging (MRI) has emerged as a leading diagnostic technique in clinical settings because it is non-destructive and yields a true volume rendering of the subject.[1,2,3] The 2003 Nobel Prize was awarded to Sir Peter Mansfield and Paul Lauterbur for their pioneering work to make this technique clinically feasible.[4,5] An MR image is created by imposing one or more orthogonal magnetic field gradients upon the specimen while exciting nuclear spins with radio frequency pulses similar to a typical NMR experiment.[6,7] After collection of data with a variety of gradient fields, de-convolution by computer yields a one, two, or three-dimensional image of the specimen. Typically, the image is based upon the NMR signal from the protons of water where the signal intensity in a given volume element is a function of the water concentration and both the T_1 and T_2 relaxation times of the water protons.[8] Local variations in these three parameters (water concentration, T_1, and T_2 relaxation times) provide the vivid signal intensity (contrast) observed in diagnostic MR images.[9,10]

The qualities that have made MRI a technique of choice in medical imaging make it an ideal imaging tool for use in biological experiments.[7,11] Unlike light-microscope imaging techniques based upon the use of dyes or fluorophores, MRI does not produce toxic photobleaching byproducts and is not limited by light scattering/adsorption to those cells within a hundred microns of the surface. In order to increase the intrinsic contrast generated in an MR image, paramagnetic complexes are used.[12]

Paramagnetic metal ions, as a result of their unpaired electrons, act as potent MRI contrast agents.[1,12] They decrease the T_1 and T_2 relaxation times of nearby water protons (r^6

dependence where *r* is the distance between the water proton and metal ion).[13] Some paramagnetic ions decrease the T_1 without causing substantial line broadening (e.g. Gd(III) and Mn(II)), while others induce line broadening that masks signal intensity (e.g. superparamagnetic iron oxide).[14] The mechanism of T_1 relaxation is generally a through space dipole-dipole interaction. This interaction is between the unpaired electrons of a paramagnetic ion, such as Gd(III), and water molecules that are in fast exchange (~10 ns) within the ion's inner-coordination sphere. If the time between successive scans in the experiment is short, regions associated with the water molecules in close proximity to the Gd(III) ion appear bright in a MR image and the aqueous solution that is not close to the Gd(III) appears as a darker background.[15] The lanthanide ion Gd(III) is by far the most frequently chosen for MRI contrast agents (CAs) because it has a very high magnetic moment ($\mu^2 = 63BM^2$), and a symmetric electronic ground state (S^8) providing a long electronic relaxation. Transition metals such as high-spin Mn(III) and Fe(III) are candidates due to their high magnetic moments. Since paramagnetic ions are generally toxic, a suitable ligand or chelate must be found to render the complex inert.[16-18] Examples of commercial MRI CA ligands are found in **Figure 1.1** and research into novel chelating ligands is a topic of intense research.[7, 19, 20]

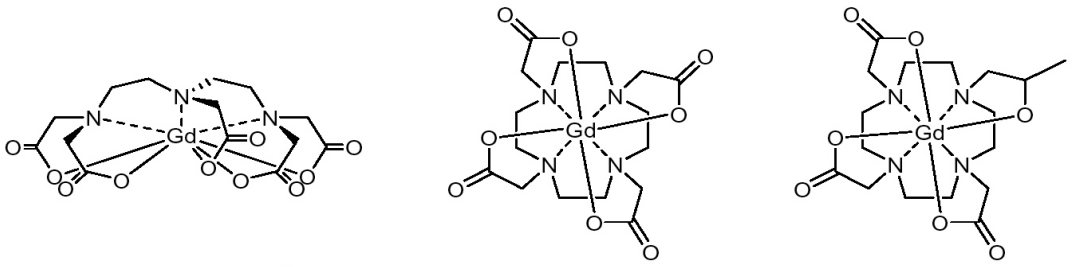

Magnevist® (r_1=4.3 $mM^{-1}s^{-1}$) Dotarem® (r_1=4.2 $mM^{-1}s^{-1}$) ProHance® (r_1=3.7 $mM^{-1}s^{-1}$)

Figure 1.1 Examples of clinically used MR CAs. All have eight coordination sites of the Gd(III) saturated and one open site for water exchange. The relaxivity data was taken at 20 MHz and 20 C.[7]

A major shortcoming of clinical and experimental MR contrast agents is that they are limited to reporting on anatomical detail only. It is difficult to synthesize CAs that are permeable to cells, contain fluorophores, or target specific cells, but work on this front is currently underway.[21-28] While significant progress has been made on the design and preparation of MR agents that are brighter, selectively target certain tissues, and remain in circulation for longer periods of time in vivo,[29] a new generation of agents capable of reporting on the physiological status and metabolic activity of cells or organisms has been pioneered by the Meade group at Northwestern University. These *procontrast* agents have been designed to exploit three fundamental physical properties of paramagnetic complexes that function as the switch or trigger to make them detectable by MRI. These properties are first, q, the number of water molecules coordinated to the paramagnetic ion; second, τ_m, the lifetime of a water molecule bound to the paramagnetic ion; and third, τ_R, the rotational correlation time of the complex. Varying q, τ_m, or τ_R can increase or decrease the observed signal intensity and

therefore manipulation of these parameters in the design of an agent produce what we call "activatable" MR agents. Here, we briefly review examples of these recently prepared agents, organized by the mechanism of activation (q, τ_m, or τ_R) and their identity as T_1, T_2, or chemical exchange saturation transfer (CEST) contrast agents.

q Modulated Contrast Agents

The first class of activated MR contrast agents reported was described by the Meade laboratory and was developed in response to the need of correlating developmental biological events with gene expression during an imaging experiment.[30, 31] The mechanism of the inner-sphere T_1 relaxation phenomena (q) suggested a means to create a contrast agent with two distinct relaxation states: one fast, one slow in response to the CAs immediate chemical environment (**Figure 1.2**). By blocking the one remaining open coordination site of Gd(III), water protons are excluded from the inner sphere and the effect of the Gd(III) ion on the T_1 of water is diminished. The agent (4,7,10-tri(acetic acid)-1-(2-β-galactopyranosylethoxy)-1,4,7,10-tetraazacyclododecane) gadolinium or "EGad" was designed to be activated by the enzyme β-galactosidase. The enzyme substrate (sugar) in addition to the chelate ligand occupies all nine coordination sites, inhibiting water access to the paramagnetic ion. The contrast agent is irreversibly turned "on" when β-galactosidase cleaves the sugar and water becomes accessible to the ion thus modulating q. These agents have been successfully used in vivo to monitor gene expression in *Xenopus laevis*.[30]

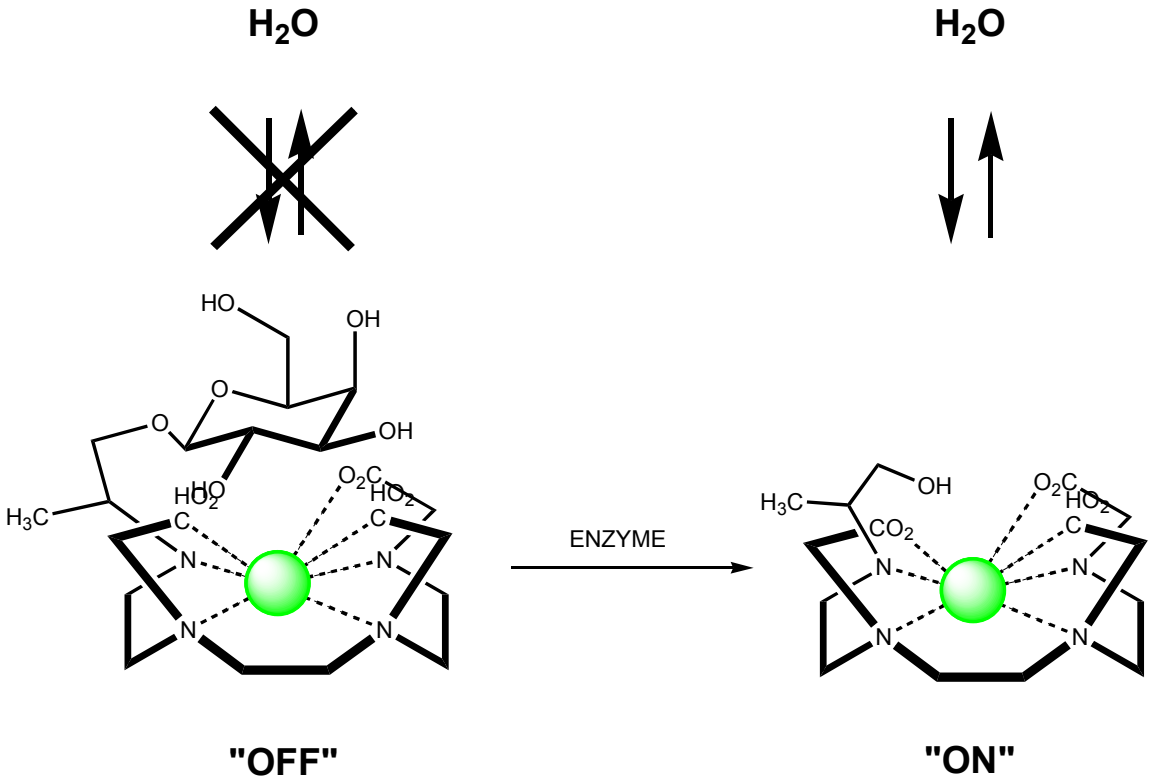

Figure 1.2 Enzyme activated MR contrast agent. Schematic of the transition of EgadMe (methyl substituted Egad) from a weak to a strong relaxivity state. Diagram representing the site-specific placement of the galactopyranosyl ring on the tetraazamacro-cycle (side view). Upon cleavage of the sugar residue by β-galactosidase, an inner sphere coordination site of the Gd(III) ion becomes more accessible to water.

Our lab has created the first iteration of MRI prodrug–procontrast agent based on a change in q. A DOTA derivative Gd(III) chelator was attached via an acid labile linker to the chemotherapeutic Doxorubicin (**Figure 1.3**). The CAs design was intended to release the Doxorubicin and CA when exposed to low pH and simultaneously change the CAs relaxivity by allowing water access to the metal center. The design was intended to switch the CA from dark to bright as the linker dissolved with sufficient contrast change to be seen with MR and simultaneously activating the Doxorubicin.[32] This class of prodrug-procontrast agents

incorporated the same q modulation theme as our enzyme-activatable CAs with the sugar being substituted with the doxorubicin as the water blocking moiety.

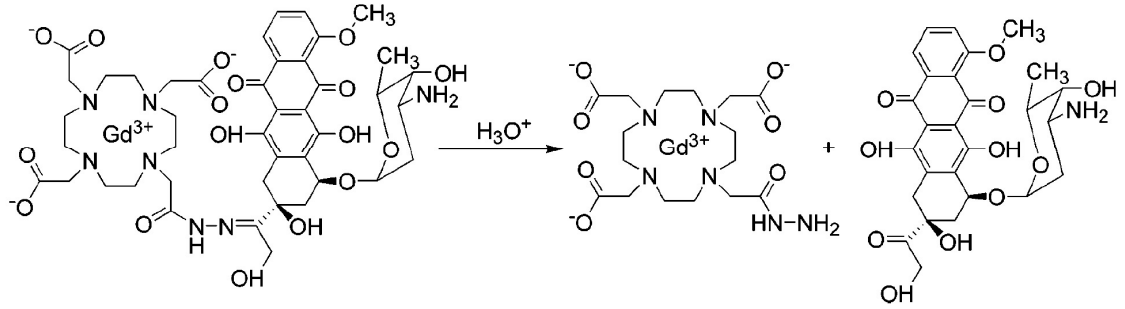

Figure 1.3 Design of the first prodrug-procontrast agent using a DOTA derivative and Doxorubicin. The design enabled the compound to fall apart at low pH (in the tumor) into the free contrast agent and free Doxorubicin changing the q and thus relaxivity.[32]

Intracellular Ca(II) plays an important role in signal transduction especially within neurons. Meade et al. [33, 34] developed the first intracellular messenger contrast agent activated by micromolar concentrations of Ca(II). The Ca(II)-sensitive contrast agent contains a calcium binding domain BAPTA (1,2-bis-(*o*-aminophenoxy)-ethane-N,N,N',N'-tetraacetic acid) which links two DO3A (1,4,7-tris(carboxymethyl)-1,4,7-10-tetraazacyclododecane) Gd(III) contrast agents. This reversible contrast agent takes advantage of stronger binding affinity of Ca(II) to the BAPTA acetate arms than with Gd(III). This leads to "switching" of the carboxylic acid arms of the BAPTA from the DO3A to the Ca(II) ion, which allows water access to the Gd(III) (**Figure 1.4**). This class of MR agents may lead to new ways of mapping brain function and signal transduction using MRI. Nagano et al. [35] have used a similar scheme for detection of zinc ions, by using a diethylenetriaminepentaacetic acid (DTPA) derived ligand with N,N,N',N'-tetrakis (2-pyridylmethyl)ethylenediamine (TPEN) as zinc-specific chelators and Que et al. [36] has worked on smart agents for copper sensing.

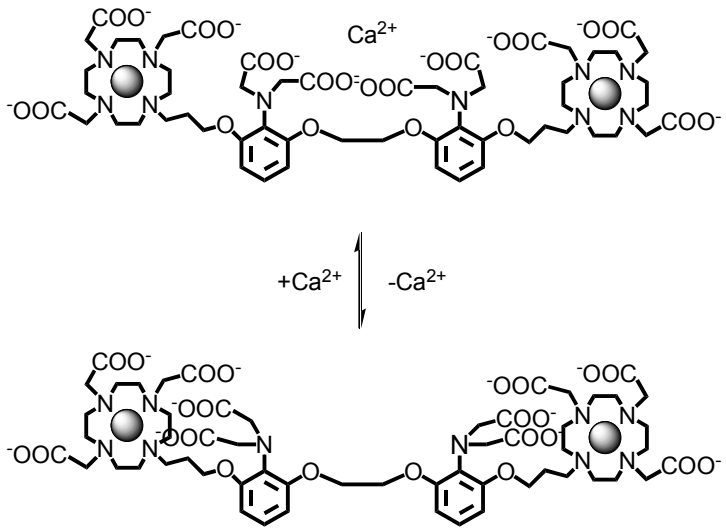

Figure 1.4 Calcium activated MR contrast agent. Proposed conformational change of a Ca(II) activated MR contrast agent. The addition of calcium induces a conformational shift allowing water access to Gd(III) and a change in observed relaxivity.

Indicators of pH are of interest as markers for abnormal tissue.[37-39] Lowe et al. [40] synthesized MR agents that exploit the difference between the pH of the extracellular matrix in tumors (pH 6.8-6.9) and healthy tissue's extracellular matrix (pH 7.4). This agent consists of a DO3A-derived chelator with a sulfonamide nitrogen, which is protonated at low pH and unable to chelate to the paramagnetic ion. As a result, water access to the ion is restored creating a detectable signal. At high pH, the deprotonated amine chelates Gd(III) thereby preventing water access to the ion resulting in a low MR signal. Work on pH sensitive CAs has been published by Woods et al.[41] and Toth et al.[42]

τ_m Modulated Contrast Agents

The use of deoxyhemoglobin as a paramagnetic MRI contrast agent was discovered by Thurlborn et al. [43] Ogawa discovered that the MR signal was dependent on the oxygenated state of the blood and that the blood oxygen level-dependent (BOLD) signal could be used for noninvasive mapping of human brain function.[44] Exploiting the BOLD method, activatable

contrast agents sensitive to pO_2 have been synthesized.[45] Instead of manipulating the ligands of the chelate to control the signal intensity, the oxidation state of a europium ion (Eu(III)) is varied by environmental pO_2 and therefore turns the signal on or off. Europium (III) is reduced to Eu(II) (isoelectronic with Gd(III)), thereby enhancing the observed MR signal upon reduction. The oxidation state of the metal is directly related to the pO_2 and allows for quantitative determination. An advantage of using Eu(III) is that its larger size allows for faster water exchange and therefore increases τ_m. The increase in τ_m enhances the already established signal given by the redox switch of the contrast agent.

τ_R Modulated Contrast Agents

Aime et al. [46] have developed a redox switch coupled to an increase in τ_R as a pO_2 sensitive contrast agent. Instead of Eu(III) as the redox ion, these agents use Mn(III) porphyrin complexes. By coupling the contrast agent to polycyclodextran, the Mn(III) porphyrin aggregates increasing the Mn(III) concentration and τ_R, resulting in greater signal intensity. It was shown that the water relaxation of Mn(II) (5 unpaired electrons) is much greater than Mn(III), creating a redox switch dependent on pO_2. This technique allows for the quantification of the oxygen concentration in the surrounding environment.

Relaxivity can be enhanced by an increase in rotational correlation time τ_R.[7, 47] This property can be altered by the viscosity of the environment, or by covalent and non-covalent interaction with a large species such as a protein.[7] Typically, τ_R agents are designed to bind to and target specific proteins. McMurry et al.[48] have developed a bioactivated contrast agent that produced an increase in τ_R after enzymatic cleavage of a peptide. The contrast agent consisted of a human serum albumin (HSA) binding inhibitor group, a HSA binding group, and a chelated

Gd(III) ion. When carboxylpeptidase B (part of the thrombin-activatable fibrinolysis inhibitor family) irreversibly cleaves the lysine-masking groups, the contrast agent facilitates the binding to HSA thereby increasing the relaxivity via τ_R. In this case, the ability to detect enzymatic cleavage is not due to the modulation of *q* as described above but is dictated by the agent binding to HSA. This dramatically shortens T_1 by an increase in τ_R yielding a significant change in MR intensity.

Sherry et al.[49] demonstrated a specific binding event of the galactose regulatory protein Gal80 to a contrast agent capped to a peptide sequence. Upon binding of the peptide sequence to Gal80, the τ_R and signal intensity were both increased. The binding event led to a τ_R increase to the near optimum level producing a relaxivity of 44.8 ± 1.7 $mM^{-1}s^{-1}$. This lock-and-key methodology can be used to target different proteins by altering the corresponding peptide sequence or simply incorporate groups for binding to large proteins and provides a facile means to increase τ_R for signal enhancement (

Figure 1.5).

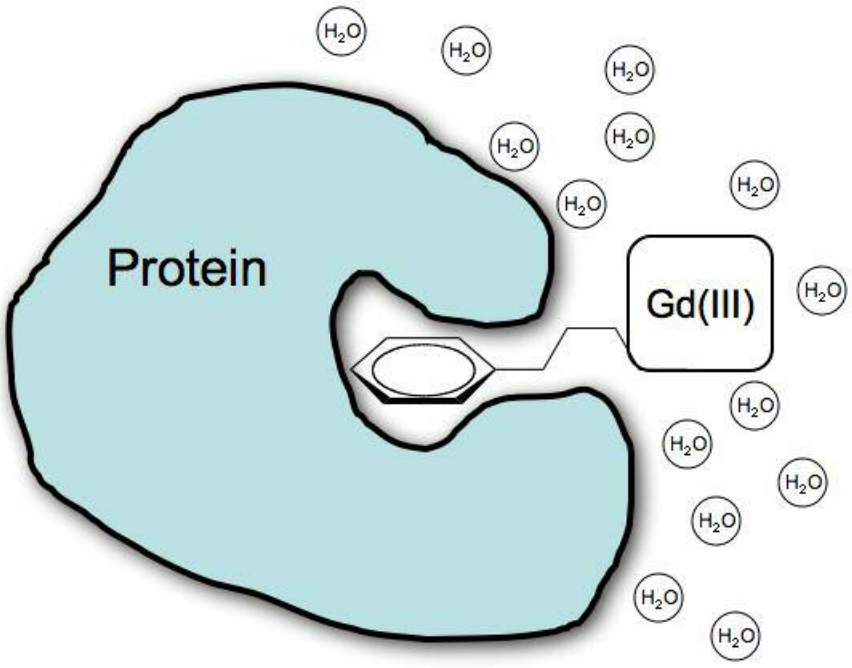

Figure 1.5 Protein binding of an MR agent. Schematic representation of the protein binding to an MR contrast agent. This size increase demonstrates the effect of signal enhancement by τ_R.

T_2 Contrast Agent

Detecting specific oligonucleotide sequences can be accomplished by using MRI techniques. Weissleder et al. [50] has developed an agent that enhances the spin-spin (T_2) relaxation by the detection of a specific oligonucleotide sequence. In order to target a specific oligonucleotide sequence, a cross-linked iron oxide (CLIO) agent was synthesized with an oligonucleotide sequence complimentary to that of a target sequence. Hybridization to the target sequence resulted in oligomerization, increasing magnetic relaxivity, thereby detecting specific DNA sequences (**Figure 1.6**).

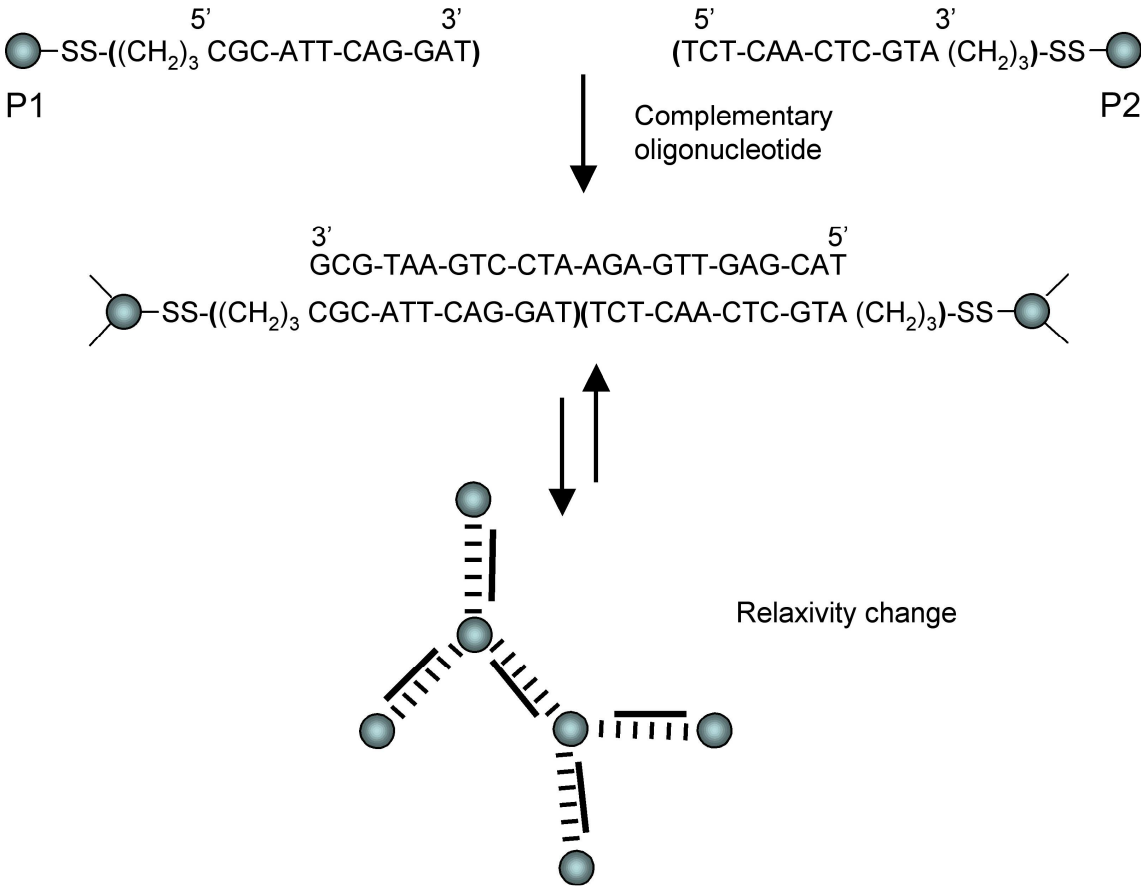

Figure 1.6 T_2-activated MR agent. Alkanethiol-substituted oligonucleotides were treated with N-succinimidyl 3-(2-pyridyldithio)propionate-activated nanoparticles to form the P1 and P2 nanosensors. P1 and P2 hybridize with complementary oligonucleotides and result in oligomerization and changes in the magnetic relaxivity.

A novel class of CA was developed by Genove et al.[51] in which a contrast agent was developed to visualize transgene expression. They used a vector to introduce a metalloprotein (from the ferritin family) into a host tissue. The reporter became superparamagnetic as the protein sequestered endogenous iron from the host. The cells were actually made to construct the MRI CA. A defective adenovirus was the vector of delivery for the ferritin transgene to transport the gene into the host's cells. This was the first report of an organism "synthesizing" its own MR reporter.

Chemical Exchange Saturation Transfer Contrast Agents

Contrast agents that can be switched on and off externally with an applied radio frequency (RF) pulse are known as chemical exchange saturation transfer (CEST) agents. CEST agents take advantage of the difference in proton relaxivity between the amide and inner-sphere water protons of the contrast agent. Aime et al. [52, 53] and Sherry et al. [54-56] have shown the advantages of concentration independence of CEST agents and their ability to be externally turned on or off. The concentration dependence is avoided by using two different exchange sites within a contrast agent as in the O-H and N-H bonds. When an external RF is directed at the frequency of one of the proton pool resonances, this causes saturation transfer to the water resonances and decreases the bulk water intensity, allowing for external manipulation of the signal intensity.

Aime et al. [53] have shown that a Yb(III) CEST agent can be sensitive to a biological substrate such as lactate. The lactate-bound Yb(III) complex, as opposed to the unbound complex, possesses two different sets of amide frequencies to irradiate. The concentration of lactate can be determined by irradiating the amide protons of the unbound complex. The

concentration of lactate-bound Yb(III) does not directly correlate with total lactate concentration. Using this methodology, Aime demonstrated that CEST can be used to measure the concentration of metabolites.

MR imaging has the promise of three-dimensional visualization of gene expression, metabolic activity and neuronal activation. The ability of MRI to report on metabolic activity in vivo could represent a substantial leap in existing diagnosis from quantifying gene expression to diagnosing brain disorders. The development of new types of contrast agents that are sensitive to a variety of biological processes will make MRI a more attractive tool for biomedical research and clinical diagnosis. Imaging these processes three-dimensionally in whole animals will allow researchers to probe events that formerly were accessible only in histologically stained and sectioned specimens. The future of MRI promises to be an exciting one as advancements in hardware, contrast agents, and image acquisition methods coalesce to bring high-resolution in vivo imaging to the biochemical sciences and to diagnostic radiology.

1.2 Introduction to Biomaterials and the Peptide Amphiphile

Through evolution, the human body has gained the ability for self-healing when presented with an injury. Unfortunately, this regenerative ability does not work with all organs nor does it last for one's entire life. When natural regeneration fails, we need to supplement the body with biomaterials to take over the roles the body is unable to perform. Biomaterials are defined as "materials of natural or manmade origin that are used to direct, supplement, or replace the function of living tissues."[57] While biomaterials have been in use for thousands of years, only recently have we rationally and systematically developed materials that are able to help supplement a damaged or diseased tissue/organ.[58]

Currently the need for organs/tissues greatly outweighs the supply of human donors, causing ethical and moral problems throughout society.[59] Most commonly cadavers are used for more complicated organs that perform a specific function e.g. tendons, hearts, skin, etc. The number of Americans waiting for organ transplants has been increasing and there are now more than 100,000 men, women, and children waiting for transplants.[60] Since the demand cannot be met with cadaveric or donated tissues, there is a great need for synthetic materials that perform the same function as natural organs.

The first materials used as biomaterials date back to prehistoric times with the evidence of sutures used to close wounds.[61] Gold was first used in dentistry more than 2000 years ago with the Aztecs,[62] and lead and silver wires were experimented with as sutures in the 1800s.[61] As materials chemistry advanced, so did the number of alloys and new materials that could be used to help support and heal the body. The 20th century saw more complex materials like stainless steel, cobalt chromium alloys, and synthetic polymers that had desirable properties to be used as biomaterials.[58, 61] Many of these materials are in use today to repair and treat various ailments of the human body.

Restoring structural function to the human body is what brought about the first-generation biomaterials. These materials are limited to structural functions rather than having a biological role in aiding regeneration (e.g. sutures). They were often susceptible to inflammation and immune response that caused the implant to fail.[63] Examples of first generation biomaterials that are still used include titanium screws used in bone repair, stainless steel hip implants, and bone cement (**Figure 1.7**). Their role throughout history has greatly increased the quality of life of the recipients but there is much room for improvement of these materials.

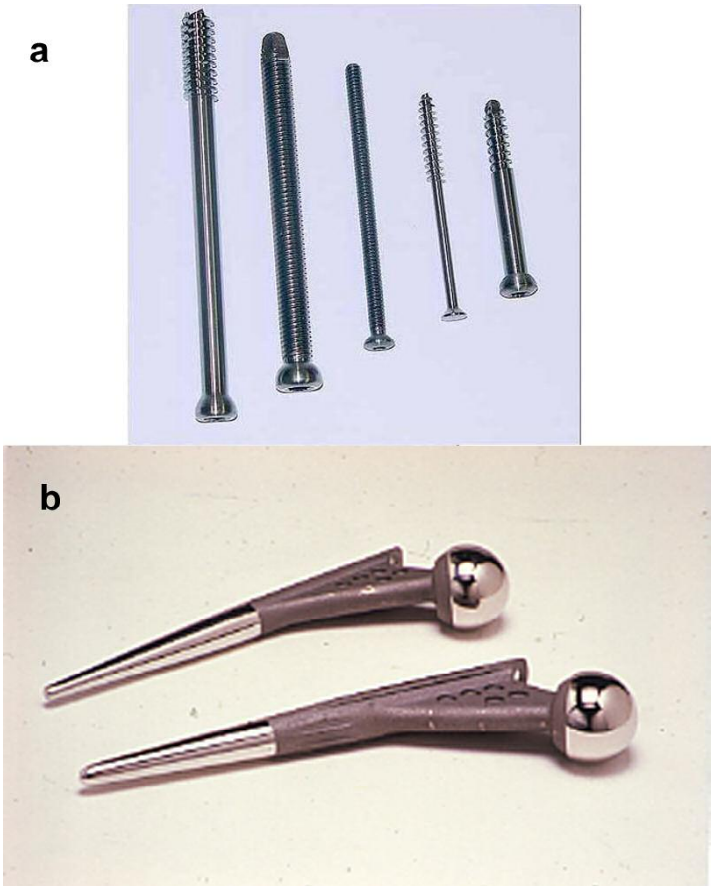

Figure 1.7 Titanium screws used in bone repair (a) and stainless steel hip implants (b).

The improvements of the first generation biomaterials came in the form of bioactivity and led to second generation biomaterials. Bioactive materials give rise to a biological response from the organism to aid in the recovery process. They combine both the mechanical aspects of the first generation with the body's natural healing mechanisms. Examples of these include titanium implants that are coated with hydroxyapatite to create a hybrid material that presents itself as a bone-like surface to the surrounding tissue.[64] Drug eluting stents fall into this second generation biomaterial category by incorporating the structural function of a stent with the bioactive drug portion to prevent restenosis (**Figure 1.8**).

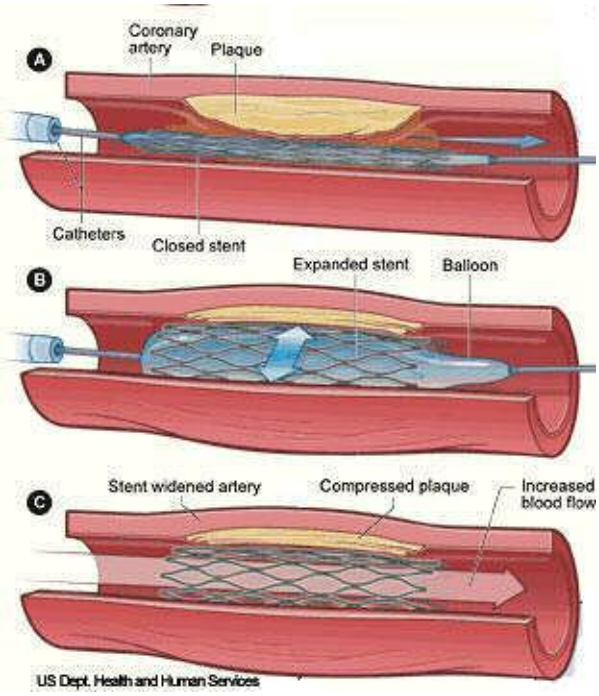

Figure 1.8 Cartoon illustrating the use of stents to open arteries blocked by plaque buildup.[65]

The second generation biomaterials gave rise to a solution for long-term use by degrading in the body over time and becoming replaced by the body's natural tissue. Polymers such as poly-L-lactide (PLLA) and poly (lactic-*co*-glycolic acid) (PLGA) are used because of their ability to be broken down in the body over time. PLLA and PLGA are both degraded by ester hydrolysis in the body into natural byproducts of the body's metabolic pathways, lactic acid and glycolic acid. These biocompatible materials are in use for devices such as grafts, sutures, and implants.[66] They offer very little toxicity and are able to be molded into different shapes and sizes. Even with the advances of the second generation biomaterials, there remains room for improvement such as faster degradation and promotion of vascularization.

Tissue engineering is the really the third generation of biomaterials where a template/scaffold is biocompatible, is bioactive, and provides signals for certain cellular

behavior. With this material, one would biopsy a patient's tissue and regrow the tissue on a three-dimensional scaffold ex vivo.[67] This new tissue would then be transferred back to the patients body after growth and degradation of the scaffold.[68] Previous literature has focused on using certain peptide sequences such as Arg-Gly-Asp (RGD) as the biomimetic component for the biomaterials.[69, 70] These sequences are frequently covalently attached to the scaffold via amides, esters, and disulfide chemistry.[69] The objective of the biomaterial is for the patient's own body to reproduce the damaged tissue (ex vivo), followed by degradation of the scaffold and subsequent implantation of the tissue back in the patient (**Figure 1.9**). This goal is being pursued in vivo by way of a direct implantation of the scaffold followed by degradation and replacement with new tissue.

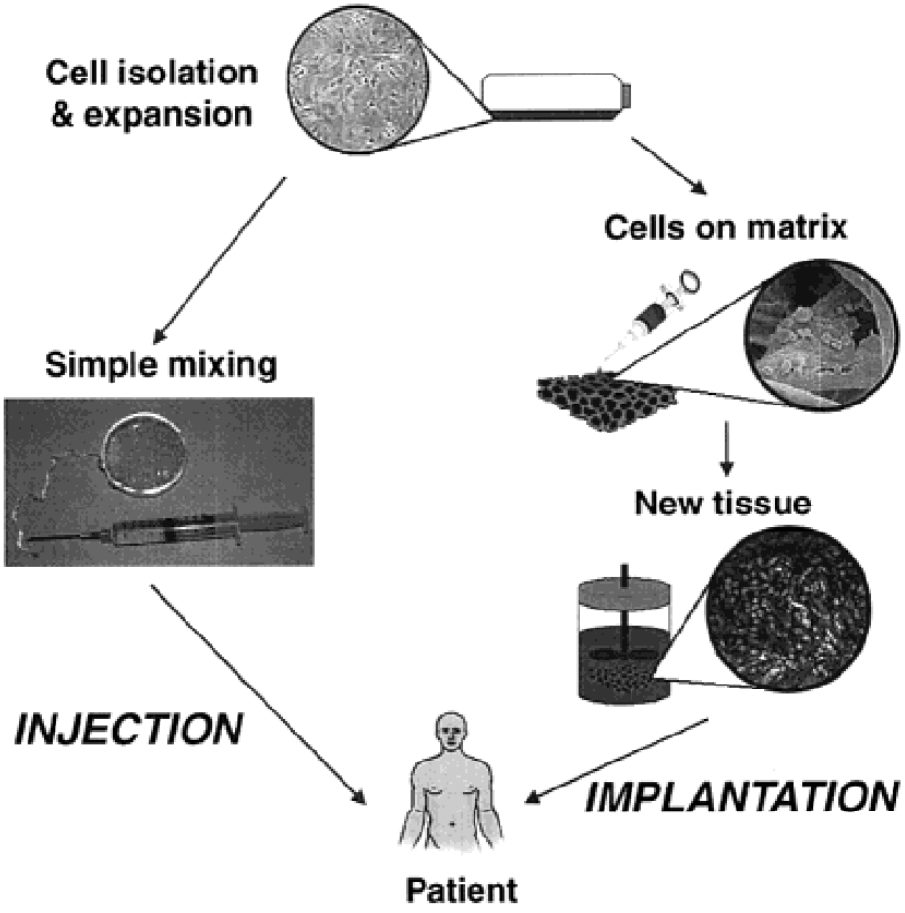

Figure 1.9 Cell-based tissue engineering methods via either scaffold use or direct injection of cells. (from Lee, K.Y. et al. *Chem. Rev.* **2001**, *101*, 1769-1779.)

A potential solution to tissue-regenerating biomaterials is in the form of self-assembly. One can define self-assembly as the organization of molecules through non-covalent bonds without outside intervention–essentially the molecules are preprogrammed to interact in a specific way.[71-73] Self-assembly is Nature's way of creating and organizing structures such as cells, the DNA double helix, and folded proteins without having to make energetically costly covalent modifications or reactions. The forces that create these supramolecular structures are

van der Waals forces, hydrophobic effects, hydrogen bonding, and electrostatics to combine one or more molecules into larger supramolecular objects.[71]

The size scale of these assemblies become very important when one considers tissue regeneration. The interactions with the extracellular matrix (ECM) are on the size of the nanometer–exactly the size scale that is being investigated today for many tissue regenerating biomaterials.[74] Cells actually recognize and are manipulated by objects in the nanoscale, which is the size regime of protein-protein interactions and the size of the ECM proteins.[75] This makes the use of bottom-up processes much more versatile in creating different shapes and sizes. The Stupp group has worked on self-assembly processes for more than a decade in designing and synthesizing zero-dimensional,[76-78] one-dimensional,[79-82] and two-dimensional structures.[83, 84] Challenges in self-assembly arise with the design of the molecules with reproducible and predictable behavior when exposed to certain environments.

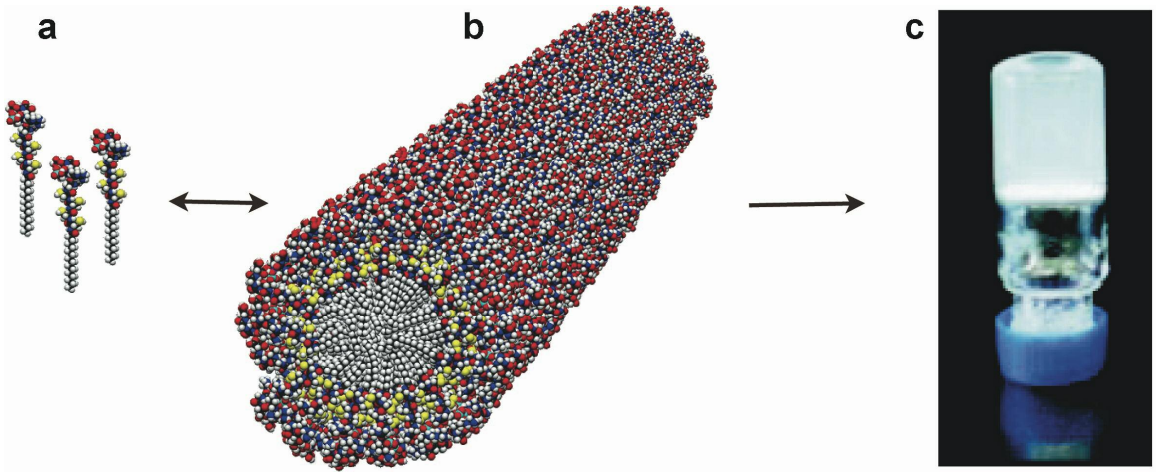

Figure 1.10 Cartoon depicting the self-assembly of PA monomers (a) into the nanofibers (b) they eventually form self-supporting hydro gels that are approximately 99% water (c).[81]

The Stupp group's preferred biomaterial is created from the self-assembly of peptide amphiphile (PA) molecules (**Figure 1.10**). These amphiphilic molecules are synthesized with

charged amino acids that act as the hydrophilic portion of the molecule and an alkyl tail for the hydrophobic portion of the molecule.[85] When dissolved in water, these molecules aggregate together which is driven by the hydrophobic collapse followed by β-sheet hydrogen bonding between monomers that extends the micelles into cylindrical micelles (nanofibers). The PA molecules self-assemble into elongated one-dimensional supramolecular polymers with diameters on the nanoscale and are able to noncovalently crosslink and encapsulate water molecules to form a hydrogel. This propagation of hydrogen bonds between successive PA molecules results in the elongation of the supramolecular polymer and prevents spherical micelle formation.[86] These PA fibers then bundle and entangle with themselves, trapping water molecules to form self-supporting gels at low weight percents (1% by weight). The PAs are robust molecules and one is able to vary the amino acid headgroup to incorporate an almost unlimited number of bioactive peptide sequences without changing the basic self-assembly and structural characteristics. We have worked with multiple PA molecules and have tested their bioactivity as well as structural characteristics ranging from gels that target the differentiation of neurons[87] to gels that promote angiogenesis.[88] The major limiting factor of using biomaterials is the inability to fate map them over time, noninvasively, and in vivo. I have decided to use MRI as the technique to overcome this drawback.

Scope of Thesis

This thesis focuses on the development of high relaxivity magnetic resonance imaging contrast agents via supramolecular chemistry for use in fate mapping of biomaterials in vivo. The thesis begins with a background on MRI contrast agents as biochemical reporters and an overview of biomaterials. The chapter breaks down biomaterials into different classes of

increasing complexity and ends with the Stupp group's work into self-assembling peptide amphiphile nanofibers as biomaterials for tissue regeneration. This chapter provides the background and inspiration for the original work done by this author that is covered in Chapters 2 through 7.

Chapter 2 describes the early work of synthesizing a template molecule to control the self-assembly of the peptide amphiphile nanofibers. The template's core took advantage of convergent synthesis and the Suzuki reaction to produce an oligophenylene hydrophobic rigid-rod core. This oligophenylene rod was then capped at each end with a hydrophilic bulky PEG end cap. This structure produced a dumbbell shaped molecule that could be tailored in length. This synthetic work was accomplished without success owing to the multiple steps and low yields and failure to reproduce results. The failure of this chapter, did however, pave the way for a more efficient synthetic methodology using Sonogashira chemistry described in Chapter 3.

Chapter 3 details the synthesis and characterization of a dumbbell-shaped molecule for use as a template in controlling the supramolecular structure of the peptide amphiphile nanofibers as well as the solution phase synthesis of peptide amphiphile molecules. Instead of using the more complicated and lower yielding Suzuki chemistry to form oligophenylenes found in Chapter 2, the synthesis was altered from an oligophenylene rod to an oligophenylene ethyneylene rod. This allowed for higher reaction yields and a more lengthy rigid-rod core. I was able to keep the benefits of having a defined length but could add more degrees of rotation within the rigid rod to help with the packing of the peptide amphiphiles around the core. Solution-phase synthesis of the peptide amphiphiles was utilized to make larger quantities of the molecule and to provide a synthesis that can be characterized after each step. Using orthogonal protection schemes with convergent peptide synthesis, the peptide amphiphiles were synthesized

in a relatively small number of steps. When the dumbbell template was added to a solution of peptide amphiphile, a shift from long one-dimensional fibers to short aggregates was observed. This shift was solely due to the addition of the template molecule providing a synthetic template for supramolecular control.

Chapter 4 describes the conjugation of magnetic resonance imaging contrast agents to self-assembling peptide amphiphiles for the use in fate mapping tissue regenerating biomaterials. This chapter reports on the synthesis of magnetic resonance active peptide amphiphile molecules that self-assemble into spherical and fiber-like nanostructures, enhancing T_1 relaxation time. These new molecules give relaxivities on the order of five times that of clinically used contrast agents. This new class of magnetic resonance contrast agents can potentially be used to combine high-resolution three-dimensional fate mapping of tissue-engineered scaffolds with targeting of specific cellular receptors.

Chapter 5 reports on the in vitro and in vivo use of the self-assembling peptide amphiphile contrast agents for use in biomaterial applications. The current interest in biomaterials for tissue engineering and drug delivery applications have spurred research into self-assembling peptide amphiphiles. Nanofiber networks formed from self-assembling peptide amphiphiles can be used as biomaterial scaffolds with the advantage of specificity by the incorporation of peptide-epitopes. Imaging the materials noninvasively will give information as to their fate in vivo. This chapter reports on the synthesis and in vitro images of self-assembling peptide amphiphile contrast agents doped into other biologically active peptide amphiphile biomaterial gels. At 400 MHz using a 0.1 mM Gd(III) conjugate of the peptide amphiphile, we observed a T_1 three times that of a control gel. The peptide amphiphile derivative was doped into various epitope-bearing amphiphile solutions and that resulted in a homogeneous biomaterial

upon gel formation as imaged by magnetic resonance. This result has proven that the peptide amphiphile contrast agent can be used as doping material to image various targeting biomaterials, extending the application of this new contrast agent. This agent was then tested in vivo in a porcine heart model and mouse organ model. These models confirmed the ease and ability to track peptide amphiphile biomaterials noninvasively within living organisms yielding insight to degradation.

Chapter 6 compares different peptide amphiphile contrast agent architectures to help elucidate the most important variables for maximum relaxivity. Within the seven different contrast agents, branched molecules as well as linear molecules were compared. It was discovered that the branched architecture provided more favorable relaxivities because of steric effects slowing down the local rotation of the chelator. Both q = 1 and q = 2 agents were synthesized to test the difference in relaxivity. It was found that the q = 2 agents provide for a higher relaxivity as expected from the increased water access to the inner sphere. I explore the effects of polymerization of the peptide amphiphiles in respect to relaxivity and discovered little to no change as well. This chapter provides insight into attaining the highest possible relaxivity for peptide amphiphile based contrast agents.

Chapter 7 describes the work performed in collaboration with Lindsay Karfeld to develop a novel class of contrast agents using protein polymers as the backbone for high relaxivity contrast agents. We transformed a plasmid into *E. coli* to induce natural production of protein polymers. Purification from these cells yielded our naturally synthesized contrast agent backbone. These protein polymers are monodisperse in length with molecular weights >20 kDa and contain regular repeats of lysine amino acids. The ε-amine on these lysines are available for conjugation to a DOTA derivative contrast agent to chelate Gd(III). Conjugation yields

approximately eight to nine contrast agents per protein with relaxivities of 7.3 $mM^{-1}s^{-1}$ yielding molecular relaxivities >60 $mM^{-1}s^{-1}$. These high-relaxivity protein polymers were designed for incorporation into hydrogels for use in tissue regenerating biomaterials.

The appendix section of this thesis describes the mechanism of relaxivity in greater detail. It is broken down into the specific parameters of relaxivity and this section is aimed to give the reader greater insight into how magnetic resonance imaging works. This chapter provides an explanation of why and how contrast agents help enable this diagnostic technique.

Chapter Two

Oligophenylene Dumbbell Synthesis

2 Oligophenylene Dumbbell Synthesis and Characterization

2.1 Introduction

Dimensional control over synthetic self-assembled supramolecular structures on the nanoscale has not been well demonstrated in literature and has yet to be realized with the peptide amphiphile (PA) self-assembling system. A possible solution to this problem is the use of a template molecule to direct the self-assembly of the PA monomers into discrete structures. Controlled self-assembly of PA systems via templation could help to explore fundamental unanswered questions including: the density of the PA monomers in the nanofibers, derivatives of the end caps could be used to explore the ends of the fibers, and the final structures could afford discrete aggregates to be filled with a drug for targeted delivery. This chapter will discuss my unsuccessful first generation template, principles behind using a template molecule, and the synthetic methodology used. Chapter 3 will provide a detailed description of a successful template.

The initial attempt to control self-assembly of the supramolecular polymer of PA molecules began with a global view of the final self-assembled structure of fibers and forces involved in creation of these fibers. PA monomers self-assemble into high aspect-ratio one-dimensional nanofibers that are <9 nm in diameter, but have uncontrolled lengths that can reach into micrometers. My research was focused on controlling the length of these nanofibers because the widths are predetermined by the PA monomer size. In determining the length control over a self-assembling fiber structure, one must think of both a beginning and end point for the structure. Considering the forces that drive the self-assembly – hydrophobic collapse, hydrogen bonding, van der Walls, and electrostatics – there is not an obvious solution to a starting point for these self-assembled fiber-like structures. Instead of developing a starting point

for fiber formation or an ending point, I developed a template molecule to counteract the forces promoting self-assembly, essentially creating two ending points (either end of the fiber) for "short" controlled fiber formation.

In aqueous solution, above the critical micelle concentration, the PA molecules will associate and arrange themselves such that the alkyl tails bundle together and collapse to minimize their interaction with solvent. This collapse is driven by the entropy gained in the individual solvent molecules released from the hydrophobic region of the PA monomers prior to collapse. This phenomena is observed because of the hydrogen-bonding network of solvent will locally rearrange to maximize hydrogen bonding around the PA monomers, thus restricting the number of configurations of the solvent molecules.[89] (The hydrophobic portion effectively orders the water around it and this decreases entropy.) Control over the self-assembly of these monomers must begin with the development of a molecule to take advantage of this hydrophobic collapse step and the template must contain a hydrophobic region. Elongation of the PAs into fibers is dominated by the β-sheet hydrogen bonds formed between adjacent PA monomers.[87] To stop the extension of the fibers one must inhibit these hydrogen bonds from propagating. One solution to prohibit extension of the fibers is to use a dumbbell shaped molecule as a template for the control over supramolecular self-assembly.

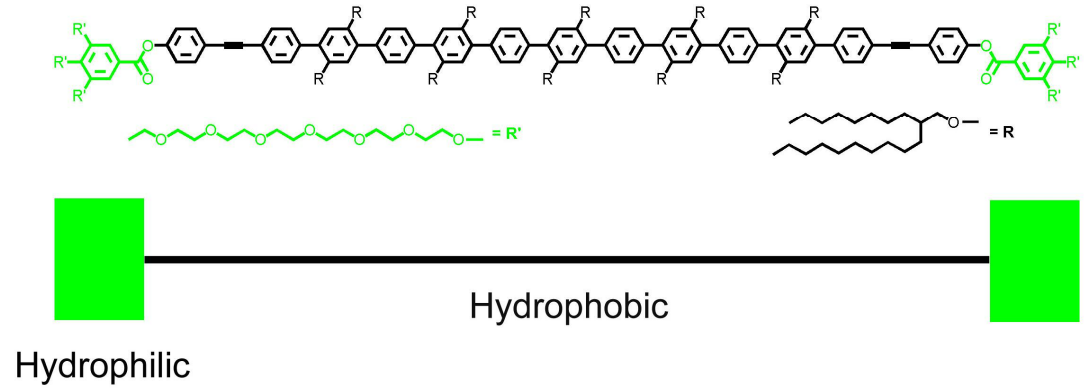

Figure 2.1 Schematic representation of a dumbbell molecule and cartoon representing the dumbbell shape of the molecule. This molecule was designed to be a hydrophobic rigid rod (in black) flanked by hydrophilic PEG end caps (in green).

The dumbbell molecules are named for their overall shape and likeness to a dumbbell found in a gymnasium. The molecular dumbbell shape consists of two bulky ends separated by a rigid-rod core. Using the dumbbell shape as the basis for a molecular template, interaction/inhibition with the PAs self-assembling driving forces are incorporated into this template molecule. A hydrophobic rigid-rod flanked by bulky hydrophilic end caps would give the correct dumbbell shape (**Figure 2.1**) and modification of the components would lead to favorable interaction between the PA and template. Making use of a hydrophobic core would allow the PA monomers to collapse with the dumbbell's rigid-rod portion within the core of the PA's fiber structure. The PAs self-assemble in water and the dumbbell must be at least sparingly soluble in aqueous solutions. Owing to the hydrophobic rigid-rod portion of the dumbbell, hydrophilic end caps must be synthesized to give the template molecule solubility in aqueous solutions.

The synthesis of a dumbbell shaped template molecule began with a hydrophobic rigid-rod core (**Figure 2.1**) to provide a controlled length determined synthetically. We theorized that the hydrophobic rod would be incorporated into the hydrophobic region of the self-assembled PA molecules during hydrophobic collapse. A rigid-rod core was chosen over a linear hydrophobic polymer to prevent its collapse (globular formation to decrease surface area in aqueous solution), thus increasing the interaction with solvent and subsequent interaction with the PA monomers. To this end, I have incorporated a 2-octyl dodecanol derivative for enhanced interaction with the alkyl segments on the PA monomers and increased solubility of the rigid-rod during synthesis. The aromatic core was chosen because of the synthetic precedence in literature, its stability, its ability to be functionalized, and its defined length.

We designed the PEG end caps to bring a hydrophilic and bulky end group to prevent further elongation of the nanofibers by saturating hydrogen bonds along the amino acid portion of the PA, to disrupt the hydrophobic collapse of the monomers, and to add steric bulk to misalign the PA monomers such that hydrogen bonding for β-sheet formation was no longer in the optimal alignment. Effectively, the PA monomers' alkyl regions would collapse, incorporating the dumbbell molecules into their core. Once the template molecules were entirely coated the self-assembly would terminate with the bulky hydrophilic end caps, leaving a discrete aggregate (**Figure 2.2**).

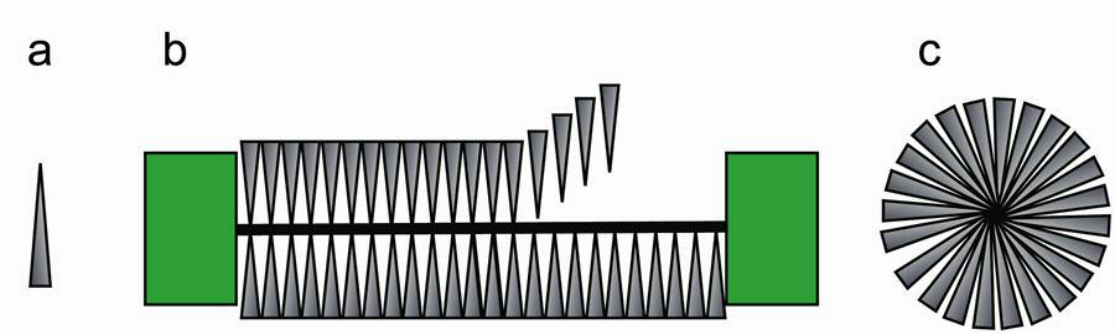

Figure 2.2 Representative cartoon of the PA (**Figure 2.3**) self-assembling around the dumbbell molecule creating a discrete nanobarrel. The PA (a) self assembles around the dumbbell stopping at the hydrophilic end caps (green) (b) and a side view taken as a slice of the dumbbell with PA surrounding it (c).

2.2 General Synthesis of Oligophenylene Dumbbells

The initial design of the dumbbell used an iterative, convergent synthesis to form a rigid hydrophobic oligophenylene (OP) rod capped at both ends by a hydrophilic bulky PEG derivative end group. Due to the insolubility of rigid-rod like molecules in organic solvents, 2-octyl dodecanol derivative was used for the dual purpose of increased solubility and interaction with the palmitic acid alkyl tails of the PA molecules assembling around the dumbbell (**Figure 2.3**).[90] Iterative Pd-catalyzed Suzuki coupling methodology afforded an OP rigid-rod (**Figure 2.3-2.8**). The end caps were synthesized by substituting a trihydroxy benzoic (gallic) acid, via etherfication, with three PEG_{350} tails. This PEG_{350} gallic acid moiety provides a bulky/hydrophilic region in stark contrast to the hydrophobic rigid-rod interior of the dumbbell template. The end caps were then attached to the rod portion using an ester bond.

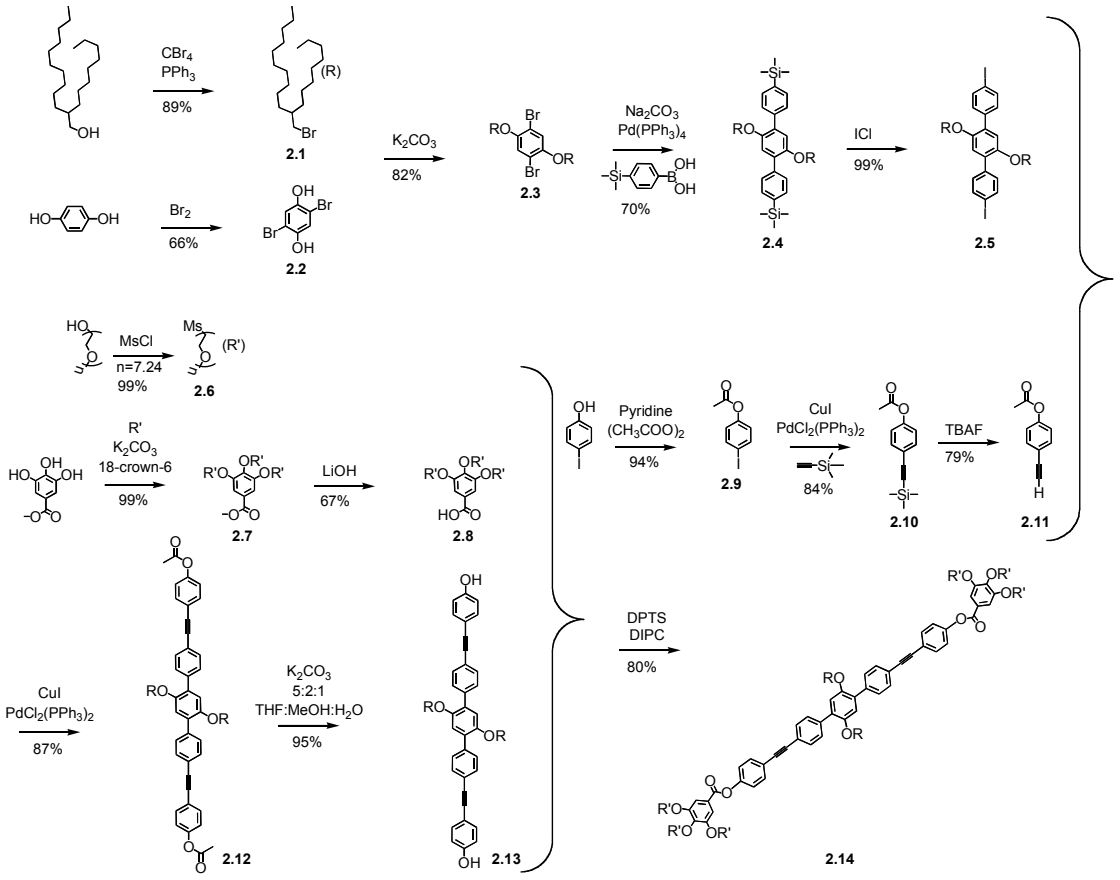

Scheme 2.1 OP3 (**2.14**) dumbbell synthesis is depicted above, and represents the general convergent synthetic scheme for all OP dumbbells.

The synthesis of the rigid-rod portion of the dumbbell began with the creation of a solubilizing moiety that could be produced in large quantities for the extension of the rigid-rod core. A 2-octyl dodecanol molecule was chosen for its more optimal solubility properties when compared to a linear alkyl solubilizing moiety as well for its similar length to that of the PA alkyl tail. Bromination of the branched tail and Williamson-ether synthesis to **2.2** (**Scheme 2.1**) afforded the complete solubilizing moiety with the ability to continue to employ Suzuki coupling chemistry owing to the bromide substituents. Making use of trimethylsilyl (TMS) phenylboronic acid for the rod extension and facile conversion of the TMS, by way of ICl,[91] to the aryl iodide

provided greater yields and the means for the subsequent Suzuki couplings to extend the rod portion of the template. Suzuki coupling of the 4-trimethylsilyl phenyl boronic acid to **2.3** resulted in **2.4**, which was used as the basic OP rod for the subsequent dumbbell templates. The TMS group could be converted to the corresponding iodide **2.5** by way of ICl for consecutive Suzuki couplings. Adding to the core OP rod molecule, **2.5** (**Scheme 2.1**), various lengths of dumbbells were prepared.

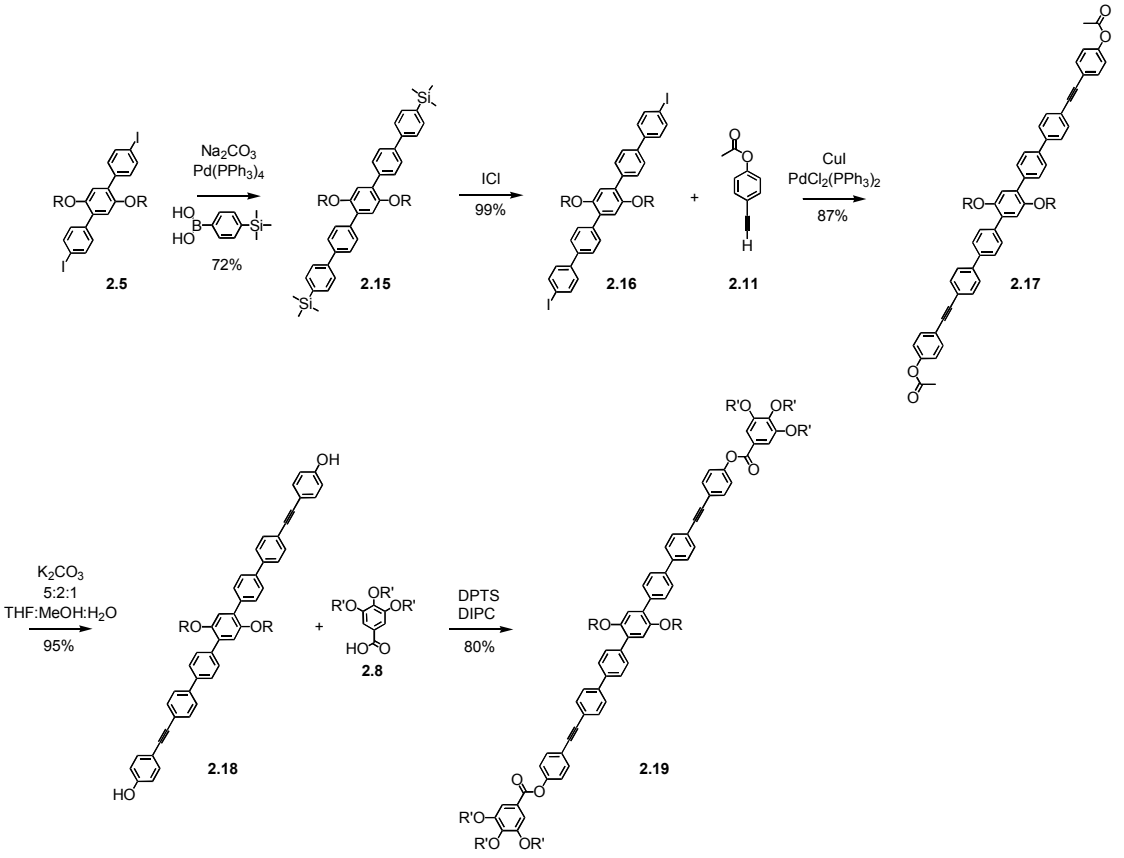

Scheme 2.2 OP5 (**2.19**) dumbbell synthesis utilizing consecutive Suzuki couplings and a final Sonogashira coupling for the end caps.

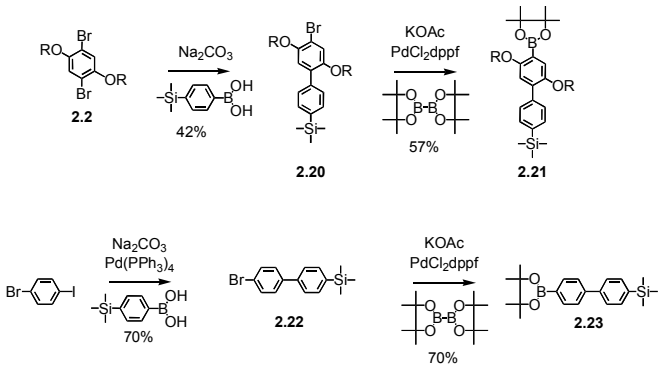

Scheme 2.3 Boronic ester synthesis (**2.21**, **2.23**) for extension of the OP dumbbell rigid-rod synthesis via Suzuki couplings.

With only one solubilizing core, **2.3** (**Scheme 2.1**), five consecutive phenylene units was the longest soluble rod that could be synthesized. This fact demanded the synthesis of another extension unit besides 4-trimethylsilylphenylboronic acid and led to the synthesis of diphenylene boronic esters **2.21** and **2.23** (**Scheme 2.3**) used for rod elongation.[92, 93] These new Suzuki units provided more efficient rod extension with a fewer number of steps and **2.21** allowed for a solubilizing group to be added with each extension unit. These boronic esters allowed for the completion of the OP7 dumbbell **2.28** (**Scheme 2.4**) and using both **2.21** and **2.23** allowed for the completion of the OP13 dumbbell **2.35** (**Scheme 2.5**).

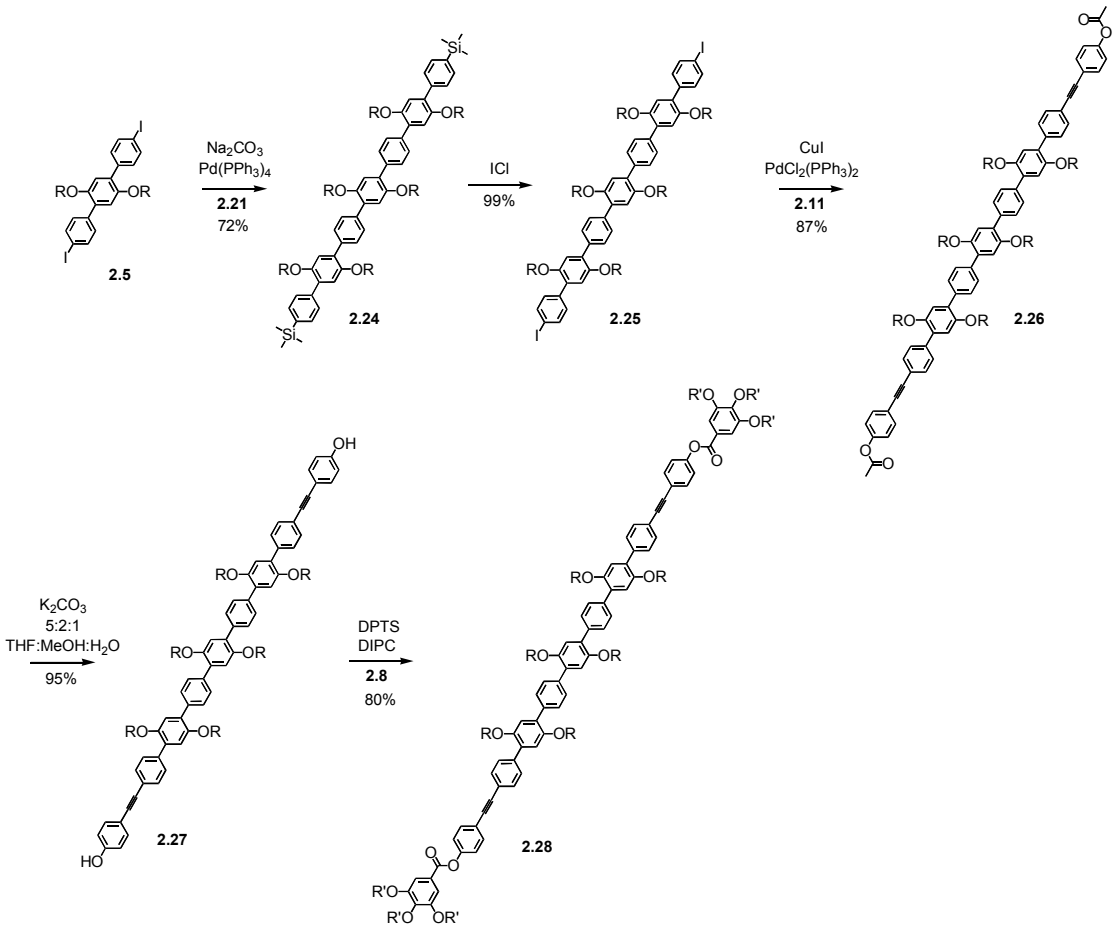

Scheme 2.4 OP7 (**2.28**) dumbbell synthesis via consecutive Suzuki couplings and a final Sonogashira coupling to attach the end caps.

The Sonogashira reaction was chosen for the final step in rod formation as the most facile procedure to add length and the hydroxide moiety as a handle for the final esterfication with the gallic acid derivative end caps **2.11**. 4-iodophenol was acetate protected and TMS-acetylene was then attached via Pd catalyzed Sonogashira coupling chemistry. Subsequent deprotection of the TMS afforded **2.11** (**Scheme 2.1**). The Sonogashira coupling between **2.5** and **2.11** provided the final step to completing the rigid rod portion of the template.

The end caps were synthesized to add steric bulk to the ends of the rigid-rod molecules, completing the dumbbells and provided solubility in aqueous solutions. The basic building block

was the gallic acid methyl ester, which provided a facile handle for attachment via ester bond formation to the rigid-rod molecule e.g. **2.14**. Three PEG_{350} units were covalently attached by ether bond formation to the gallic acid forming **2.7** (**Scheme 2.1**). Deprotection of the methyl group by base hydrolysis afforded the end cap moiety **2.8**.

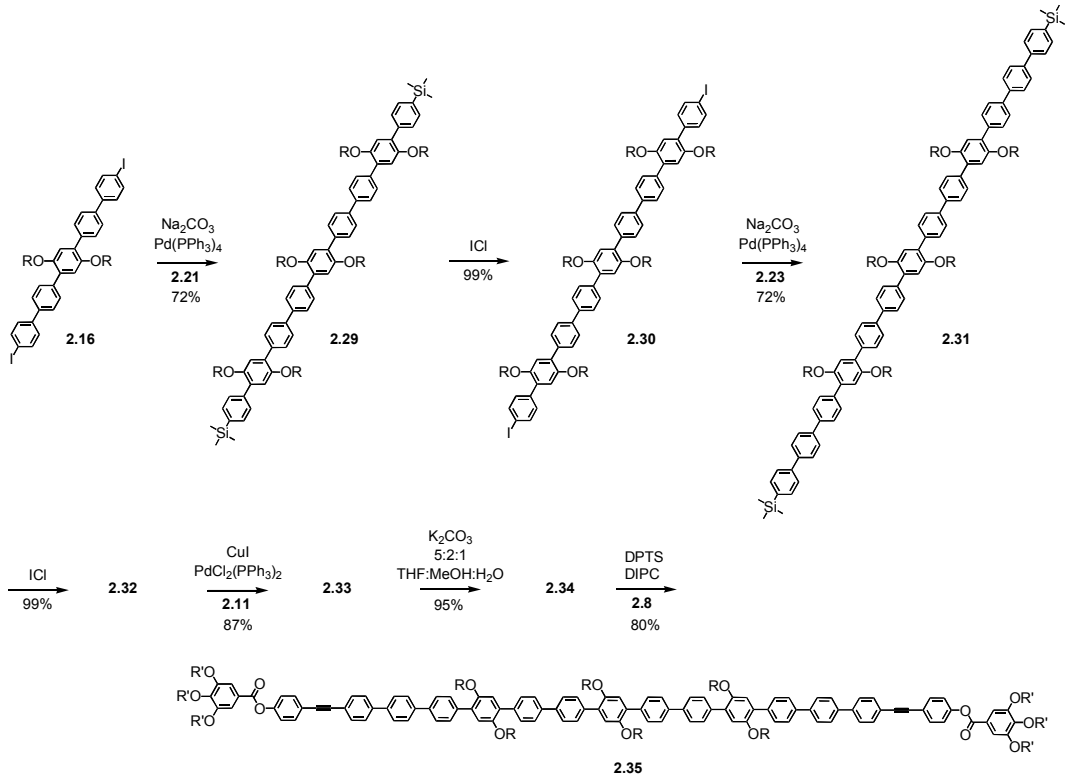

Scheme 2.5 OP13 (**2.35)** dumbbell synthesis via consecutive Suzuki couplings and a final Sonogashira coupling to attach the end caps.

2.3 Preliminary Results

Stock solutions of both the OP3 and OP5 dumbbells **2.14** and **2.19** with PA **2.36** (**Figure 2.3**) were prepared in THF and water respectively. These solutions were mixed in different ratios of **2.14** to **2.36** corresponding to 3:1, 1:2, 1:8, 1:15, 1:30, 1:60, 1:120 and then drop cast onto carbon transmission electron microscopy (TEM) grids for imaging. It was found that when the PA concentration was about eight times that of the template concentration fibers were present

and below that ratio fibers were not present. At the 1:7 ratio of **2.14**:**2.36**, instead of long fibers, small spherical micelle like structures were seen but the lengths were unable to be calculated. When ratios greatly favored the PA molecules, fibers were seen and the structures were indistinguishable from the control PA sample. The control samples of just the PA showed only fibers and the control sample of **2.14** showed no discernable supramolecular structure at all (**Figure 2.4**, **Table 2.1**).

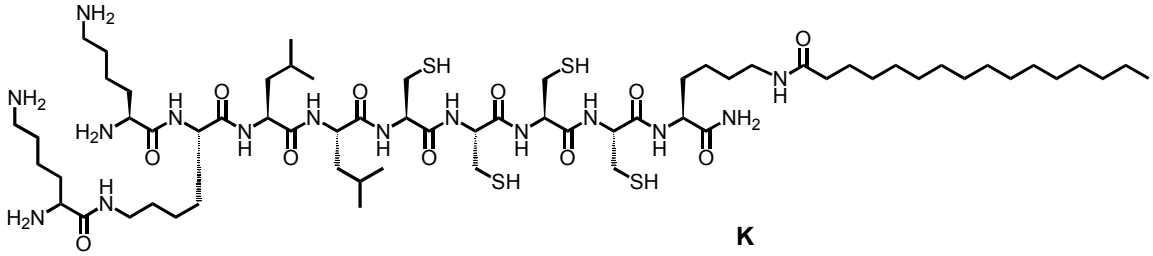

Figure 2.3 Molecular structure of PA **2.36** used with **2.14** and **2.19** for length control studies.

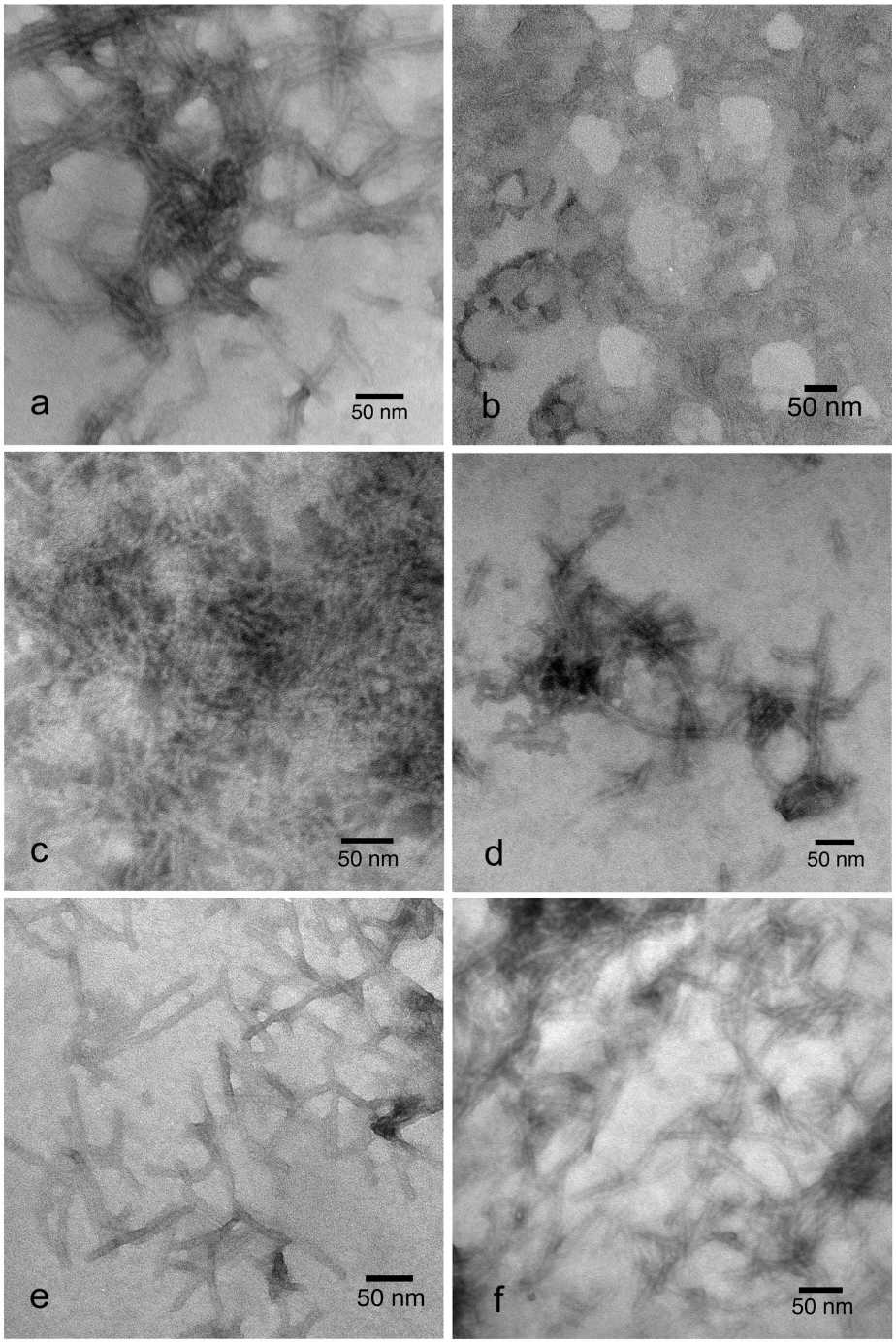

Figure 2.4 Representative TEM images of **2.14** mixed with **2.36** (**Figure 2.3**). a) **2.36** alone b) 3:1 **2.14**:**2.36** c) 1:8 **2.14**:**2.36** d) 1:30 **2.14**:**2.36** e) 1:60 **2.14**:**2.36** f) 1:120 **2.14**:**2.36**. One is able to see that defined supramolecular structures appear with a ratio of 1:30 and greater. All images were drop cast on carbon grids with uranyl acetate staining.

2.14:**2.36** ratio	AFM results
2.36	Fiber
2.14	No structure
3:1	No structure
1:2	No structure
1:8	Beads on a string
1:15	Fiber
1:30	Fiber
1:60	Fiber
1:120	Fiber

Table 2.1 Results of mixing **2.14** and **2.36** in different ratios drop, casting onto mica, and imaging by AFM.

Equivalent AFM experiments were performed with **2.19**:**2.36** in the ratios of 1:1, 1:10, 1:100, 1:200, 1:400. Data by AFM again showed that above the 1:10 dumbbell to PA concentrations fibers were present and below that concentration indiscernible spherical micelles were again present (**Table 2.2**).

2.19:**2.36 ratio**	AFM results
2.36	Fiber
2.19	No structure
1:1	Spherical micelles
1:10	Spherical micelles
1:100	Fibers
1:200	Fibers
1:400	Fibers

Table 2.2 Results of mixing **2.19** and **2.36** in different ratios drop, casting onto mica, and imaging by AFM.

Fluorescence studies were completed on dumbbells **2.14** and **2.19**. The goal of these studies was to observe a shift in fluorescence with the environment surrounding the dumbbell templates (aqueous solution vs. hydrophobic solution). This outcome would help conclude that the dumbbell molecules were indeed internalized within the PA nanofibers. Fluorescence studies were first prepared with **2.14** and **2.19** in both hexanes and THF to simulate a nonpolar environment and polar environment mimicking both the aqueous and hydrophobic environments of inside and outside the self-assembled PA fibers (**Figure 2.5**). The decrease in intensity in THF verses hexanes is attributable to quenching from the association of the rigid-rod portions (π stacking) of the dumbbell molecules. The fluorescence data when the **2.14** and **2.19** were mixed with the PA **2.36** (**Figure 2.6**) showed a decrease in intensity with the addition of PA but again not a shift in absorbance. The decrease in intensity with an increase of PA concentration

suggests encapsulation of the dumbbell within the PA fibers with energy transfer to the PA **2.36** resulting in vibrational enhancement and less photon emission in the form of fluorescence.[94]

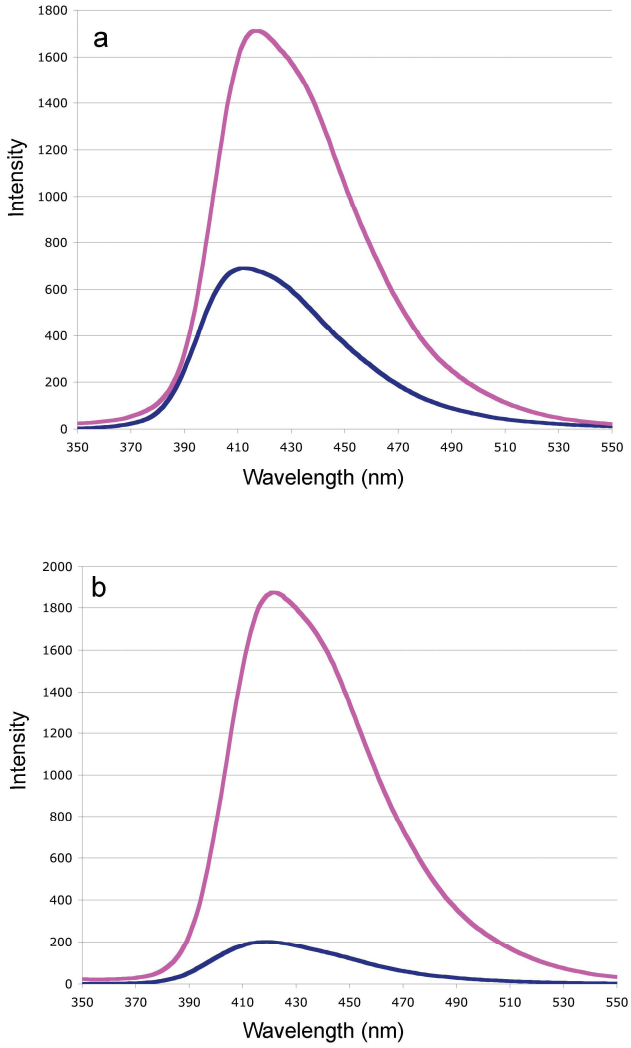

Figure 2.5 Emission spectrum of **2.14** in (a) and **2.19** (b) when excited at 204 nm and 216 nm respectively. The pink curves are spectra taken in hexanes and the blue curves are spectra taken in THF. There is not a shift in maximum emission wavelength only intensity.

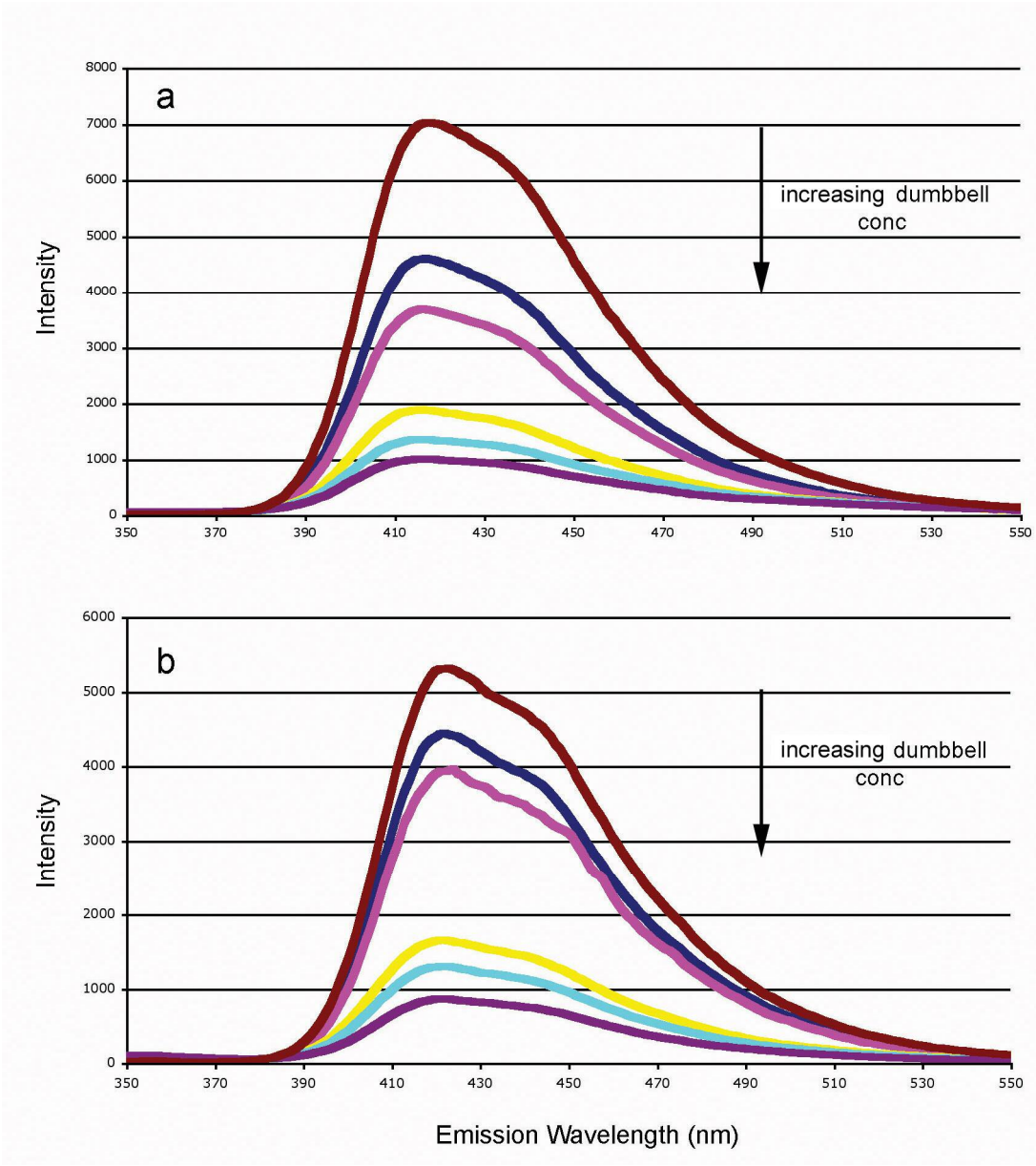

Figure 2.6 Emission spectra of **2.14** (a) and **2.19** (b) at 1 μM with varying concentrations of PA **2.36** (**Figure 2.3**) added. Brown line is the dumbbell itself, dark blue is 1:1, pink is 1:10, yellow is 1:50, light blue is 1:100, and purple is 1:200 ratio of dumbbell to PA respectively. All spectra were taken in H_2O and the dumbbell concentration remained constant.

2.4 Conclusions

These data gave promise that the dumbbell molecule were acting as templates for the self-assembly of the PA, but the AFM and TEM data were not consistently reproducible. Compounds **2.28** and **2.34** were synthesized with the purpose of showing that longer dumbbell molecules might allow for more reproducible results but were difficult to synthesize with very low yields of product where the decision was made to synthesize the second-generation dumbbell. Chapter 3 will go into detail with a target dumbbell molecule incorporating many of the same characteristics as those found in Chapter 2 but with simplified characterization and synthesis. The new method would allow for more lengthy structures and will be discussed in Chapter 3.

2.5 Experimental

Unless otherwise noted, all starting materials were obtained from Sigma-Aldrich or Strem and used without further purification. Analytical TLC was performed on Merck KgaA silica gel 60 F254 TLC plates. Silica gel for flash chromatography was ICN Silitech 32-63 D 60 Å. Water was used from a MilliQ water source. ^{1}H NMR and ^{13}C NMR spectra were recorded on Varian 500, 400 or 300 MHz NMR spectrometers. MALDI-TOF mass spectrometry was performed on a PE Voyager DE-Pro instrument using dithrinol as the matrix. Fluorescence was performed on a Hitachi F-4500 Fluorescence Spectrophotometer and UV experiments were performed on a Hewlett Packard 8452A Diode Array Spectrophotometer.

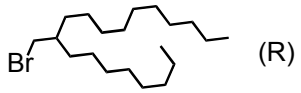

2.1

9-(bromomethyl)nonadecane (2.1): 2-octyl dodecanol (10.0 g, 33.5 mmol) and carbon tetrabromide (11.1 g, 33.5 mmol) were combined and stirred at 0 C with DCM (200 mL). After the materials were in solution, a solution of triphenyl phosphine (11.4 g, 43.5 mmol) in DCM (50 mL) was added slowly over 10 min. The reaction proceeded for 30 min and turned clear and yellow in color. After reacting for 10 h, the reaction was diluted in DCM and washed three times with water, the organic layer was dried over $MgSO_4$ and the solvent was removed by rotary evaporation. Flash chromatography in hexanes afforded a clear colorless oil (10.8 g, 89% yield). ^{1}H NMR (300 MHz, $CDCl_3$): δ 3.46 (d, *J*=4.8 Hz, 1H), 1.28 (bs, 34H), 0.90 (t, *J*=7.2, 6H). ^{13}C NMR (150MHz, $CDCl_3$): δ 40.02, 39.73, 32.81, 32.18, 32.15, 30.05, 29.91, 29.86, 29.82, 29.62, 29.57, 26.82, 22.96, 14.41.

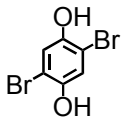

2.2

2,5 dibromohydroquinone (2.2): Br_2 (95.6 ml, 1.9 mol) was placed in DCM (100 mL) which was added dropwise over 2 h to a solution of hydroquinone (102.5 g, 928.0 mmol) in DCM (500 mL) and reacted for 15 h. The precipitate was filtered, the filtrate was dried, and recrystallized twice from isopropanol and provided a white solid (88.0 g pure, 35% yield). ^{1}H NMR (400 MHz, $CDCl_3$): δ 8.58 (s, 2H), 7.16 (s, 2H). ^{13}C NMR (100MHz, $CDCl_3$): δ 147.74, 119.93, 108.78. ESI MS Calcd. 267.86, found 267.45.

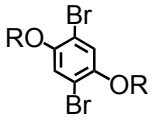

2.3

1,4 dibromo 2,5 di 2-octyl-dodecyl ether benzene (2.3): To DMF (100 mL), 9-(bromomethyl)nonadecane (**2.1**) (4.3 g, 11.8 mmol) and K_2CO_3 (8.8 g, 65.2 mmol) were stirred under N_2 for 20 min. 2,5 dibromohydroquinone (**2.2**) (12.7 g, 4.7 mmol) was added to DMF (50 mL) and dripped into the previous solution which was reacted under N_2 at 60 C for 15 h. The reaction was diluted in DCM, washed with 5% citric acid in water three times, dried over $MgSO_4$, and the solvent was removed by rotary evaporation. Flash chromatography in hexanes provided a clear, colorless oil (5.65 g, 43% yield). ^{1}H NMR (400 MHz, $CDCl_3$): δ 7.07 (s, 2H), 3.82 (d, *J*= 5.6 Hz, 2H), 1.80 (m, 2H), 1.27 (m, 34H), 0.89 (t, *J*=6.4 Hz, 12H). ^{13}C NMR (100MHz, $CDCl_3$): δ 150.36, 118.39, 111.27, 73.19, 38.24, 32.21, 31.88, 31.59, 30.28, 29.96, 29.94, 29.89, 29.86, 29.65, 27.10, 22.99, 14.41.

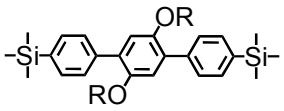

2.4

1,12 ditrimethylsilyl triphenol 6,17 2-octyl-dodecyl ether (2.4): 1,4 dibromo 2,5 di 2-octyl-dodecyl ester benzene (**2.3**) (1.8 g, 2.2 mmol) was added to toluene (190 mL), EtOH (48 mL), and water (48 mL). Trimethylsilyl phenylboronic acid (1.48 g, 2.64 mmol) and Na_2CO_3 (1.55 g, 17.6 mmol) was added to the reaction mixture. The reaction mixture was purged with N_2 for 30 min, $Pd(PPh_3)_4$ (0.3 g, 0.2 mmol) was added, and the reaction was refluxed under N_2 for 24 h.

The reaction was diluted with DCM, washed with water three times, dried over $MgSO_4$, and the solvent was removed by rotary evaporation. Flash chromatography in hexanes provided a white solid (1.95 g, 92% yield). ^{1}H NMR (400 MHz, $CDCl_3$): δ 7.68 (dd, *J*=8 Hz, 8H), 7.02 (s, 2H), 3.87 (d, *J*=5.6 Hz, 4H), 1.70 (m, 2H), 1.26 (m, 68H), 0.89 (t, *J*=6.4 Hz, 12H), 0.30 (s, 18H). ^{13}C NMR (100MHz, $CDCl_3$): δ 150.54, 139.07, 133.86, 133.05, 130.89, 129.10, 116.11, 72.52, 38.31, 32.25, 31.92, 31.70, 30.36, 30.03, 29.98, 29.92, 29.67, 27.09, 23.02, 14.47, 0.01.

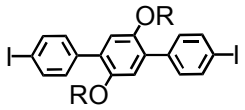

2.5

1,12 diiodo triphenol 6, 17 2-octyl-dodecyl ether (2.5): Under N_2 at 0 C, to a solution of DCM (100 mL) and 1,12 ditrimethylsilyl triphenol 6,17 2-octyl-dodecyl ester (**2.4**) (1.9 g, 1.9 mmol), ICl (4.3 mL, 4.2 mmol) was added dropwise and reacted for 2 h. The reaction mixture was diluted with DCM and washed with water three times, dried over $MgSO_4$, and the solvent was removed by rotary evaporation. Flash chromatography in hexanes provided a white solid (1 g, 48% yield). ^{1}H NMR (500 MHz, $CDCl_3$): δ 7.73 (d, *J*=8 Hz, 4H), 7.34 (d, *J*=6.8 Hz, 4H), 6.92 (s, 2H), 3.79 (d, *J*=5.5 Hz, 4H), 1.72 (m, 2H), 1.26 (m, 68H), 0.89 (t, *J*=7 Hz, 12H). ^{13}C NMR (125MHz, $CDCl_3$): δ 150.46, 138.05, 137.20, 131.72, 130.18, 115.73, 92.92, 72.44, 38.30, 32.19, 31.68, 30.28, 29.97, 29.92, 29.89, 29.85, 29.63, 27.05, 22.96, 14.40.

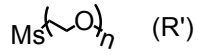

2.6

MePEO$_{350}$ Ms (2.6): To a solution of DCM (250 mL) and PEG$_{350}$ (10.4 g, 29.7 mmol), a solution of mesylchloride (2.8 mL, 32.7 mmol) in DCM (40 mL) was added to the PEG$_{350}$ solution and reacted for 20 min. The reaction mixture was diluted with DCM, washed with 5% citric acid three times, dried over $MgSO_4$, and the solvent was removed by rotary evaporation that provided a clear colorless liquid (12.7 g, 99% yield). ^{1}H NMR (300 MHz, $CDCl_3$): δ 4.37 (t, *J*=4.5 Hz, 2H), 3.76 (t, *J*=4.2 Hz, 2H), 3.64 (m, 32H), 3.74 (s, *J*=5.5 Hz, 3H), 3.08 (s, 3H).

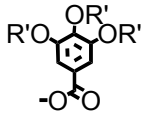

2.7

Tri MePEO$_{350}$ 3,4,5trihydroxybenzoate (2.7): To dry acetone (125 mL) was added MePEO$_{350}$Ms (**2.6**) (12.7 g, 33 mmol), 3,4,5trihydroxybenzoate (1.7 g, 11 mmol), K_2CO_3 (6.2 g, 55 mmol), and 18-crown-6 (0.3 g, 1.8 mmol). The reaction was refluxed for 48 h. The acetone was removed by rotary evaporation and the reaction mixture was diluted in DCM, washed with water two times, once with saturated $NaHCO_3$ in water, dried over $MgSO_4$, and the solvent was removed by rotary evaporation. This provided a clear colorless liquid (10.6 g, 99% yield). ^{1}H NMR (400 MHz, $CDCl_3$): δ 7.35 (s, 2H), 4.21 (m, 6H), 3.89 (m, 8H), 3.64 (m, 96H), 3.39 (s, 9H).

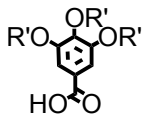

2.8

Tri MePEO$_{350}$ 3,4,5trihydroxybenzoic acid (2.8): In THF (50 mL) and water (10 mL), Tri MePEO$_{350}$ 3,4,5trihydroxybenzoate (**2.7**) (10.6 g, 8.5 mmol) was added with LiOH (1.9 g, 42.5

mmol) and reacted for 2 h. The reaction mixture was diluted in DCM and washed once with water, twice with 5% citric acid in water, dried over $MgSO_4$, and the solvent was removed by rotary evaporation. This provided a clear colorless liquid (7 g, 66% yield). ^{1}H NMR (400 MHz, $CDCl_3$): δ 7.34 (s, 2H), 4.20 (m, 4H), 3.92 (m, 8H), 3.61 (m, 96H). ^{13}C NMR (125MHz, $CDCl_3$): δ 152.39, 109.71, 72.49, 70.98, 70.81, 70.77, 70.71, 70.69, 70.67, 69.83, 68.99, 59.17.

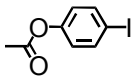

2.9

4-iodophenyl acetate (2.9): 4-iodophenol (5.0 g, 22.8 mmol) was added to pyridine (2.0 mL) and acetic anhydride (2.8 g, 27.4 mmol). The reaction was stirred overnight and diluted with DCM, washed with water twice, dried over $MgSO_4$, and the solvent was removed by rotary evaporation. Flash chromatography in 50/50 DCM/Hex afforded a white solid (5.6 g, 95% yield). ^{1}H NMR (400 MHz, $CDCl_3$): δ 7.72 (d, *J*=8 Hz, 2H), 6.92 (d, *J*=8 Hz, 2H), 2.12 (s, 3H).

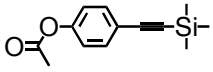

2.10

4-(2-(trimethylsilyl)ethynyl)phenyl acetate (2.10): 4-iodophenyl acetate (**2.9**) (4.1 g, 15.8 mmol), $PdCl_2(PPh_3)_2$ (0.6 g, 0.79 mmol), CuI (0.2 g, 0.8 mmol), and TEA (50 mL) was purged with N_2 for 30 min. Under N_2, trimethylsilyl acetylene (4.4 mL, 17.4 mmol) was added and the reaction was heated to 70 C for 14 h. The reaction was filtered and flash chromatography in 50% hexanes and 50% DCM provided a white solid (3.1 g, 84% yield). ^{1}H NMR (400 MHz,

$CDCl_3$): δ 7.47 (d, *J*=8.8 Hz, 2H), 7.04 (d, *J*=8.4 Hz, 2H), 2.29 (s, 3H), 0.25 (s, 9H). ^{13}C NMR (100MHz, $CDCl_3$): δ 169.10, 150.68, 133.26, 121.69, 120.97, 104.38, 94.52, 21.54, 0.39.

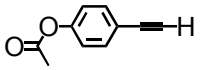

2.11

4-ethynylphenyl acetate (2.11): 4-(2-(trimethylsilyl)ethynyl)phenyl acetate (**2.10**) (3.1 g, 19.3 mmol), was added to TBAF (13.4 mL) in THF (60 mL) and was cooled to –78 C. The reaction proceeded for 15 min and was quenched with silica gel (50 mL), solvent was removed by rotary evaporation and loaded on a flash chromatography column in 50/50 DCM/Hex. This provided a white solid (1.7 g, 79% yield). ^1H NMR (400 MHz, $CDCl_3$): δ 7.51 (d, *J*=8.4 Hz, 2H), 7.06 (d, *J*=8.8 Hz, 2H), 2.30 (s, 3H). ^{13}C NMR (100MHz, $CDCl_3$): δ169.18, 151.04, 133.51, 121.91, 119.98, 83.05, 77.59, 21.38.

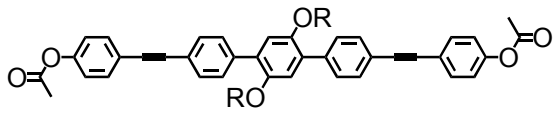

2.12

Compound 2.12: 1,12 diiodo triphenol 6, 17 2-octyl-dodecyl ester (**2.5**) (0.3 g, 1.6 mmol), 4-ethynylphenyl acetate (**2.11**) (0.1 g, 3.5 mmol), CuI (0.01 g, 0.16 mmol), and TEA (100 mL) was degassed with N_2 for 30 min. $PdCl_2(PPh_3)_2$ (0.2 g, 0.16 mmol) was added and the reaction was heated to 70 C for 15 h. The reaction was filtered and the solvent was removed by rotary evaporation leaving a yellow solid. Flash chromatography in 60/40 Hex/DCM and provided a yellow solid (0.24 g, 87% yield). ^1H NMR (400 MHz, $CDCl_3$): δ 7.62 (m, 12H), 7.12 (d, *J*=4 Hz, 4H), 6.99 (s, 2H), 3.79 (d, *J*=5.5 Hz, 4H), 2.33 (s, 6H), 1.72 (m, 2H), 1.26 (m, 68H), 0.89 (t, *J*=7

Hz, 12H). ^{13}C NMR (100MHz, $CDCl_3$): δ 150.55, 138.60, 132.89, 131.27, 130.45, 129.74, 121.86, 121.29, 115.73, 89.92, 89.00, 72.31, 38.35, 32.19, 31.85, 31.69, 30.29, 29.98, 29.93, 29.86, 29.64, 27.07, 22.96, 21.43, 14.41.

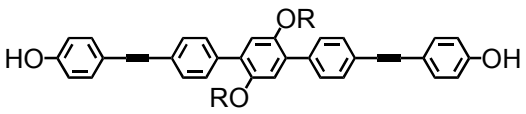

2.13

Compound 2.13: Compound **2.11** (0.2 g, 0.21 mmol) was added to THF (50 mL), MeOH (20 mL), H_2O (10 mL), and K_2CO_3 (0.09 g, 0.6 mmol) and stirred for 15 h. The reaction mixture was rotary evaporated to a brown solid, diluted in DCM and washed once with saturated $NaHCO_3$, once with 5% citric acid, once with water, dried over $MgSO_4$, and the solvent was removed by rotary evaporation. Flash chromatography in DCM provided a yellow solid (0.2 g, 95% yield). ^{1}H NMR (300 MHz, $CDCl_3$): δ 7.64 (d, *J*=4.8 Hz, 8H), 7.46 (d, *J*=8.4 Hz, 4H), 6.98 (s, 2H), 6.83 (d, *J*=8.4 Hz, 4H), 3.82 (d, *J*=5.5 Hz, 4H), 1.72 (m, 2H), 1.29 (m, 68H), 0.90 (t, *J*=7 Hz, 12H).

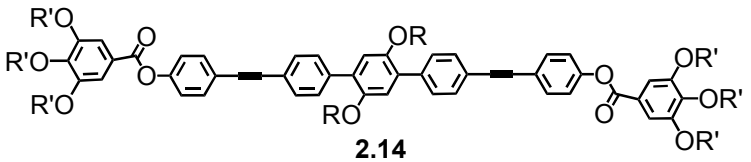

2.14

Compound 2.14: In DCM (40 mL), **2.13 (**0.2 g, 0.2 mmol), **2.8** (0.6 g, 0.4 mmol), DPTS (0.2 g, 0.2 mmol), and DIPC (0.1 mL, 0.5 mmol) were combined and reacted at room temp for 15 h. The reaction solvent was removed by rotary evaporation and flash chromatography in 8/92 MeOH/DCM provided a clear colorless liquid (0.6 g) that was dialyzed in a 1000MW dialysis bag in H_2O for five days (changing water twice daily) yielding a clear colorless liquid (0.35g,

52% yield). ^{1}H NMR (400 MHz, $CDCl_3$): δ 7.60 (m, 12H), 7.46 (s, 4H), 7.21 (d, *J*=8 Hz, 4H), 6.99 (s, 2H), 4.30-3.50 (m), 1.7-1 (m), 0.89 (t, *J*=7 Hz, 12H).

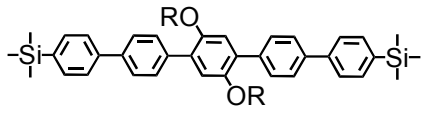

2.15

Compound 2.15: Reference synthesis of **2.4**. ^{1}H NMR (400 MHz, $CDCl_3$): δ 7.68 (m, 16H), 7.09 (s, 2H), 3.87 (d, *J*=5.6 Hz, 4H), 1.70 (m, 2H), 1.25 (m, 68H), 0.89 (m, 12H), 0.35 (s, 18H). ^{13}C NMR (100MHz, $CDCl_3$): δ 134.03, 130.21, 126.76, 126.59, 38.38, 32.22, 30.37, 29.96, 23.00, 14.45, -0.75.

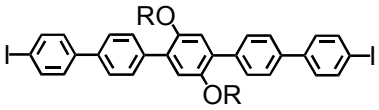

2.16

Compound 2.16: Reference synthesis of **2.5**. ^{1}H NMR (400 MHz, $CDCl_3$): δ 7.79 (d, *J*=8.4 Hz, 4H), 7.69 (d, *J*=8 Hz, 4H), 7.61 (d, *J*=8.4 Hz, 4H), 7.40 (d, *J*=8.4 Hz, 4H), 7.04 (s, 2H), 3.87 (d, *J*=5.6 Hz, 4H), 1.70 (m, 2H), 1.26 (m, 68H), 0.89 (m, 12H).

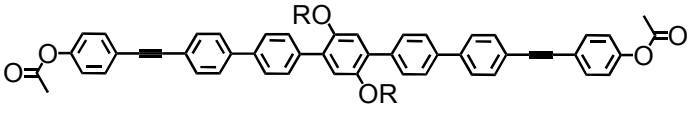

2.17

Compound 2.17: Reference synthesis of **2.12**. ^{1}H NMR (400 MHz, $CDCl_3$): δ 7.72-7.62 (m, 16H), 7.57 (d, *J*=8 Hz, 4H), 7.12 (d, *J*=8.4 Hz, 4H), 7.05 (s, 2H), 3.87 (d, *J*=5.6 Hz, 4H), 2.33 (s, 6H), 1.70 (m, 2H), 1.26 (m, 68H), 0.89 (m, 12H).

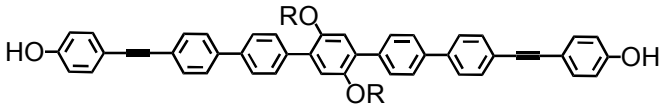

2.18

Compound 2.18: Reference synthesis of **2.13**. ^{1}H NMR (400 MHz, $CDCl_3$): δ 7.72-7.62 (m, 16H), 7.57 (d, *J*=8 Hz, 4H), 7.10 (d, *J*=8.4 Hz, 4H), 7.06 (s, 2H), 3.87 (d, *J*=5.6 Hz, 4H), 1.70 (m, 2H), 1.24 (m, 68H), 0.90 (m, 12H). MALDI MS Calcd. 1206.8, found 1207.2 M+H.

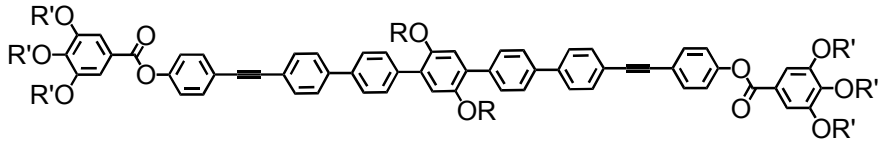

2.19

Compound 2.19: Reference synthesis of **2.15**. ^{1}H NMR (500 MHz, $CDCl_3$): δ 7.72-7.62 (m, 16H), 7.46 (s, 4H), 7.21 (d, *J*=8 Hz, 4H), 6.99 (s, 2H), 4.21 (m, 6H), 3.80-3.30 (m), 1.7-1 (m), 0.89 (s, 12H).

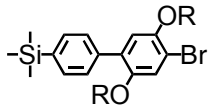

2.20

1-bromo12-trimethylsilyl triphenol 6,17 2-octyl-dodecyl ether 2.20: Under N_2, to toluene (75 mL), EtOH (18 mL), and H_2O (18 mL) was added **2.2** (5.0 g, 6.0 mmol), TMS phenylboronic acid (0.6 g, 3.0 mmol), Na_2CO_3 (5.1 g, 48 mmol), and $Pd(PPh_3)_4$ (0.348 g, 3.0 mmol). The solution was refluxed for 18 h. The reaction mixture was diluted with DCM, washed with water three times, dried with $MgSO_4$, and the solvent was removed by rotary evaporation. Flash

chromatography was performed in hexanes and afforded a clear colorless liquid (2.27 g, 42% yield). ^{1}H NMR (400 MHz, $CDCl_3$): δ 7.53 (dd, *J*=8 Hz, *J*=18.4 Hz, 4H), 7.17 (s, 1H), 6.91 (s, 1H), 3.87 (d, *J*=5.2 Hz, 2H), 3.75 (d, *J*=5.6 Hz, 2H), 1.78 (m, 1H), 1.56 (m, 1H), 1.5-1 (m), 0.89 (t, *J*=6.8 Hz, 12H), 0.31 (s, 9H). ^{13}C NMR (125MHz, $CDCl_3$): δ 150.75, 150.16, 139.28, 138.55, 133.10, 131.07, 128.95, 118.29, 116.60, 116.28, 111.42, 73.08, 72.56, 38.25, 38.14, 32.16, 31.55, 30.25, 29.89, 29.86, 29.82, 29.60, 27.06, 26.97, 22.93, 14.36, -0.86. MALDI MS (theo. 898.35) 899.00 M+H.

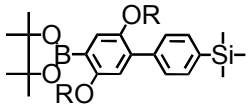

2.21

1-boronic ester12-trimethylsilyl triphenol 6,17 2-octyl-dodecyl ether 2.21: Under N_2, to dry DMF (100 mL), **2.20** (3.4 g, 3.7 mmol), bis(pinacolato)diboron (1.9 g, 7.5 mmol), potassium acetate (1.2 g, 12.3 mmol), and $PdCl_2$(dppf) (0.2 g, 0.23 mmol). The reaction was heated to 70 C overnight. The mixture was diluted in DCM, washed with H_2O three times, and the solvent was removed by rotary evaporation. Flash chromatography was performed with 10/90 DCM/Hex and afforded a white solid (1.7 g, 57% yield). ^{1}H NMR (400 MHz, $CDCl_3$): δ 7.54 (s, 4H), 7.24 (s, 1H), 6.85 (s, 1H), 3.87 (d, *J*= 8 Hz, 2H), 3.75 (d, *J*=8 Hz, 2H), 1.78 (m, 1H), 1.56 (m, 1H), 1.5-1 (m), 0.89 (t, *J*=6.8 Hz, 12H), 0.31 (s, 9H). ^{13}C NMR (100MHz, $CDCl_3$): δ 139.24, 133.07, 129.45, 128.91, 118.23, 115.54, 38.28, 32.22, 31.59, 30.31, 29.93, 29.89, 29.66, 27.11, 27.03, 23.00, 14.45, -0.90. MALDI MS Calcd. 945.1, found 946.3 M+H.

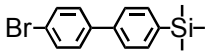

2.22

1-bromo 8-trimethylsiyl diphenyl 2.22: Under N_2, to toluene (442 mL), H_2O (110 mL), and EtOH (110 mL) was added 1-bromo 4-iodo benzene (8.0 g, 28.3 mmol), 4-trimethylsilyl phenyl boronic acid (3.4 g, 17.7 mmol), sodium carbonate (15.0 g, 142 mmol), $Pd(PPh_3)_4$ (1.0 g, 0.9 mmol). The reaction was refluxed overnight, diluted with DCM, washed with H_2O three times, dried with $MgSO_4$, and the solvent was removed by rotary evaporation. Flash chromatography was performed with 40/60 DCM/Hex to afford a white solid (3.76 g, 70% yield). ^{1}H NMR (500 MHz, $CDCl_3$): δ 7.62 (d, *J*=8.5 Hz, 2H), 7.57 (d, *J*=8.5 Hz, 4H), 7.48 (d, *J*=8.5 Hz, 2H), 0.32 (s, 9H). ^{13}C NMR (125MHz, $CDCl_3$): δ 140.25, 139.27, 134.16, 133.65, 132.08, 128.93, 126.45, 121.82, -0.90.

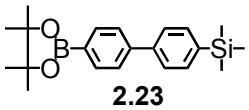

2.23

8-Trimethylsilyl diphenyl boronic ester 2.23: A dry flask with dry DMF (60 mL), **2.22** (2.4 g, 7.8 mmol), bis(pinacolato)diboron (2.9 g, 11.6 mmol), and potassium acetate (2.7 g, 27.2 mmol) was stirred under N_2 for 30 min. $PdCl_2$(dppf) (0.4 g, 0.5 mmol) was added and the reaction was heated to 80 C overnight. The reaction was diluted with ether and washed with H_2O twice, dried with $MgSO_4$, and the solvent was removed by rotary evaporation. Flash chromatography was performed using 40/60 DCM/Hex to afford a white solid (1.7 g, 70% yield). ^{1}H NMR (400 MHz, $CDCl_3$): δ 7.90 (d, *J*=8 Hz, 2H), 7.63 (s, 6H), 1.38 (s, 12H), 0.32 (s, 9H). ^{13}C NMR

(125MHz, $CDCl_3$): δ 143.94, 141.49, 139.80, 135.41, 133.98, 126.69, 126.62, 84.02, 25.13, -0.81. MALDI MS Calcd. 945.1, found 946.2.

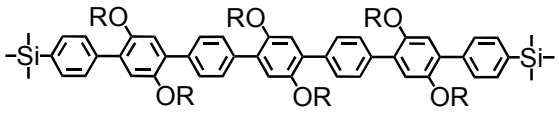

2.24

Compound 2.24: Reference synthesis **2.22**. ^{1}H NMR (500 MHz, $CDCl_3$): δ 7.68 (s, 8H), 7.60 (dd, *J*=8 Hz, *J*=21 Hz, 8H), 7.07 (d, *J*=6.5 Hz, 4H), 7.02 (s, 2H), 3.83 (m, 12H), 1.72 (s, 6H), 1.24 (m), 0.89 (m, 36H), 0.32 (s, 18H). ^{13}C NMR (125MHz, $CDCl_3$): δ 150.73, 150.61, 139.16, 138.84, 137.24, 137.14, 133.06, 130.81, 130.69, 129.85, 129.26, 129.13, 116.08, 72.51, 72.15, 38.32, 32.16, 31.63, 30.30, 29.90, 29.61, 27.03, 22.92, 14.35, -0.82. MALDI MS Calcd. 2456.2, found 2457.8 M+H.

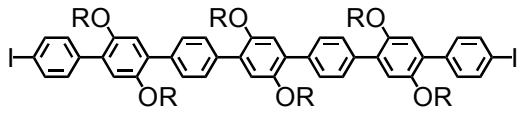

2.25

Compound 2.25: Reference synthesis **2.5**. ^{1}H NMR (500 MHz, $CDCl_3$): δ 7.50 (d, *J*=8 Hz, 8H), 7.67 (m, 8H), 7.37 (d, *J*=7.6 Hz, 4H), 7.07 (d, *J*=7.6 Hz, 4H), 6.96 (s, 2H), 3.83 bs, 12H), 1.72 (s, 6H), 1.24 (m), 0.89 (m, 36H). ^{13}C NMR (100MHz, $CDCl_3$): δ 150.96, 150.66, 138.60, 137.70, 137.42, 132.06, 131.31, 130.77, 129.67, 129.57, 129.50, 116.27, 116.14, 115.75, 92.86, 72.54, 38.68, 32.53, 30.66, 30.33, 30.28, 29.99, 27.39, 23.30, 14.52.

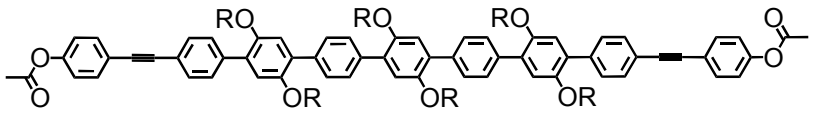

2.26

Compound 2.26: Reference synthesis **2.12**. ^{1}H NMR (500 MHz, $CDCl_3$): δ 7.68-7.57 (app s, dd, 20H), 7.12 (d, *J*=8 Hz, 4H), 7.08 (d, *J*=4.8 Hz, 2H), 7.02 (s, 2H), 3.83 (bs, 12H), 2.36 (s, 6H), 1.22 (m), 0.88 (m, 36H). MALDI MS Calcd. 2628.2, found 2653.2 M+Na.

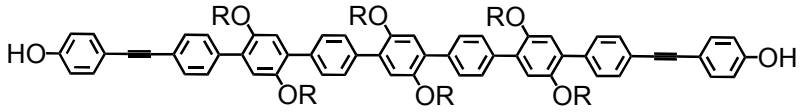

2.27

Compound 2.27: Reference synthesis **2.13**. ^{1}H NMR (500 MHz, $CDCl_3$): δ 7.68-7.57 (app s, dd, 20H), 7.12 (d, *J*=8 Hz, 4H), 7.08 (d, *J*=4.8 Hz, 2H), 7.02 (s, 2H), 3.83 (bs, 12H), 1.24 (m), 0.89 (m, 36H). MALDI MS Calcd. 2546.1, found 2542.4.

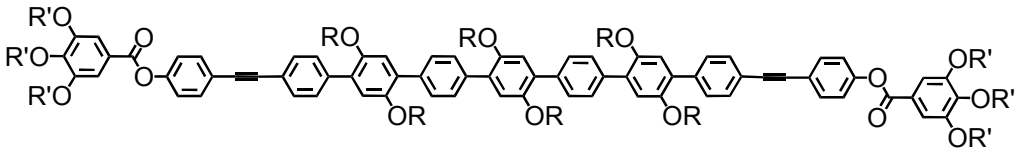

2.28

Compound 2.28: Reference synthesis **2.14**. ^{1}H NMR (500 MHz, $CDCl_3$): δ 7.68-7.57 (bm), 7.46 (s, 4H), 7.22 (d, *J*=8 Hz, 2H), 7.07 (d, *J*=4.5, 4H), 7.01 (s, 2H), 4.39 (m, 4H), 4.23 (m, 12H), 3.80-3.30 (m), 3.09 (s, 6H), 1.7-1 (m), 0.89 (bs, 36H). MALDI MS Calcd. polymer dispersity around 4946.5, found 5053.2.

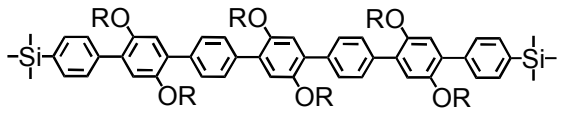

2.29

Compound 2.29. Reference synthesis **2.22**. ^{1}H NMR (500 MHz, $CDCl_3$): δ 7.73 (bs, 16H), 7.60 (dd, *J*=8 Hz, *J*=16 Hz, 8H), 7.08 (s, 2H), 7.06 (s, 2H), 7.03 (s, 1H), 3.83 (app d-d, 12H), 1.72 (bs, 6H), 1.56 (s, 9H), 1.21 (bs), 0.89 (m, 36H), 0.32 (s, 18H). ^{13}C NMR (125MHz, $CDCl_3$): δ 150.69, 139.12, 137.66, 133.09, 130.56, 130.23, 129.13, 126.65, 116.16, 116.03, 72.56, 47.88, 38.32, 32.16, 31.67, 30.29, 29.94, 29.89, 29.84, 29.60, 28.77, 27.03, 22.92, 14.34, -0.82. MALDI MS Calcd. 2610.4, found 2606.2.

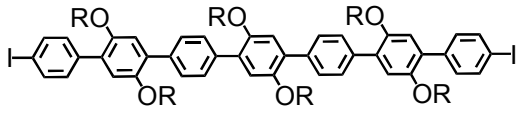

2.30

Compound 2.30: Reference synthesis **2.5**. ^{1}H NMR (500 MHz, $CDCl_3$): δ 7.24 (s, 20H), 7.37 (d, *J*=8 Hz, 4H), 7.08 (s, 2H), 7.05 (s, 2H), 6.97 (s, 2H), 3.83 (app d-d, 12H), 1.72 (bs, 6H), 1.56 (s, 9H), 1.24 (bs), 0.89 (m, 36H).

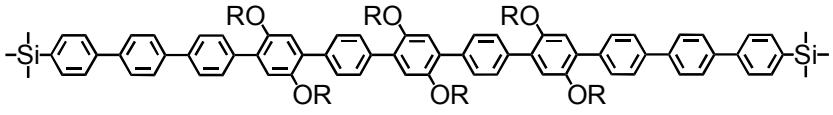

2.31

Compound 2.31. Reference synthesis **2.22**. ^{1}H NMR (500 MHz, $CDCl_3$): δ 7.79-7.66 (m, 30H), 7.11 (d, *J*=6.5 Hz, 6H), 3.89 (s, 12H), 1.74 (bs, 6H), 1.23 (bs), 0.90 (m, 36H), 0.36 (s, 18H). ^{13}C NMR (125MHz, $CDCl_3$): δ 150.785, 150.74, 150.68, 141.35, 140.21, 139.53, 139.23, 137.88, 137.29, 137.14, 134.10, 130.93, 130.70, 130.36, 130.30, 129.26, 127.73, 127.60, 126.62, 126.58,

116.14, 72.46, 72.16, 38.37, 32.16, 31.65, 30.32, 29.91, 29.62, 27.07, 22.92, 14.36, -0.85. MALDI MS Calcd. 2760.3, found 2761.1 M+H.

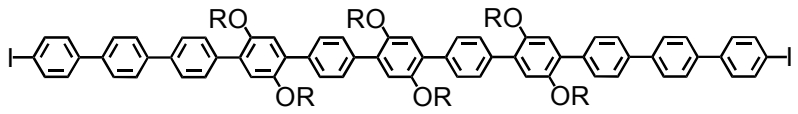

2.32

Compound 2.32. Reference synthesis **2.5**. ^{1}H NMR (500 MHz, $CDCl_3$): δ 7.82-7.67 (m, 24H), 7.11 (d, *J*=8 Hz, 2H), 7.10 (m, 4H), 3.89 (s, 12H), 1.76 (bs, 6H), 1.24 (bs), 0.89 (m, 36H). ^{13}C NMR (125MHz, $CDCl_3$): δ 150.74, 150.66, 140.61, 140.46, 139.02, 128.12, 137.29, 131.10, 130.69, 130.34, 129.29, 129.07, 127.73, 127.46, 126.62, 116.15, 93.28, 72.16, 38.37, 32.15, 31.64, 31.32, 30.31, 29.91, 29.61, 27.06, 22.92, 14.35. MALDI MS Calcd. 2868.4, found 2865.8.

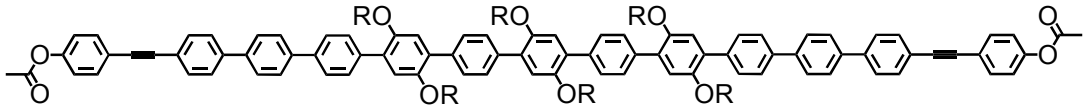

2.33

Compound 2.33. Reference synthesis **2.12**. ^{1}H NMR (500 MHz, $CDCl_3$): δ 7.80-7.64 (m, 36H), 7.59 (d, *J*=8.5 Hz, 4H), 7.10 (m, 10H), 3.89 (s, 12H), 2.34 (s, 6H), 1.76 (bs, 6H), 1.59 (s, 9H), 1.24 (bs), 0.89 (m, 36H). ^{13}C NMR (125MHz, $CDCl_3$): δ 169.42, 150.77, 150.73, 150.66, 140.77, 140.53, 139.28, 139.04, 137.99, 137.11, 132.98, 132.30, 130.68, 130.33, 129.24, 127.68, 127.58, 127.09, 126.61, 122.24, 121.95, 121.21, 89.54, 72.45, 72.15, 38.34, 32.14, 31.63, 30.31, 29.89, 29.61, 27.06, 22.92, 31.38, 14.34. MALDI MS Calcd. 2932.5, found 2933.9 M+H.

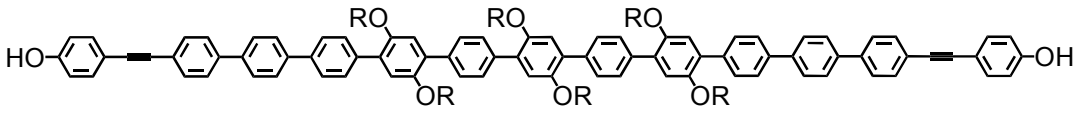

2.34

Compound 2.34. Reference synthesis **2.13**. ^{1}H NMR (500 MHz, $CDCl_3$): δ 7.80-7.62 (m, 36H), 7.47 (d, *J*=8.5 Hz, 2H), 7.10 (m, 6H), 6.84 (d, *J*=9 Hz, 2H), 3.89 (s, 12H), 1.75 (bs, 6H), 1.22 (bs), 0.88 (m, 36H). ^{13}C NMR (125MHz, $CDCl_3$): δ 156.20, 150.82, 150.77, 150.70, 140.45, 140.36, 139.42, 139.13, 138.00, 137.16, 133.53, 132.17, 130.99, 130.73, 130.37, 129.30, 137.70, 127.59, 127.08, 126.65, 122.78, 116.22, 115.82, 115.68, 90.37, 88.19, 72.54, 72.21, 38.41, 32.19, 31.68, 31.54, 30.35, 29.94, 29.65, 2.10, 22.96, 14.39. MALDI MS Calcd. 2850.3, found 2851.5 M+H and 28573.6 M+Na.

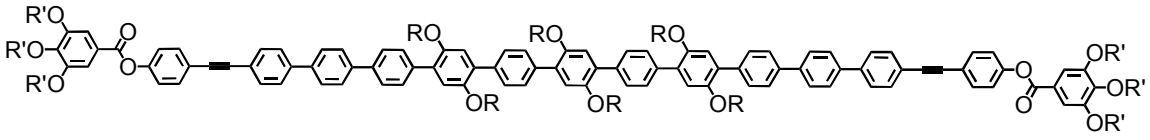

2.35

Compound 2.35. Reference synthesis **2.14**. ^{1}H NMR (500 MHz, $CDCl_3$): δ 7.80-7.62 (m, 38H), 7.47 (ds, 4H), 7.22 (d, *J*=8 Hz, 2H), 6.08 (m, 6H), 4.24 (m, 14H), 3.89-3.55 (m), 3.38 (s, 18H), 1.76 (bs, 6H), 1.24 (bs), 0.89 (m, 36H). ^{13}C NMR (125MHz, $CDCl_3$): δ 164..62, 152.64, 150.68, 150.62, 143.51, 143.51, 140.73, 139.3, 133.01, 132.27, 130.29, 129.21, 127.64, 127.54, 127.06, 126.57, 124.09, 122.12, 121.20, 116.11, 109.84, 89.59, 72.68, 72.43, 72.09, 71.00, 70.83, 70.77, 70.73, 70.69, 69.78, 69.49, 69.12, 59.22, 42.26, 38.33, 37.91, 32.10, 31.59, 30.27, 29.86, 29.56, 27.01, 23.67, 23.32, 22.87, 14.30. MALDI MS (dithrinol matrix) Calcd. polymer dispersity around 5056.4, found around 5188.1.

Chapter Three

Oligo(phenylene ethynylene) Dumbbell Synthesis and Studies

3 Oligo(phenylene ethynylene) Dumbbell Synthesis and Characterization

3.1 Introduction

An increasing body of literature describing the non-covalent self-assembly of molecules to form supramolecular nanostructures has been realized.[95-99] In systems that routinely generate supramolecular objects with nano and micrometer dimensions, it is critical to understand the inhibition in addition to the promotion of molecular self-assembly in order to precisely control nanostructure size in all dimensions.[100, 101] Specifically, the control of one-dimensional supramolecular systems via template-mediated self-assembly is desired, that is the manipulation of self-assembling molecules through use of an external template molecule in order to fabricate discrete sized self-assembled aggregates. This technique could potentially provide information concerning the structure's density and mechanism of nucleation.

Control over supramolecular structures is found in a number of examples in nature from the membranes of cells to entire organisms. An example of nature using a template to control self-assembly is that of the tobacco mosaic virus (TMV) coat proteins assembling around a single strand of RNA, where more than 2100 coat proteins assemble into a 300 nm long rod-shaped structure. The length is predetermined by the length of the enclosed viral RNA template.[102, 103] This self-assembly is spontaneous and without RNA, the TMV coat proteins assemble similarly to the native caspids but are not length templated, affording structures with correct diameters, but variable lengths.[103] The RNA template inhibits/controls the unlimited self-assembly of the caspid proteins through specific interactions between constituent molecules.

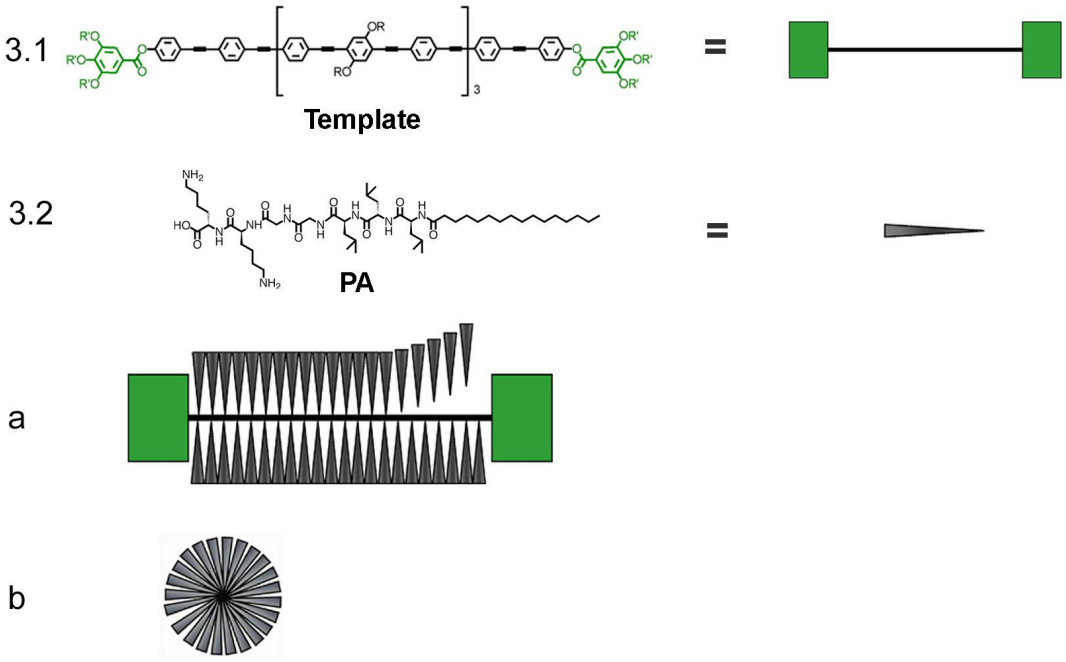

Figure 3.1 (1, left) Oligo(phenylene ethyneylene) (OPE) dumbbell where R is 2-octylodocecane and R' is PEG_{350} and (1, right) cartoon representation of **3.1**. (2, left) Molecular structure of PA **3.2** used in this chapter, synthesized by solution phase methods and (2, right) cartoon representation of **3.2**. (a) Representative cartoon of the PA self-assembling around the dumbbell molecule creating a discrete aggregate. (b) Cross section of the aggregate.

Inspired by the TMV caspid protein-RNA interaction, I have focused on constructing a synthetic template to control the self-assembly of peptide amphiphile (PA) molecules (**Figure 3.1**).[81, 104] The PA monomers consist of a charged linear amino acid sequence coupled to a hydrophobic alkyl chain. In aqueous conditions, the alkyl chain undergoes hydrophobic collapse and the peptide segments hydrogen-bond in a β-sheet configuration to form high aspect ratio cylindrical objects with a hydrophobic core.[105] In our model, PA monomers behave in an analogous fashion to the TMV caspid proteins without a template, enabling them to grow to uncontrollable lengths (micrometer scale). In the presence of our molecular dumbbell-shaped template, the PAs to assemble into discrete supramolecular structures (nanometer scale).

To this end, I designed a template molecule that contains a hydrophobic rigid-rod core with large hydrophilic end caps resembling the shape of a dumbbell (**Figure 3.1**).[106] The rigid-rod interior defines a precise length that can be encapsulated within the hydrophobic core of the PA nanofibers. In an aqueous solution of both **3.1** and **3.2**, we hypothesize that the PA and dumbbell will co-aggregate upon hydrophobic collapse. In this manner, the template will help nucleate the formation self-assembled aggregates that are defined by the template. The bulky and hydrophilic PEG end-caps located at each end of the rigid-rod disrupt one-dimensional PA assembly and terminate fiber growth, resulting in well-defined nanoscale aggregates (**Figure 3.1**). Without these end caps a mixture of PA monomers and rigid-rods (**3.19**) produce fibers that are indistinguishable from the control sample of PA (**3.2**).

3.2 General Synthesis of Oligo(phenylene ethyneylene) Dumbbell

The template was convergently synthesized over 20 steps using iterative Sonogashira couplings[107, 108] and orthogonal protection/deprotection chemistry from a difunctional core (**Scheme 3.1**). Beginning with commercially available 4-iodophenol, acetate protection of the hydroxyl, and a subsequent Sonogashira reaction with 4-bromophenylacetylene afforded **3.4**. Mesylation of PEG_{350} and subsequent conjugation to gallic acid via ether bonds provided **3.6** as the hydrophilic end caps for the template molecule. The rigid rod was then prepared around a central solubilizing dibromo benzyl unit **3.9**. We used a branched alkyl tail for solubility and favorable interaction with the hydrophobic tails of the PA monomers. After iterative Sonogashira reactions and TMS deprotections, **3.12**, **3.13**, and **3.14** were isolated. These became the basic building block for rod elongation and subsequent conjugation to **3.4** and **3.7** that provided **3.1**.

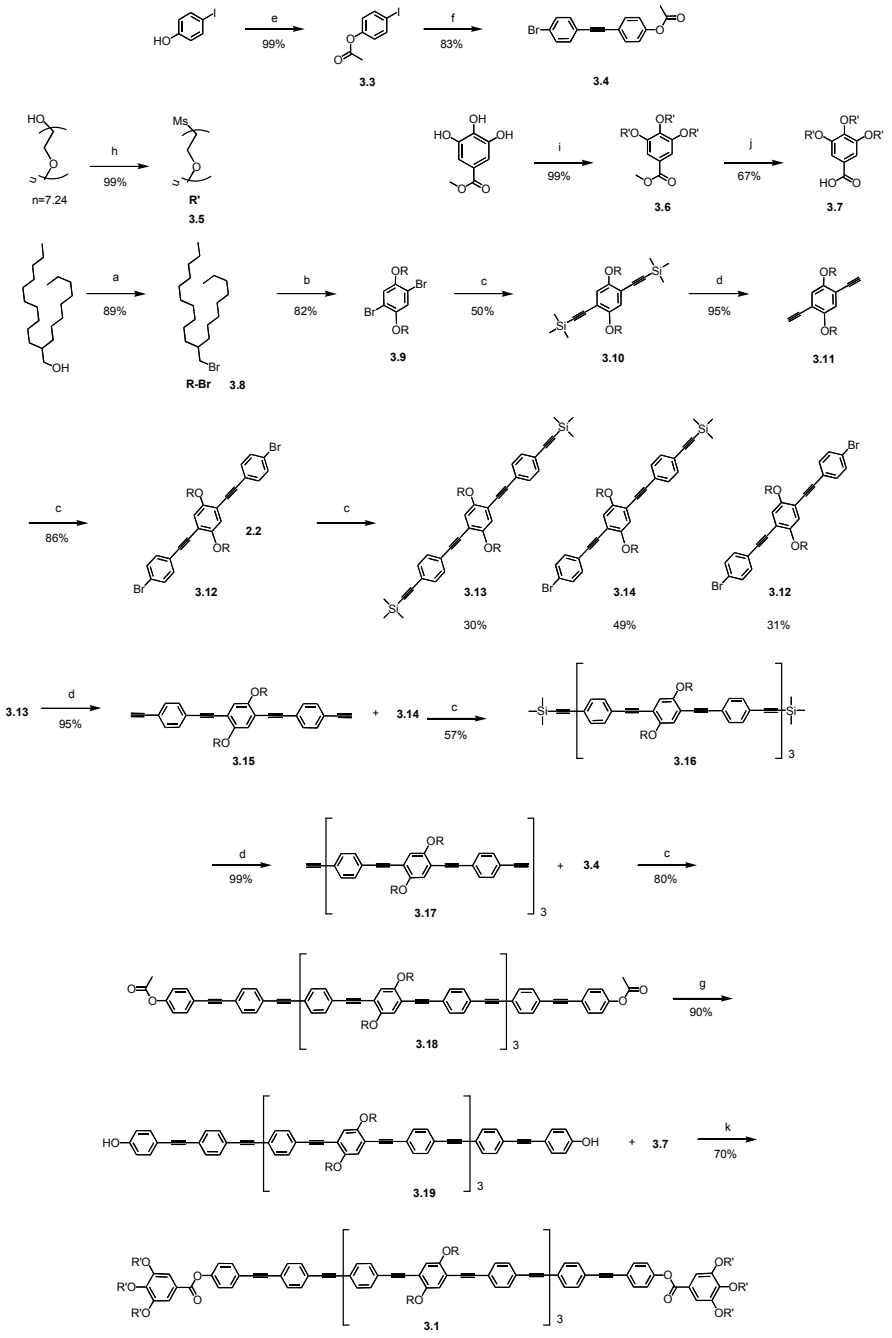

Scheme 3.1 Synthesis of **3.1** using iterative Sonogashira chemistry for rod elongation. Reaction conditions: (a) CBr_4 triphenylphosphine. (b) K_2CO_3. (c) ethynyltrimethylsilane, CuI, TEA, $PdCl_2(PPh_3)_2$. (d) THF, MeOH, TBAF. (e) pyridine, acetic anhydride. (f) ethynyltrimethylsilane, CuI, TEA, $PdCl_2(PPh_3)_2$. (g) THF, MeOH, H_2O, K_2CO_3. (h) methanesulfonyl chloride. (i) acetone, K_2CO_3, 18-crown-6. (j) THF, H_2O, LiOH. (k) DIPC, DPTS.

The PA was convergently synthesized by solution phase methods, making use of Cbz and Boc orthogonol protection schemes (**Scheme 3.2**). The reaction of Boc-Lys(Z)-OH with NH-Lys(Z)-OBz and subsequent Boc cleavage afforded **3.21**. Following the same general scheme used to synthesize **3.21** was used to produce the diglycine **3.23**. Finally, a third portion of the convergent synthesis using leucine conjugation to form a trileucine complex was conjugated to a palmitic acid tail using standard coupling techniques. Subsequent deprotection of the benzyl group afforded **3.31**. Conjugation of **3.31** to **3.21** and **3.23** followed by hydrogenation provided **3.2** (**Scheme 3.2**).

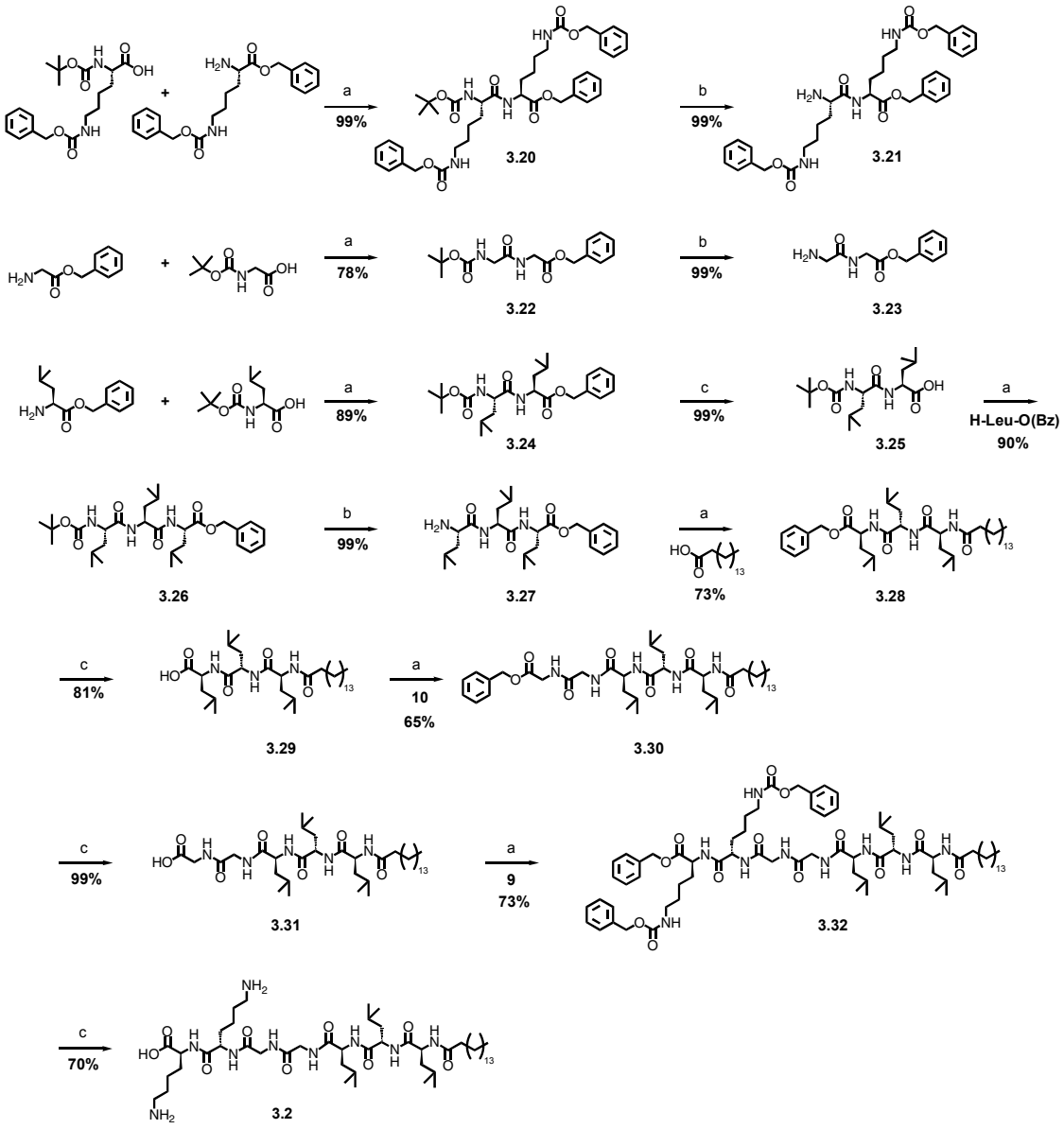

Scheme 3.2 Convergent solution phase synthetic scheme of **3.2** using iterative Boc and benzyl deprotections followed by amide couplings. Reaction conditions: (a) EDCI, HOBT, TEA. (b) HCl/Dioxane. (c) Pd/C, H_2.

3.3 Results

AFM/TEM. The typical self-assembly behavior of PA molecules is the formation of a high-aspect ratio nanostructure of well-defined widths in TEM and heights in AFM.[109] These fibers are formed via the hydrophobic collapse of the alkyl segments in addition to β-sheet

hydrogen bonding interactions in the amino acid repeats of the PA monomers. The average fiber height of **3.2**, determined by AFM, was measured to be 5.3 ± 0.6 nm, which is in good agreement with the widths determined from TEM as 5.1 ± 0.7 nm (**Figure 3.2**). Small aggregate structures are not observed in samples prepared for AFM and TEM microscopies from aqueous solutions composed solely of PA (**3.2**), only extended fibers were visible.

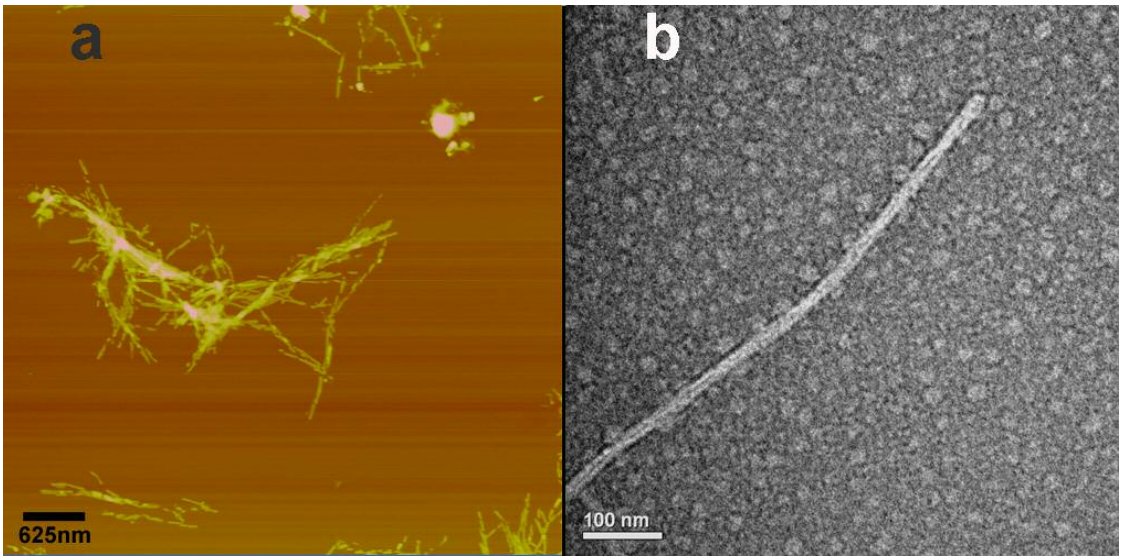

Figure 3.2 (a) AFM of **3.2** cast on mica from water as a control sample. The fiber heights were measured to be 5.3 ± 0.6 nm. (b) TEM of **3.2** cast from water as a control sample. The fiber widths were in agreement with AFM and measured to be 5.1 ± 0.8 nm.

When drop cast from aqueous solution on mica, AFM of **3.1** alone revealed ribbon-like supramolecular structures. We believe that these dumbbell molecules aggregate upon drying on the hydrophilic substrate, maximizing π-stacking interactions between rigid-rods, and lie flat on the mica surface. AFM measurements indicate nanostructure heights of 1.1 ± 0.2 nm and inter-ribbon spacing of 11.8 ± 2.8 nm (**Figure 3.3**). This is consistent with the calculated length of fully extended dumbbells with interdigitating poly(ethylene glycol) units. Under a polarized optical microscope, birefringence is observed for dried solutions of **3.1** on glass substrate,

indicating nanoscale order resulting in an anisotropic index of refraction upon drying (**Figure 3.4**). Self-assembly has been observed previously for this class of dumbbell molecules and finding order in **3.1** was not a surprising development.[106] In aqueous solution at the concentrations employed for these experiments, however, **3.1** exists as discreet molecular entities evidenced by dynamic light scattering (DLS).

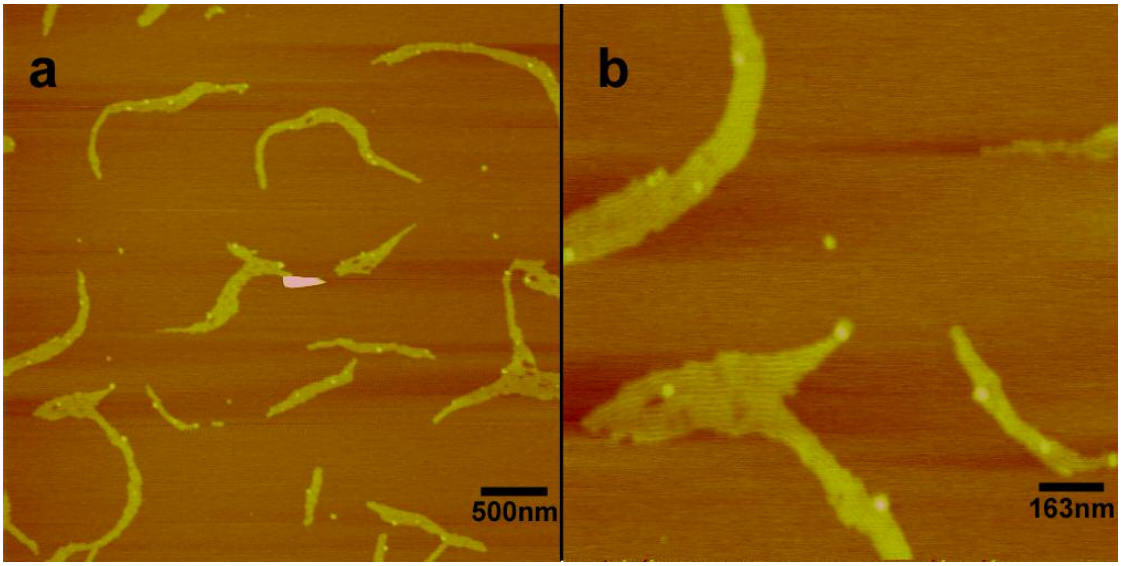

Figure 3.3 (a) AFM image of **3.1** cast on mica from water as a control sample. (b) Zoomed-in AFM image of **3.2**, depicting the dumbbell-ribbon striations. The dumbbell self-assembles into a fiber-like structure that readily aggregates upon drying. The average structure height was measured to be 1.1 ± 0.2 nm and the distance between aligned fibers to be 11.8 ± 2.6 nm.

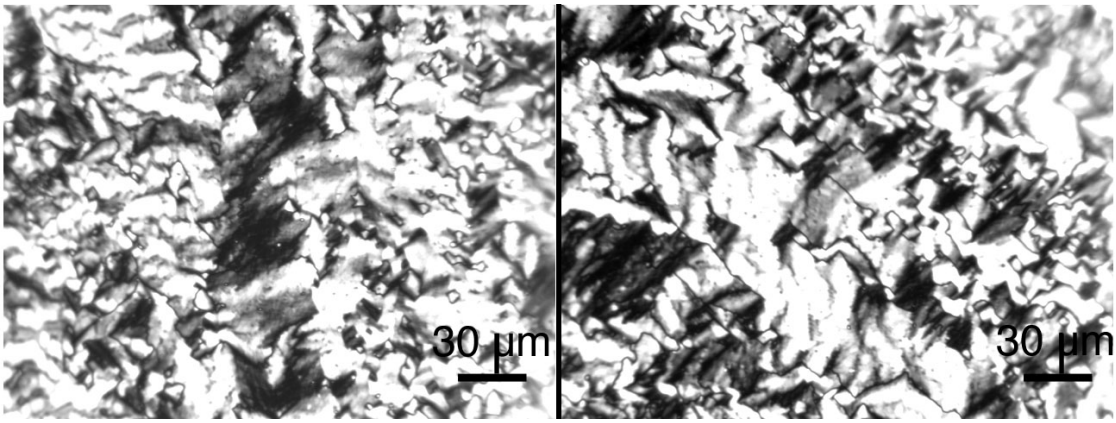

Figure 3.4 Optical microscopy under cross polarizers showing the birefringence of **3.1** dropcast onto a glass coverslide.

Mixtures of **3.1** and **3.2** were studied using a molar ratio of 1:200, 1:500, and 1:1000. AFM images of the 1:200 mixture of **3.1**:**3.2** revealed small aggregates (**Figure 3.5**). There is a marked difference between the 1:200 mixture over the control sample of **3.2** alone keeping the PA at the same concentration in both samples. There is a clear interaction between **3.1** and **3.2** resulting in the formation of small nanoscale aggregates as opposed to high-aspect ratio nanofibers (**Figure 3.5**). The **3.1/3.2** aggregates have heights of 5.5 ± 0.7 nm by AFM, comparable to **3.2** fiber heights of 5.3 ± 0.6 nm showing that the aggregates are composed of **3.2** and not the result of a structure formed from the **3.1**. Similarly, TEM images of the mixture show micelle-like structures (**Figure 3.6**) that we attribute to an end on view of the **3.1/3.2** aggregate. The widths measured in the TEM sample were 5.6 ± 0.6 nm compared to 5.1 ± 0.8 nm widths determined by TEM of **3.33** as a control sample. TEM images of uranyl acetate-stained samples are consistent with this hypothesis as the interior of the aggregates are more lightly stained than the exterior, as expected with an end on view.[81] These data indicate that the **3.1/3.2** aggregate has similar diameters to that of the PA alone, as predicted by our model of

assembly. Using quick freeze deep etch (QFDE) to prepare the TEM samples, we were able to image a single aggregate revealing an aspect ratio of 14.0 nm by 8.8 nm, which is larger than our proposed model. The size difference is due to the sputter coating of the mask which adds ~2.5 nm to the dimensions. Taking this into account, the actual dimensions of 11.5 nm by 6.3 nm is consistent with our other microscopy. In mixed samples with a molar ratio of **3.1**:**3.2** of 1:500 and 1:1000, we observed a mixture of small micelle-like and larger fiber-like nanostructures, indicating that there was not enough **3.1** to suppress the extensive one-dimensional assembly of **3.2**. As a control to understand the function of the completed dumbbell shape a mixture of **3.2** and **3.19** was imaged (**Figure 3.7**). This data confirms the need for the entire dumbbell shape and aqueous solubility because only fibers were observed that were indistinguishable from **Figure 3.2**.

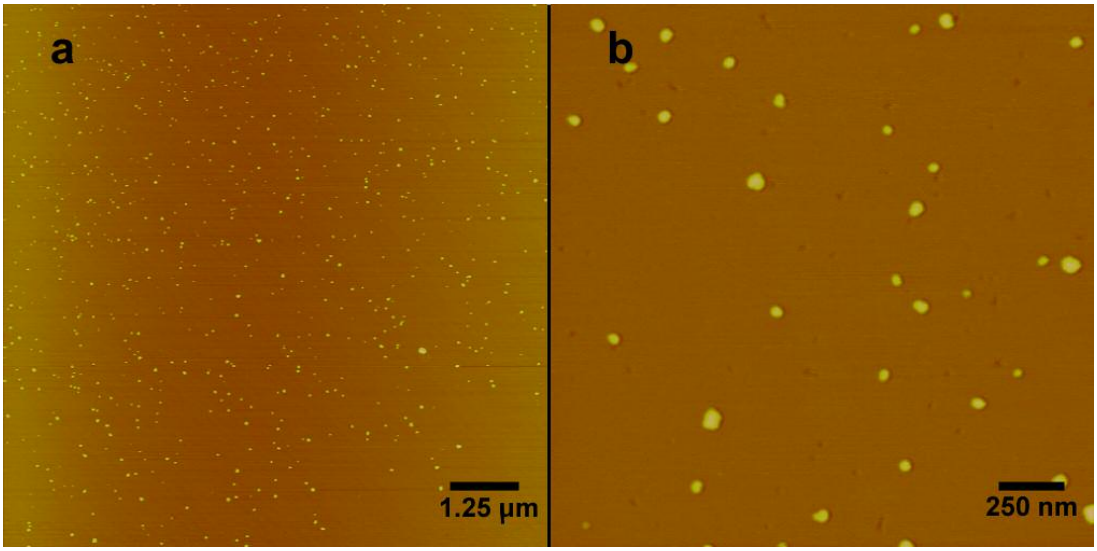

Figure 3.5 AFM image of 1:200 molar ratio mixture of **3.1** and **3.2**, cast from water on mica. The samples did not produce any visible fibers. The average height of the aggregates were measured to be 5.5 ± 0.7 nm. Height image (a) and a magnified height image (b) depicting the individual nanostructures.

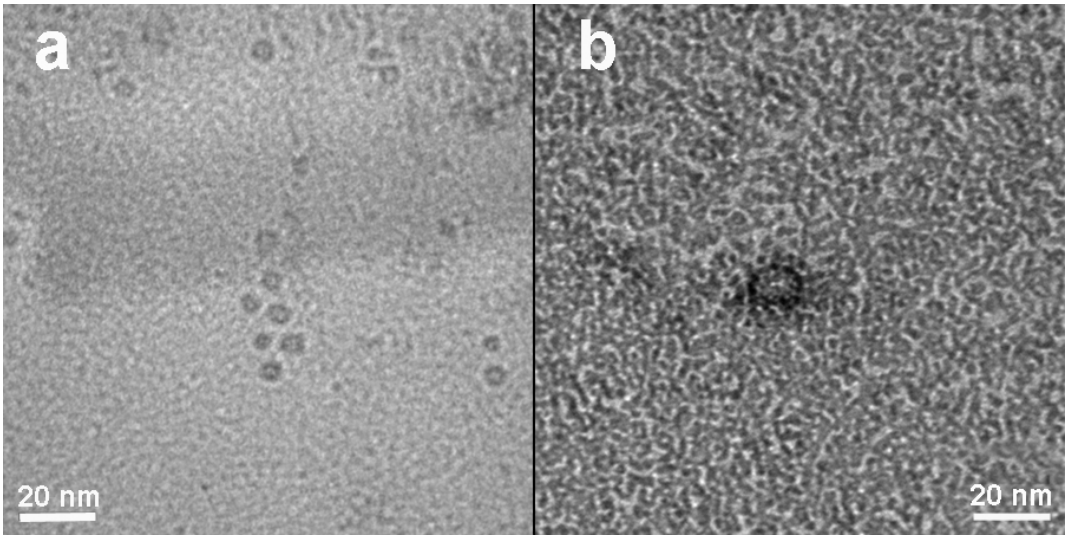

Figure 3.6 TEM images of 1:200 molar ratio mixture of **3.1** to **3.2**, cast from water and stained with uranyl acetate (a). The representative TEM shows spherical micelles that are believed to be the aggregates standing on end due to the PEG end cap interacting with the carbon film on the TEM grid. The average widths of these aggregates were measured as 5.6 ± 0.6 nm which correspond to the width of the fibers observed by TEM. The TEM (b) shows an aspect ratio of the small aggregates by using quick freeze deep etch technique. The length and widths correspond to 14.0 nm by 8.8 nm and are consistent with the predicted model.

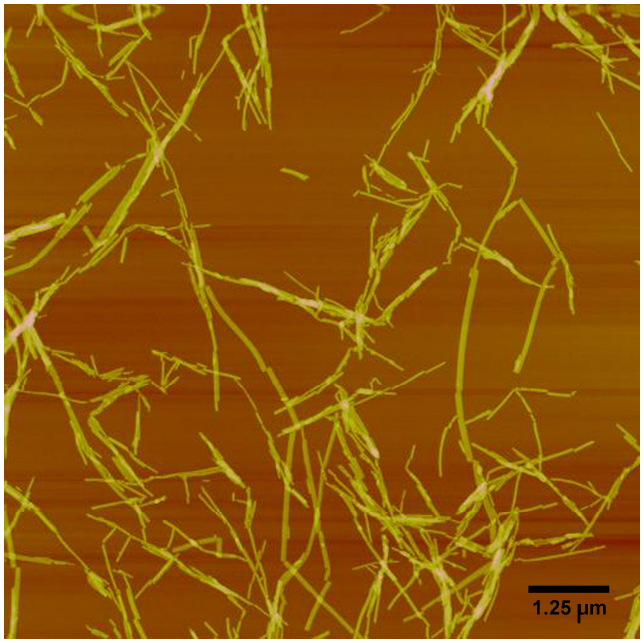

Figure 3.7 AFM of **3.2** mixed with **3.19** depicting the original fibrous structure. This data indicates the necessity of the entire dumbbell molecule for templation to occur.

DLS. Dynamic light scattering (DLS) was used to characterize the effect of the dumbbell template on PA assembly in solution. We chose this technique as a bulk characterization method in solution for mixed and control samples of **3.1** and **3.2**. A change in the self-assembled structures from nanofibers to small aggregates should result in a change in hydrodynamic radii observed by DLS and is confirmed in the DLS measurements. Solution of **3.2** analyzed by DLS confirmed the presence of large structures in solution. While **3.1** was observed to form ribbon-like structures when drop cast from solution on mica (attributed to drying effects), DLS indicates that in solution, **3.1** has a hydrodynamic radius of ~17.4 nm. The mixed sample consisting of 1:200 **3.1**:**3.2** gave a size distribution centered at ~17.9 nm (**Figure 3.8**). We did not expect a significant change in hydrodynamic radius of the dumbbell molecule with and without the PA because the dumbbell length is greater than the width, making length the determining factor in the hydrodynamic radius. In the mixed samples of 1:500 and 1:1000, consistent with the microscopy data, we observed larger structures, indicating the existence of fibers within the samples.

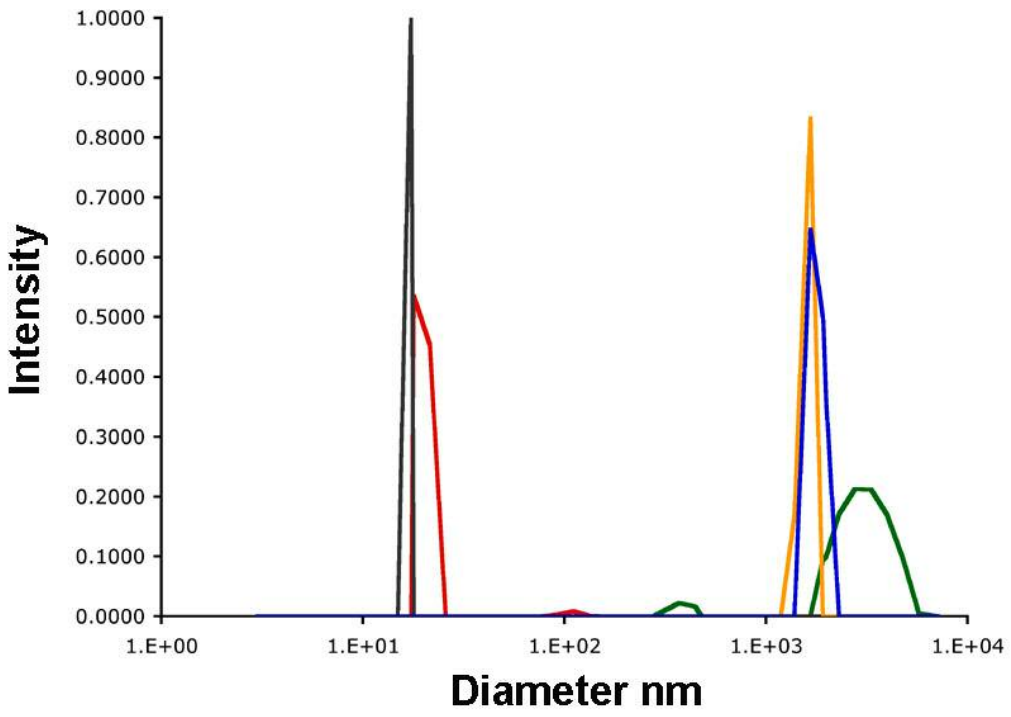

Figure 3.8 Dynamic light scattering of **3.1** (black), **3.2** (green) and mixed sample 1:200 (red), 1:500 (yellow), 1:1000 (blue). DLS did not show a significant difference between the mixed 1:200 and dumbbell samples, but does show a distinct difference from the PA alone, 1:500, and 1:1000 samples.

CD. In order to confirm that the structures observed for the **3.1/3.2** aggregates were indeed self-assembled structures and not random aggregates, CD was used to probe the peptide structure. The CD spectra displays a similar secondary structure for **3.2** and the 1:200 **3.1**:**3.2** mixture (**Figure 3.9**). These data are consistent with a β-sheet conformation between **3.2** molecules despite the presence of **3.1**. This observation indicated that the intermolecular interactions of self-assembly for the PA molecule are not perturbed significantly by the presence of **3.1**. While **3.1** limits the ability of **3.2** to form extended supramolecular structures, the intermolecular basis of self-assembly remained unchanged.

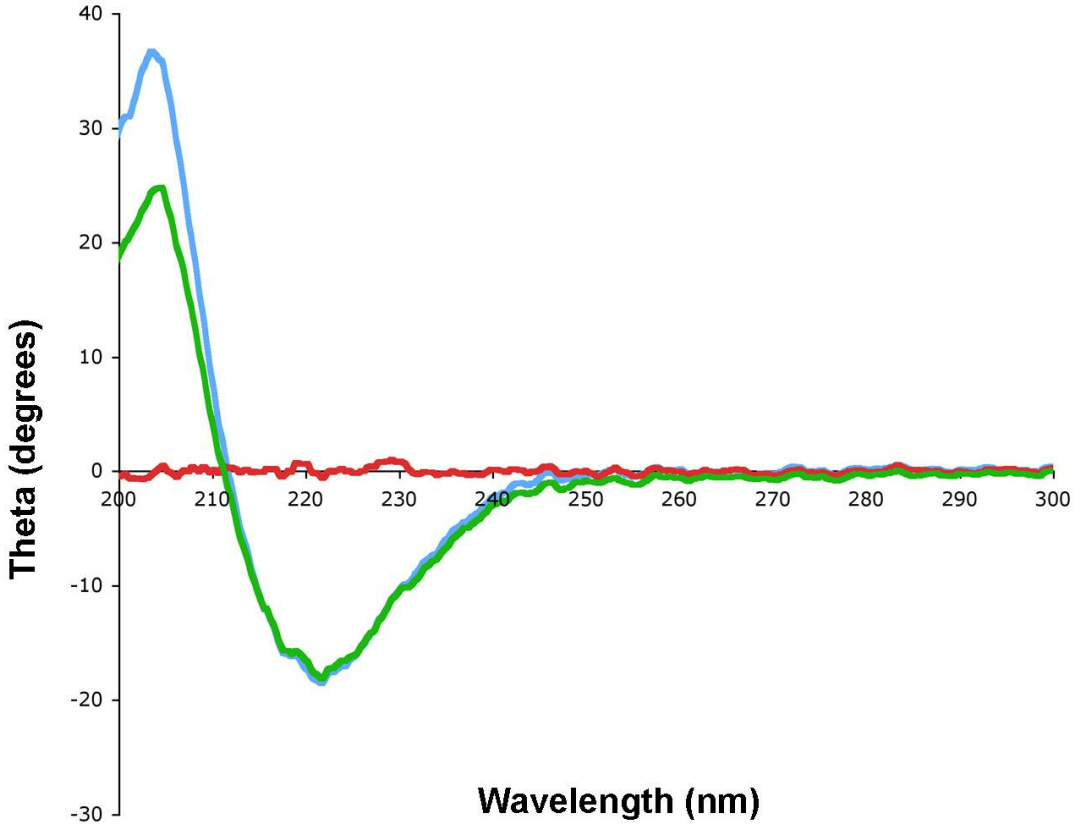

Figure 3.9 CD spectra depicting **3.1** (red line), **3.1**:**3.2** (1:200 molar ratio) (blue), **3.2** (yellow) that shows the β-sheet character of the PA aggregates and lack of β-sheet character in the dumbbell structure.

3.4 Conclusions

In conclusion, we have demonstrated the formation of supramolecular aggregates of controlled dimensions utilizing a rigid-rod dumbbell molecule that serves as a template for the self-assembly of PA molecules. The dumbbell molecule was specifically designed as a hydrophobic rod with hydrophilic and bulky end-caps to impede extensive one-dimensional PA self-assembly. AFM and TEM data show a dramatic change in the PA supramolecular aggregates upon addition of the dumbbell template. By itself, **3.2** shows high aspect-ratio nanofibers typical of these systems. In great contrast, **3.1**:**3.2** mixtures show small, discrete

nanoscale aggregates. DLS and CD were employed to evaluate these aggregates in solution supporting this behavior. We are able to suppress and thereby control the self-assembly behavior of PA molecules using a molecular template. The template approach could be a universal strategy for controlling aqueous self-assembling systems, and could be applied to medical applications like drug delivery and imaging.

3.5 Experimental

Synthesis. Unless otherwise noted, all stating materials were obtained from commercial sources and used without further purification. 4-(Dimethylamino)-pyridinium-4-toluenesulfonate (DPTS) was prepared according to literature.[110] The ^{1}H NMR and ^{13}C NMR spectra were recorded on a Varian Inova 500 (500 MHz) or Varian Unity 400 (400 MHz) spectrometer using the residual solvent proton signal as a standard. Mass spectra were obtained with an Applied Biosystems Voyager-DE Pro Matrix-assisted laser desorption ionization-time-of-flight (MALDI-TOF MS) or a Varian quadrupole ESI mass spectrometer. Dithrinol was used as the matrix for the template intermediates and α-cyano-4-hydroxycinnamic acid was used as the matrix for the PA. Silica for flash chromatography was ICN silitech 32-63 D 60 A.

Self-Assembly. Atomic force microscopy (AFM) was performed with a Nanoscope Multimode Scanning Probe Microscope (Veeco, Woodbury, NY). Tapping mode at 1 Hz was performed on freshly cleaved mica (Ted Pella, Redding, CA). Transmission electron microscopy (TEM) was performed on a Hitachi HF2000 cold field-emission gun (cFEG-TEM) operated at 200 KeV. Carbon-coated copper grids (Ted Pella, Redding, CA) were used as the substrate. AFM and TEM samples were prepared by drop casting a 1 mg/mL solution onto the substrates, removing excess liquid via wicking with filter paper, and allowing the remaining solvent to

evaporate. The TEM samples were then stained with a solution of uranyl acetate in water (30 mg/mL). Approximately 20 μl of solution was dropcast onto the EM sample, which was allowed to sit for 2 min before being wicked away. The sample was allowed to air dry overnight.

Dynamic light scattering was performed on samples of **3.1**, **3.2**, and mixtures of both dissolved in basic water. The concentration was optimized for the instrument. The samples (ca. 200 μL) were loaded into a quartz cuvette and measurements were taken on a Precision Detectors/90T dynamic light scattering instrument. All measurements were performed using a 682 nm laser at a 90˚ scattering angle with at least ten measurements for each sample. Using the accompanying software (Precision Deconvolve) the correlation function was fitted in order to obtain the hydrodynamic radius, which we used to estimate the length of the particles. The fit was weighted using molecular weight normalization with a scaling law exponent corresponding to a rigid rod (R^1) as determined by the anticipated shape for each sample.

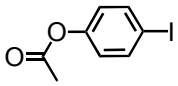

3.3

4-iodophenyl acetate (3.3). In a roundbottom flask was combined 4-iodophenyl (5.0 g, 22.8 mmol), pyridine (1.98 g, 25.0 mmol), acetic anhydride (2.59 mL, 27.4 mmol) and stirred overnight. The reaction was diluted in DCM and washed with water once, with saturated $NaHCO_3$ once, dried over $MgSO_4$, and the solvent was removed by rotary evaporation. Flash chromatography was performed with 50/50 DCM/Hex to afford a white solid at 99% yield. ^{1}H NMR (500 MHz, $CDCl_3$) δ 7.87 (d, *J*=8 Hz, 2H), 7.69 (d, *J*=8.5 Hz, 2H), 2.29 (s, 3H). ^{13}C (125 MHz, $CDCl_3$) δ 169.21, 150.61, 138.59, 123.93, 90.04, 21.25.

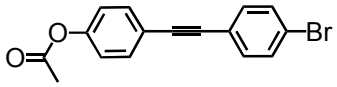

3.4

4-(2-(4-bromophenyl)ethynyl)phenyl acetate (3.4): In a roundbottom flask, under N_2, was combined 1-bromo-4-ethynylbenzene (0.80 g, 4.4 mmol), **2.44** (1.27 g, 4.8 mmol), CuI (0.004 g, 0.2 mmol) and TEA (50 mL). The solution was stirred for 30 min and $PdCl_2(PPh_3)_2$ (0.155 g, 0.2 mmol) was added. The reaction was heated to 80 C with a secured cap and reacted overnight. The reaction was diluted in DCM and washed with H_2O twice, dried with $MgSO_4$, and the solvent was removed by rotary evaporation. Flash chromatography was performed with 50/50 DCM/Hex that afforded a yellow solid at 80% yield. ^{1}H NMR (500 MHz, $CDCl_3$) δ 7.54 (d, *J*=8.5 Hz, 2H), 7.49 (d, *J*=8 Hz, 2H), 7.39 (d, *J*=8 Hz, 2H), 7.10 (d, *J*=8 Hz, 2H), 2.32 (s, 3H). ^{13}C (125 MHz, $CDCl_3$) δ 169.35, 150.85, 133.23, 132.97, 131.85, 122.77, 122.29, 121.99, 120.80, 89.88, 88.58, 21.37. MALDI ESI Calcd. 314.1, found 315.0 M+H.

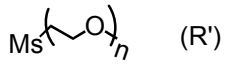

3.5

MePEO$_{350}$ Ms (3.5): To a solution of DCM (250 mL) and PEG_{350} (10.4 g, 29.7 mmol), a solution of mesylchloride (2.8 mL, 32.7 mmol) in DCM (40 mL) was added to the PEG_{350} solution and reacted for 20 min. The reaction mixture was diluted with DCM, washed with 5% citric acid three times, dried over $MgSO_4$, and the solvent was removed by rotary evaporation that provided a clear colorless liquid (12.7 g, 99% yield). ^{1}H NMR (300 MHz, $CDCl_3$): δ 4.37 (t, *J*=4.5 Hz, 2H), 3.76 (t, *J*=4.2 Hz, 2H), 3.64 (m, 32H), 3.74 (s, *J*=5.5 Hz, 3H), 3.08 (s, 3H).

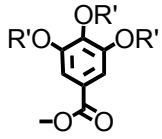

3.6

Tri MePEO$_{350}$ 3,4,5trihydroxybenzoate (3.6): To dry acetone (125 mL) was added MePEO$_{350}$Ms (**2.6**) (12.7 g, 33 mmol), 3,4,5trihydroxybenzoate (1.7 g, 11 mmol), K_2CO_3 (6.2 g, 55 mmol), and 18-crown-6 (0.3 g, 1.8 mmol). The reaction was refluxed for 48 h. The acetone was removed by rotary evaporation and the reaction mixture was diluted in DCM, washed with water two times, once with saturated $NaHCO_3$ in water, dried over $MgSO_4$, and the solvent was removed by rotary evaporation. This provided a clear colorless liquid (10.6 g, 99% yield). ^{1}H NMR (400 MHz, $CDCl_3$): δ 7.35 (s, 2H), 4.21 (m, 6H), 3.89 (m, 8H), 3.64 (m, 96H), 3.39 (s, 9H).

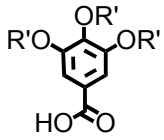

3.7

Tri MePEO$_{350}$ 3,4,5trihydroxybenzoic acid (3.7): In THF (50 mL) and water (10 mL), Tri MePEO$_{350}$ 3,4,5trihydroxybenzoate (**3.6**) (10.6 g, 8.5 mmol) was added with LiOH (1.9 g, 42.5 mmol) and reacted for 2 h. The reaction mixture was diluted in DCM and washed once with water, twice with 5% citric acid in water, dried over $MgSO_4$, and the solvent was removed by rotary evaporation. This provided a clear colorless liquid (7 g, 66% yield). ^{1}H NMR (400 MHz, $CDCl_3$): δ 7.35 (s, 2H), 4.21 (m, 4H), 3.89 (m, 8H), 3.64 (m, 96H), 3.39 (s, 9H). ^{13}C NMR (125MHz, $CDCl_3$): δ 152.39, 109.71, 72.49, 70.98, 70.81, 70.77, 70.71, 70.69, 70.67, 69.83, 68.99, 59.17.

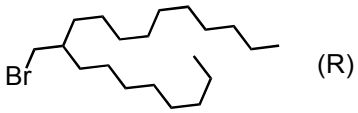

3.8

9-(bromomethyl)nonadecane (3.8): 2-octyl dodecanol (10.0 g, 33.5 mmol) and carbon tetrabromide (11.1 g, 33.5 mmol) were combined and stirred at 0 C with DCM (200 mL). After the materials were in solution, a solution of triphenyl phosphine (11.4 g, 43.5 mmol) in DCM was added slowly over 10 min. The reaction proceeded for 30 min and turned clear and yellow in color. After reacting for 10 h, the reaction was diluted in DCM and washed three times with water, the organic layer was dried over $MgSO_4$ and the solvent was removed by rotary evaporation. Flash chromatography in hexanes afforded a clear colorless oil (10.8 g, 89% yield). ^{1}H NMR (300 MHz, $CDCl_3$): δ 3.46 (d, *J*=4.8 Hz, 1H), 1.28 (bs, 34H), 0.90 (t, *J*=7.2, 6H). ^{13}C NMR (150MHz, $CDCl_3$): δ 40.02, 39.73, 32.81, 32.18, 32.15, 30.05, 29.91, 29.86, 29.82, 29.62, 29.57, 26.82, 22.96, 14.41.

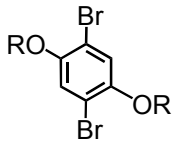

3.9

1,4 dibromo 2,5 di 2-octyl-dodecyl ether benzene (3.9): To DMF (100 mL), 9-(bromomethyl)nonadecane (**3.8**) (4.3 g, 11.8 mmol) and K_2CO_3 (8.8 g, 65.2 mmol) were stirred under N_2 for 20 min. 2,5 dibromohydroquinone (12.7 g, 4.7 mmol) was added to DMF (50 mL) and dripped into the previous solution which was reacted under N_2 at 60 C for 15 h. The reaction was diluted in DCM, washed with 5% citric acid in water three times, dried over $MgSO_4$, and the

solvent was removed by rotary evaporation. Flash chromatography in hexanes provided a clear, colorless oil (5.65 g, 43% yield). ^{1}H NMR (400 MHz, $CDCl_3$): δ 7.07 (s, 2H), 3.82 (d, *J*= 5.6 Hz, 2H), 1.80 (m, 2H), 1.27 (m, 34H), 0.89 (t, *J*=6.4 Hz, 12H). ^{13}C NMR (100MHz, $CDCl_3$): δ 150.36, 118.39, 111.27, 73.19, 38.24, 32.21, 31.88, 31.59, 30.28, 29.96, 29.94, 29.89, 29.86, 29.65, 27.10, 22.99, 14.41.

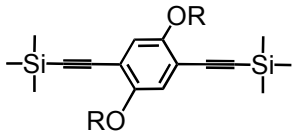

3.10

Compound 3.10: To a flame dried round bottom flask, 1,4-bis(2-octyldodecyloxy)-2,5-dibromobenzene (1.01 g, 1.2 mmol), $PdCl_2(PPH_3)_2$ (0.01 g, 0.12 mmol), CuI (0.02 g, 0.12 mmol), and triethylamine (15 mL) was stirred under N_2 for 20 min. Ethynyltrimethylsilane was then added and the reaction was heated to 80 C overnight. Excess TEA was added and the reaction was filtered and the solvent was evaporated under reduced pressure to an orange liquid. This was run through a silica column eluting with 5/95 DCM/Hex eluent to afford a viscous liquid product in 89% yield. ^{1}H NMR (500 MHz, $CDCl_3$) δ 6.83 (2H, s, CH), 3.82 (4H, d, *J*=5, CH_2), 1.78 (2H, m, CH), 1.49 (4H, m, CH_2), 1.36 (60H, m, CH_2), 0.89 (12H, t, *J*=6.5, CH_3), 0.26 (18H, s, CH_3). ^{13}C (125 MHz, $CDCl_3$) δ 154.31, 116.79, 113.85, 101.35, 100.03, 72.00. 38.37, 32.13, 31.43, 30.30, 29.86, 29.58, 27.08, 22.91, 14.34, 0.20. MALDI MS Calcd. 862.7, found 862.4.

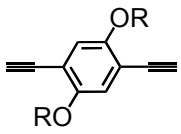

3.11

Compound 3.11: To a round bottom flask containing THF (3 mL), MeOH (1 mL), and **3.10** (0.73 g, 0.8 mmol) cooled to 0 C, tetrabutylammonium fluoride (1.0 mL, 1.0 mmol) was added dropwise and allowed to react overnight. A 5% by weight solution of citric acid (2 mL) was added to quench the reaction and the reaction was diluted with DCM and washed with the citric acid solution (150 mL). The organic layer was dried with anhydrous $MgSO_4$ and a silica gel column was run eluting with 7/93 DCM/Hex mixture yielding a clear liquid (0.55 g, 95% yield). ^{1}H NMR (500 MHz, $CDCl_3$) δ 6.95 (2H, s, CH), 3.84 (4H, d, *J*=5.5, CH_2), 3.30 (2H, s, CH), 1.81 (2H, m, CH), 1.26 (60H, m, CH_2), 0.89 (12H, t, *J*=6.5, CH_3). ^{13}C (125 MHz, $CDCl_3$) δ 154.42, 117.67, 113.38, 82.49, 80.02, 72.68, 38.08, 32.15, 31.53, 30.24, 29.89, 29.81, 29.58, 27.02, 22.92, 14.36. MALDI MS (dithrinol matrix) Calcd. 718.7, found 719.9 (MH^+).

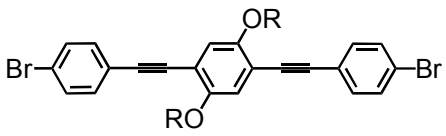

3.12

Compound 3.12: To a flame dried round bottom were added 1,4-Diethynyl-2,5-bis-hexyloxybenzene (0.74 g, 1.0 mmol), 1-bromo-4-iodobenzene (0.58 g, 2.1 mmol), and CuI (0.04 g, 0.2 mmol). To the system, dry TEA (50 mL) was added and flushed with N_2 for 15 min. Bis(triphenylphosphine)-palladium dichloride (0.15 g, 0.02 mmol) was added and the reaction was heated to 70 C overnight. The mixture was diluted with TEA and filtered. The TEA was removed by vacuum and the resulting liquid was purified by column chromatography eluting

with 10/90 DCM/Hex eluent yielding a yellow solid in 86% yield. ^{1}H NMR (500 MHz, $CDCl_3$) δ 7.49 (4H, d, *J*=8, CH), 7.39 (4H, d, *J*=8, CH), 7.00 (2H, s, CH), 3.90 (4H, d, *J*=5.5, CH_2), 1.85 (2H, m, CH), 1.53 (4H, m, CH_2), 1.24 (56H, m, CH_2), 0.89 (12H, t, *J*=6.5, CH_3). ^{13}C (125 MHz, $CDCl_3$) δ 154.02, 133.12, 131.81, 122.67, 116.59, 113.91, 93.98, 87.39, 72.51, 38.36, 32.14, 31.67, 30.32, 29.93, 29.88, 29.59, 27.17, 22.92, 14.36. MALDI MS Calcd. 1029.2, found 1029.9.

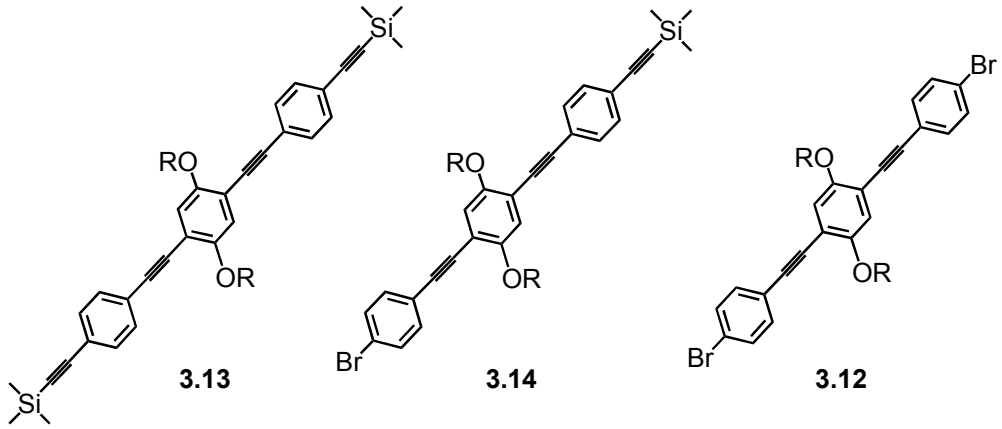

Compounds 3.13, 3.14, 3.12: In a roundbottom flask under N_2 were combined 1,4-bis(2-octyldodecyloxy)-2,5-bis(2-(4-bromophenyl)ethynyl)benzene (0.34 g, 0.33 mmol), TEA (10 mL), CuI (0.003 g, 0.017 mmol), and trimethylsilyl acetylene (0.05 mL, 0.331 mmol). After stirring for 10 min, $PdCl_2(PPh_3)_2$ (0.012 mg, 0.017 mmol) was then added. The reaction was sealed and heated to 80 C overnight. The reaction was then diluted in TEA, filtered, and the solvent was removed under reduced pressure. The crude reaction mixture was brought up in DCM (100 mL) and washed with water (150 mL). The DCM was removed under reduced pressure and purified by column chromatography affording 110 mg of starting material (**3.12**), 170 mg of **3.13**, and 110 mg of **3.14**.

3.13 ^{1}H NMR (500 MHz, $CDCl_3$) δ 7.48 (2H, d, *J*=8, CH), 7.45 (4H, CH), 7.39 (2H, d, *J*=8, CH), 7.00 (2H, s, CH), 3.90 (4H, d, *J*=5.5, CH_2), 1.85 (2H, m, CH), 1.53 (4H, m, CH_2), 1.24-1.52 (56H, m, CH_2), 0.89 (12H, m, CH_3), 0.27 (9H, s, CH_3). ^{13}C (125 MHz, $CDCl_3$) δ 154.02, 133.12, 132.07, 131.80, 131.50, 123.74, 123.05, 122.67, 122.65, 116.58, 114.00, 113.84, 104.87, 96.45, 94.76, 93.97, 88.19, 87.41, 72.46, 38.34, 32.13, 31.65, 30.32, 29.92, 29.87, 29.59, 27.15, 22.91, 14.34, 0.12. MALDI MS Calcd. 1044.7, found 1045.0.

3.14 ^{1}H NMR (500 MHz, $CDCl_3$) δ 7.49 (4H, d, *J*=8, CH), 7.39 (4H, d, *J*=8, CH), 7.00 (2H, s, CH), 3.90 (4H, d, *J*=5.5, CH_2), 1.85 (2H, m, CH), 1.53 (4H, m, CH_2), 1.24 (56H, m, CH_2), 0.89 (12H, t, *J*=6.5, CH_3). ^{13}C (125 MHz, $CDCl_3$) δ 154.02, 133.12, 131.81, 122.67, 116.59, 113.91, 93.98, 87.39, 72.51, 38.36, 32.14, 31.67, 30.32, 29.93, 29.88, 29.59, 27.17, 22.92, 14.36. MALDI MS Calcd. 1029.2, found 1029.9.

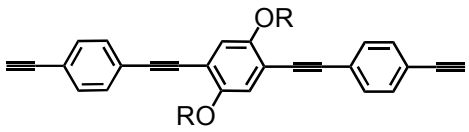

3.15

Compound 3.15: To a round bottom flask containing THF (20 mL), MeOH (5 mL), and **3.13** (0.82 g, 0.77 mmol) cooled to 0C, tetrabutylammonium fluoride (1.7 mL, 1.7 mmol) was added dropwise. The solution was stirred and warmed to RT overnight. 5% by weight solution of citric acid (2 mL) was added to quench the reaction and the reaction was diluted with DCM and washed with the citric acid solution (150 mL). The organic layer was dried with anhydrous $MgSO_4$ and a silica gel column was run eluting with 20/93 DCM/Hex mixture yielding a clear liquid (0.67 g,95% yield). ^{1}H NMR (500 MHz, $CDCl_3$) δ 7.48 (8H, s, CH), 7.00 (2H, s, CH), 3.91 (4H, d, *J*=5.5, CH_2), 3.19 (2H, s, CH), 1.81 (2H, m, CH), 1.57-1.27 (78H, m, CH_2), 0.89

(12H, m, CH_3). ^{13}C (125 MHz, $CDCl_3$) δ 154.05, 132.24, 131.58, 124.19, 122.03, 116.03, 113.97, 94.55, 88.30, 83.50, 79.10, 72.49, 38.36, 32.14, 31.66, 30.32, 29.93, 29.88, 29.84, 29.59, 27.16, 22.92, 14.36. MALDI MS (dithrinol matrix) Calcd. 918.73, found 918.93.

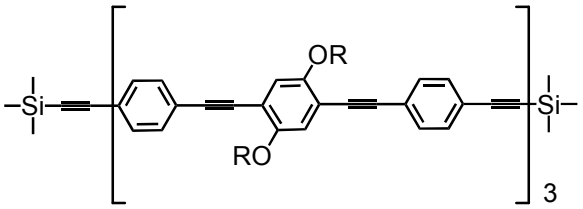

3.16

Compound 3.16: In a roundbottom flask under N_2 were combined **3.15** (0.24 g, 0.26 mmol), **3.14** (0.58 mg, 0.55 mmol), TEA (25 mL), tritolylphosphine (0.079 g, 0.26 mmol). After stirring for 10 min, $Pd(DBA)_3$ (0.024 g, 0.026 mmol) was then added. The reaction was sealed and heated to 80 C overnight. The crude reaction mixture was brought up in DCM (100 mL) and washed with water (150 mL). The DCM was removed under reduced pressure and purified by column chromatography using 20/80 DCM/Hex affording a yellow solid (0.42 g, 57% yield). ^1H NMR (500 MHz, $CDCl_3$) δ 7.51 (s, 18H), 7.45 (s, 6H), 7.01 (m, 6H), 3.91 (s, 12H), 1.86 (s, 6H), 1.57-1.25 (m), 0.89 (m, 36H), 0.26 (s, 18H). ^{13}C (125 MHz, $CDCl_3$) δ 154.08, 132.09, 131.75, 131.71, 131.53, 123.77, 123.05, 116.65, 114.04, 95.01, 91.29, 88.39, 72.57, 53.67, 38.40, 32.16, 31.67, 30.35, 29.91, 29.63, 27.19, 22.94, 14.38, 0.144. MALDI MS Calcd. 2848.2, found 2849.8 M+H.

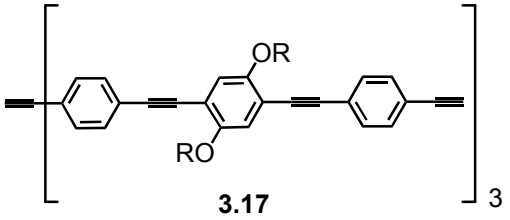

3.17

Compound 3.17: Reference synthesis of **3.11**. ^{1}H NMR (500 MHz, $CDCl_3$) δ 7.51 (s, 18H), 7.48 (s, 6H), 7.01 (m, 6H), 3.91 (s, 12H), 1.86 (s, 6H), 1.57-1.25 (m), 0.89 (m, 36H): ^{13}C (125 MHz, $CDCl_3$) δ 150.08, 132.26, 131.73, 131.69, 131.59, 124.22, 123.76, 123.04, 116.65, 114.08, 114.04, 113.94, 94.86, 94.57, 91.28, 88.35, 83.52, 79.10, 72.55, 38.39, 32.15, 31.68, 30.35, 29.95, 29.89, 29.61, 27.18, 22.93, 14.36. MALDI MS Calcd. 2702.2, found 2703.8 M+H.

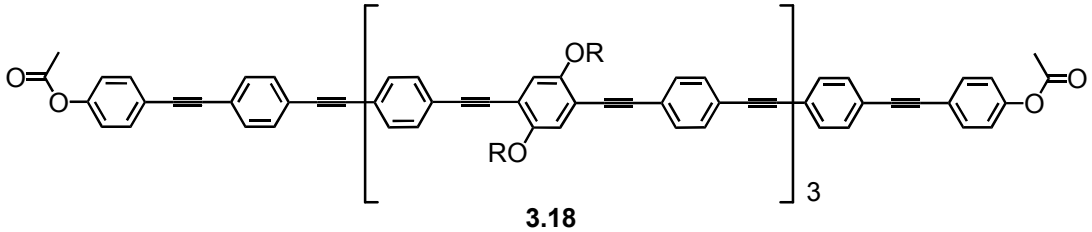

3.18

Compound 3.18: Reference synthesis of **2.12**. ^{1}H NMR (500 MHz, $CDCl_3$) δ 7.51 (m, 30H), 7.11 (d, *J*=8.5 Hz, 4H), 7.02 (s, 6H), 3.93 (d, *J*=5.5 Hz, 12H), 2.32 (s, 6H), 1.86 (m, 6H), 1.57-1.25 (m), 0.89 (m, 36H): ^{13}C (125 MHz, $CDCl_3$) δ 169.37, 154.32, 150.84, 133.02, 131.73, 131.69, 123.75, 123.03, 121.99, 120.90, 116.63, 114.02, 94.85, 91.27, 90.76, 89.36, 88.39, 72.54, 38.39, 32.15, 31.68, 30.34, 29.95, 29.89, 29.86, 29.61, 27.18, 23.47, 22.93, 21.38, 14.37. MALDI MS Calcd. 3172.3, found 3175.6.

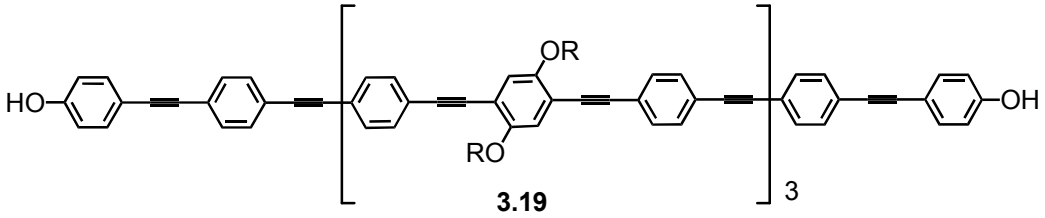

Compound 3.19: Reference synthesis of **2.13**. ^{1}H NMR (500 MHz, $CDCl_3$) δ 7.56-7.44 (m, 30H), 7.11 (d, *J*=8 Hz, 4H), 7.02 (s, 6H), 6.83 (d, *J*=8 Hz, 4H), 3.93 (d, *J*=5.5 Hz, 12H), 1.87 (m, 6H), 1.57-1.25 (m), 0.89 (t, *J*= 6.5 Hz, 36H). MALDI MS Calcd. 3089.4, found 3129.3 M+K.

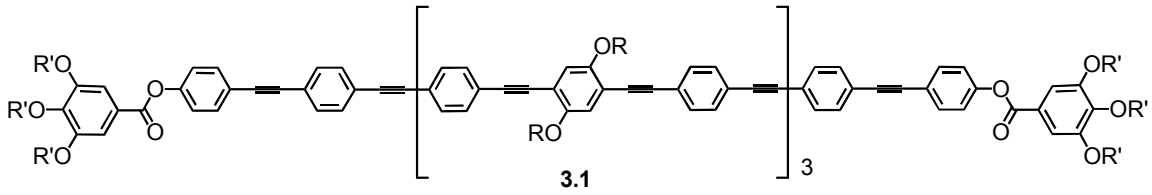

Compound 3.1: Reference synthesis of **2.14**. ^{1}H NMR (500 MHz, $CDCl_3$) δ 7.56-7.44 (m, 30H), 7.28 (m, 12H), 7.01 (s, 6H), 4.19 (m), 3.91-3.54 (m), 3.37 (s), 1.87 (m, 6H), 1.57-1.25 (m), 0.89 (t, *J*= 7.5 Hz, 36H). ^{13}C (125 MHz, $CDCl_3$) δ 166.70, 153.99, 152.61, 152.41, 142.64, 132.99, 131.69, 131.64, 125.07, 122.12, 116.54, 113.94, 109.82, 109.09, 72.53, 72.46, 72.05, 70.94, 70.78, 70.73, 70.69, 70.65, 69.73, 69.09, 68.93, 59.17, 52.31, 38.29, 32.06, 31.59, 30.24, 29.79, 29.51, 27.08, 22.84, 14.28. MALDI MS Calcd. polymer dispersion around 5433, found around 5388.

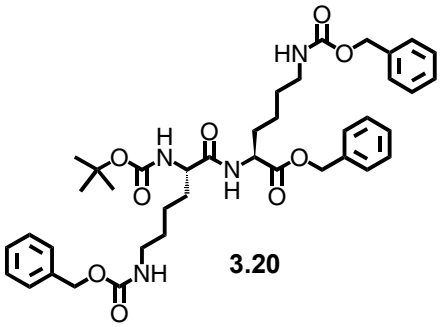

3.20

Boc(dilysine)Bn 3.20: Reference synthesis of **3.24** (99% yield). ^{1}H NMR (500 MHz, $CDCl_3$) δ 7.81 (s, 15H), 5.99 (s, 1H), 5.3 (d, *J*=8 Hz, 1H), 5.32 (s, 1H), 5.15-4.97 (m, 6H), 4.53 (s, 1H), 4.31 (s, 1H), 3.15 (m, 2H), 3.05 (m, 2H), 1.67 (bs, 4H), 1.40 (s, 15H), 1.24 (bm, 4H). ^{13}C (125 MHz, CD_3OD) δ 173.19, 172.01, 156.60, 156.12, 136.68, 136.52, 35.34, 128.57, 128.52, 128.48, 128.38, 128.15, 128.05, 127.84, 80.01, 67.08, 66.69, 66.54, 53.79, 52.29, 40.44, 40.37, 32.47, 31.43, 29.27, 29.16, 28.42, 22.68, 22.23. ESI MS (methanol) Calcd. 732.37, found 733.4 M+H.

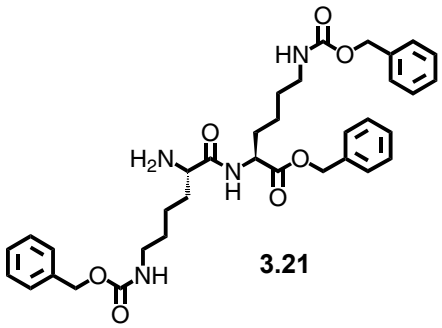

3.21

(dilysine)Bn 3.21: Reference synthesis of **3.27** (99% yield). TLC showed complete conversion as well as MS. ESI MS (methanol) Calcd. 632.32, found 633.3 M+H.

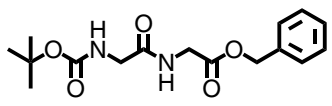

3.22

Diglycine 3.22: Reference synthesis of **3.24** with flash chromatography using 5/95 MeOH/DCM as eluent (78% yield). ^{1}H NMR (500 MHz, $CDCl_3$) δ 7.33 (s, 5H), 7.21 (t, *J*=6 Hz, 1H), 5.13 (s, 2H), 4.04 (s, 2H), 3.83 (s, 2H), 1.43 (s, 9H). ^{13}C (125 MHz, CD_3OD) δ 170.33, 169.76, 156.24, 141.21, 135.27, 135.16, 128.39, 128.29, 127.34, 126.93, 80.04, 67.11, 64.84, 43.95, 42.45, 41.16, 28.29. ESI MS (methanol) Calcd. 322.15, found 323.3 M+H.

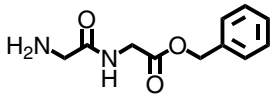

3.23

Compound 3.23: Reference synthesis of **3.27 (**100% yield): Monitored by TLC and MS and used without further purification. ESI MS (methanol) Calcd. 221.10, found 222.2 M+H.

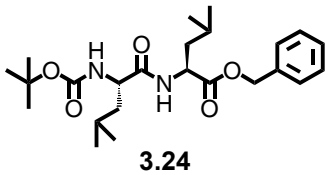

3.24

Boc(dileu)Bn 3.24: To a roundbottom flask was combined NH_2(leu)Bn (3.0 g, 13 mmol), EDCI (2.99 g, 15.6 mmol), HOBT (1.76 g, 13 mmol), TEA (1.32 g, 13 mmol), DCM (300 mL), and stirred until in solution. Boc(leu)OH (3.0 g, 13 mmol) was then added and the mixture was stirred overnight. The mixture was diluted with DCM and washed with brine three times, dried over $MgSO_4$, and the solvent was removed by rotary evaporation. Flash chromatography was performed using 5/95 MeOH/DCM affording a white solid (5.0 g, 89% yield). ^{1}H NMR (500 MHz, $CDCl_3$) δ 7.34 (s, 5H), 6.50 (s, 1H), 5.15 (d, *J*= 9, 2H), 4.92 (s, 1H), 4.66 (m, 2H), 4.10 (s, 1H), 1.63 (m, 6H), 1.45 (s, 9H), 0.91 (s, 12H). ^{13}C (125 MHz, $CDCl_3$) δ172.70, 172.43, 155.91,

135.53, 128.77, 128.58, 128.43, 80.21, 67.21, 53.06, 50.90, 41.57, 41.02, 28.44, 24.81, 23.02, 21.49. ESI MS (methanol) Calcd. 434.28, found 457.34 M+Na.

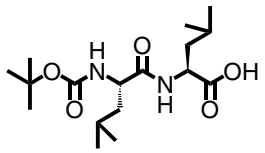

3.25

Boc(dileu) 3.25: To a roundbottom flask was combined **3.24** (4.9 g, 11.2 mmol), Pd/C (0.70 g), DCM (100 mL), and EtOH (100 mL). The solution was stirred overnight under a balloon of H_2. The mixture was filtered through celite, and the solvent was removed by rotary evaporation affording (3.72 g, 96% yield). TLC showed the absence of starting material and this material was carried on without further purification.

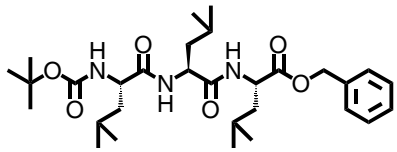

3.26

Boc(trileu)Bn (3.26): Reference synthesis of **3.24** (89% yield). ^{1}H NMR (500 MHz, $CDCl_3$) δ 7.34 (s, 5H), 7.16 (s, 1H), 6.98 (s, 1H), 5.36 (s, 1H), 5.12 (dd, *J*=12 Hz, *J*=18.5, 2H), 4.62 (m, 1H), 4.54 (s, 1H), 4.18 (s, 1H), 1.58 (bm, 8H), 1.41 (s, 11H), 0.91 (s, 18H). ^{13}C (125 MHz, $CDCl_3$) δ 172.84, 172.64, 171.88, 155.84, 135.58, 128.65, 128.55, 128.43, 128.35, 127.52, 127.03, 79.88, 67.04, 65.12, 52.97, 51.68, 50.88, 41.35, 41.11, 40.97, 28.44, 24.81, 24.77, 24.65, 22.98, 22.84, 22.44, 22.31, 21.91. ESI MS (methanol) Calcd. 547.36, found 548.34 M+H.

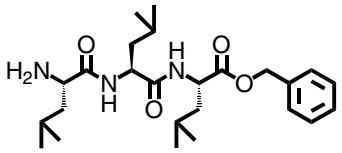

3.27

NH_2(trileu)Bn (3.27): To a roundbottom flask was combined **3.26** (6.4 g, 11.7 mmol), DCM (100 mL), and HCl in Dioxanes (4 M, 5 mL) was stirred into the solution and the reaction was monitored by TLC. After 15 minutes the solvent was removed by rotary evaporation to give a white solid (4.73 g, 90% yield). The material was used without further purification. ESI MS (methanol) Calcd. 434.28, found 448.3 M+H.

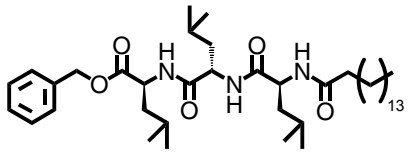

3.28

Compound 3.28: Reference synthesis of **3.24** with flash chromatography using 5/95 MeOH/DCM as eluent (73% yield). ^{1}H NMR (500 MHz, $CDCl_3$) δ 7.34 (s, 5H), 5.14 (dd, *J*=12.5 Hz, *J*=35.5 Hz, 2H), 4.84 (s, 1H), 4.77 (s, 1H), 4.65 (s, 1H), 2.27 (m, 1H), 2.15 (m, 1H), 1.86 (s, 1H), 1.67-1.36 (bm, 10H), 1.22 (s, 24H), 0.88 (s, 21H). ^{13}C (125 MHz, $CDCl_3$) δ 173.04, 172.81, 172.48, 172.33, 135.76, 128.68, 128.40, 128.21, 66.96, 53.61, 51.77, 50.81, 42.53, 41.36, 40.68, 36.24, 34.29, 32.10, 29.89, 29.69, 29.55, 25.92, 24.91, 24.72, 23.47, 22.87, 22.54, 22.09, 21.58, 14.30. ESI MS (methanol) Calcd. 685.54, found 708.6 M+Na.

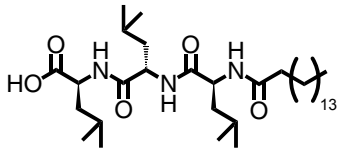

3.29

Compound 3.29: Reference synthesis of **3.25** (81% yield). ^{1}H NMR (500 MHz, $CDCl_3$) δ 8.36 (s, 1H), 4.56 (m, 2H), 4.47 (m, 1H), 2.25 (m, 2H), 1.76-1.55 (bm, 9H), 1.30 (s, 20H), 0.92 (m, 17H). ^{13}C (125 MHz, CD_3OD) δ 174.85, 174.68, 173.52, 173.43, 173.39, 173.40, 173.32, 51.59, 50.92, 50.84, 41.09, 40.86, 40.62, 35.76, 32.03, 29.77, 29.67, 29.49, 29.45, 29.27, 25.98, 24.78, 24.60, 22.70, 22.47, 21.56, 21.38, 21.00, 13.57. ESI MS (methanol) Calcd. 595.49, found 618.6 M+Na.

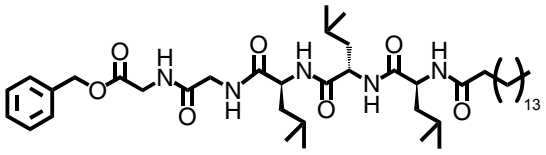

3.30

Compound 3.30: Reference synthesis of **3.24** with flash chromatography using 5/95 MeOH/DCM as eluent (58% yield). ^{1}H NMR (500 MHz, CD_3OD) δ 7.38 (s, 5H), 5.20 (s, 2H), 4.37 (m, 3H), 3.48-3.23 (m, 4H), 2.25 (t, *J*=7.5 Hz, 2H), 1.71-1.56 (m, 11H) 1.31 (s, 24H), 1.32-0.92 (m, 21H). ESI MS (methanol) Calcd. 799.58, found 822.7 M+Na.

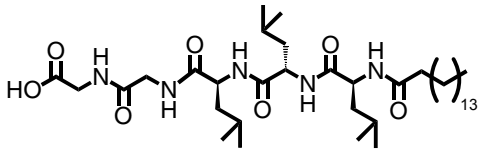

3.31

Compound 3.31: Reference synthesis of **3.25** (100% yield). ^{1}H NMR (500 MHz, dDMSO) δ 8.15 (s, 1H), 8.07 (s, 1H), 7.95 (s, 1H), 7.85 (s, 1H), 4.28 (m, 3H), 3.74 (m, 4H), 2.09 (m, 2H), 1.57 (m, 3H), 1.47-1.38 (bm, 9H), 1.23 (s, 24H), 0.87-0.81 (m, 21H). ^{13}C (125 MHz, CD_3OD) δ 172.96, 172.91, 172.83, 172.60, 171.81, 169.68, 51.79, 51.49, 42.44, 41.34, 35.79, 32.02, 29.76, 29.44, 29.22, 26.01, 24.67, 23.75, 22.82, 22.24, 14.64. ESI MS (methanol) Calcd. 709.54, found 732.7 M+H.

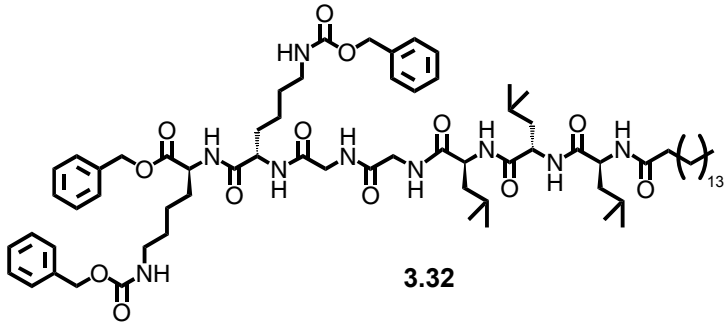

3.32

Compound 3.32: Reference synthesis of **3.24** with flash chromatography using 10/90 MeOH/DCM as eluent (70% yield). ^{1}H NMR (500 MHz, $CDCl_3$) δ 7.34 (s, 15H), 5.10 (s, 2H), 5.00 (s, 4H), 4.30 (s, 4H), 3.74 (s, 4H), 2.95 (s, 4H), 2.01 (s, 2H), 1.58-1.23 (bm, 47H), 0.87-0.83 (app s, s, 21H). ESI MS (methanol) Calcd. 1323.85, found 1346.8 M+Na.

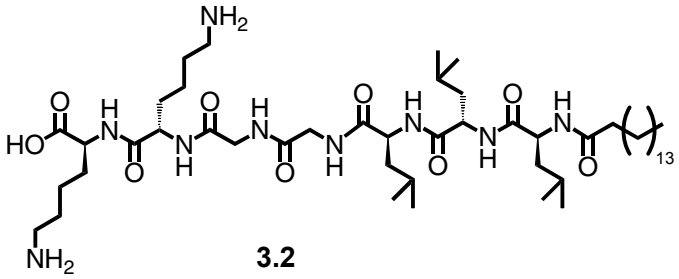

3.2

Compound 3.2: To a roundbottom flask was combined **3.32** (0.16 g, 0.12 mmol), Pd/C (30 mg), DCM (10 mL), and EtOH (10 mL). The solution was stirred overnight under a balloon of H_2. The mixture was filtered through celite using MeOH as eluent, and the solvent was removed by rotary evaporation. The solid was taken up in H_2O (10 mL) and acetonitrile (5 mL) and lyophilized. The white powder was then taken up in acidic water (0.1% TFA) and filtered through a syringe filter (0.22 μm) and lyophilized to a white powder. HPLC purification was performed with a gradient from 0-100% acetonitrile and H_2O/0.01% TFA. ESI MS (methanol) Calcd. 965.73, found 966.7 M+H.

Chapter Four

Self-Assembled Peptide Amphiphile Nanofibers Conjugated to Magnetic Resonance Imaging Contrast Agents

Adapted from:

Bull, S. R.; Guler, M. O.; Bras, R. E.; Meade, T. J.; Stupp, S. I. "Self-Assembled Peptide Amphiphile Nanofibers Conjugated to MRI Contrast Agents." *Nanoletters* **2005**, 5 (1), 1-4.

4 Peptide Amphiphile Contrast Agents (PACA) Synthesis and Characterization

4.1 Introduction

Magnetic resonance imaging (MRI) has evolved as one of the most important diagnostic techniques in clinical radiology.[7, 111, 112] The advent of high magnetic fields, improved gradient coils and pulse sequences has provided the means to obtain three-dimensional images of whole animals at near cellular resolution.[12] Typically, intrinsic contrast is augmented by the use of paramagnetic agents to increase the spin lattice relaxation rate (T_1) of nearby water protons.[113] The majority of MR contrast agents (CAs) use the paramagnetic metal ion Gd(III) because it has seven unpaired electrons and a long electronic relaxation time which is ideal for shortening the T_1 relaxation time which in turn increases contrast in the MR image.[114, 115] When chelated to a suitable ligand, the Gd(III) ion is detoxified and provides a powerful tool for a number of clinical and experimental applications that include tumor identification,[116] perfusion analysis,[117] cell tracking,[24, 118] and monitoring gene expression.[30, 34]

A principle barrier to the efficacy of MRI is the inherent lack of in vivo sensitivity. Essentially, there is a lack of sufficient contrast between different tissues of the body. A solution to this problem is in the form of CAs that can provide greater image contrast in specific organs/areas within the body where the CA has accumulated. In order to obtain significant contrast over long periods of time, the observed relaxivity of MR agents must be increased. Because of the low efficacy of small molecule CAs, large amounts need to be used in clinical settings (grams). A common method of relaxivity enhancement of small molecule MR CAs is to increase the rotational correlation time (τ_R).[7, 119] This τ_R enhancement is accomplished by

increasing the molecular weight of the CA by conjugation to proteins, polymers, use of nanoparticles, or the preparation of micellar structures.[7, 12, 120-127]

Our approach to increasing the relaxivity of new MR agents utilizes self-assembly, specifically the use of peptide amphiphiles (PAs) that have been developed over the past decade as scaffolds for regenerative medicine.[81, 82, 87] I have coupled a small molecule MR CA to the self-assembling PA in varying positions and tested the effect on relaxivity. We chose PAs due to their biocompatibility and bioactivity, and because of their well characterized robust self-assembly into cylindrical nanofibers and hydro gels.[81, 82, 87] In this chapter, I describe the synthesis and supramolecular structure of two modified self-assembling PAs covalently linked to a derivative of DOTA. We chose to use a macrocyclic DOTA (**Figure 1.1**) derivative for its high association constant with lanthanide ions (log K ~21)[128] and for its ease of conjugation to the PA during solid phase peptide synthesis.[117] This class of peptide amphiphile contrast agent (PACA) conjugates can form either self-assembled nanofibers or spherical micelles that can be cross-linked through disulfide bonds.[81] The PACA systems described here (**Figure 4.2**) are examples of self-assembling PAs in which the peptide sequence is modified to enable tracking of the molecule by MRI. These PA biomaterial monomers self-assemble into nanofibers with diameters on the order of six to eight nanometers and form self-supporting bioactive gels that can be implanted into the body.[81, 87] Ideally, one would like to extend the benefits of MRI for three-dimensional non-invasive visualization of the PA gel scaffolds when they are used as biomaterial implants. The in vivo use of these gels would benefit greatly from the ability to detect and track their fate, migration and degradation by MRI.

4.2 General Synthesis of Peptide Amphiphile Contrast Agents

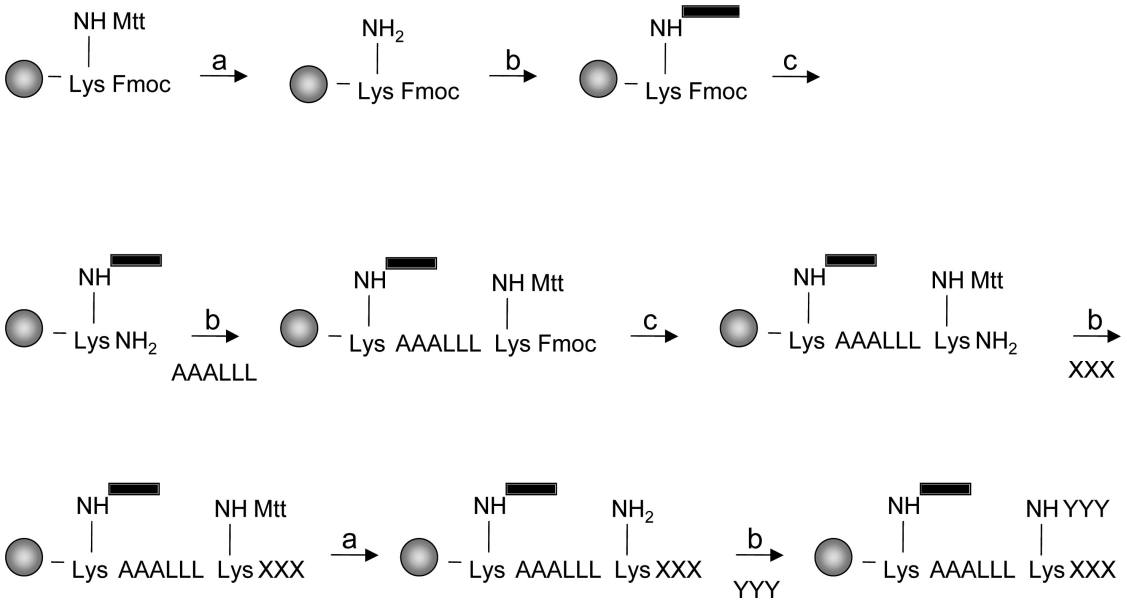

Figure 4.1 Cartoon depicting general solid phase peptide synthesis couplings. (a) 1.5% TFA/DCM (10 min). (b) 0.4 mmol amino acid, 0.39 mmol HBTU, 0.39 mmol HOBT, 0.41 mmol DIPEA (2.5 h). (c) 30% piperidine/DMF (10 min). The amino acids described as A, L, X, Y can be substituted with any Fmoc amino acid.

Both PACA **4.1** and **4.2** were synthesized using standard Fmoc solid phase peptide synthesis. HBTU was used as the activating agent for the acids and DIPEA was used as the base. Branching was accomplished by use of an orthogonally protected lysine (Mtt protection) that could be deprotected while on the solid phase leaving a free ε amine for further conjugation (**Figure 4.1**). Addition of the tris-t-butyl DOTA, was exactly the same as an amino acid. Cleavage from the resin provided a global deprotection for the PACA molecules and subsequent reaction with $GdCl_3$ afforded the final products.

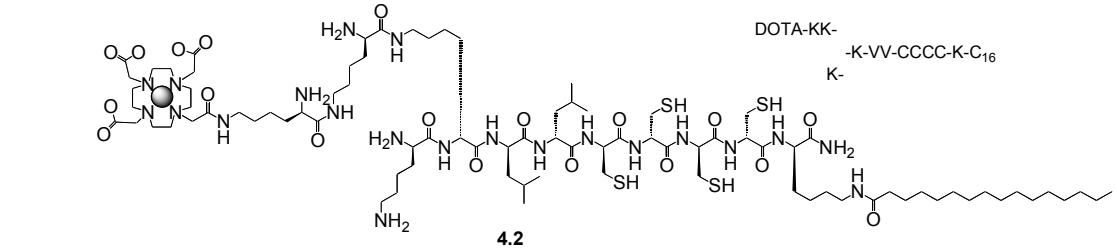

4.2

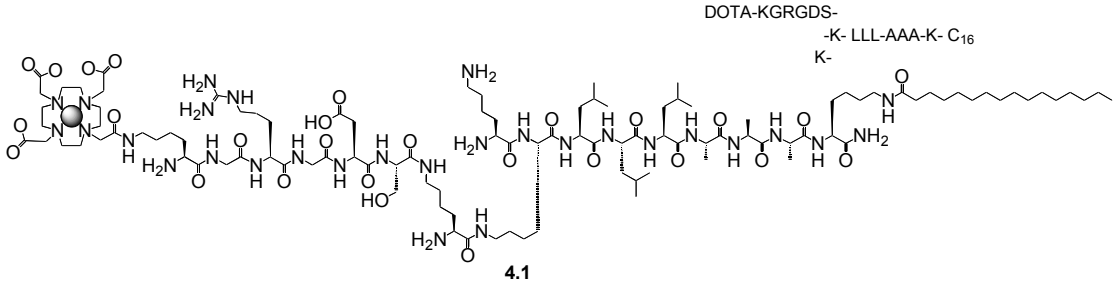

4.1

Figure 4.2 Monomer structures of a chelate conjugated to **4.1**, an RGD bioactive epitope and **4.2**, a crosslinkable PA scaffold. Both structures self-assemble into nanostructures upon raising the pH to basic conditions, PACA **4.1** assembles into fibers and PACA **4.2** assembles into spherical micelles.

4.3 Results

Of the two PACA derivatives only **4.1** forms nanofibers in solution at a pH greater than 7.0. It is believed to be the result of β-sheet forming amino acids, AAALLL, present in the peptide sequence of this PACA compared to **4.2** that does not have strong β-sheet forming amino acid section (two leucines).[86] The relaxivity of **4.1** in its self-assembled state was measured at 14.7 ± 0.8 $mM^{-1}s^{-1}$ (**Figure 4.3**). The relaxivity of the uncrosslinked **4.2** was 22.8 ± 1.2 $mM^{-1}s^{-1}$ (**Figure 4.5**) and became 20.8 ± 0.8 $mM^{-1}s^{-1}$ upon crosslinking by I_2 oxidation. The crosslinking of **4.2** does not appreciably change the relaxivity due to the flexible linker between the DOTA moiety and the aggregate, resulting in the linker as the limiting factor in τ_R. The observed relaxivities of these derivatives are significantly higher than that of typical monomer contrast agents by 3-6 times (**Figure 1.1**).[17] This increased relaxivity is due to the self-assembly of the

monomers into nanofibers in basic conditions, thereby increasing τ_R. PACA **4.2** results in a higher relaxivity than **4.1** due to its lower degree of molecular flexibility (it is more rigid) since the DOTA moiety is closer to the core of the nanofiber with less degrees of flexibility. The oxidation modulation of cysteines in **4.2** was through the addition of excess aqueous iodine to covalently crosslink the monomers after self-assembly. Further work on systems with different epitopes is currently as well as varying the position of the DOTA derivative will be described in Chapter 6.

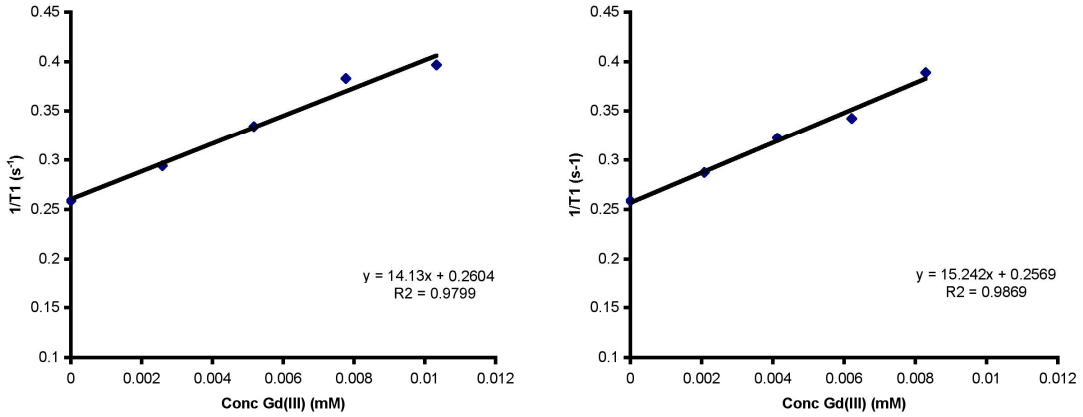

Figure 4.3 Relaxivity graphs of **4.1** in its self-assembled state at pH 7.4. Each point represents the average of three repetitions and the Gd(III) concentration was determined by ICP-MS. The final relaxivity was taken by averaging the above graph's slopes to be 14.7 ± 0.8 $mM^{-1}s^{-1}$. The measurements were obtained at 37 C with a 60 MHz magnet.

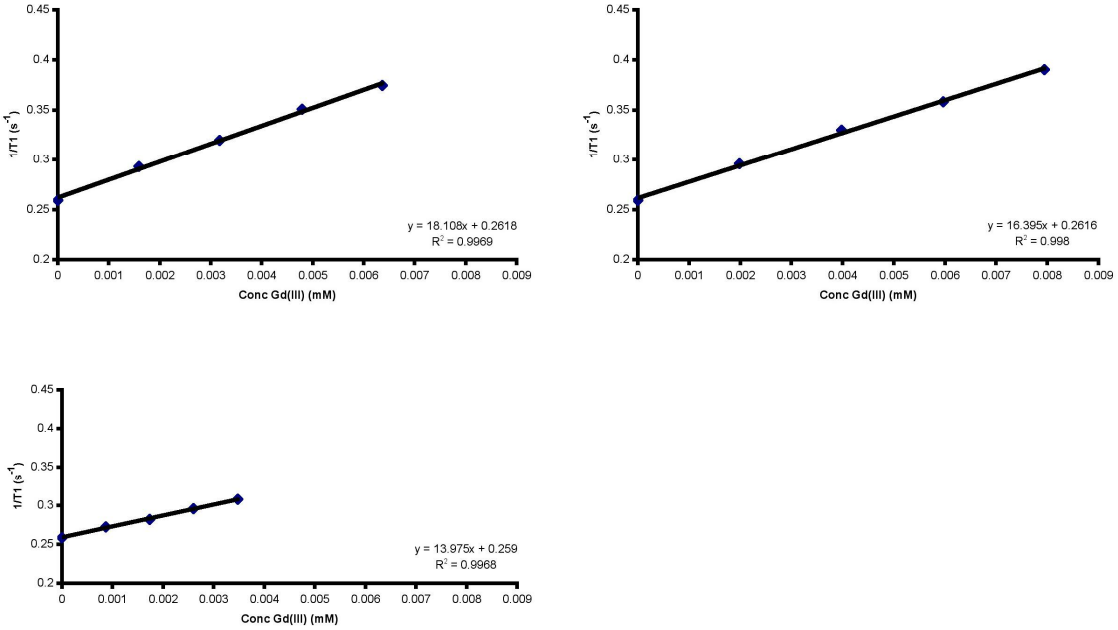

Figure 4.4 PACA **4.1** at pH 3 resulting in a relaxivity of 16.2 ± 2.1 $mM^{-1}s^{-1}$. Each point represents the average of three repetitions and the Gd(III) concentration was determined by ICP-MS. The measurements were obtained at 37 C with a 60 MHz magnet.

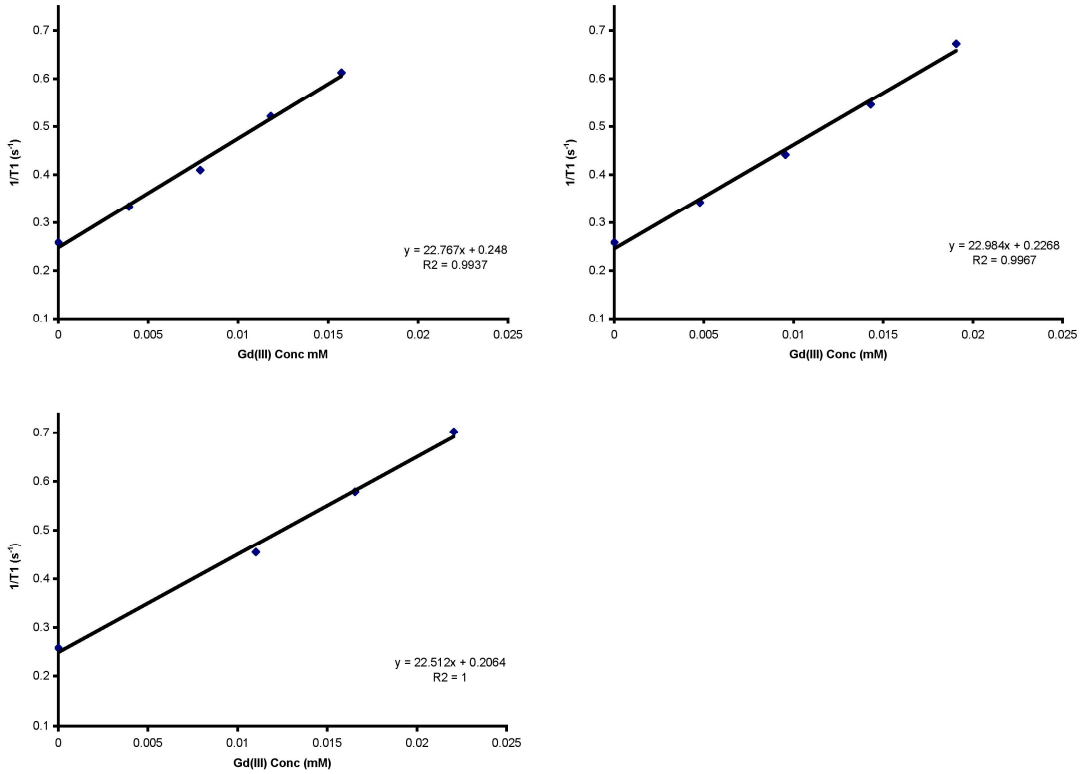

Figure 4.5 Relaxivity graphs of **4.2** in its self-assembled state at pH 7.4 without crosslinking the sulfides. Each point represents the average of three repetitions and the Gd(III) concentration was determined by ICP-MS. The final relaxivity was taken by averaging the above graph's slopes resulting in a relaxivity of 22.8 ± 1.2 mM^{-1} s^{-1}. The measurements were obtained at 37 C with a 60 MHz magnet.

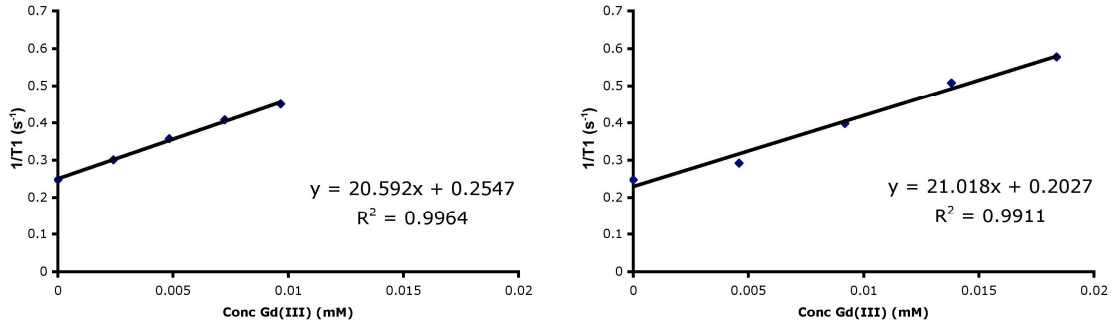

Figure 4.6 Relaxivity graphs of **4.2** in its self-assembled state after crosslinking the sulfides via iodine oxidation. Each point represents the average of three repetitions and the Gd(III) concentration was determined by ICP-MS. The final relaxivity was taken by averaging the above graph's slopes resulting in a relaxivity of 20.8 ± 0.8 mM^{-1} s^{-1}. The measurements were obtained at 37 C with a 60 MHz magnet.

Transmission electron microscopy (TEM) images and atomic force microscopy (AFM) reveal the supramolecular structure of aggregates from **4.1** and **4.2**. The contrast observed under the electron beam is provided by the Gd(III) attached to the surface of the PACAs (unstained) and provides evidence that Gd(III) is indeed chelated (**Figure 4.8**). PACA **4.1** forms uniform fibers with lengths beyond 100 nm and widths corresponding to 22 ± 2 nm, which can be explained by the tendency of nanofibers to bundle, and is not indicative of the individual nanofiber widths (**Figure 4.7**). In contrast, uncrosslinked **4.2** does not self-assemble into fibers but rather into spherical micelles (**Figure 4.8**). Circular dichroism spectroscopy (CD) confirmed the difference in supramolecular structure seen in **4.1** and **4.2** (**Figure 4.9**). PACA **4.1** shows an intense Cotton effect corresponding to a β-sheet structural motif, and in contrast PACA **4.2** reveals a less intense structural signal that is a combination of random coil, α-helix, and β-sheet.[129] The less defined molecular conformation in the self-assembled state is consistent with the formation of spherical micelles.[86] On the other hand, the nanofiber formation observed in **4.1** by AFM and TEM supports the CD signature for an extended β-sheet structure.

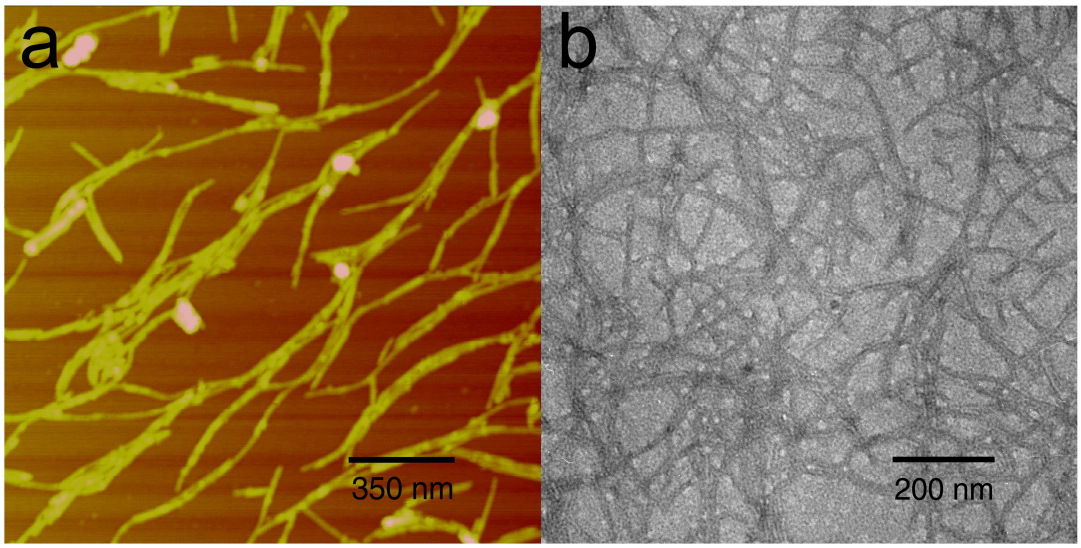

Figure 4.7 AFM (a) and TEM (b) images of molecule **4.1** with Gd(III). (b) was not stained because the Gd(III) density provided enough contrast to be imaged.

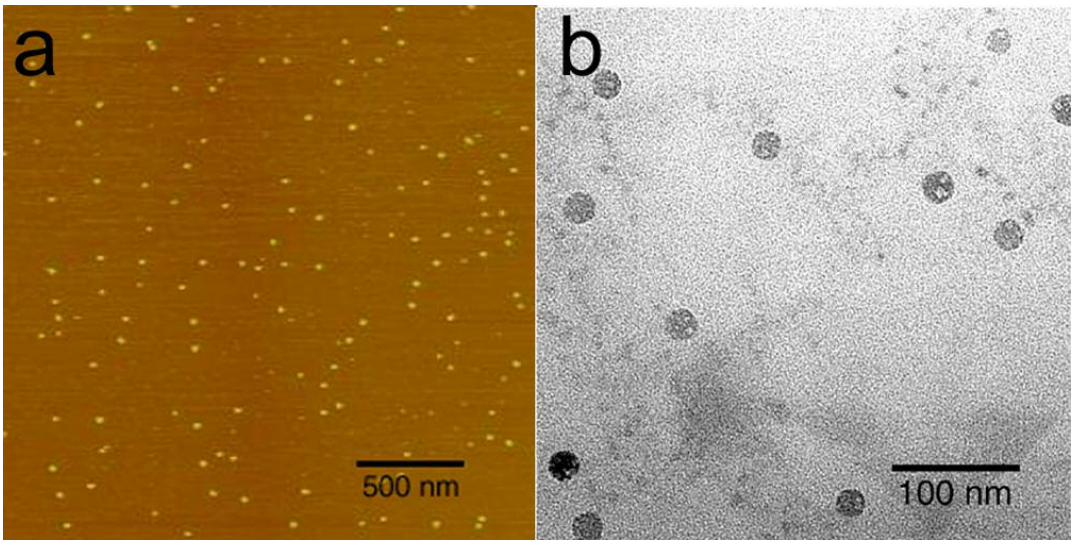

Figure 4.8 AFM (a) drop cast on mica and TEM (b) unstained of molecule **4.2**. These images depict a spherical nanostructure and the contrast in (b) is due to the Gd(III) chelation.

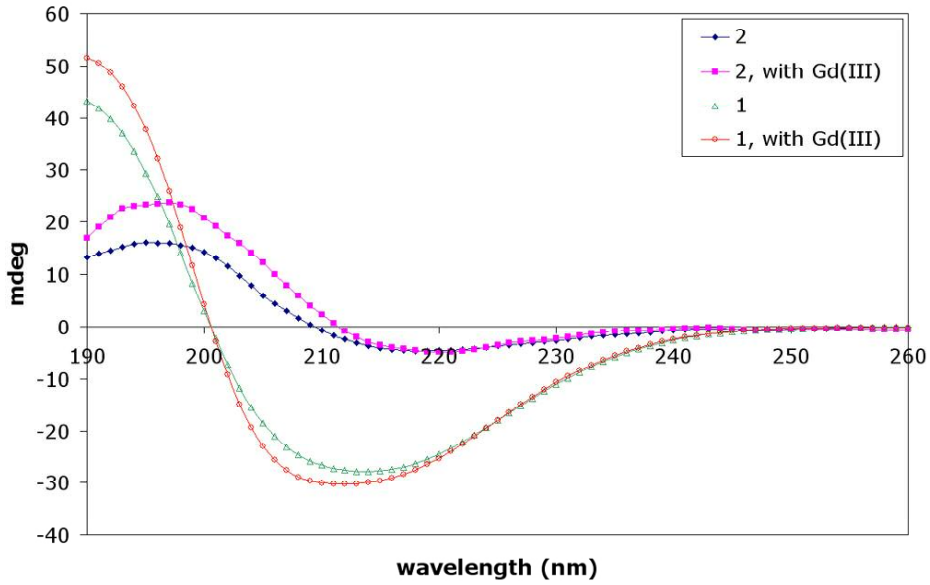

Figure 4.9 CD spectra of molecules **4.1** and **4.2** with and without Gd(III) chelation taken at 0.025 mM and pH of 7.4. PACA **4.2** without Gd(III) (blue curve), PACA **4.2** with Gd(III) (pink curve), PACA **4.1** without Gd(III) (green curve), and PACA **4.1** with Gd(III) (orange curve).

The spectra show an atypical β-sheet motif in PACA **4.1** and a weaker and structurally less defined signal for PACA **4.2**.

4.4 Conclusions

In this chapter, I have described the design and synthesis of two MRI active PA monomers that self-assemble into different supramolecular structures, fibers and spherical micelles. The PA structure and architecture allow for an increase in τ_R as a result of self-assembly in basic water and will allow the integration of additional bioactive functions in these systems for variability in bioactivity of the amino acid sequence. The incorporation of a Gd(III) chelator does not change the self-assembly of the monomers as evidenced by AFM, TEM, and CD. The PACAs produce a supramolecular polymer that allow for the delivery of a high Gd(III) payload to the implanted region which is necessary for good imaging.[130] We envision using these molecules to non-invasively track PA gel scaffolds in vivo, allowing for a complete time-series of high-resolution three-dimensional MR images to reconstruct their fate.

4.5 Experimental

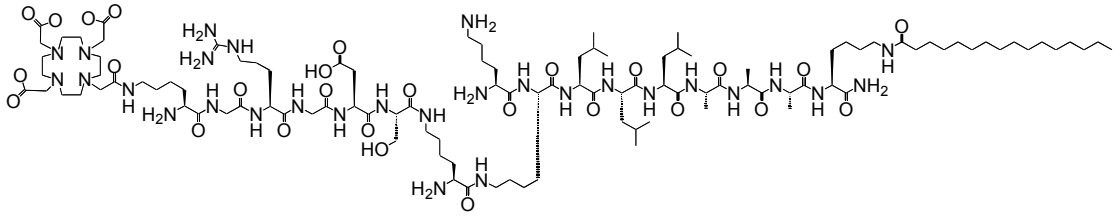

The branched PACA, **4.1**, was prepared by Fmoc solid phase peptide synthesis (SPPS) on a 0.1 mmol scale. The amino acids were purchased from NovaBiochem and the reagents from Sigma-Aldrich and used without further purification. The branching of the peptide head group was achieved using orthogonal protection group chemistry for the amines at the α and ε positions of the lysine residue.[131] Fmoc-Lys(Mtt)-OH, (Mtt: 4-methyl trityl) was coupled to MBHA Rink

Amide resin (NovaBiochem), followed by selective cleavage of the Mtt protecting group (1.5% TFA/DCM solution, shaken for 10 min) on the ε amine for palmitic acid coupling.[132] This was followed by Fmoc removal (30% piperidine in DMF for 10 min) on the α amine to grow the peptide segment of the PA. Amino acid coupling entailed use of the respective Fmoc amino acid (0.4 mmol), HBTU (3.9 mmol), HOBT (3.9 mmol), and DIEA (4.1 mmol) where each coupling reaction was shaken for 2.5 hours. The branching point in PACA **4.1** was introduced at a lysine again using Fmoc-Lys(Mtt)-OH. For PACA **4.1**, Boc-Lys(Boc)-OH was coupled at the end of the first branch where the branch was terminated. Both α and ε amine positions of the lysine were blocked with Boc protection as it is more stable under the cleavage conditions employed for the removal of Fmoc and Mtt. Mtt was removed and the peptide branch was grown by first using Boc-Lys(Fmoc)-OH. The peptide sequence RGDS,[133] important in cell adhesion where the RGD sequence binds to the integrin receptor, was elongated on the branch (using the ε amine) in order to combine bioactivity and MR functionality. The DOTA moiety was coupled on SPPS to the ε amine of a final Fmoc-Lys(Mtt)-OH using a tri-t-butyl ester protected DOTA purchased from Macrocyclics and the same coupling conditions of an Fmoc amino acid.[132] Global deprotection was achieved simultaneously with cleavage from the resin in 95:2.5:2.5 TFA:TIS:H_2O. Excess TFA was evaporated under reduced pressure and the crude PA solution was triturated using cold ether. PACA **4.1** was then dried under vacuum and characterized by MS-MALDI with a single peak found at 2308.66 (calcd. 2308.87).

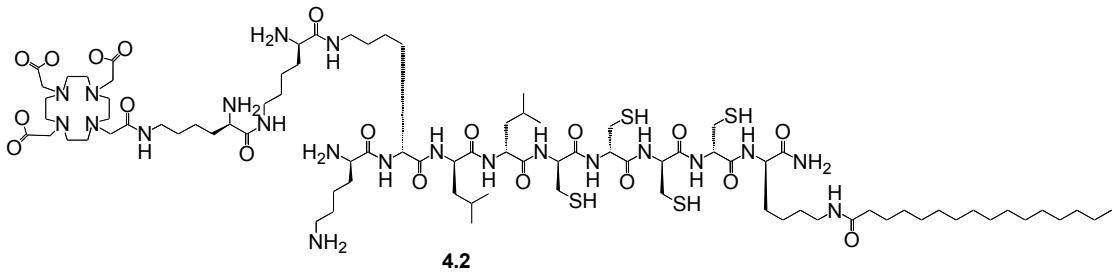

4.2

The branched PACA, **4.2**, was prepared by Fmoc solid phase peptide synthesis (SPPS) on a 0.1 mmol scale. Fmoc-Lys(Mtt)-OH, was coupled to MBHA Rink Amide resin (NovaBiochem), followed by cleavage of the Mtt protecting group on the ε amine for palmitic acid coupling via selective deprotection of the Mtt using a 1.5% TFA/DCM solution (10 min).[132] This was followed by Fmoc removal via a 30% piperidine in DMF solution (10 min) on the α amine to grow the peptide segment of the PA. Amino acid coupling entailed use of the respective Fmoc amino acid (0.4 mmol), HBTU (3.9 mmol), HOBT (3.9 mmol), and DIEA (4.1 mmol), where each coupling was shaken for 2.5 h. The branching point in PACA **4.2** was introduced at a lysine again using Fmoc-Lys(Mtt)-OH. For PACA **4.2**, Boc-Lys(Boc)-OH was coupled at the end of the first branch. Both α and ε amine positions of the lysine were blocked with Boc protection as it is more stable under the cleavage conditions employed for the removal of Fmoc and Mtt. Mtt was removed and Boc-Lys(Fmoc)-OH was attached. The ε-amine was deprotected and the DOTA moiety was coupled using a tri-t-butyl ester protected DOTA molecule purchased from Macrocyclics and the same coupling conditions of an Fmoc amino acid. Global deprotection was achieved simultaneously with cleavage from the resin in 95:2:2:1 TFA:EDT:TIS:H_2O (1,2-ethanedithiol was used to prevent sulfur crosslinking). Excess TFA was evaporated under reduced pressure and crude PA solutions were triturated using cold ether.

PACA **4.2** was then dried under vacuum and characterized by MS-MALDI with a single peak found at 1920.25 (calcd. 1920.12)

The final products, **4.1** and **4.2**, were obtained by the addition of $GdCl_3$ stirred at pH 6.5 for two days at RT and purified by dialysis in MilliQ water for three days (1000 MWC Spectrum Laboratories Inc.) changing the MilliQ twice per day.[134] PACA **4.2** was designed to have reversibly crosslinkable thiol bonds that can contribute to the stability of the supramolecular polymer (

Figure 4.2).[81, 135, 136]

CD measurements were performed on a Jasco J-715 CD spectrometer at concentrations of $2.50X10^{-5}$ M with a 1 mm cell path length. TEM microscopy was performed on a Hitachi H-8100 TEM instrument. Samples were prepared on holey carbon coated TEM grids by dipping the grid in the PA solution, rinsing, and wicking dry.

Inductively coupled plasma mass spectrometry (ICP-MS) was performed on a Thermo Jarrell Ash Atomscan Model 25 Sequential ICP Spectrometer. Samples were prepared by taking an aliquot of **5.2** and **5.3** from the stock solution used for relaxivity measurements and placed in 600 μL of neat nitric acid. Five mL of deionized water was added and the solution was sonicated for three minutes. The volume was brought up to 9990 μL with deionized water and 10 μL of an indium standard was added to bring the total volume to 10 mL.

Relaxivity measurements were performed on **5.2** and **5.3** by reconstituting the samples in deionized water to form stock solutions and the relaxivity experiments were performed on a Bruker mq60 NMR Analyzer (Bruker Canada, Milton, Ont., Canada) in pH 7.4 buffer (10mM 3-(N-morpholino)propane sulfonic acid (MOPS), 100 mM sodium chloride, 20 mM sodium bicarbonate, and 4 mM sodium phosphate monobasic) at 37 C. Four samples were prepared of

each **5.2** and **5.3** at concentrations of about 0.005, 0.01, 0.015, 0.02 mM (actual concentrations of Gd(III) were calculated from ICP-MS) with a total volume of 500 μL. Measurements were performed in at least triplicate and plotted as $1/T_1$ vs. mM Gd(III). The slope of this line provided the molar relaxivity per Gd(III) ion.

Chapter Five

Magnetic Resonance Imaging of Self-Assembled Biomaterial Scaffolds

Adapted from:

Bull, S. R.; Guler, M. O.; Bras, R. E.; Venkatasubramanian, P. N.; Stupp, S. I.; Meade, T. J. "Magnetic resonance imaging of self-assembled biomaterial scaffolds." *Bioconjugate Chemistry* **2005**, 16 (6), 1343-1348.

5 Peptide Amphiphile Contrast Agent (PACA) Imaging and Mixing Studies

5.1 Introduction

Current interest in human tissue repair has prompted the development of biomaterial scaffolds to envelop cells, mimicking the natural extracellular matrix and to help mediate processes such as cell proliferation and differentiation.[68, 137-139] Tissue repair in mature organisms can be crippled because many of the molecular cues present in early development are absent in later life. Peptide sequences (epitopes) can be used to influence specific cell matrix interactions leading to tissue formation, cellular differentiation, or for use as targeting moieties.[87, 140, 141] Therefore, providing a synthetic scaffold with specific epitopes affords the possibility of in vivo tissue regeneration.[139, 140]

Nanofiber networks derived from self-assembling peptide amphiphiles (PAs) have been used to mimic the bone's extracellular matrix and provide a scaffold to direct the differentiation of neural progenitor cells in vitro.[81, 87] PA molecules contain a peptide sequence at one terminus that is hydrophilic relative to the hydrophobic alkyl segment (**Figure 5.1**). The PA's charge and amphiphilic nature provides solubility and promotes self-assembly in aqueous media into long cylindrical structures that are nanometers in diameter and up to microns in length (**Figure 1.10**).[81, 82, 87, 142-144] These supramolecular structures preferentially form fibrous strands because of hydrogen bond formation between the amino acids of adjacent PA molecules producing a β-sheet motif and stabilizing the elongated structures. In our case, the β-sheet forming sequence of LLLAAA together with the hydrophobic alkyl tail's (palmitoyl chain) collapse is thought to be the driving force to form extended structures, rather than spherical micelles.[144] Upon charge screening by pH change or divalent cations, the high aspect ratio nanofibers form a three-

dimensional network trapping water, to create a self-supporting gel that is 99% water by mass.[81, 144] Since the hydrophilic portion of the PA contains charged amino acids and are accessible to the aqueous environment, the self-assembled nanofibers can present a high density of epitopes on the periphery[81, 143, 144] of the nanofibers to interact with cells trapped/doped within.[87] In order to understand the scaffolds properties in vivo, it is necessary to noninvasively elucidate the structural degradation and migration of the self-assembled materials post-implantation.[145-149]

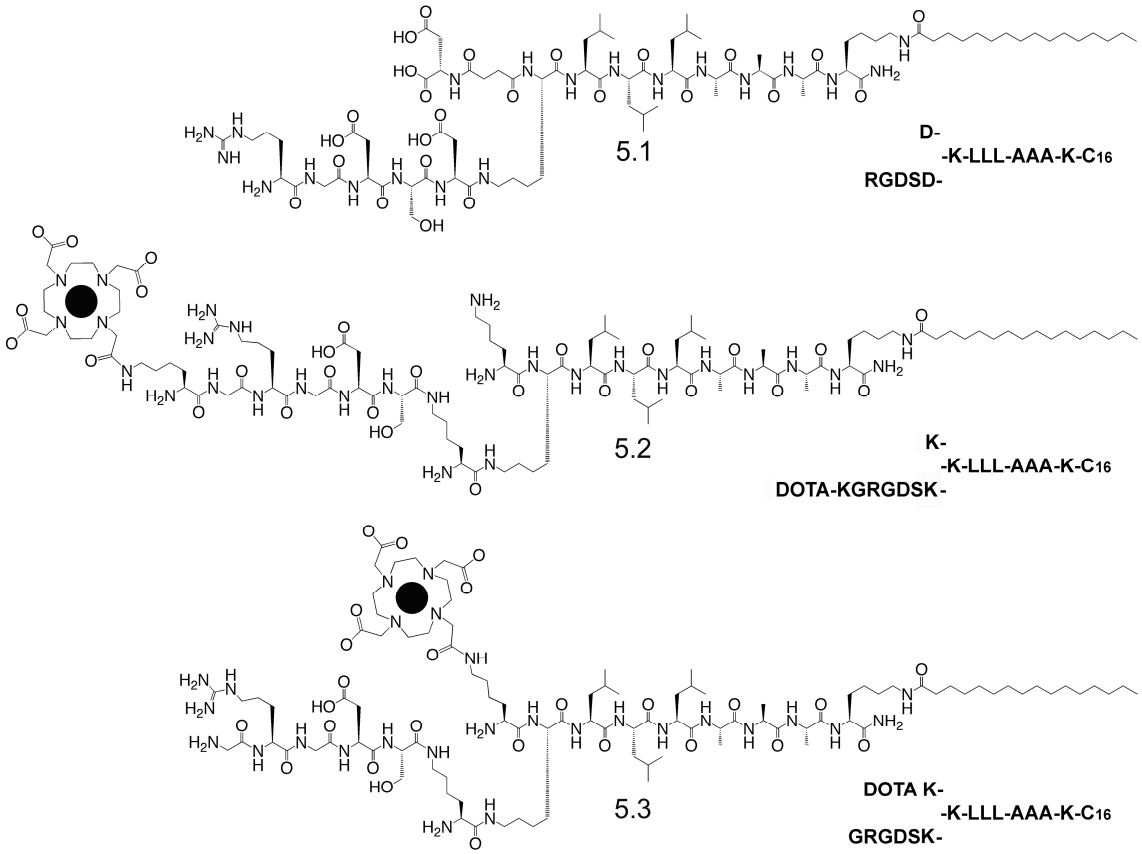

Figure 5.1 Structures of the PA molecules with the black circles representing the Gd(III) ion. PA **5.1** is an example of a filler PA and does not contain the Gd(III) chelate. PACAs **5.2** and **5.3** are the PACA molecules used in this chapter that containing Gd(III).

Magnetic Resonance Imaging (MRI) is a noninvasive technique for in vivo imaging and is an ideal tool for fate mapping of tissue scaffolds at near cellular resolution.[112, 148, 150] MRI does not contain high energy photons as does computed tomography, instead it relies upon only a

magnetic field and low energy radio waves. We have chosen this modality to image self-assembled gels that integrate into their structure PA molecules conjugated to Gd(III) contrast agents (PACAs). In Chapter 4, I reported on the synthesis and characterization of PACA derivatives of PA molecules that were capable of self-assembling into nanofibers or spherical micelles.[98] In this chapter, I report on the synthesis, in vitro, and in vivo images of two PACA derivatives mixed with a variety of epitope bearing PA biomaterials describing the versatility in the PACAs' utility. A number of reports have described the use of MRI to track implants in vivo, [145, 147, 148, 151-154] however, to our knowledge this is the first demonstration that rationally designed self-assembled biomaterials conjugated with MR contrast agents can be imaged.

5.2 General Synthesis of Peptide Amphiphiles

Peptide amphiphiles **5.1**-**5.3** were all synthesized using Fmoc solid phase synthesis technique. Branching was accomplished by use of an orthogonally protected lysine (with Mtt) that could be deprotected while on the solid phase leaving a free ε amine for further conjugation (**Figure 4.1**). Cleavage from the resin provided a global deprotection for the PACA molecules and subsequent reaction with $GdCl_3$ afforded the final PACA products **5.2** and **5.3** (**Figure 5.1**). The filler PAs found in **Figure 5.5** were synthesized on the solid phase by either Mustafa Guler or Krista Niece. Details of these PA synthesis can be found in their dissertations and will not be discussed in this document.

5.3 Results

The Gd(III) chelator is a DOTA derivative (**Figure 1.1**) selected because of its high binding affinity with lanthanide ions and synthetic versatility.[7] PA **5.1** (filler PA) is a self-assembling PA that forms self-supporting gels and is similar in sequence to **5.2** and **5.3** but does

not contain the Gd(III) chelator, and thus was used as a standard to compare to the MR images of the gels with Gd(III). Gels of **5.1** and **5.2** or **5.1** and **5.3** were prepared to demonstrate the minimal concentration of peptide amphiphile contrast agent (PACA) needed to obtain good MR contrast, leaving the remaining PA molecules free to present different epitopes on the nanofibers giving rise to more bioactive versatility. Varying the position of the tethered DOTA derivative on the PAs induces changes in the molecule's relaxivity (efficiency) and imaging utility.[98] The PACA derivatives described contain the RGD peptide sequence, a well-known epitope in integrin-binding domains of extracellular proteins that is critical for adhesion of many types of cells to the extracellular matrix.[155] We have observed that positioning the chelate close to the core of the molecule results in a higher relaxivity.[98] PACAs **5.2** and **5.3** differ in the position of the Gd(III) chelator, that results in a change in relaxivity in the self-assembled state from 14.7 ± 0.8 $mM^{-1}s^{-1}$ [98] to 21.5 ± 1.1 $mM^{-1}s^{-1}$ respectively (normalized to ICP measurements of Gd(III) conentration) at pH 7.4 (buffer, 10mM 3-(N-morpholino)propane sulfonic acid (MOPS), 100 mM sodium chloride, 20 mM sodium bicarbonate, and 4 mM sodium phosphate monobasic). The difference in relaxivity between **5.2** and **5.3** is likely due to a difference in the rotational correlation time, τ_R, arising from decreased internal flexibility (increased rigidity) from increased steric hindrance of the chelator in **5.3** as compared to **5.2**.[112, 156, 157]

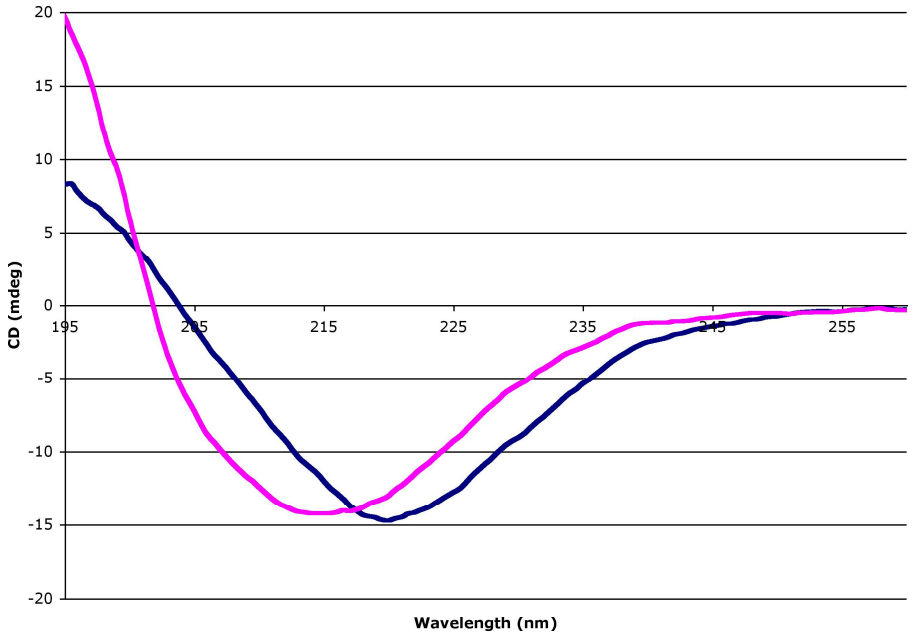

Figure 5.2 CD of **5.3** with Gd(III) (blue) without Gd(III) (pink). CD shows characteristic β-sheet absorbance in the 220 nm region. There is a slight shift in the curves because of a less perfect extended β-sheet without Gd(III). This less perfect self-assembly is believed to be caused by the steric bulk and charge of the DOTA moiety without Gd(III).

Transmission electron microscopy (TEM) and atomic force microscopy (AFM) reveal the supramolecular structural aggregates from **5.1**, **5.2**,[98] and **5.3**. Both **5.2** and **5.3** self-assemble into fibers at pH greater than 7.0 and **5.1**, **5.2**, and **5.3** form uniform nanofibers microns in length. The fiber diameter of structures formed by **5.3** was calculated from AFM height measurements to be 6.0 ± 0.1 nm with 95% confidence (**Figure 5.3**). A self-supporting gel is formed upon mixing **5.2** or **5.3** with **5.1**, followed by sonication and buffer addition. Circular dichroism (CD) spectroscopy was used to probe the hydrogen bonding interaction in the supramolecular polymer to compare with the structural observations in dried films obtained by TEM and AFM (**Figure 5.2**). The minima of **5.2** and **5.3** without Gd(III) revealed a peak at 212 nm, signifying a β-sheet like hydrogen bonding character,[129] which supports fiber formation in the samples seen by microscopies. These shifts in spectra from ideal β-sheets (218 nm), are thought to be from the

change in hydrogen bonding caused by both the chelator and the branching motif used in synthesis.

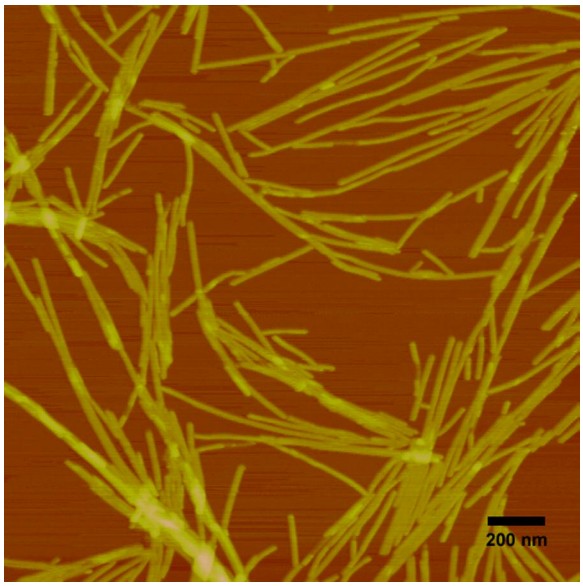

Figure 5.3 AFM micrograph of nanofibers formed from **5.3**. This image depicts the supramolecular assembly of the PACAs into fibers. These high aspect fibers then form a network trapping water and creating a gel. The fiber heights correspond to 6.0 ± 0.1 nm.

We found the resulting gel formed from the mixing PACAs **5.2** or **5.3** with filler PA **5.1** could be successfully imaged by MR (**Figure 5.4**). The gels are homogeneous in image intensity throughout the samples, which implies uniform mixing of the PACA molecules within the filler PA at MR resolution. If heterogeneous mixing of PAs occur on a large enough scale domains of bright and dark intensity would be observed. **Figure 5.4** shows the difference in observed contrast between **5.1** (without Gd(III)), **5.2** mixed with **5.1**, **5.3** mixed with **5.1**, and a standard small molecule MR contrast agent diethylenetriamene pentaacetate (DTPA) doped into **5.1** (0.1 mM Gd(III)). The gels were formed using a 0.75 weight percent of filler PA. The PACA molecule was mixed into this solution before inducing gelation as was the DTPA for images created in **Figure 5.4**. The T_1 of these gels were measured at 3.03 ± 0.05 s, 1.89 ± 0.06 s, 1.08 ±

0.06 s, and 2.81 ± 0.05 s respectively, the shorter T_1's resulting in higher contrast. There is difference of over 35% in T_1 relaxation time providing facile imaging. This clearly demonstrates the utility of using a contrast agent with a high relaxivity for imaging biomaterials.

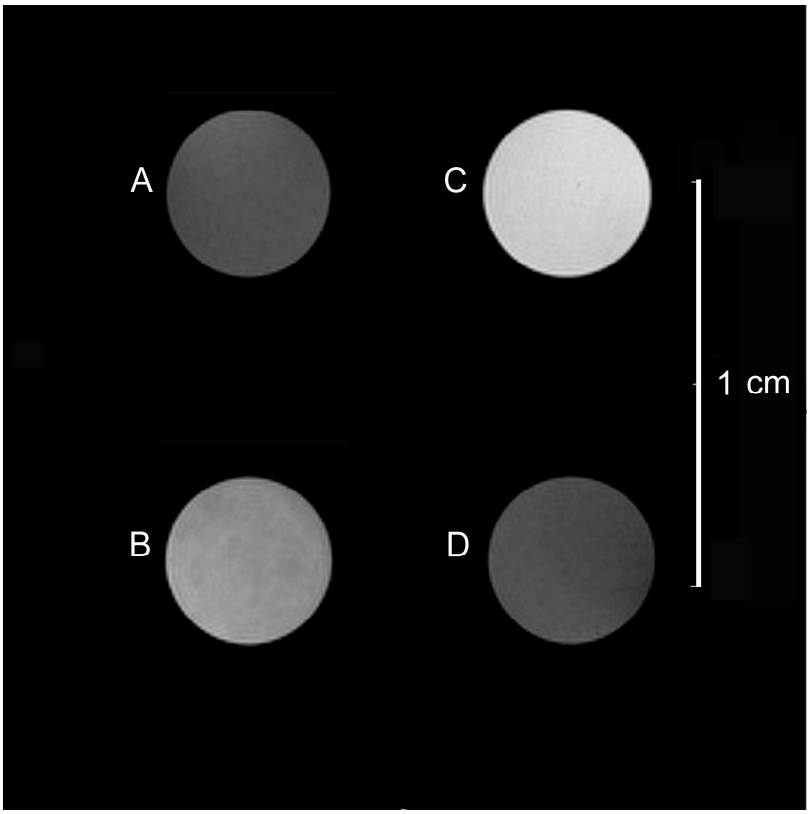

Figure 5.4 MR images of the phantom gels formed from **5.1**, **5.1** and **5.2**, **5.1** and **5.3**, and a Gd(III) DTPA standard corresponding to A, B, C, and D respectively. The contrast arising from **5.3** is the greatest due to an increase of τ_r for the Gd(III) chelator.

A PACA that is able to mix homogeneously with a variety of different epitope containing PAs is important for biomaterial specificity. Using a PACA that universally mixes with other PAs simplifies the in vivo tests for fate mapping of different gels and allows for differing bioactivity without synthesizing a new PACA for every material. We tested the ubiquitous nature of **5.3**, owing to its higher relaxivity, with differing types of PA. We used a variety of PAs similar and different in structure and sequence (**Figure 5.5**) to the PACA to gain a full

understanding of the imaging properties. The filler PAs were chosen based on their structure, epitopes, and sequence terminus (either C-terminus or N-terminus). **Figure 5.5**, **h**, **i, j**, are all linear PAs synthesized C to N-terminus with an IKVAV epitope [87] used for neuronal stem cell differentiation. PAs **e** and **f** are branched PAs containing the IKVAV epitope and **e** contains the YIGSR epitope as well for use in neuronal stem cell differentiation. PA **g** is branched and contains the RGD epitope for cell adhesion. All samples formed aqueous self-supporting gels at 1% by weight and were imaged in a 400 MHz magnet. All of the gels imaged were of homogeneous signal intensity and the T_1's of the gels were all similar values when doped with equal amounts of **5.3** (**Figure 5.5**). This finding shows the robustness and consistency of **5.3** and its ability to be used in differently structured and epitope presenting biomaterials.

Not every PACA made will mix homogeneously as in the case of the cystine containing PA previously published.[98] Depicted in **Figure 5.6**, one is able to see that the areas of light and dark are due to the incomplete mixing or phase separation of the cystine containing PA from the filler PA. The gel was prepared in the same manner as **Figure 5.4**. We believe phase separation of the spherical micelles from the fibers account for the lack of homogeneity seen in the MR image.

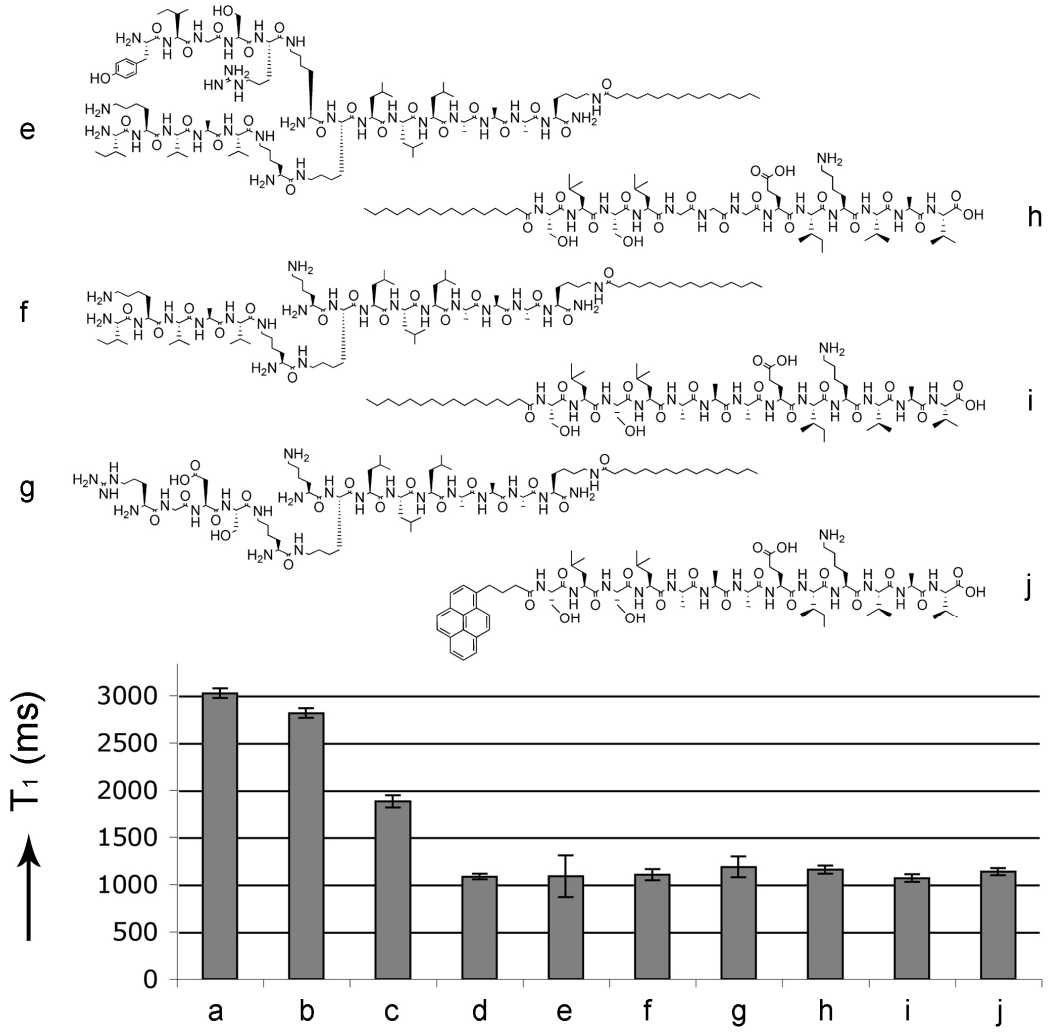

Figure 5.5 Results of T_1 study of PA gels and mixed PA gels. The concentration of Gd(III) is 0.1 mM in all samples except a and the concentration of filler PA is 1% by weight in each case (all samples form self-supporting gels). (a) corresponds to **5.1** alone and is used as a standard, (b) refers to **5.1** mixed with DTPA, (c) refers to **5.1** mixed with **5.2**, (d) refers to **5.1** mixed with **5.3**, (e) – (j) are mixed with **5.3** and their structures are depicted above. Error bars represent one standard deviation.

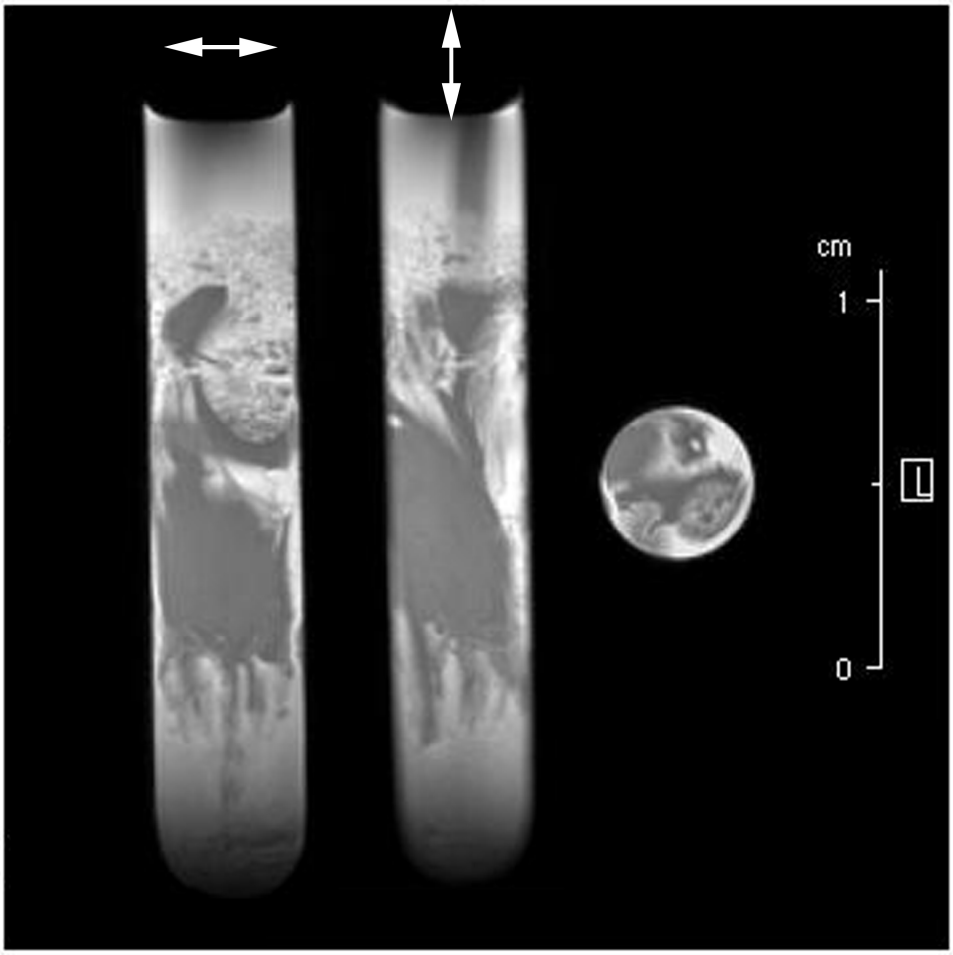

Figure 5.6 MR images of the phantom gels formed from **5.1** and **4.2**. The bright areas arise from **4.2** and the darker areas are from the filler PA. This mixture is not homogeneous owing to phase separation of the spherical micelles and the nanofibers.

This work has spurred the in vivo testing of the PACA mixing with a PA specific for promotion of vasculogenesis within a porcine heart in collaboration with the Beohar group at Northwestern University (**Figure 5.8**). The porcine was induced with an infarct, cutting the blood supply and causing death to part of the heart muscle. The function of the PA mixture was to induce vasculogenesis to promote regeneration of the dead heart muscle and to visualize this process using MRI. The functional PA used has an epitope designed to bind to heparin for the promotion of vasculogenesis (**Figure 5.10**).[88] These experiments were the first in vivo imaging

of the PA biomaterial, giving rise to the first data describing the temporal fate of the biomaterials.

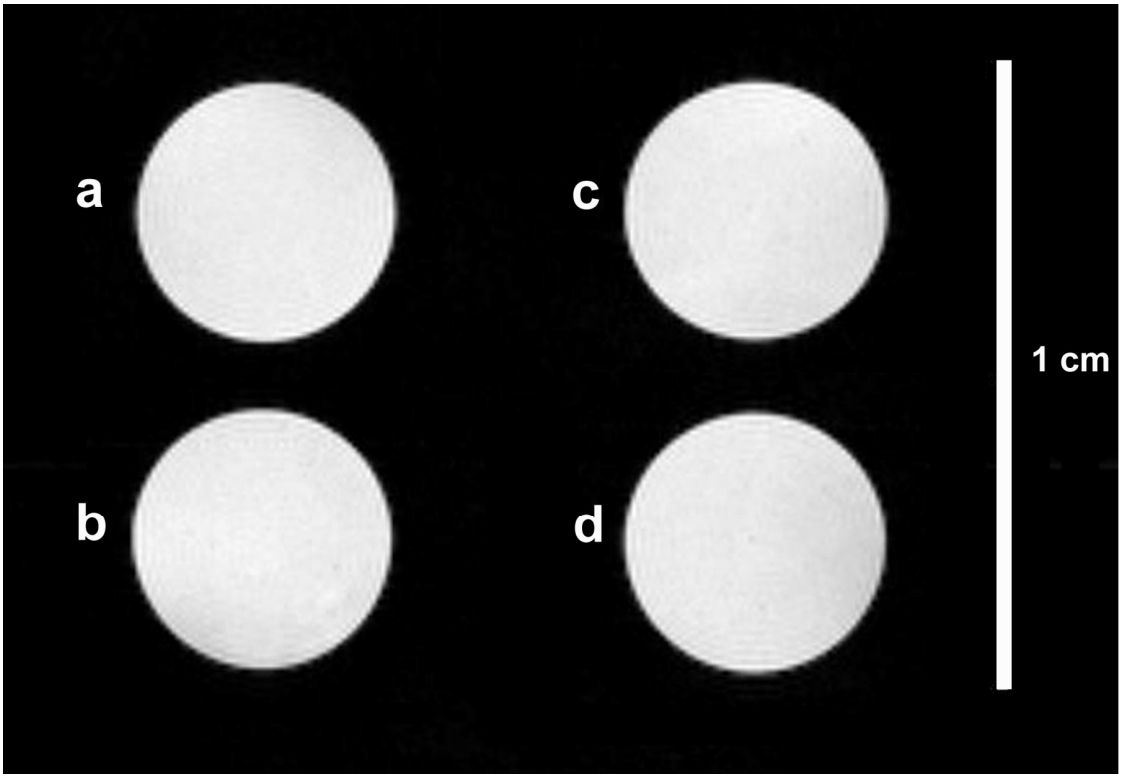

Figure 5.7 MR image of phantoms depicting **g**, **h**, **i**, **j** (**Figure 5.5**) in **a**, **b**, **c**, and **d** respectively. There is no apparent visible difference owing to the similar relaxivities of each gel using **1** as the filler PA. All samples were found to be homogeneous throughout.

The gel was easily distinguishable in the heart for up to two weeks post implantation but was not visible at four weeks (**Figure 5.8**). The heart muscle is colored black and the blood, owing to the blood pool contrast agent, is colored white. The PACA was used as a 0.1 mM concentration of Gd(III) mixed with the heparin binding PA. These PA solutions were designed to gel in vivo and promote the vascularization of the dead heart muscle. Time points did not cover the time in between these and further work is required, but this preliminary data vividly shows the utility of the PACA for use in fate mapping the PA biomaterial. As seen in **Figure 5.9**, we are able to vary the concentration of PACA doped into bioactive PA gels and customize

the T_1 relaxation times (the contrast) observed. This variation will allow one to customize the contrast for different areas in the body depending upon background signal.

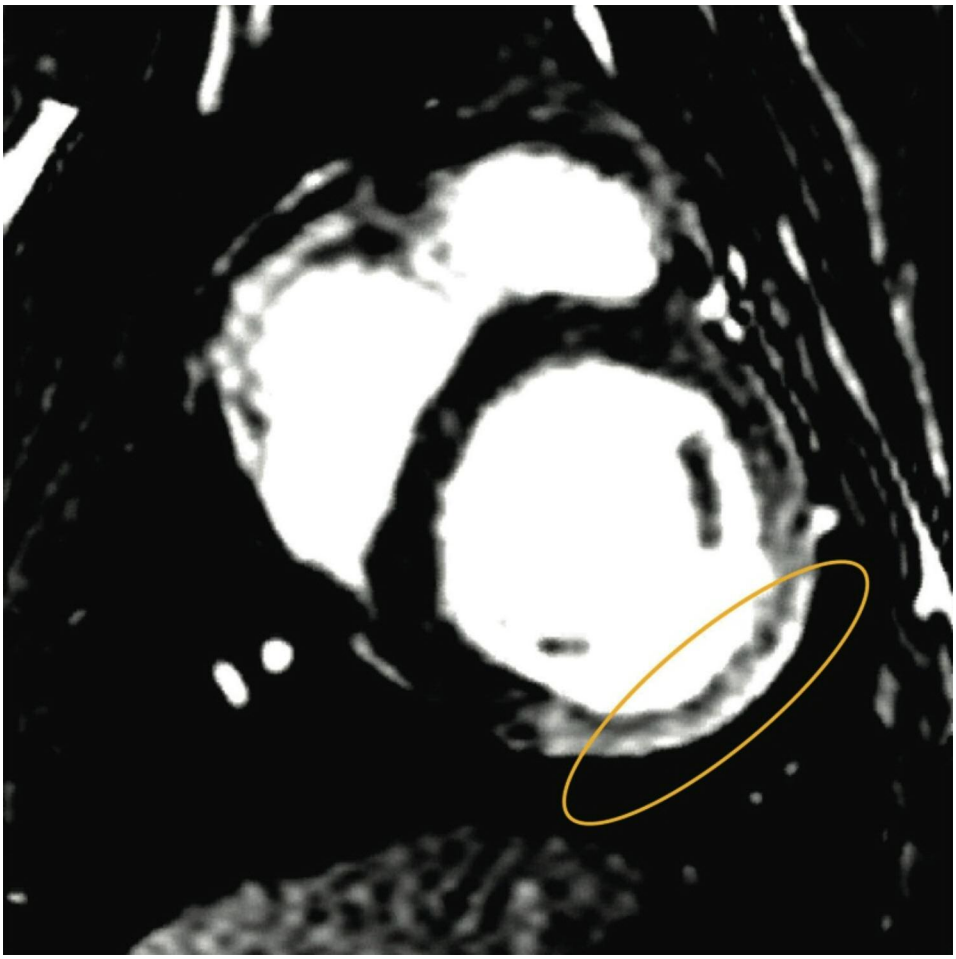

Figure 5.8 Image of porcine heart with a mixed gel of PACA (**5.3**) and heparin binding PA. The muscle is colored black (contrast was adjusted for optimal viewing) and the blood is colored white (owing to the use of a blood pool CA). The circle portion of the heart is dead and does not beat with the rest of the heart muscle, and the enhanced contrast is from the injection of the PA mixture. This image was taken 96 hours post injection of the PA mixture on a 1.5 T MRI unit.

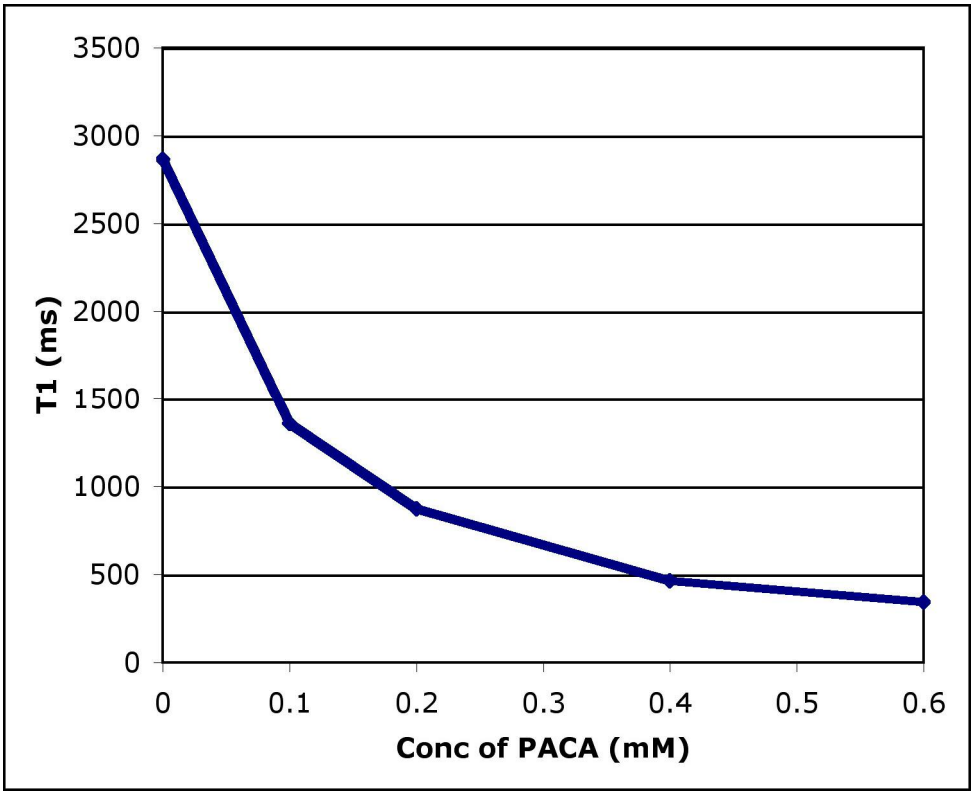

Figure 5.9 Graph depicting the T1 relaxation time versus concentration for the PACA. The measurements were taken at 60 MHz with **5.1** as the filler PA in each sample.

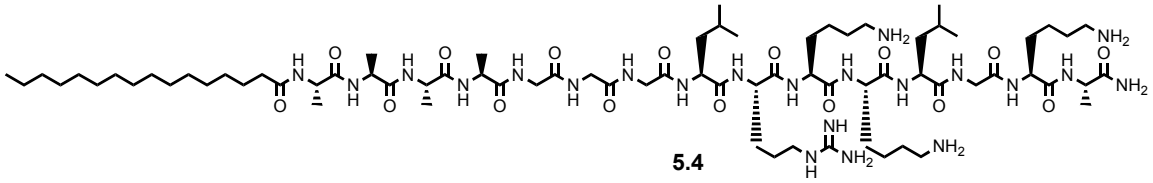

Figure 5.10 Heparin binding PA (HBPA) (**5.4**) that was mixed with the PACA to perform in vivo porcine heart experiments.

Further experiments were carried out using a mixture of **5.4** and **5.3** on mouse models for β-islet transplantation. This work was completed by Ellen Kohlmeir and Lesley Chow and all details of the experiment can be found with them but are beyond the scope of this thesis. The first experiment used the kidney capsule as a model site for PA gel transplantation (**Figure 5.11**). It was discovered that using 0.1 mM of **5.3** doped into a 2% by weight gel of **5.4**, one is able to clearly depict the implanted gel. Without PACA addition, one is unable to find the implanted gel

owing to the lack of differentiating contrast between the biomaterial and surrounding tissue. This kidney model experiment was accomplished by injection of 10 μL of a solution containing 0.1 mM of **5.3** with a 2% by weight solution of **5.4**. This was followed by a 10 μL solution

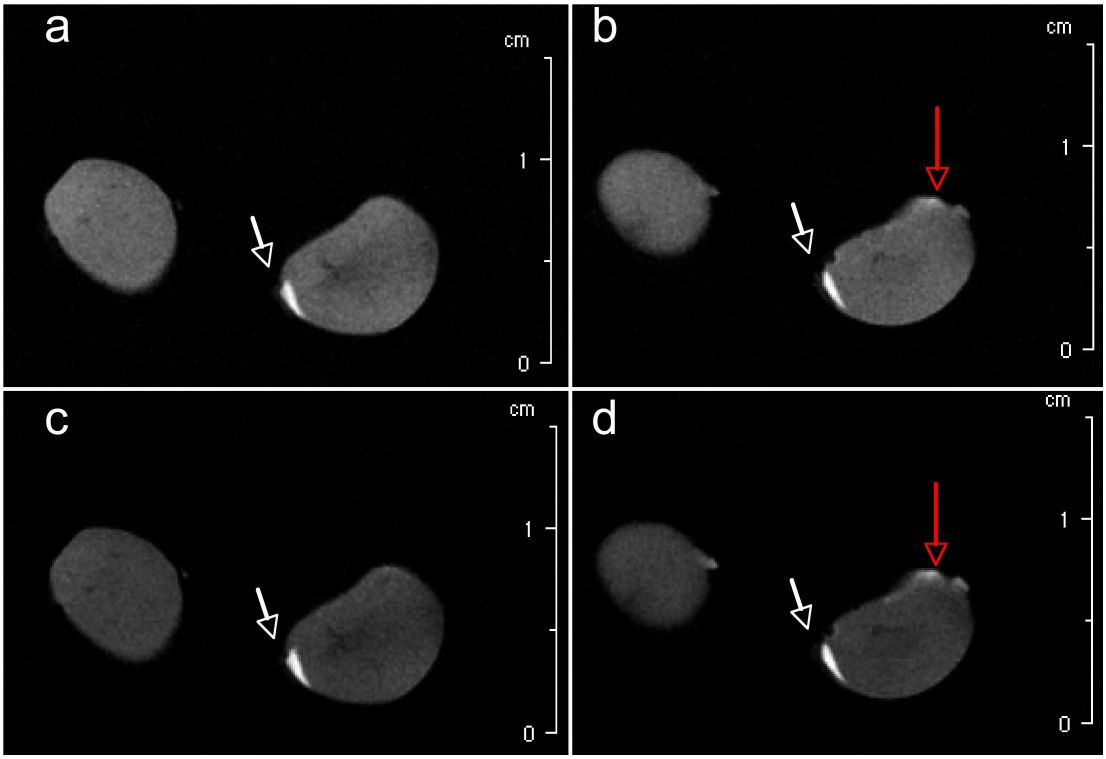

Figure 5.11 Mouse kidneys where the right kidney was injected with the HBPA (**5.4**) and PACA (**5.3**, 0.1mM) mixture and the left kidney was injected with HBPA only where the white arrow corresponds to the PACA gel mixture and the red arrow corresponds to fat. Images (a) and (b) are without fat suppression and images (c) and (d) mirror those of (a) and (b) respectively with fat suppression. Imaging with a T_1 weighted pulse sequence with a TE of 14.6 ms and a TR of 200 ms on a 4.7 T magnet.

of heparin to initiate gellation, after which the mouse was sacrificed and the kidneys were excised and fixed in a 10% buffered neutral formalin solution. Further in vivo experiments with mice are currently underway but this preliminary data exemplifies the utility of PACA **5.4** in regards to noninvasively fate mapping the biomaterial in vivo.

Another experiment using **5.4** in combination with **5.3** was to form gels for encapsulation of pancreatic islets that were labeled with a T_2 iron oxide particle. This work was done in collaboration with Ellen Kohlmeir and Lesley Chow and the details of the experiment can be found with them. The phantoms showed that using a T_1 weighted pulse sequence there is a distinct difference between the gel with and without **5.3**. Using a T_2 pulse sequence it is evident that the islets are labeled and able to be visualized (**Figure 5.12**). This demonstrates that the PACA could feasibly be used in combination with a T_2 cellular label in a system where you could take advantage of the different MR pulse sequences to image the islets and their scaffold in vivo. One could envision a system where both the gel and islets are visible initially and as the gel degrades the T_1 signal diminishes and the T_2 signal remains. Further work with labeled islets is underway.

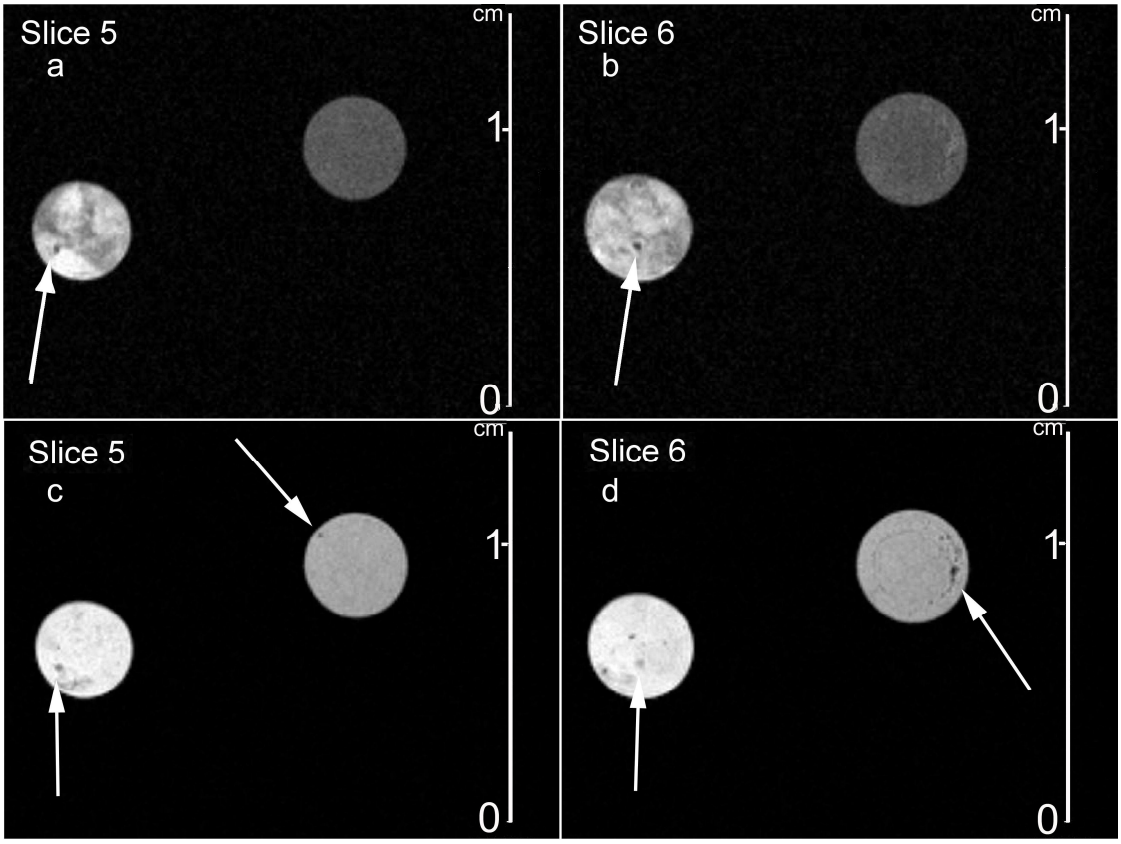

Figure 5.12 These samples are phantom gels of HBPA (**5.4)** with (right image in each pane) and without PACA (**5.3**) (left image in each pane) with embedded β-islets labeled with an iron oxide T_2 contrast agent. The white arrows depict the labeled islets and one is unable to see any islets in the HBPA sample without **5.3** mixing. Images (a) and (b) were taken with a T_1 weight sequence with a TE of 14.6 ms and TR of 500 ms on a 4.7 T magnet and images (c) and (d) were taken with a T_2 weighted pulse sequence with a TE of 30 ms and TR of 2000 ms on a 4.7 T magnet.

5.4 Conclusions

The ability to noninvasively image gels formed by scaffolds of PA nanofibers doped with self-assembling PACA molecules, provides a means for in vivo fate mapping of these new biomaterials. Our study compared two PACA molecules differing in the position of the Gd(III) chelator and used a variety of mixed systems to elucidate the minimal amount of PACA needed to achieve a homogeneous and significant signal intensity throughout the gel. We discovered that placing the Gd(III) closer to the hydrophobic region of the self-assembling molecules provides an increase in relaxivity and that **5.3** can be used with a variety of different PA gels.

Further studies included the in vivo fate mapping of a heparin binding PA within a porcine heart and mouse kidney model. Our study showed that the gel was clearly visible up to two weeks but not four weeks after implantation signifying the material is indeed degraded within the body. We have demonstrated the PACA utility when it comes to imaging T_2 labeled β-islet cells within a PA gel.

5.5 Experimental

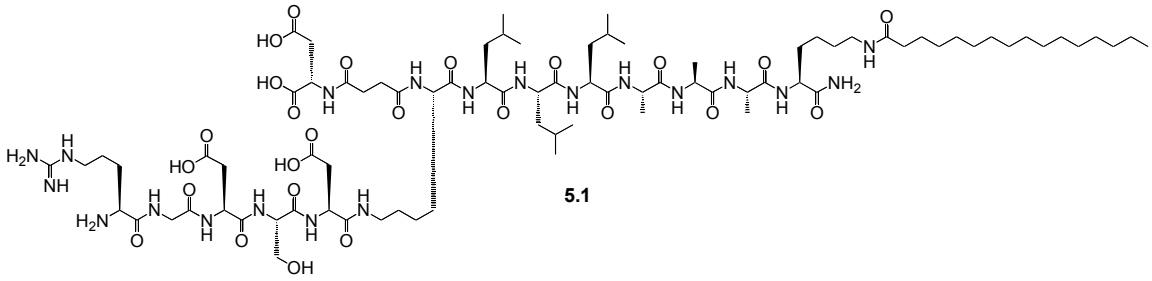

5.1

Preparation of 5.1. Amino acids were purchased from NovaBiochem and all other reagents were purchased from Sigma-Aldrich and used without further purification unless otherwise stated. The branched PAs **5.1** was prepared by 9-fluorenylmethoxycarbonyl (Fmoc) solid phase peptide synthesis (SPPS) on a 0.1 mmol scale. PACA **5.1** was prepared by SPPS, and branching of the peptide head group was achieved using orthogonal protecting group chemistry for the amines at the α and ε positions of the lysine residue.[98, 131] Fmoc-Lys(Mtt)-OH, (Mtt: 4-methyl trityl) was coupled to MBHA Rink Amide resin, followed by cleavage of the Mtt protecting group on the ε-amine to couple palmitic acid without affecting Fmoc protection with a 5% TFA in DCM solution for 5 minutes. This was followed by Fmoc removal on the α-amine to grow the LLLAAA peptide segment of the PA using 30% piperidine/DMF solution for (10 min). The branching point was introduced at a lysine dendron using Fmoc-Lys(Mtt)-OH. To grow the

first arm of the PA, Fmoc on the α-amine was removed before the Mtt protecting group. L-Aspartic acid di-tert-butyl ester hemisuccinate residue was coupled to the first branch. The Mtt on the ε-amine of the lysine residue was removed (5% TFA in DCM for 5 min) and bioactive peptide sequence RGDS was grown. The aspartic acid residue prior to the RGDS was coupled to increase solubility of the molecule in water. PA **5.1** was cleaved from the resin in 95:2.5:2.5 TFA:TIS:H_2O. Excess TFA was evaporated under reduced pressure and the crude PA solution was triturated using cold ether. MALDI-TOF Mass Spec. 1810.40 (calcd. 1810.14)

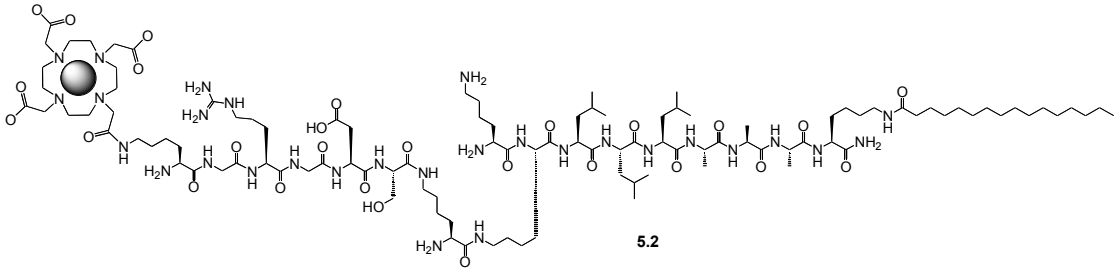

5.2

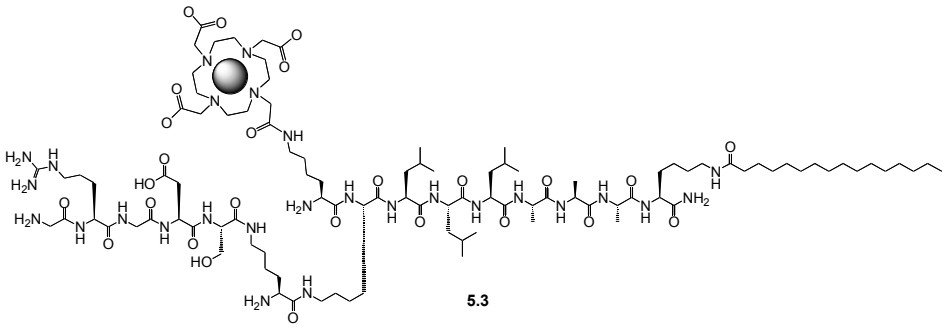

5.3

PACAs **5.2** and **5.3** were synthesized using orthogonal protection group chemistry for the amines at the α and ε positions of the lysine residue. Fmoc-Lys(Mtt)-OH was coupled to MBHA Rink Amide resin, followed by cleavage of the Mtt protecting group on the ε-amine for palmitic acid coupling without affecting the Fmoc protection. This was followed by Fmoc removal on the α-amine to extend the peptide segment of the PA. The branching point in the PAs was

introduced at a lysine dendron using Fmoc-Lys(Mtt)-OH. To extend the first arm of PAs, Fmoc on the α-amine was removed prior to Mtt removal. For molecule **5.2**, Boc-Lys(Boc)-OH was coupled at the end of the first branch. Both α and ε-amine positions of the lysine were protected with Boc as it is more stable under the cleavage conditions employed for the removal of Fmoc and Mtt. For **5.3**, Boc-Lys(Fmoc)-OH was coupled as the first branch. Fmoc was deprotected and tris-t-butyl protected DOTA (purchased from Macrocyclics) was coupled at the end of the first branch. Mtt was removed and the other branch was grown using Boc-Lys(Fmoc)-OH. The peptide sequence RGDS (important in cell adhesion) was coupled to the ε-amine in order to combine bioactivity and MR functionality. For **5.2**, the DOTA moiety was coupled on SPPS to the N-terminus of the peptide sequence by using a t-butyl ester protected DOTA molecule. PACAs **5.2** and **5.3** were cleaved from the resin in 95:2.5:2.5 TFA:TIS:H_2O. Excess TFA was evaporated under reduced pressure and crude PA solutions were triturated using cold ether. PACAs **5.2** and **5.3** were then dried under vacuum and characterized by MALDI-MS with a single peak found at 2308.66 (calcd. 2308.87) and 2180.02 (calcd. 2179.69) respectively. The final product was obtained by the addition of $GdCl_3$ with stirring at pH 6.5 for 72 h and purified by dialysis in deionized water (1000MWC Spectrum Laboratories Inc.).[132] Samples were then lyophilized into a white powder. MALDI-MS showed peaks at 2464.40 (calcd. 2463.09) and 2336.08 (calcd. 2335.61) corresponding to **5.2** and **5.3** M+H respectively.

Inductively coupled plasma mass spectrometry (ICP-MS) was performed on a Thermo Jarrell Ash Atomscan Model 25 Sequential ICP Spectrometer. Samples were prepared by taking an aliquot of **5.2** and **5.3** from the stock solution used for relaxivity and T_1 measurements and placed in 600 μL of neat nitric acid. Five mL of deionized water was added and the solution was

sonicated for three minutes. The volume was brought up to 9990 μL with deionized water and 10 μL of an indium standard was added to bring the total volume to 10 mL.

Relaxivity measurements were performed on **5.2** and **5.3** by reconstituting the samples in deionized water to form stock solutions and the relaxivity experiments were performed on a Bruker mq60 NMR Analyzer (Bruker Canada, Milton, Ont., Canada) in pH 7.4 buffer (10mM 3-(N-morpholino)propane sulfonic acid (MOPS), 100 mM sodium chloride, 20 mM sodium bicarbonate, and 4 mM sodium phosphate monobasic) at 37 C. Four samples were prepared of each **5.2** and **5.3** at concentrations of about 0.005, 0.01, 0.015, 0.02 mM (actual concentrations of Gd(III) were calculated from ICP-MS). Measurements were performed in quadruplicate and plotted as $1/T_1$ vs. mM Gd(III). The slope of this line provided the molar relaxivity per Gd(III) ion.

T_1 measurements were performed on a 9.4 T Oxford superconducting magnet (Bruker). The samples were prepared by making a 4% by weight solution of **5.1** in water. This solution was then aliquoted into four separate three-dram vials. The appropriate amount of Gd(III) containing molecules in aqueous solution was added to each vial to bring the concentration of Gd(III) to 0.1 mM (normalized to ICP measurements of Gd(III) concentration). Excess water was added to bring the total volume to 250 μL. These solutions were sonicated for 30 s and transferred to 5 mm NMR tubes. 50 μL of 0.1 M calcium carbonate buffer was added to each tube to increase the pH and induce gelation. Four sample tubes were bound together using parafilm wax and inserted into the magnet. Images were acquired using a spin-echo pulse sequence with TR of 152, 200, 400, 750, 1000, 1400, 1800, 2500, 4000, 10,000 ms, TE 12 ms, slice thickness of 1 mm (eight slices taken), and FOV of 2 cm.

Circular Dichroism (CD) was performed on a Jasco J-715 CD spectrophotometer using a 2 mm quartz cuvette. Samples were prepared from the stock solution in water to a final concentration of 3.33×10^{-6} M at a pH of 7.4 in PBS buffer. Five spectra from 190 nm to 260 nm were averaged together.

AFM preparation was from the same stock solutions of **5.1**, **5.2**, and **5.3** (0.005 mM) that were used to determine relaxivity, diluted 1:10 with deionized water. Samples were prepared by drop casting 5 μl of the diluted solutions onto freshly cleaved mica substrates. Samples were allowed to rest for two minutes prior to excess solution was wicked away. After drying in air AFM was preformed with a Digital Instruments MultiMode III SPM with a Quadrex extender and Olympus AC240TS cantilevers in tapping mode. Height measurements were taken on 149 straight fiber segments using the cross sectional averaging tool included in Digital Instruments Nanoscope III acquisition analysis software.

PA mixing for the in vivo porcine experiment, mouse kidney, and islet phantoms were carried out with addition of about 1:200 PACA to heparin binding PA monomers. These solutions were then gelled with the addition of heparin in vivo for the case of the porcine and mouse kidney experiments. Four separate injections of the PA mixtures were performed on the heart and imaging was performed at 48 hr, 72 hr, and four weeks on a 1.5 T MR magnet with a total injection volume of ~100 μL. The mouse kidneys were excised within one hour after injection of a 20 μL gel sample and imaging was performed on a 4.7 T MR magnet. The islet phantoms were gelled in 5 mm NMR tubes and imaged on a 4.7 T MR magnet in a total of 300 μL.

Chapter Six

Systematic Study of Peptide Amphiphile Contrast Agents (PACAs): Insights into Relaxivity Enhancement

6 Systematic Study of the Peptide Amphiphile Contrast Agents: Insights into Relaxivity Enhancement

6.1 Introduction

Current need for high relaxivity contrast agents (CAs) in magnetic resonance imaging (MRI) applications arises from the relatively poor relaxation rates achieved by clinically used small molecule CAs. These small molecules normally contain a single Gd(III) ion bound by a ligand that coordinates via actetate arms and a nitrogen containing backbone, e.g. DOTA and DTPA (**Figure 1.1**), leaving one site for water coordination.[7] These small molecule CAs' relaxivities are limited by their fast rotational correlation time (τ_R) which makes them rather poor at enhancing MR images.[158] Because these molecules have MWs below 1000 Da they have τ_R values ~0.05 ns, which is ~2-3 orders of magnitude below optimal levels.[7, 126] Typical proteins have τ_R values >10 ns (human serum albumin has a τ_R of ~30 ns), which are close to optimal for a MR CA in clinically used field strengths. Hence size is a major determining factor in controlling τ_R and relaxivity.[7, 159] Researchers have used this insight to attach small molecule CAs to larger molecules via covalent and non-covalent interactions in order to increase the relaxivity e.g. attachment to proteins,[160, 161] linear polymers,[162, 163] dendrimers,[164, 165] viruses,[166] and micellar structures.[98, 109, 121] These attempts to enhance τ_R do increase relaxivity but the results are still below the theoretical maximum values. In order to understand why this is the case, one must look at the way the CA is attached to the macromolecule not just the macromolecule itself (**Figure 6.1**) and to the other relevant parameters like the water exchange lifetime and the hydration number.

Small molecule CAs attached to macromolecules have been reported to increase their relaxivity from ~4 $mM^{-1}s^{-1}$ to values greater than 25 $mM^{-1}s^{-1}$ (20 MHz, 37 C).[167, 168] These CAs

often do not attain the theoretical maximum of >90 mM^{-1} s^{-1} [7] (20 MHz, 37 C) because the attachment typically has too many degrees of freedom (theoretical calculations for an optimal value of relaxivity using τ_m of 20 ns, q=1, 25 C, and 20 MHz). These "floppy" attachments decrease the local τ_R of the CA in relation to the global τ_R of the macromolecule (**Figure 6.1**).[169, 170] This local "fast" spinning of the CA moiety makes it the determining factor in the CA's efficiency.

This chapter describes the different paths used to increase relaxivity of small molecule CAs. As in Chapters 4 and 5, I have chosen to use the PA monomer as the backbone for CA attachment and to take advantage of its ability to self-assemble into high aspect ratio nanofibers to increase τ_R. To this end, different portions of the PA molecule and the attachment of the chelator were modified in order to achieve greater relaxation enhancement. This chapter is built upon Chapters 4 and 5, but contains a small library of PACA molecules and gives direct comparisons of their relaxivity efficiencies.

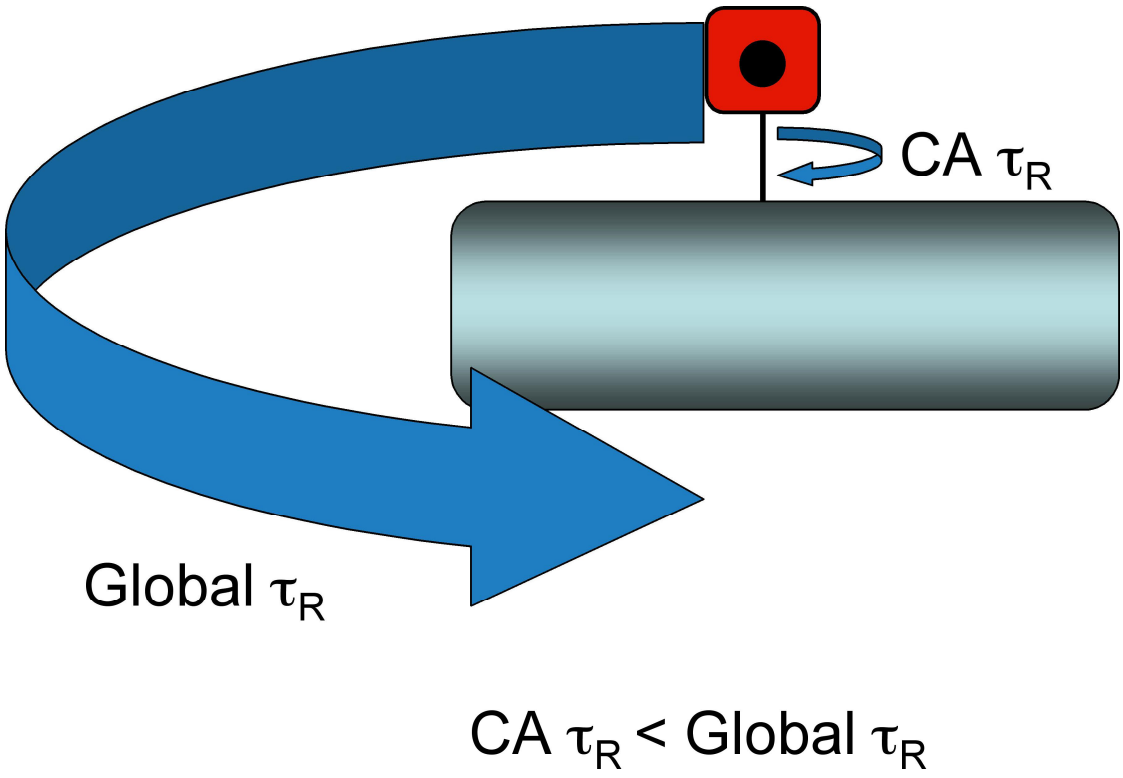

Figure 6.1 Cartoon representation illustrating the difference in τ_R when attaching a small molecule CA to a macromolecule. The linker between the CA and the macromolecule becomes the limiting factor to increasing relaxivity.

6.2 Effects of linker length on relaxivity of PACA

The linker of the Gd(III) chelator to the PACA monomers has a dramatic effect on relaxivity. To this end I synthesized **6.6** and **6.7** (**Figure 6.2**). These PACAs gave a direct comparison of the effect of the linker length on the relaxivity of the PACAs with linker lengths ranging from four to six methylene units. For these comparisons all the PACAs form nanofibers (**Figure 6.3**) and it is assumed that they have equivalent global τ_R and q values. These assumptions give rise to the relaxivity difference were only from the local τ_R of the Gd(III) on the PACA. The local τ_R stems from the degrees of freedom present in the chelators linker arms which allows for the fast rotation of the Gd(III) compared to the nanofibers.[171-173] PACA's **6.6**, and **6.7** both maintain a linear architecture, have a q of two, and have the chelator attached to the

N-terminus of the PACA. The linkers vary from four to six methylene units and provide relaxivities of 14.0 ± 0.6 and 10.2 ± 0.8 mM^{-1} s^{-1} respectively (60 MHz, 37 C). These data clearly show that linker length is a major contributor to the local τ_R of the Gd(III) providing up to ~40% enhancement in relaxivity for the shorter linker chelates. The shorter the linker the less degrees of freedom for rotation. leading to a higher relaxivity.

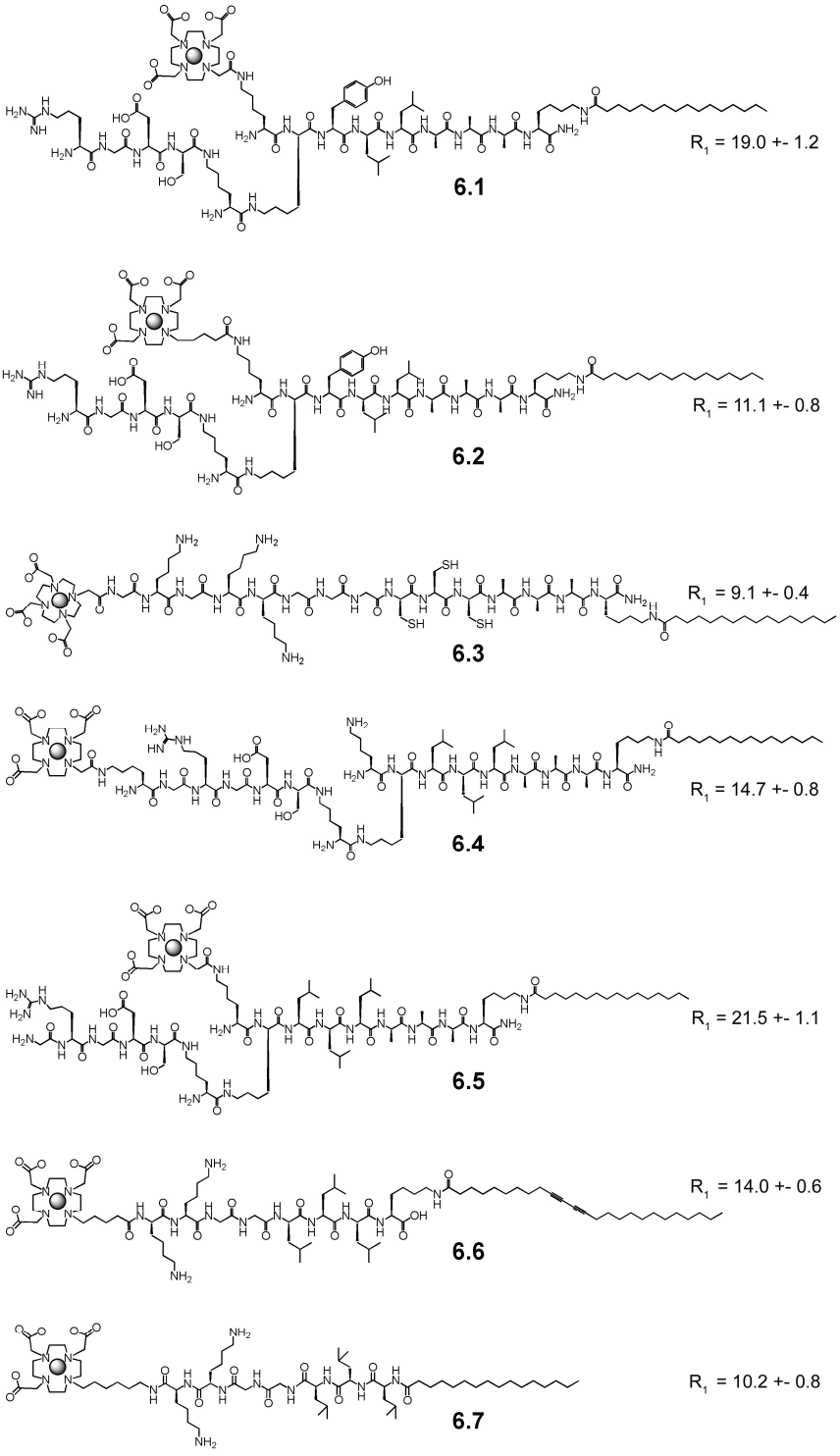

Figure 6.2 Molecular structure of PACA molecules with different MWs and linkers between the CA and PA. All PACAs contain the DOTA derivative as the chelating moiety.

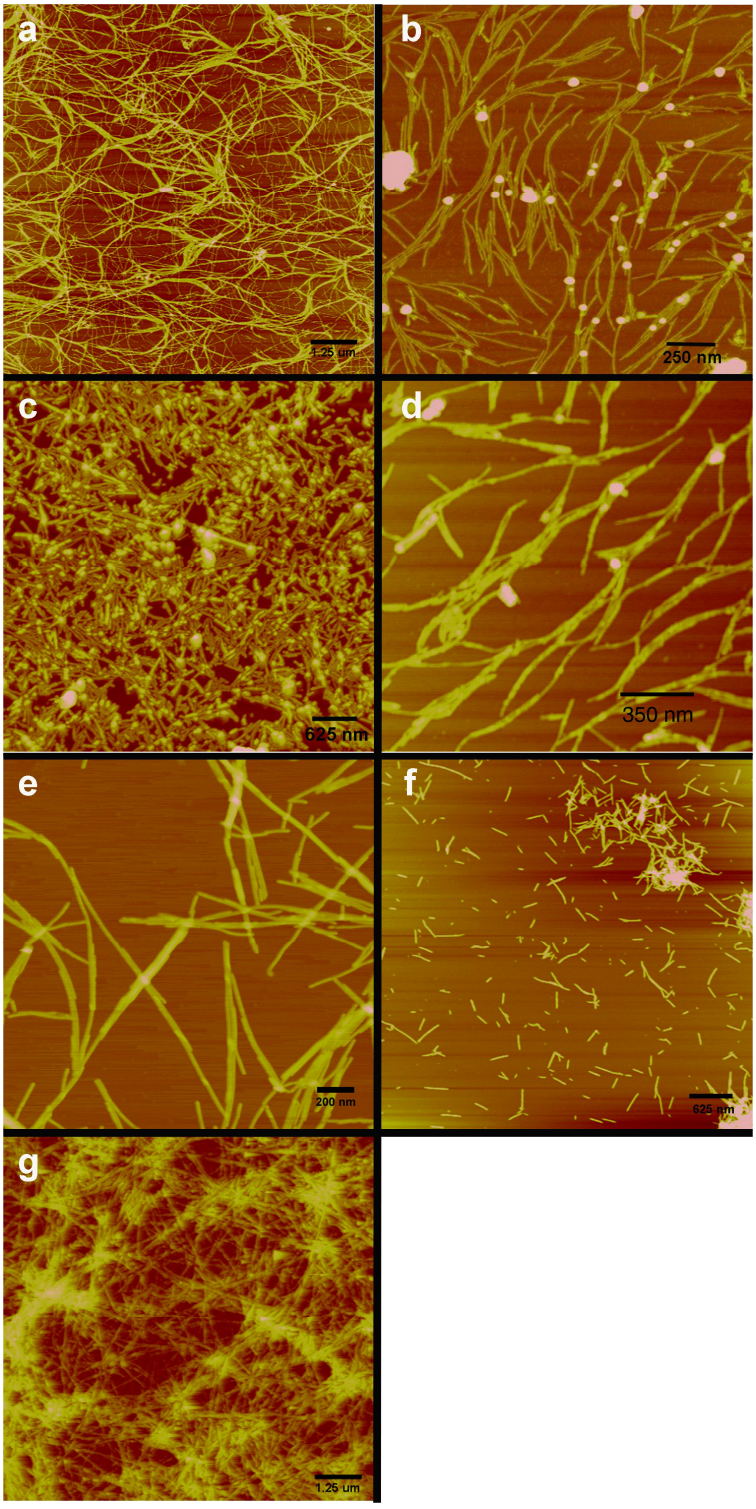

Figure 6.3 AFM height images of PACAs **6.1** - **6.7** corresponding to (a) – (g) respectively. Each PACA forms fiber structures. The samples were prepared by drop casting solutions onto freshly cleaved mica and fiber heights ranged between 6 and 8 nm.

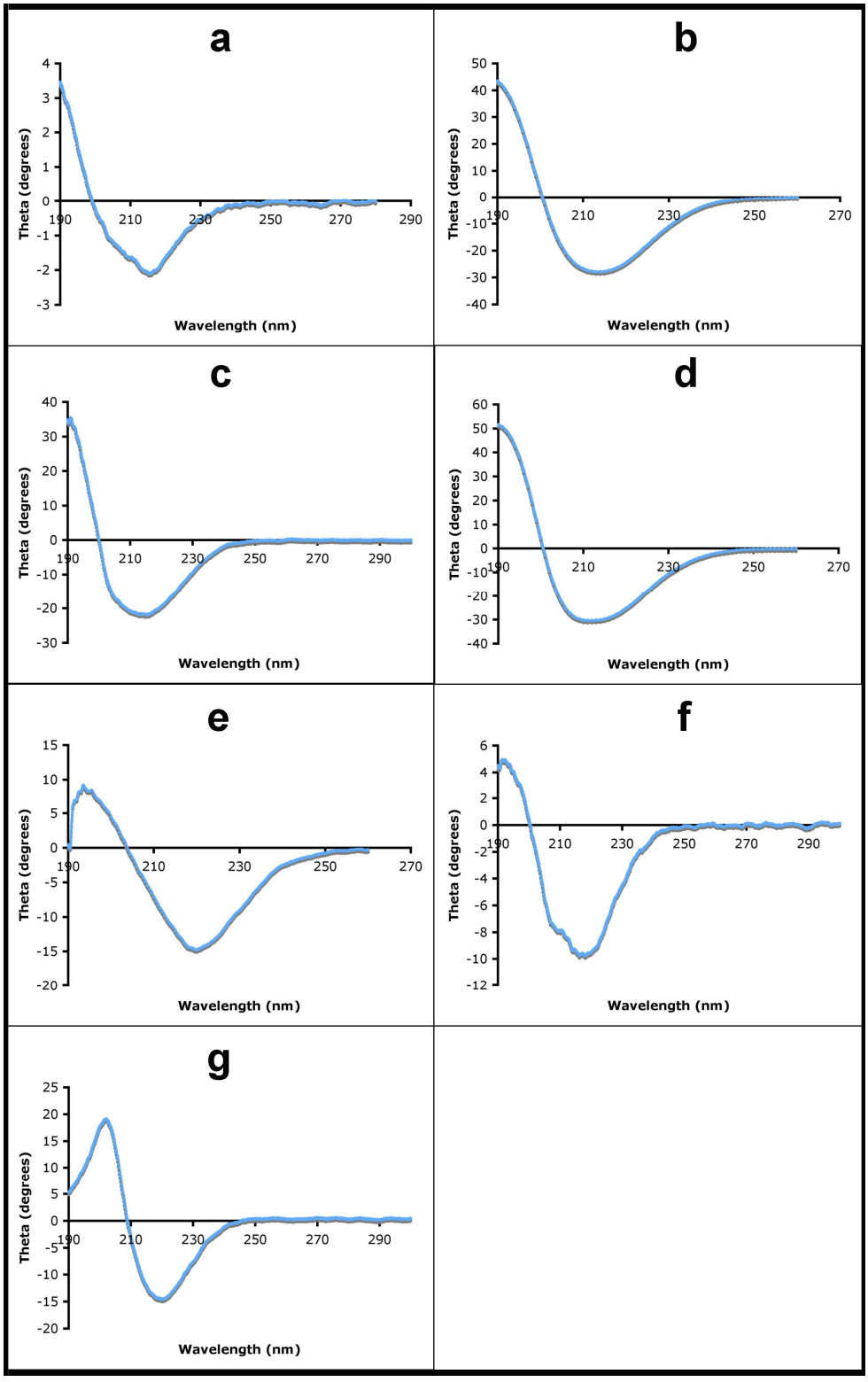

Figure 6.4 CD spectra depicting PACAs **6.1** - **6.7** (a) – (g) respectively. All spectra contain a minima at ~220 nm, displaying significant β-sheet formation.

6.3 Effect of MW on relaxivity

Unlike small molecule CAs, the molecular weight of the PACA monomer does not play a role in the difference in relaxivity. PACAs **6.1 – 6.7** have MWs, as monomers, of 2325, 2367, 2116, 2461, 2334, 1795, and 1547 Da, respectively, but are orders of magnitude larger when in the self-assembled state. When self-assembled, the exact molecular weight cannot be determined owing to the different lengths of fibers formed and the density of the fibers. Calculations have estimated that the density of the PACA molecules on the surface of the fibers is $7.5*10^{11}$ cm^{-2},[87] giving rise to a MW of ~10^{14} Da cm^{-2}. **Figure 6.5** illustrates the relationship between molecular weight and relaxivity for small molecule contrast agents, showing a clear indication of increased relaxivity with the increase of molecular weight. PACA **6.2** illustrates the limited importance of monomer MW; it has the largest mass at 2367 Da yet one of the lowest relaxivities of 11.0 ± 0.8 $mM^{-1}s^{-1}$. When the PACAs are in their self-assembled state, the τ_R increase is from the supramolecular polymer and not due to the monomers themselves. As a comparison, spherical micelles that have a r_{eff} = 18 Å give a τ_R ~ 5 ns for the global rotation.[126] This indicates that our fibers should have a τ_R >5 ns, which is in the ideal range for theoretical maximum relaxivity enhancement and the linker is the limiting factor in not achieving theoretical maximums. The differences in the PACA monomer masses do not have a bearing on the relaxivity of the nanofibers therefore one is not able to use this as a variable to increase relaxivity

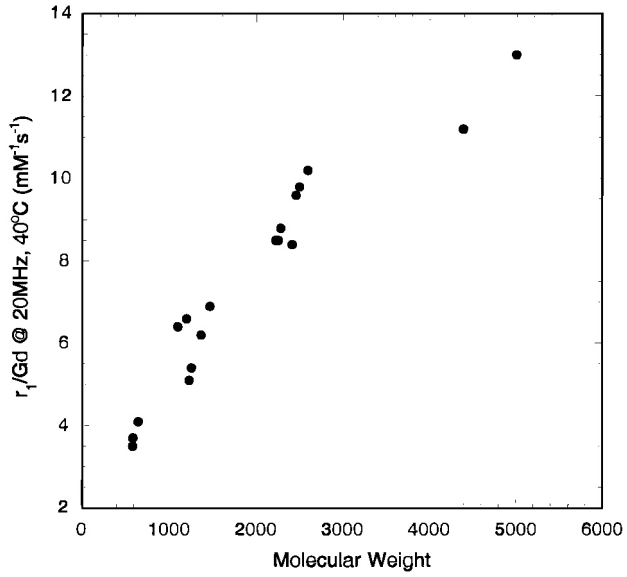

Figure 6.5 Graph depicting the relaxivity of Gd(III) vs. the molecular weight of multiple complexes.[7]

6.4 Effects of chelator position on relaxivity

PAs **6.4** and **6.5** were synthesized with the Gd(III) chelator positioned off of the ε amine of a lysine residue and these PACAs were synthesized with the chelator directly after the branch of the PACA. The position of the chelator results in a dramatic shift in the relaxivity from 21.5 ± 1.1 to 14.7 ± 0.8 mM^{-1} s^{-1} (60 MHz, 37 C). The only difference in these two PACA monomers is the chelate position, either directly after the branch point (inside the fiber) as in **6.4** or on the outer edge of the PACA and fiber as in **6.5**. This positional change has an effect on the degrees of freedom[173] of the CA with **6.5** being more sterically hindered than **6.4**, accounting for the difference in relaxivity.[29, 157, 174] In general, as the chelator moves closer to the core of the nanofibers the relaxivity is increased. This trend is followed by **6.1** and **6.5** both having relaxivities greater than 19 $mM^{-1}s^{-1}$ and both have chelators placed directly after the branch, providing the steric hindrance of the chelator and the increase in relaxivity. This is not the case

with **6.2** (even though the chelator is directly after the branch) because of the extra four methylene units – giving it much greater molecular flexibility thereby decreasing the relaxivity. The optimal position of the chelator is one where there is plentiful water access as well as steric hindrance to decrease the local τ_R of the Gd(III), which occurs directly after the branch in the PA model.

6.5 Effects of polymerization on relaxivity

Two self-assembling PACA molecules were synthesized incorporating the ability to either crosslink or polymerize the monomers. PACA **6.3** employed a crosslinking scheme that used the oxidation of the thiols on the side chains of Cys amino acids to form intermolecular bonds between adjacent PAs after self-assembly into the fiber. Relaxivity was measured at 8.60 ± 0.4 mM^{-1} s^{-1} (60 MHz, 37 C) prior to oxidation. Upon oxidation via aqueous I_2,[81] aggregation/precipitation of the fibers took place providing unreliable relaxivity measurements of the crosslinked fibers.[29] FT-IR was performed on the oxidized sample confirming the lack of a S-H stretch and the oxidation of the PACA monomers (**Figure 6.9**). Subsequent acidification of the precipitated solution (pH 3.5), made the precipitate soluble and the crosslinked fibers gave a relaxivity of 9.11 ± 0.5 mM^{-1} s^{-1}. Unfortunately there is not statistically significant difference between the samples before and after oxidation. Compound **6.6** uses photopolymerization as the mechanism for polymer formation (**Figure 6.6**). Using 254 nm light, the diacetylenes in the alkyl tail region (core) of the fibers polymerize. The relaxivity did not change significantly, from 14.0 ± 0.6 to 14.2 ± 0.4 $mM^{-1}s^{-1}$ (60 MHz, 37 C), upon polymerization. Over 24 h, aggregation/precipitation was seen with this polymer scheme as well. The difference between τ_R of a supramolecular self-assembled fiber and a macromolecular polymer is negligible and leads

to the conclusion that the limiting factor is local rotation due to the linker between the structure and the chelator, which remains unchanged during the polymerization.

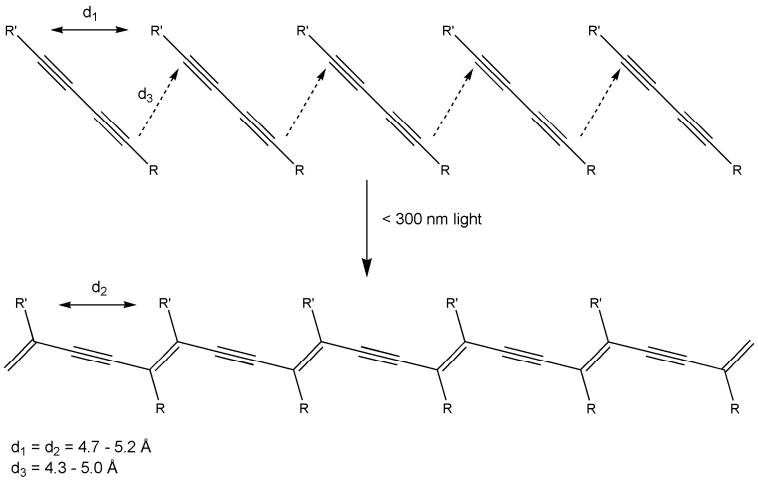

Figure 6.6 Mechanism of diacetylene polymerization within the PA nanofibers. The polymerization is accompanied by a color change.[175, 176]

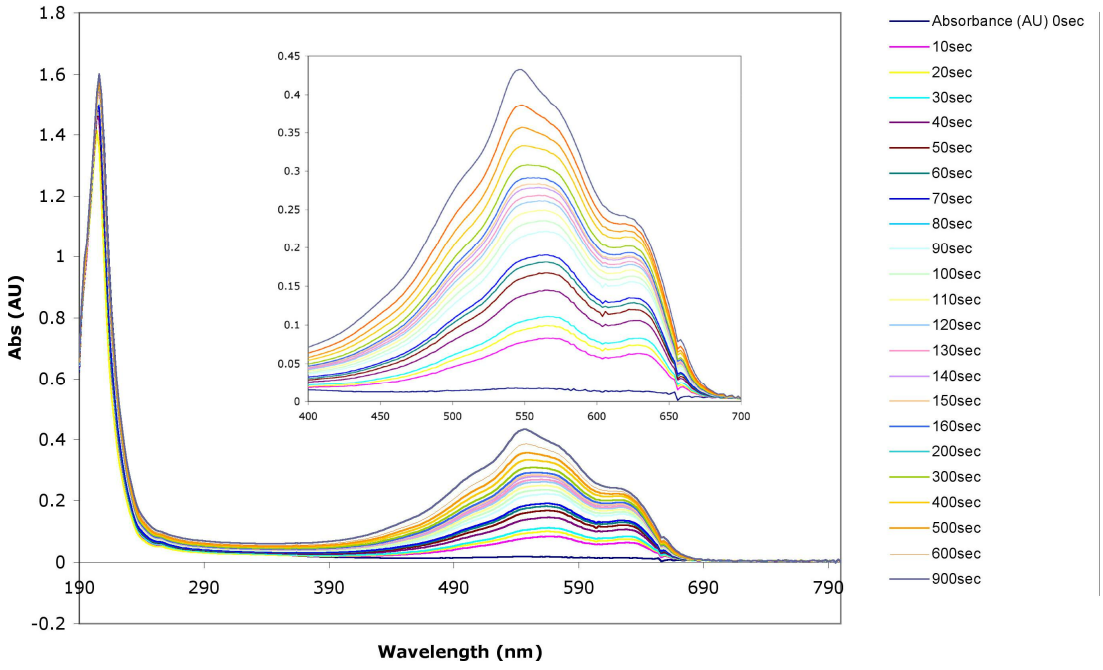

Figure 6.7 UV-Vis spectra depicting **6.6** with varying exposure times to 254 nm light. The increase in the absorbance ~550 nm is indicative of polymerization of the diacetylenes.

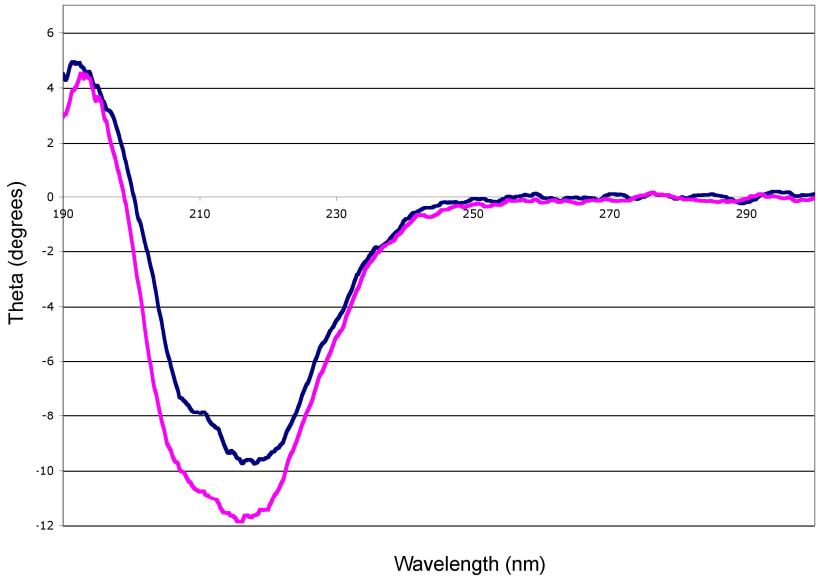

Figure 6.8 CD spectra of **6.6** with a maximum absorbance at ~220 nm and a shoulder at ~210 nm confirming the presence of β-sheet and some random coil configuration. The blue line is after 5 min of exposure to 254 nm light and the pink line is without light exposure.

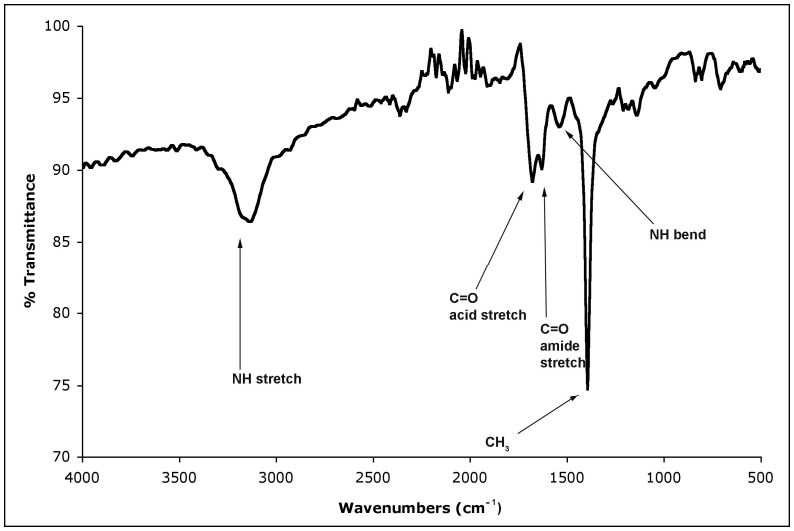

Figure 6.9 FT-IR spectra of **6.2** depicting the absence of a peak at 2555 cm^{-1} which would correspond to the free S-H.

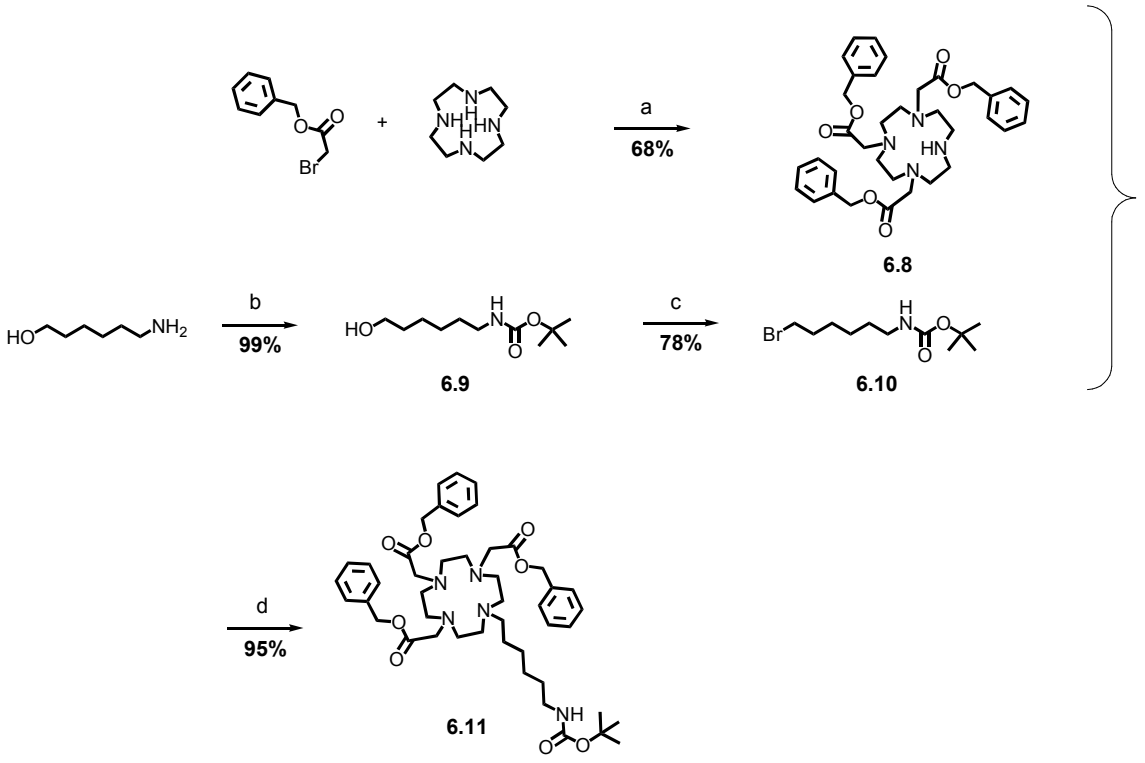

Scheme 6.1 DOTA derivative chelator for solution phase PACA synthesis. (a) $NaHCO_3$. (b) Boc Anhydride, TEA. (c) CBr_4, PPh_3. (d) K_2CO_3.

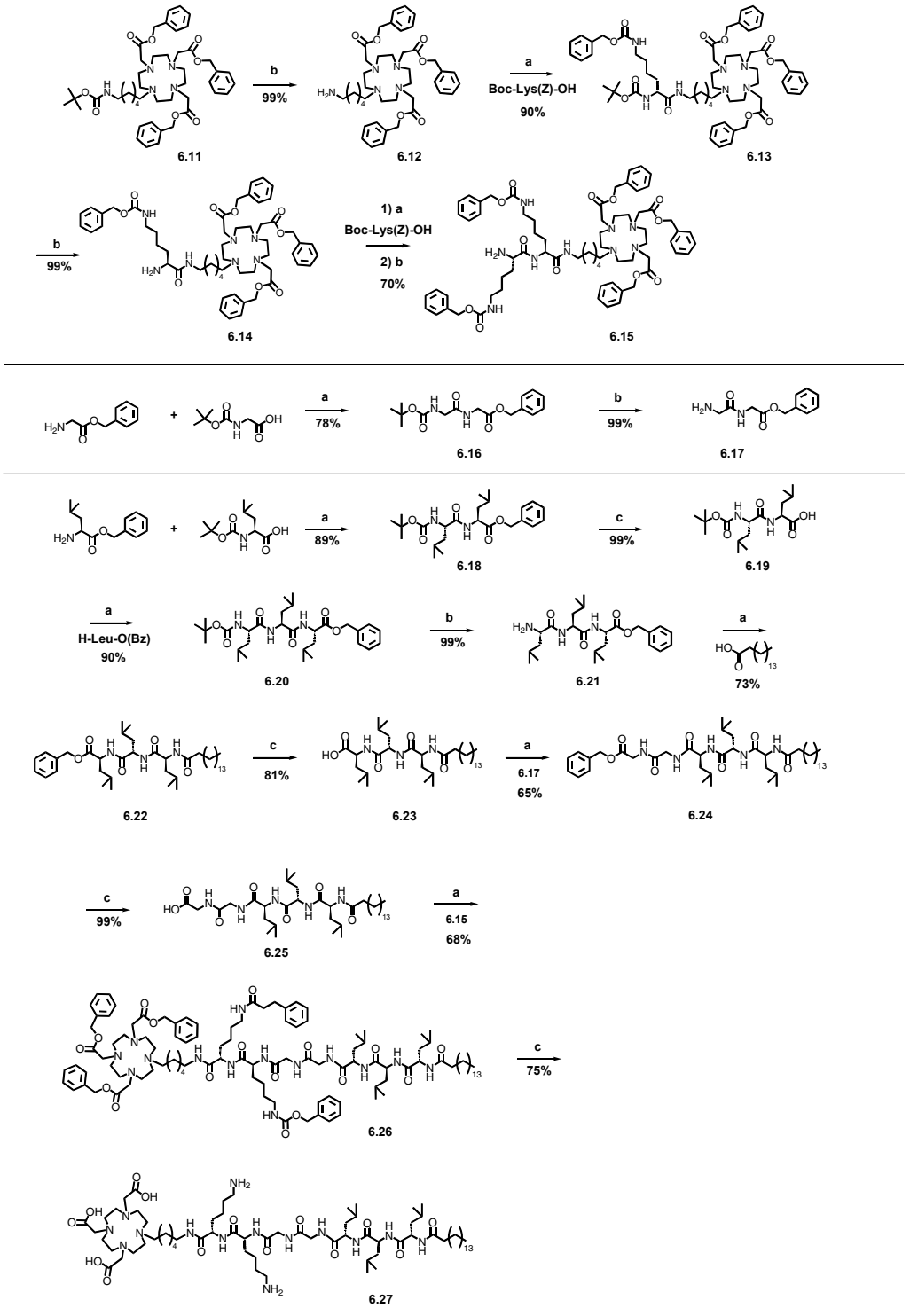

Scheme 6.2 Convergent solution phase synthesis of PACA DOTA-KK-GG-LLL-C_{16}. (a) EDCI, HOBT, TEA. (b) HCl/Dioxane. (c) Pd/C, H_2.

6.6 Effect of q on Relaxivity

The number of water molecules directly associated with the paramagnetic center corresponds to the q value for the molecule. Ample studies have been conducted on small molecule and macromolecular contrast agents explaining that the changes outside the inner sphere can be considered to be the same for all species in solution.[121, 159, 169, 171, 177] Taking this research into consideration when synthesizing PACAs **6.1** – **6.7** allowed for the synthesis of both q = 1 and q = 2 PACA molecules. PACAs **6.1**, **6.3**, **6.4**, and **6.5** all were designed as q = 1 agents and **6.2**, **6.6**, and **6.7** were designed as q = 2 agents. The difference in relaxivity between the q = 1 set of PACAs provided a difference in relaxivity from 9.1 ± 0.4 to 21.5 ± 1.1 mM^{-1} s^{-1} depending on the position of the chelator and the architecture of the PACA molecule (the change in the local τ_R of the chelate). The difference in the relaxivity of the q = 2 PACAs provided a wide distribution of relaxivities from 10.2 ± 0.8 to 14.0 ± 0.4 mM^{-1} s^{-1}. Normally q = 2 agents should have a higher relaxivity than q = 1 agents, and this is the case with the PACA molecules. A direct comparison of **6.3** and **6.7** gives relaxivities of 9.1 ± 0.4 compared to 10.2 ± 0.8 mM^{-1} s^{-1} with q = 1 and q = 2 PACAs respectively. According to the linker length trend, **6.3** would have a relaxivity much higher than **6.7** if it was not for the difference in q values.

6.7 Conclusion

In conclusion, one is able to ascertain the most important variable of relaxivity from the self-assembling PACA molecules as the linker between the PA and chelator. The separation of the different variables (MW, q, flexibility) is impossible because all variables are intertwined in governing the overall relaxivity of the PACAs. By comprising the most significant modifications of position, q value, and chelator length, **6.5** is very close to the optimal CA. It

uses steric hindrance of the nanofiber self-assembly as well as the shorter linker length of the chelator to provide the highest relaxivity.

6.8 Experimental

Unless otherwise noted, all starting materials were obtained from Sigma-Aldrich and/or Strem and used without further purification. Analytical TLC was performed on Merck KgaA silica gel 60 F254 TLC plates. Silica for flash chromatography was ICN Silitech 32-63 D 60 Å. ^{1}H and ^{13}C NMR spectra were recorded on Varian 500 and 400 MHz NMR spectrometers. MALDI-TOF mass spectra were performed on a Voyager DE instrument using α-cyano-4-hydroxycinnamic acid as a matrix. Amino acids were purchased from NovaBiochem and used without further purification unless otherwise stated. Circular Dichroism (CD) was performed on a Jasco J-715 CD spectrophotometer using a 2 mm quartz cuvette.

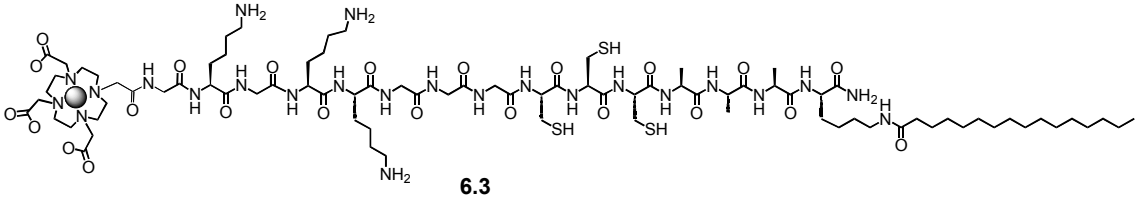

6.3

The linear PA **6.3** was prepared by 9-Fluorenylmethoxycarbonyl (Fmoc) solid phase peptide synthesis (SPPS) on a 0.1 mmol scale. Fmoc-Lys(Mtt)-OH, (Mtt: 4-methyl trityl) was coupled to MBHA Rink Amide resin, followed by cleavage of the Mtt protecting group on the ε-amine to couple palmitic acid without affecting Fmoc protection with a 5% TFA in DMF solution for 5 minutes. This was followed by Fmoc removal on the α-amine to grow the AAA peptide segment of the PA using 30% piperidine/DMF solution for 10 min. The branching point was introduced at a lysine dendron using Fmoc-Lys(Mtt)-OH. The addition of the Cys groups

was accomplished using a preactivated Fmoc-Cys(Trt)-OPfp ligand in DMF with DIEA as a base. Coupling times were increased to 8 hr per Cys monomer. PACA **6.3** was cleaved from the resin in 95:2.5:2.5 TFA:TIS:H_2O. Excess TFA was evaporated under reduced pressure and crude PA solutions were triturated using cold ether. Preparatory HPLC was preformed on the crude product providing pure **6.3** in an overall 16% yield. The Gd(III) complex was completed by the addition of $GdCl_3$ solution in water at pH 6.5 to the PACA ligand. The chelation was monitored by Arzenazo III colorimetric titrations.[172] MALDI-TOF Mass Spec. 1962.40 (calcd. 1961.14).

SPPS was used to synthesize **6.1**, **6.2**, and **6.6** as well. They followed a similar procedure as that described in the synthesis of **6.3** and were obtained in a similar yield.

Solid phase synthesis is a fantastic technique used for the ease of synthesis of a large number of amino acids. The technique facilitates the removal of unreacted substrates by filtering because the desired product remains on polystyrene beads. SPPS relies on the high efficiency of the peptide bond formation to make the technique feasible. The coupling efficiencies are usually ~99% and these reactions can be done robotically. SPPS has the advantage of large scale synthesis with the use of large amounts of resin and amino acid monomers (~4 eq for every coupling). The ease of synthesis and the ability of a robot to complete the synthesis makes this an attractive feature of PAs.

Although there are many benefits to the use of SPPS, there are some drawbacks. SPPS proceeds in a linear fashion thereby creating a fairly slow reaction process when long amino acid sequences are desired. When there is a mistake in the synthesis, there is no way to purify out the impurities until the final product is cleaved from the resin. Even though the coupling efficiencies are very high, when combining 20 or more amino acids, the yield is reduced to <78% yield (taken from 99% yield on each step). The process of SPPS is likened to a “black box” where you

are only qualitatively able to test when the addition of an amino acid is complete using the Kaiser test. SPPS uses a large excess of amino acid for each coupling step in which ~3 equivalents are wasted each coupling and this can be a problem when using a specialty amino acid.

Solution phase chemistry has the possibility to get around many of these drawbacks for the synthesis of the PA. Solution phase chemistry can utilize convergent synthesis, purification after every step, and allows for extremely large scale couplings without the use of resin and using only one equivalent per reaction. The waste is reduced, the cost is reduced and the scale is increased.

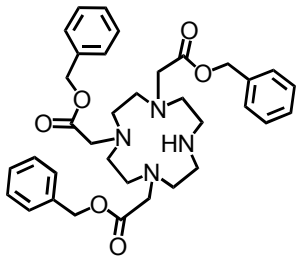

6.8

Compound 6.8: In a dry round bottom flask was combined cyclen (2.89 g, 17 mmol), sodium bicarbonate (4.71 g, 56 mmol) and dry acetonitrile (200 mL). The solution was stirred under N_2, for 5 minutes and a solution of dry acetonitrile (30 mL) and benzyl bromoacetate (11.6 g, 51 mmol) was added dropwise. The reaction proceeded overnight then the solid was filtered, and the solvent was removed by rotary evaporation. Flash chromatography was performed using 1/9/90 KNO_3/H_2O/ACN to give a white hygroscopic solid (10 g, 68% yield). ^{1}H NMR (500 MHz, $CDCl_3$) δ 7.34 (s, 15H), 5.12 (s, 6H), 3.48 (s, 4H), 3.42 (s, 2H), 3.08 (s, 4H), 2.88-2.83

(bm, 12H). ^{13}C (125 MHz, $CDCl_3$) δ 171.09, 170.28, 135.44, 128.79, 128.72, 128.66, 128.55, 66.71 (2 C), 57.28, 51.55, 49.42, 47.38. ESI MS (methanol) Calcd. 616.33, found 639.63 M+Na.

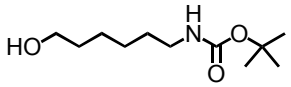

6.9

***tert*-butyl 6-hydroxyhexylcarbamate 6.9:** In a round bottom flask was combined 6-aminohexanol (3.0 g, 25.6 mmol), TEA (3.57 mL, 25.6 mmol), and DCM (100 mL). To that solution was added boc anhydride (5.9 g, 26.9 mmol) and the reaction was stirred overnight. The reaction mixture was diluted with DCM and washed three times with water, dried over $MgSO_4$, and the solvent was removed by rotary evaporation. Flash chromatography was performed using 5/95 MeOH/DCM affording a clear liquid (5.6 g, 99% yield). ^{1}H NMR (500 MHz, $CDCl_3$) δ 3.54 (t, *J*=6.5 Hz, 2H), 3.06 (t, *J*=6.8 Hz, 2H), 1.48 (m, 2H), 1.41 (m, 2H), 1.36 (s, 9H), 1.27 (bm, 4H). ^{13}C (125 MHz, CD_3OD) δ. 156.26, 79.11, 62.97, 40.49, 32.57, 30.06, 28.44, 25.39. ESI MS (methanol) Calcd. 217.17, found 240.02 M+Na.

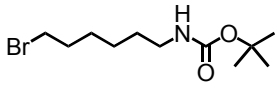

6.10

***tert*-butyl 6-bromohexylcarbamate 6.10:** In a round bottom flask was combined *tert*-butyl 6-hydroxyhexylcarbamate (**6.09**) (5.60 g, 25.8 mmol), CBr_4 (8.55 g, 25.8 mmol), and DCM (200 mL). To that solution was added PPh_3 (10.11 g, 38.7 mmol) and the reaction was stirred overnight. The reaction mixture was diluted in DCM and washed three times with water, dried over $MgSO_4$, and the solvent was removed by rotary evaporation. Flash chromatography was

performed using 50/50 DCM/Ethyl Acetate affording a clear colorless liquid (5.6 g, 78% yield). ^{1}H NMR (500 MHz, $CDCl_3$) δ 3.38 (t, *J*=6.6 Hz, 2H), 3.09 (t, *J*=6.9 Hz, 2H), 1.84 (m, 2H), 1.47 (m, 2H), 1.42 (s, 9H), 1.33 (bm, 4H). ^{13}C (125 MHz, CD_3OD) δ. 156.22, 79.23, 40.64, 34.03, 32.86, 30.14, 28.65, 28.03, 26.15. ESI MS (methanol) Calcd. 279.08, found 280.02 M+H.

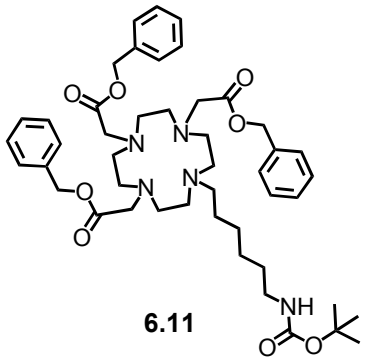

6.11

Synthesis of **6.11**: In a dry roundbottom flask was combined **6.8** (1.1 g, 1.79 mmol), potassium carbonate (0.74 g, 5.4 mmol) and dry acetonitrile (30 mL). The solution was stirred under N_2, for five min and a solution of dry acetonitrile (5 mL) and *tert*-butyl 6-bromohexylcarbamate (**6.10**) (0.65 g, 2.3 mmol) was added dropwise. The reaction proceeded overnight, the and solid was filtered, and the solvent was removed by rotary evaporation. Flash chromatography was performed using 1/9/90 KNO_3/H_2O/ACN to give a white hygroscopic solid (1.3 g, 95% yield). ^{1}H NMR (500 MHz, $CDCl_3$) δ 7.28 (s, 15H), 5.07 (s, 6H), 3.63-2.50 (bm, 26H), 1.57 (s, 2H), 1.37 (m, 9H), 1.26 (m, 6H). ^{13}C (125 MHz, $CDCl_3$) δ 170.80, 170.44, 155.93, 135.32, 135.13, 128.28, 128.23, 128.17, 127.98, 78.52, 66.19, 55.41, 55.78, 52.74, 52.31, 49.79, 47.20, 28.26. ESI MS (methanol) Calcd. 815.48, found 816.29 M+H, 838.49 M+Na.

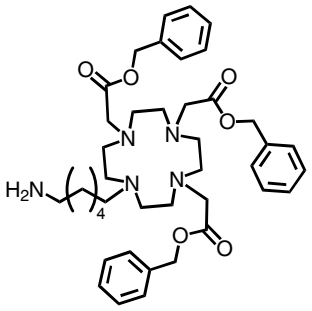

6.12

Compound 6.12: Reference synthesis of **6.21** with flash chromatography using 1/9/90 KNO_3/H_2O/ACN to give a white hygroscopic solid (75% yield). ^1H NMR (500 MHz, $CDCl_3$) δ 8.17 (bs, 3H), 7.29 (s, 15H), 5.07 (s, 6H), 3.63-2.50 (bm, 26H), 1.72 (bs, 2H), 1.64 (bs, 2H), 1.39 (bs, 2H), 1.28 (bs, 2H). ^{13}C (125 MHz, $CDCl_3$) δ 170.96, 170.77, 135.52, 135.41, 128.60, 128.57, 128.36, 128.31, 128.14, 66.49, 66.29, 55.93, 54.25, 53.54, 52.77, 52.49, 49.98, 47.42, 39.55, 26.16, 25.22, 25.06. ESI MS (methanol) Calcd. 715.32, found 716.41 M+H, 738.43 M+Na.

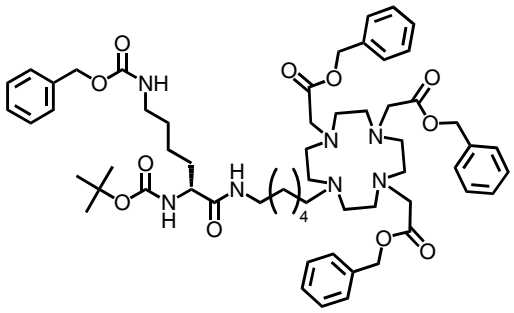

6.13

Compound 6.13: Reference synthesis of **6.18** with flash chromatography using 1/9/90 KNO_3/H_2O/ACN to give a white hygroscopic solid (75% yield). Characterization was by ESI MS and TLC. ESI MS (methanol) Calcd. 1077.53, found 1078.62 M+H.

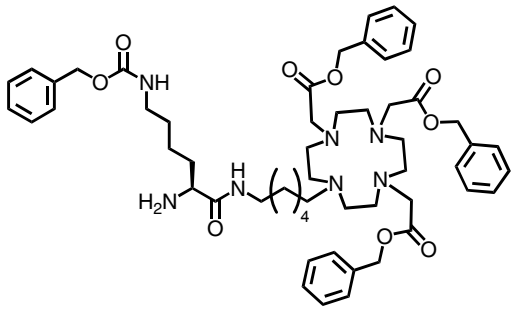

6.14

Compound 6.14: Reference synthesis of **6.21** (99% yield) and used without further purification. Characterization was by ESI MS and TLC. ESI MS (methanol) Calcd. 977.56, found 978.62 M+H, 888.51 M-CBz+H.

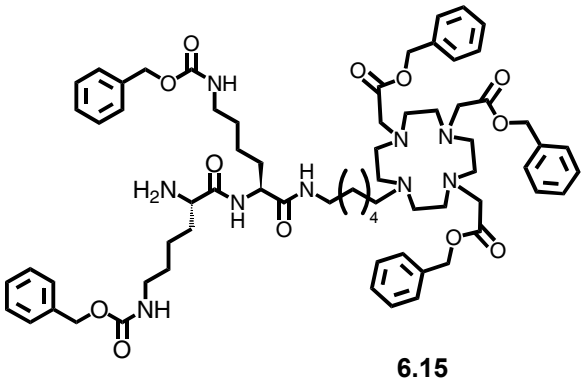

6.15

Compound 6.15: Reference synthesis of **6.18** and **6.21** (99% yield) with flash chromatography using 1/9/90 KNO_3/H_2O/ACN to give a white hygroscopic solid (90% yield). Characterization was by ESI MS and TLC. ESI MS (methanol) Calcd. 1239.71, found 1240.62 M+H, 621.17 M/2.

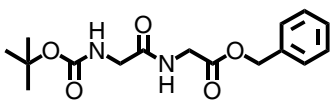

6.16

Diglycine 6.16: Reference synthesis of **6.18** with flash chromatography using 5/95 MeOH/DCM as eluent (78% yield). ^{1}H NMR (500 MHz, $CDCl_3$) δ 7.33 (s, 5H), 7.21 (t, *J*=6 Hz, 1H), 5.13 (s, 2H), 4.04 (s, 2H), 3.83 (s, 2H), 1.43 (s, 9H): ^{13}C (125 MHz, CD_3OD) δ 170.33, 169.76, 156.24, 141.21, 135.27, 135.16, 128.39, 128.29, 127.34, 126.93, 80.04, 67.11, 43.95, 41.16, 28.29. ESI MS (methanol) Calcd. 322.15, found 323.3 M+H.

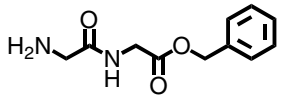

6.17

(diglycine)Bn 6.17: Reference synthesis of **6.21 (**99% yield): Monitored by TLC and ESI MS and used without further purification. ESI MS (methanol) Calcd. 221.10, found 222.2 M+H.

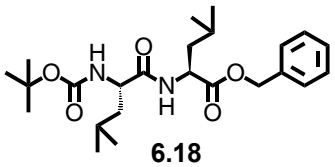

6.18

Boc(dileu)Bn 6.18: To a roundbottom flask was combined NH_2(leu)Bn (3 g, 13 mmol), EDCI (2.99 g, 15.6 mmol), HOBT (1.76 g, 13 mmol), TEA (1.32 g, 13 mmol), DCM (300 mL), and stirred until a homogeneous solution formed. Boc(leu)OH (3 g, 13 mmol) was then added and the mixture was stirred overnight. The mixture was diluted with DCM and washed with brine three times, dried over $MgSO_4$, and the solvent was removed by rotary evaporation. Flash chromatography was performed using 5/95 MeOH/DCM affording a white solid (5 g, 89% yield). ^{1}H NMR (500 MHz, $CDCl_3$) δ 7.34 (s, 5H), 6.50 (s, 1H), 5.15 (d, *J*= 9, 2H), 4.92 (s, 1H), 4.66 (m, 2H), 4.10 (s, 1H), 1.63 (m, 6H), 1.45 (s, 9H), 0.91 (s, 12H): ^{13}C (125 MHz, $CDCl_3$)

δ172.70, 172.43, 155.91, 135.53, 128.77, 128.58, 128.43, 80.21, 67.21, 53.06, 50.90, 41.57, 41.02, 28.44, 24.81, 23.02, 21.49. ESI MS (methanol) Calcd. 434.28, found 457.34 M+Na.

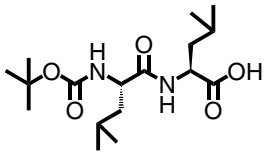

6.19

Boc(dileu) 6.19: To a roundbottom flask was combined **6.18** (4.9 g, 11.2 mmol), Pd/C (0.71 g), DCM (100 mL), and EtOH (100 mL). The solution was stirred overnight under a balloon of H_2. The mixture was filtered through celite, and the solvent was removed by rotary evaporation affording (3.72 g, 96% yield). TLC showed the absence of starting material and this material was carried on without further purification.

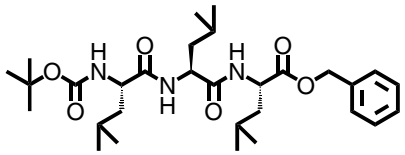

6.20

Boc(trileu)Bn 6.20: Reference synthesis of **6.18** (89% yield). ^{1}H NMR (500 MHz, $CDCl_3$) δ 7.34 (s, 5H), 7.16 (s, 1H), 6.98 (s, 1H), 5.36 (s, 1H), 5.12 (dd, *J*=12 Hz, *J*=18.5, 2H), 4.62 (m, 1H), 4.54 (s, 1H), 4.18 (s, 1H), 1.58 (bm, 8H), 1.41 (s, 11H), 0.91 (s, 18H). ^{13}C (125 MHz, $CDCl_3$) δ 172.84, 172.64, 171.88, 155.84, 135.58, 128.65, 128.55, 128.43, 128.35, 127.52, 127.03, 79.88, 67.04, 65.12, 52.97, 51.68, 50.88, 41.35, 41.11, 40.97, 28.44, 24.81, 24.77, 24.65, 22.98, 22.84, 22.44, 22.31, 21.91. ESI MS (methanol) Calcd. 547.36, found 548.34 M+H.

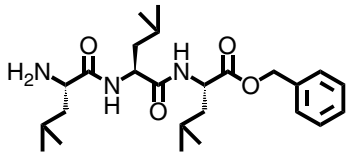

6.21

NH_2(trileu)Bn 6.21: To a roundbottom flask was combined **6.3** (6.41 g, 11.7 mmol), DCM (100 mL), and HCl in Dioxanes (4 M, 5 mL) was stirred into the solution and the reaction was monitored by TLC. After 15 minutes the solvent was removed by rotary evaporation to give a white solid (4.73 g, 90% yield). The material was used without further purification. ESI MS (methanol) Calcd. 447.28, found 448.3 M+H.

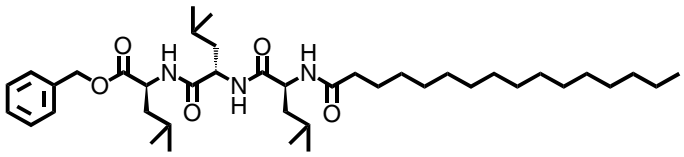

6.22

Compound 6.22: Reference synthesis of **6.18** with flash chromatography using 5/95 MeOH/DCM as eluent (73% yield). ^{1}H NMR (500 MHz, $CDCl_3$) δ 7.34 (s, 5H), 5.14 (dd, *J*=12.5 Hz, *J*=35.5 Hz, 2H), 4.84 (s, 1H), 4.77 (s, 1H), 4.65 (s, 1H), 2.27 (m, 1H), 2.15 (m, 1H), 1.86 (s, 1H), 1.67-1.36 (bm, 10H), 1.22 (s, 24H), 0.88 (s, 21H). ^{13}C (125 MHz, $CDCl_3$) δ 173.04, 172.81, 172.48, 172.33, 135.76, 128.68, 128.40, 128.21, 66.96, 53.61, 51.77, 50.81, 42.53, 41.36, 40.68, 36.24, 34.29, 32.10, 29.89, 29.69, 29.55, 25.92, 24.91, 24.72, 23.47, 22.87, 22.54, 22.09, 21.58, 14.30. ESI MS (methanol) Calcd. 685.54, found 708.6 M+Na.

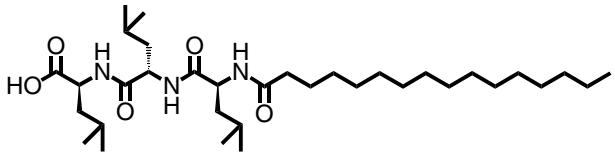

6.23

Compound 6.23: Reference synthesis of **6.19** (81% yield). ^{1}H NMR (500 MHz, $CDCl_3$) δ 8.36 (s, 1H), 4.56 (m, 2H), 4.47 (m, 1H), 2.25 (m, 2H), 1.76-1.55 (bm, 9H), 1.30 (s, 31H), 0.92 (m, 17H). ^{13}C (125 MHz, CD_3OD) δ 174.85, 174.68, 173.52, 173.43, 173.39, 173.40, 173.32, 51.59, 50.92, 50.84, 41.09, 40.86, 40.62, 35.76, 32.03, 29.77, 29.67, 29.49, 29.45, 29.27, 25.98, 24.78, 24.60, 22.70, 22.47, 21.56, 21.38, 21.00, 13.57. ESI MS (methanol) Calcd. 595.49, found 618.6 M+Na.

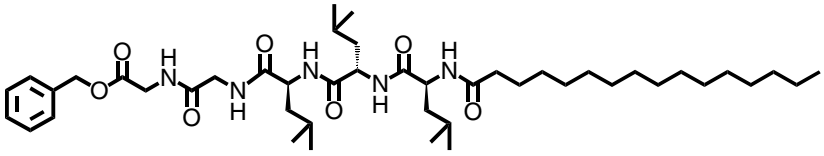

6.24

Compound 6.24: Reference synthesis of **6.18** with flash chromatography using 5/95 MeOH/DCM as eluent (58% yield). ^{1}H NMR (500 MHz, CD_3OD) δ 7.38 (s, 5H), 5.20 (s, 2H), 4.37 (m, 3H), 3.48-3.23 (m, 4H), 2.25 (t, *J*=7.5 Hz, 2H), 1.71-1.56 (m, 11H) 1.31 (s, 24H), 1.32-0.92 (m, 21H). ESI MS (methanol) Calcd. 799.58, found 822.7 M+Na.

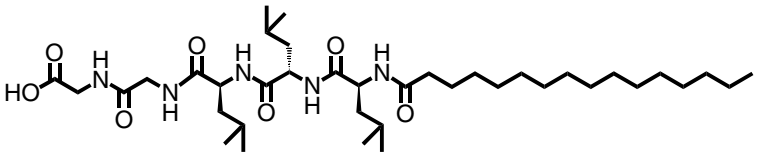

6.25

Compound 6.25: Reference synthesis of **6.19** (99% yield). ^{1}H NMR (500 MHz, dDMSO) δ 8.15 (s, 1H), 8.07 (s, 1H), 7.95 (s, 1H), 7.85 (s, 1H), 4.28 (m, 3H), 3.74 (m, 4H), 2.09 (m, 2H), 1.57 (m, 3H), 1.47-1.38 (bm, 9H), 1.23 (s, 24H), 0.87-0.81 (m, 21H). ^{13}C (125 MHz, CD_3OD) δ 172.96, 172.91, 172.83, 172.60, 171.81, 169.68, 51.79, 51.49, 42.44, 41.34, 35.79, 32.02, 29.76, 29.44, 29.22, 26.01, 24.67, 23.75, 22.82, 22.24, 14.64. ESI MS (methanol) Calcd. 709.54, found 732.7 M+H.

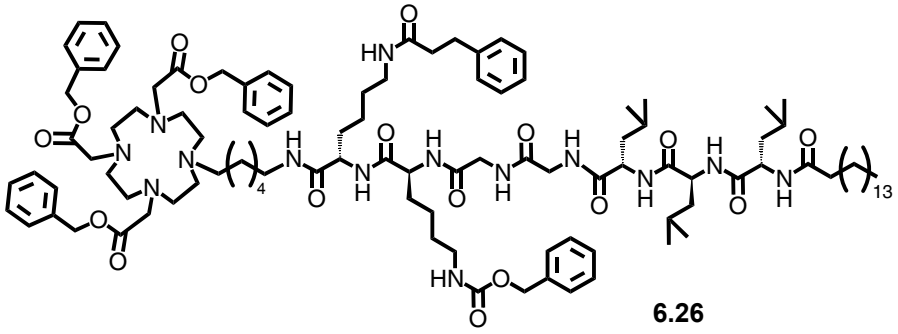

6.26

Compound 6.26: Reference synthesis of **6.18** with flash chromatography using 1/9/90 KNO_3/H_2O/ACN to give a white hygroscopic solid. The column yielded two spots that were not able to be separated so the combination of both spots was taken to the next step for deprotection. ESI MS (methanol) Calcd. 1931.22, found 965.56 M/2.

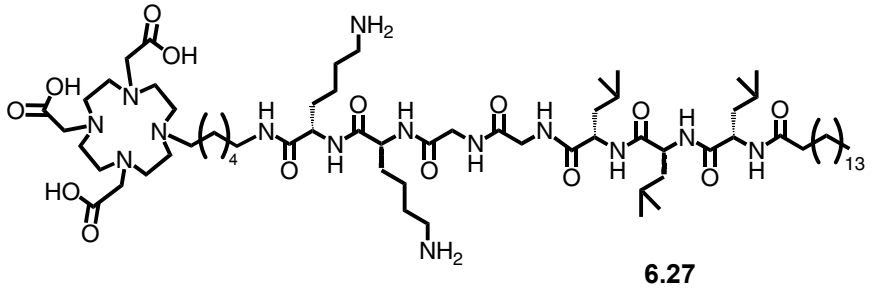

6.27

Compound 6.27: Reference synthesis of **6.19**. Hydrogenation continued for five days until MS showed complete removal of the benzyl groups. After filtration through celite, the product was taken up in 0.05% TFA/H_2O and filtered through a 0.200 μm syringe filter. HPLC was then performed on an Waters Atlantis semiprep RP column using a gradient from 100% 0.05%TFA/H_2O to 40% ACN over 15 min, to 70% ACN over 25 min, and 100% ACN over 20 min at 15 mL/min flow rate. The product eluted in 32 min (60% yield). MS MALDI Calcd. 1393.88, found 1394.64 M+H.

Chapter Seven

Genetically Engineered Protein Polymer Multivalent Magnetic Resonance Imaging Contrast Agents for Use in Tissue Engineering Applications

7 Genetically Engineered Protein Polymer Multivalent Magnetic Resonance Imaging Contrast Agents for Use in Tissue Engineering Applications

7.1 Introduction

Tissue engineering is a field that combines chemistry, biology, and materials science to design biocompatible materials that provide cellular signals for tissue regeneration. The scaffold is a key component of tissue engineering, supplying the physical support and chemical signals for cellular proliferation and ingrowth.[138, 178-180] Mechanical strength, degradation rate, porosity, chemical composition, incorporated bioactive factors, and other scaffold variables determine its efficacy, indicated by the survival and proliferation of the regenerating cells implanted with the scaffold.[138, 178] It is valuable to track the degradation of the scaffold and the ingrowth of the new tissue cells temporally and noninvasively to ascertain the biomaterials fate within a subject.[154, 181] This fate mapping would lead to greater care for the patient and better understanding into the healing process of that patient. Magnetic resonance imaging (MRI) affords advantages over other existing imaging modalities, providing whole animal imaging in four dimensions (x, y, z, and time) without the use of radiation or high energy, making it an ideal imaging tool for tracking tissue engineering scaffolds within the subject over time.[98, 109, 182, 183] Contrast agents (CAs) improve the sensitivity of MRI by increasing the relaxation rate of water protons, allowing for greater image contrast and decreased scan times.[7] T_1 CAs provide positive contrast enhancement by employing a paramagnetic ion, typically gadolinium, Gd(III), and the currently approved CAs' effectiveness are commonly governed by the rotational correlation time (τ_R). As the τ_R increases, the efficiency (measured as relaxivity in $mM^{-1}s^{-1}$) of the CA is increased.[7] The increase in relaxivity translates to a brighter image as taken by the magnet, providing a greater

contrast between the background of the body's tissue and the area containing the CA. Current clinically used CAs are small molecules that chelate Gd(III) with short τ_R, but research has turned to macromolecular CAs, including those based on protein binding,[7, 160, 161, 184] carbohydrates,[185, 186] linear polymers,[162, 163, 172, 187-189] dendrimers,[164, 165, 167-170] macromolecules,[190-193] self-assembly,[121, 194] and liposomes,[195] to increase the τ_R, the concentration of Gd(III), and retention of the CA in vivo. The increase in retention allows for longer scans and the ability for magnetic resonance angiography (labeling the blood with a CA to visualize the brain). To date, researchers have tracked tissue engineering scaffolds with MRI either without a CA or using one with a single Gd(III).[151-154, 181, 196] In Chapters 4, 5, and 6, I synthesized a number of self-assembling biomaterial scaffolds conjugated with a Gd(III) chelator,[98, 109] but we describe here for the first time a macromolecular CA based on artificial proteins covalently incorporated into tissue engineering hydrogels.

We report the design, synthesis, relaxivity, and in vitro images of a cutting-edge class of multivalent T_1 MRI CAs based on a synthetic bacterial protein. Artificial protein polymers that were generated through cloning and recombinant protein expression were naturally produced for use as the macromolecular backbone of a CA. Effectively, we have designed and synthesized the gene for a protein polymer, transformed it into *E. coli*, and induced them to naturally produce large quantities of this protein. These protein polymers were designed to obtain specific desirable properties, including solubility, reactivity, length, and the ability for these proteins to be incorporated into hydrogels for tissue engineering applications. In contrast to both natural biological (e.g. dextran) and synthetic polymers, we can exactly control the chemical makeup and length of these protein polymers, which are determined by the plasmid transformed into the

bacteria. We are able to obtain long monodisperse proteins with evenly spaced reactive sites, creating a construct that is an ideal backbone for a defined multivalent CA.

7.2 General Synthetic Scheme

The genetically engineered protein polymer backbone of these multivalent CAs consists of a repetitive amino acid monomer unit. The protein contains thirty repeats of the monomer, GKAGTGSA, providing thirty evenly spaced reactive lysines that are available for modification. The 21,825 Da protein polymer was designed to be water soluble (by use of multiple charged sites from the lysines), which is necessary for in vivo applications, and to have a random coil configuration. This random coil configuration was preprogrammed into the polymer to prevent protein collapse and allow for exposure of the lysines for contrast agent conjugation. A macrocyclic 1, 4, 7, 10-tetraazacyclocododecane-1, 4, 7, 10-tetra acetic acid (DOTA) derivative was used as the Gd(III) chelator and covalently attached to the lysines. The three acetate arms chelate the Gd(III) while the carboxyl group on the valeric acid arm was used for covalent attachment with the ε amine on the protein's lysine residues.

The multi-step controlled cloning method was used to create the gene for the protein polymer.[197] Standard transformation and expression protocols were used to produce the protein polymer, **7.1**. The pET19 plasmid that the gene was ligated into contains an N-terminal histidine fusion tag, GH_{10}SSGHIDDDDKHM, enabling protein purification via Ni-NTA affinity chromatography under denaturing conditions. Effectively, after the DNA synthesis and transformation into expression cells, the CA backbone can be produced in large quantities by the bacteria and then followed with a facile column purification process. Details of this procedure can be found in my collaborator's, Lindsay Karfeld's, thesis.

The Gd(III) chelator was synthesized using a hydrogenation labile protection scheme with benzyl 2-bromoacetate and benzyl 5-bromopentanoate as the chelating arms of the macrocycle (**Scheme 7.1**).[198] Addition of three benzyl 2-bromoacetate arms to cyclen was followed by addition of benzyl 5-bromopentanoate. Global deprotection by hydrogenation of the chelator and subsequent metallation with $GdCl_3$ afforded **7.6** to be conjugated to the protein polymer.

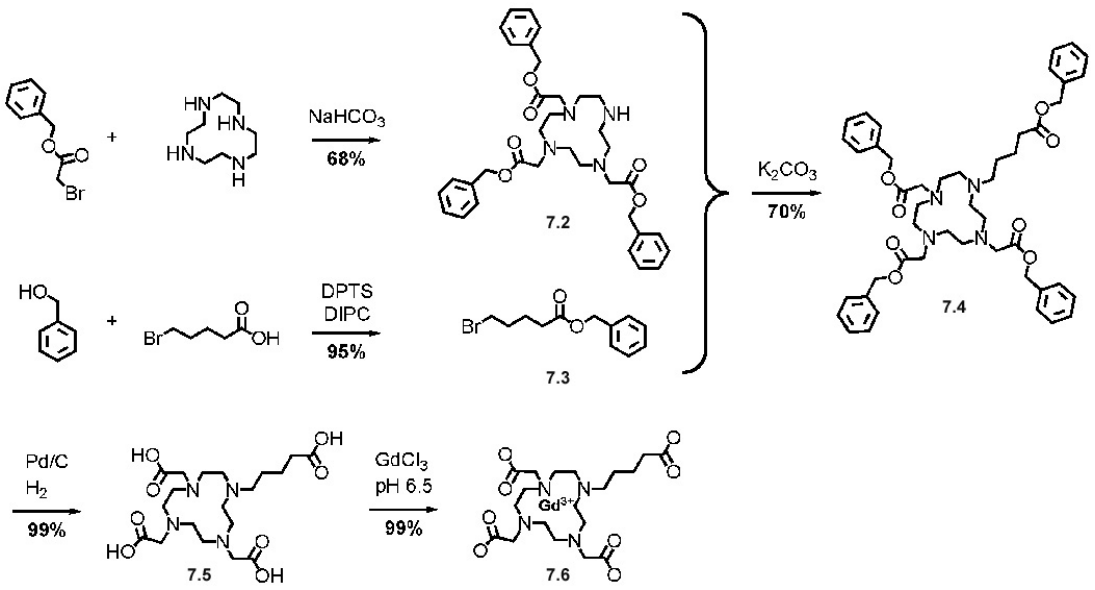

Scheme 7.1 Synthesis of Gd(III) chelator using a global deprotection scheme. The Gd(III) was chelated prior to conjugation to the protein to ensure all chelators contained Gd(III).

The coupling reaction between the lysine residues on **7.1** and **7.6** (**Figure 7.1**), was carried out in an aqueous 0.1 M MES, 0.5 M NaCl buffer with EDC and Sulfo-NHS, peptide coupling agents. We performed this conjugation in water owing to the solubility restrictions of the chelator and protein and chose to conjugate premetallated chelators to the protein polymer in order to guarantee that every chelate had Gd(III) conjugated.

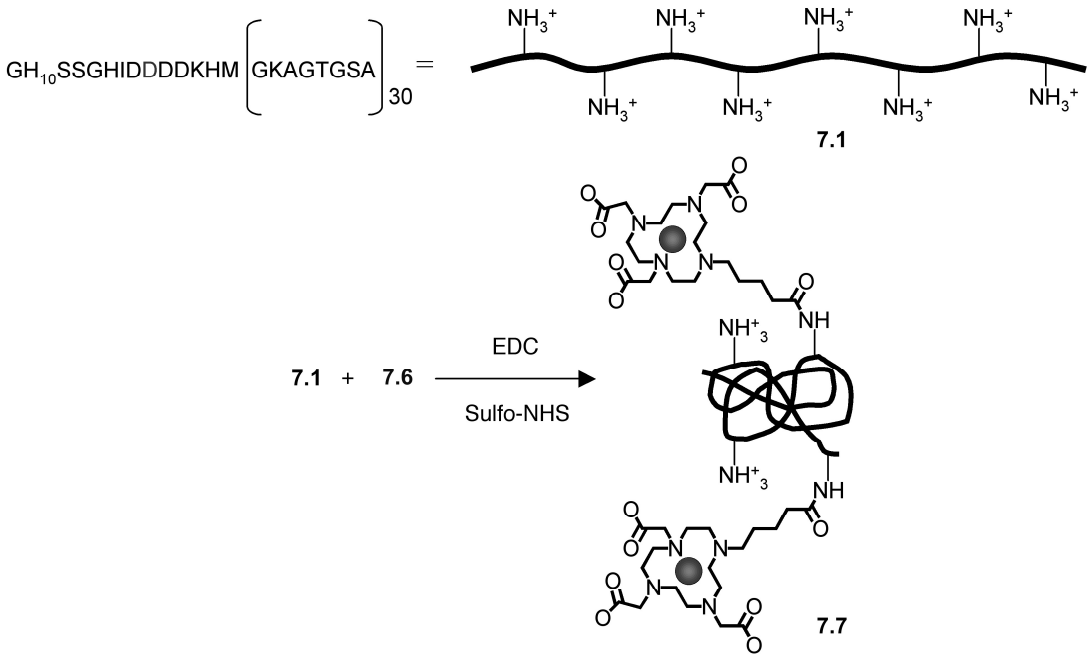

Figure 7.1 Conjugation of Gd(III) chelator to protein polymer backbone by standard coupling conditions. This provided ~8-9 Gd(III) per protein molecule.

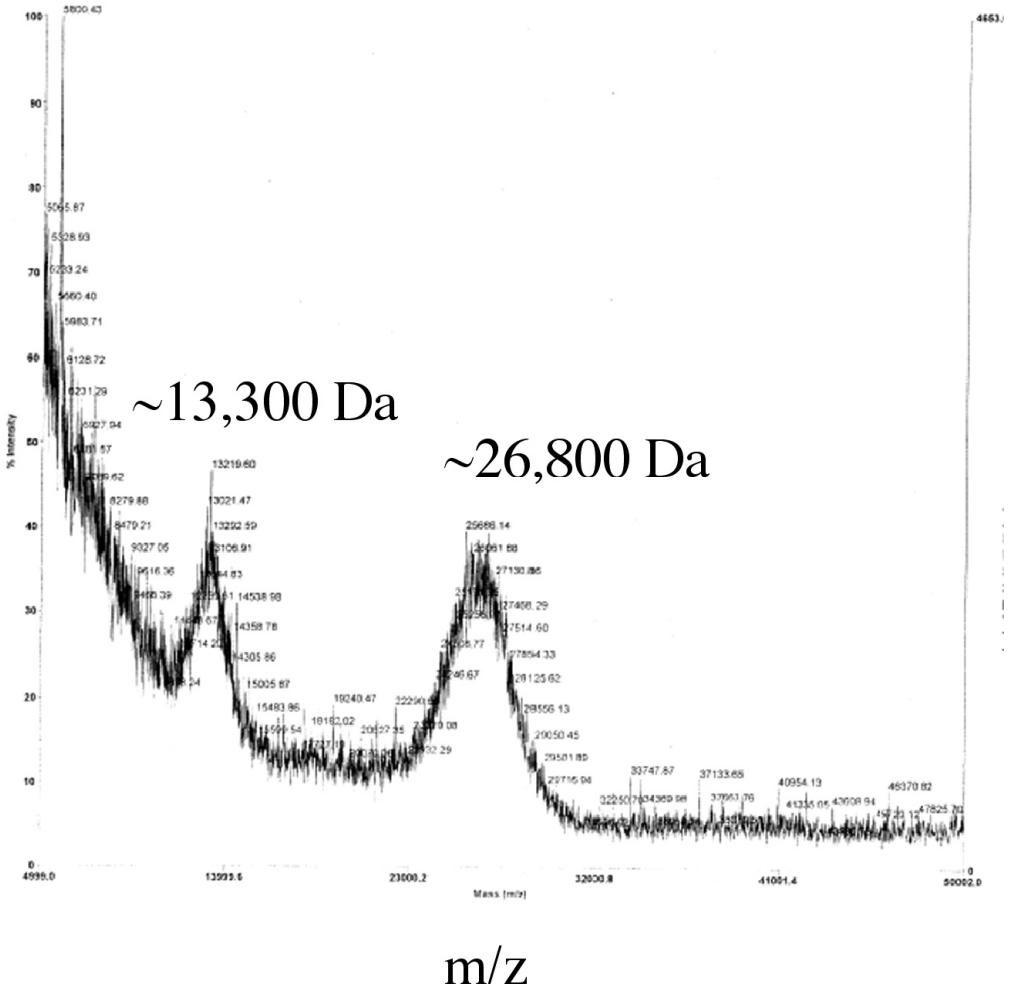

Figure 7.2 MALDI-MS of **7**. Depicted are the mass and M/2 peaks.

7.3 Results

Using these synthesis conditions, we have consistently produced CAs that display a relaxivity of 62.6 ± 3.5 $mM^{-1}s^{-1}$ per molecule and 7.3 ± 0.4 $mM^{-1}s^{-1}$ per Gd. This relaxivity is about double that of DOTA alone and is expected with the increase of τ_r experienced by the protein polymer and the local τ_R experienced by the linker flexibility. We obtained a 4.5% reproducibility difference in the relaxivity using this procedure for conjugation, and MALDI-MS

confirms ~8-9 lysines per molecule are being conjugated to the contrast agent resulting in a reliable synthetic methodology.

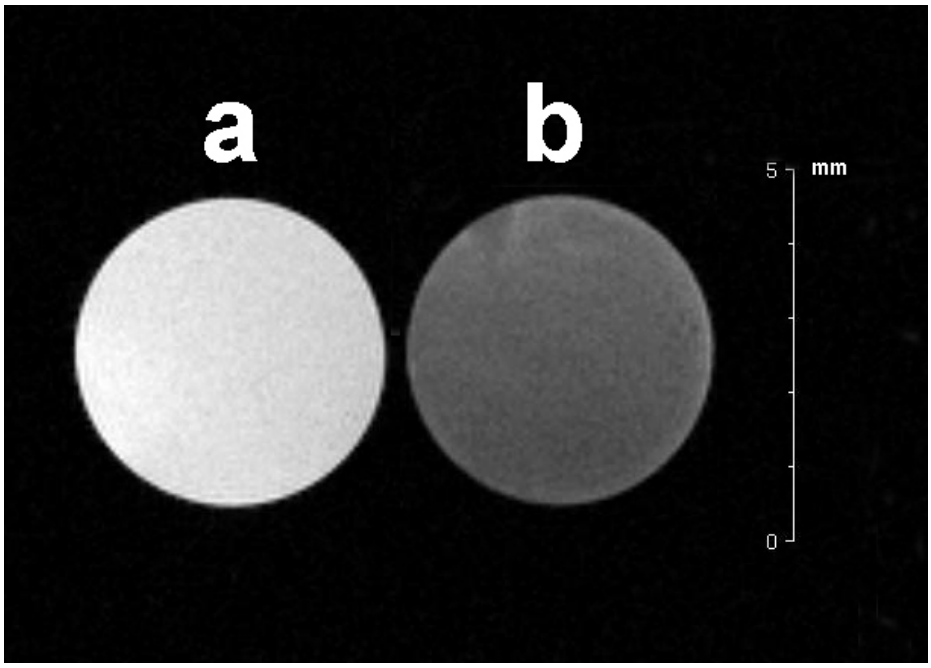

Figure 7.3 MR image taken at 600 MHz, **a** is the gel doped with **7.7**, Gd(III) concentration of 0.8 mmol, and **b** is the control gel without CA.

As indicated above, these protein polymer CAs enable the use of MRI to track tissue engineering gel scaffolds to be used in vivo. To demonstrate the proof of concept, we created gels in 5 mm NMR tubes for MR imaging. The protein polymer (not containing any CA) and the free amines were crosslinked with glutaraldehyde to form a hydrogel. An advantage of these protein polymer-based CAs is that they covalently crosslink to assist in forming the hydrogel and can only be removed as a result of hydrolysis of the scaffold, not from diffusion. This ensures the presence of the CA until complete degradation of the scaffold. The gel with **7.7** shows dramatically higher contrast than the unconjugated protein polymer control (**Figure 7.3**) and can be varied by the concentration of the CA doped protein added. Although glutaraldehyde itself is

toxic and other crosslinking mechanisms would be more favorable in a biological system, these images demonstrate the significant contrast enhancement as well as feasibility for different crosslinking reactions.

7.4 Conclusion

In conclusion, a combination of biosynthetic and chemical methods has been used to create high contrast, multivalent, protein polymer-based MRI CAs. We have demonstrated that we have a reliable synthetic protocol that produces reproducible relaxivity results and can be accomplished on large scales. As shown in the MR images, this protein polymer-based CA can be incorporated into a hydrogel and display a dramatic contrast enhancement, which is important for fate mapping the evolution of the tissue engineering scaffolds within a subject. We can optimize reaction conditions to increase the extent of grafting as well as the relaxivity of the CAs. In the future, we will employ other crosslinking mechanisms and hydrogel media to create a biocompatible tissue engineering scaffold to be fate mapped by MRI, enabling tracking of both the cellular ingrowth and the scaffold degradation over time. We can attach targeting epitopes to the backbone for induce specificity for the CA to be used in vivo.

7.5 Experimental

Unless otherwise noted, all starting materials were obtained from commercial sources and used without further purification. Analytical TLC was performed on Merck KgaA silica gel 60 F254 TLC plates. Silica for flash chromatography was ICN Silitech 32-63 D 60 Å. ^{1}H NMR spectra were recorded on Varian 500, 400 or 300 MHz NMR spectrometers. ^{13}C NMR spectra were on a Varian 500, 400 or 300 MHz NMR spectrometer. MALDI-TOF mass spectrometry was performed on a PE Voyager DE-Pro MALDI-TOF-MS instrument.

Relaxivity measurements were performed in triplicate using a Bruker mq60 NMR Analyzer (Bruker Canada, Milton, Ont., Canada). Inductively coupled plasma mass spectrometry (ICP-MS) was used to determine Gd(III) concentration and was performed on a Thermo Jarrell Ash Atomscan Model 25 Sequential ICP Spectrometer.

The synthesis of the protein polymer was completed by Lindsay Karfeld of the Barron Group at NWU and will not be added to this thesis.

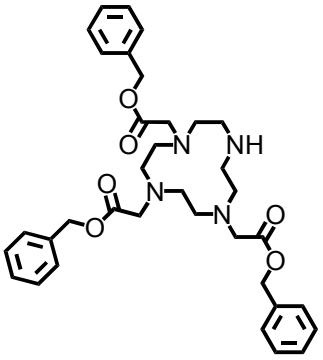

Synthesis of **7.2**: In a dry round bottom flask was combined cyclen (2.89 g, 17 mmol), sodium bicarbonate (4.71 g, 56 mmol) and dry acetonitrile (200 mL). The solution was stirred under N_2, for 5 min and a solution of dry acetonitrile (30 mL) and benzyl bromoacetate (11.61 g, 51 mmol) was added dropwise. The reaction proceeded overnight then the solid was filtered, and the solvent was removed by rotary evaporation. Flash chromatography was performed using 1/9/90 KNO_3/H_2O/ACN to give an off white hygroscopic solid (10 g, 68% yield). ^{1}H NMR (500 MHz, $CDCl_3$) δ 7.34 (s, 15H), 5.12 (s, 6H), 3.48 (s, 4H), 3.42 (s, 2H), 3.08 (s, 4H), 2.88-2.83 (bm, 12H). ^{13}C (125 MHz, $CDCl_3$) δ 171.09, 170.28, 135.44, 128.79, 128.72, 128.66, 128.55, 66.71, 57.28, 51.55, 49.42, 47.38. ESI MS (methanol) Calcd. 616.33, found 639.63 M+Na.

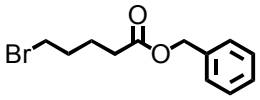

Synthesis of benzyl 5-bromopentanoate (**7.3**): In a dry roundbottom flask was combined 5-bromo valeric acid (2.00 g, 11 mmol), DTPS (3.56 g, 12.1 mmol), DIPC (1.81 g, 14.3 mmol) and DCM (200 mL). The solution was stirred for five min and a solution of benzyl alcohol (1.79 g, 16.6 mmol) and DCM (10 mL) was added dropwise. The reaction proceeded overnight then was diluted in DCM and washed with H_2O three times, dried over $MgSO_4$, and the solvent was removed by rotary evaporation. Flash chromatography was performed using 5/95 MeOH/DCM to afford a clear colorless liquid (2.82 g, 95% yield). ^{1}H NMR (500 MHz, $CDCl_3$) δ 7.36 (s, 5H), 5.14 (s, 2H), 3.43 (t, *J*=7 Hz, 2H), 2.41 (t, *J*=7 Hz, 2H), 1.90 (q, *J*=7 Hz, *J*=14 Hz, 2H), 1.83 (q, *J*=7 Hz, *J*=14 Hz, 2H). ^{13}C (125 MHz, $CDCl_3$) δ 173.19, 136.19, 128.86, 128.54, 128.51, 66.55, 33.53, 33.33, 32.21, 23.74. ESI MS (methanol) Calcd. 270.03, found 271.23 M+H.

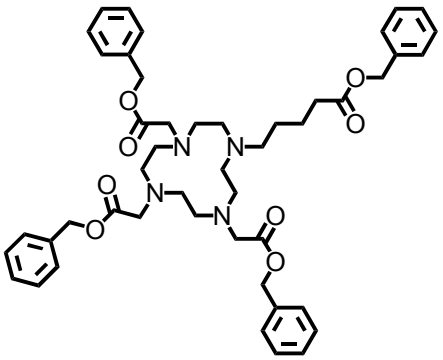

Synthesis of **7.4**: In a dry roundbottom flask was combined **7.2** (0.35 g, 0.57 mmol), potassium carbonate (0.24 g, 1.7 mmol) and dry acetonitrile (30 mL). The solution was stirred under N_2, for 5 minutes and a solution of dry acetonitrile (5 mL) and benzyl 5-bromopentanoate (**3**) (0.167

g, 0.74 mmol) was added dropwise. The reaction proceeded overnight then the solid was filtered, and the solvent was removed by rotary evaporation. Flash chromatography was performed using 1/9/90 KNO_3/H_2O/ACN to give a white solid (0.458 g, 70% yield). ^{1}H NMR (500 MHz, $CDCl_3$) δ 7.28 (s, 20H), 5.07 (s, 8H), 3.63-2.28 (bm, 24H), 1.65 (s, 4H), 1.48 (m, 2H), 1.35 (m, 2H). ^{13}C (125 MHz, $CDCl_3$) δ 172.77, 170.98, 170.57, 135.83, 135.45, 135.22, 134.96, 128.66, 128.62, 128.57, 128.51, 128.41, 128.30, 128.24, 128.18, 66.67, 66.43, 66.26, 56.09, 53.00, 52.72, 52.44, 50.17, 47.53, 33.18. ESI MS (methanol) Calcd. 806.43, found 807.52 M+H.

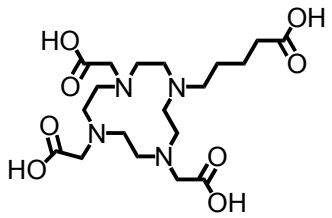

Synthesis of **7.5:** In a falcon tube was placed **7.4** (0.17 g, 0.70 mmol), MeOH (10 mL), DCM (10 mL), and Pd/C (0.04 g). The solution was stirred under a balloon of H_2 for two days. The solution was then filtered through celite, the solvent was removed by rotary evaporation providing a hygroscopic white solid. ^{1}H NMR (500 MHz, D_2O) δ 3.66 (s, 2H), 3.46-2.96 (bm, 22H), 2.28 (t, *J*=7.5 Hz, 2H), 1.60 (s, 2H), 1.48 (m, 2H). ^{13}C (125 MHz, $CDCl_3$) δ 177.86, 174.34, 169.40, 53.91, 53.11, 51.79, 49.93, 49.01, 48.47, 48.19, 33.12, 22.31, 21.34. ESI MS (methanol) Calcd. 446.24, found 469.42 M+Na.

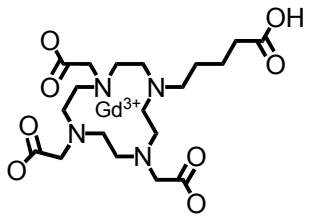

Synthesis of **7.6:** In a falcon tube was placed **5** (0.17 g, 0.37 mmol), MilliQ H_2O (4 mL), and $GdCl_3$ (0.15 g, 0.4 mmol). The pH was adjusted to 6.5 using ammonium hydroxide and the solution was stirred for 2 days. The solution was then brought up to pH 10, the ppt was centrifuged at 4000 rpm for 10 min, and the liquid decanted. The water was removed by lyophilization giving a white powder (mass and yield inaccurate because of NaOH salt in the final product). ESI MS (negative mode) (methanol) Calcd. 600.16, found 600.21 M.

A 5.8 wt% hydrogel was made in 5 mm NMR tubes. The hydrogel with **7.7** contained 5.30 x 10^{-7} mol of Gd(III). The remaining weight was made up of the unconjugated protein polymer. The solids were dissolved in 650 μL of 0.01 M sodium phosphate, 0.15 M sodium chloride, pH 7.4 buffer and then put in the NMR tube. Glutaraldehyde (45 μL) was then added, the NMR tube was mixed by sonication, and then put on ice. Imaging was performed on a 4.7 T MR magnet.

Chapter 8: Appendix

Principles and Details of Magnetic Resonance Imaging

8 Principles of Magnetic Resonance Imaging

A.1 Basic Concepts of Magnetic Resonance Imaging

Here I will briefly explain the basics of NMR which are the basics of MRI. When an atomic nucleus has an odd number of protons or neutrons it will produce a magnetic field. One can think of this as a tiny ball of charge spinning, creating a magnetic field (a magnet). When placed in an external magnetic field (B), these tiny magnets (nuclei) want to align with the field. Depending on both the inherent gyromagnetic ratio of the nuclei (Γ) and the strength of the external B field, the energy that is required to flip these nuclei 180^0 is related to the Larmor frequency. This flipping and relaxing phenomenon is what NMR and MRI makes use of because we can measure the time it takes for the nuclei to return to the lowest energy state (aligned with the B field) which emits recordable energy. (In real terms, the energy needed to flip the proton spins of water is on the order of 0.6 μeV, which is millions of times lower energy than X-rays.) The required energy to flip the nuclei is the same energy as the Larmor frequency and because the MR scanner is built with the ability to generate a gradient magnetic field, it effectively creates "slices" of differing B field. The protons in these slices all require the same Larmor frequency radio frequency (RF) pulse to excite them. This gradient field is created by coils inside the homogeneous B field that are turned on and off (giving rise to the sound one hears). The computer can tell when to send an RF pulse and detect the relaxation of the protons.

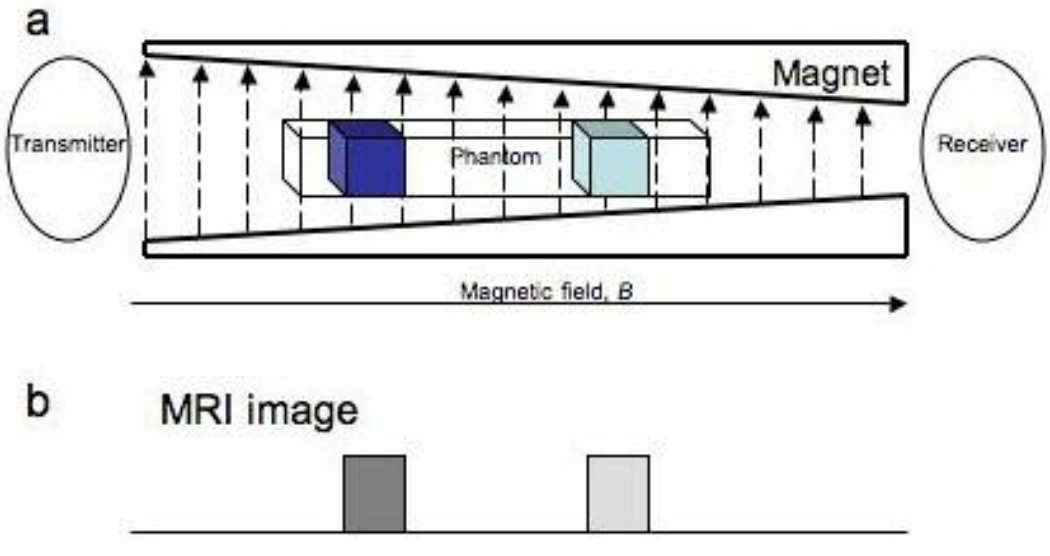

Figure 8.1 A gradient magnetic field has been created with a phantom inserted. The dark blue box is filled with water and the light blue box is filled with half as much water. The water samples are in different field strengths and have different water contents. These properties allows for the specific excitation of each phantom giving rise to signals that are spatially encoded and have different intensities based upon water content.

Because most of the samples for MRI are heterogeneous and large, orthogonal magnetic gradients are used to give the 3-D spatial encoding of voxels. A voxel is the smallest distinguishable unit in an image, one can liken this to a pixel on a LCD monitor. The computer applies varying magnetic field gradients and RF pulses and records the energy given off when the nuclei relax, giving rise to spatial resolution with the sample (**Figure 8.1**).

A.2 Relaxation Equations

Proton relaxation is composed of the longitudinal relaxation rate and the transverse relaxation rate. This thesis is concerned with the longitudinal relaxation rate because the CAs used augment the longitudinal relaxation rate. A great review has been published by Caravan et al. and I direct anyone interested in further understanding and detail to read it.[7, 158] There are

many other reviews and papers published on the equations and how to augment relaxivity.[11, 112, 114, 199, 200]

Observed relaxation rate can be expressed as the sum of the diamagnetic (d) and paramagnetic (p) relaxation rates.

$(1/T_i)_{obs}=(/T_i)_d + (1/T_i)_p \;\; i = 1, 2$ **equation 1**

The diamagnetic contribution is inherent to the sample and its surroundings. The paramagnetic contribution is proportional to the concentration of the paramagnetic species. Therefore, relaxivity (r_1) is defined by the concentration dependence of the relaxation rate of the paramagnetic ion.

$(1/T_i)_{obs}=(/T_i)_d + r_1[Gd] \;\; i = 1, 2$ **equation 2**

Relaxivity is measured as the slope of $1/T_1$ versus the concentration of the paramagnetic species in $mM^{-1}s^{-1}$ and is basically the efficiency of the CA.

The paramagnetic component can then be expressed from two different terms, the inner-sphere and the outer-sphere relaxation.

$(1/T_i)_p=(1/T_i)_{inner\,sphere} + (1/T_i)_{outer} \; i = 1, 2$ **equation 3**

Outer-sphere relaxation is the interaction between the paramagnetic center and the neighboring water molecules that are not directly coordinated to the metal ion. The inner-sphere relaxation represents the interaction between the paramagnetic center and its bound water molecules.

Inner-sphere relaxation

The inner-sphere relaxation rate ($1/T_1^{IS}$) is the most important portion for MRI CAs. One is able to modulate the factors affecting the relaxation time and thus can control the efficacy of the CA. *c* is the molar concentration of the paramagnetic species, *q* is the number of water

molecules bound to the paramagnetic center, τ_m is the mean residence lifetime of the bound water molecule, and T_{1m} is the longitudinal relaxation rate of the bound water molecules.

$$1\frac{1}{T_1^{IS}} = \frac{cq}{55.5}\left(\frac{1}{T_{1m} + \tau_m}\right) \qquad \textbf{equation 4}$$

We can further break down this longitudinal relaxation rate in the sum of the dipole-dipole (DD) relaxation and the scalar (SC) relaxation rates.

$$\frac{1}{T_{1m}} = \frac{1}{T_1^{DD}} + \frac{1}{T_1^{SC}} \qquad \textbf{equation 5}$$

When the water exchange rate becomes fast as is the case with Gd(III) ions, the scalar interaction becomes negligible and the relaxation rate then is dependent on the dipolar interaction between the water molecule and the paramagnetic center.

From the previous equations, T_1^{DD} is affected by τ_{ci}, which is the correlation time that defines the dipole-dipole relaxation. This correlation time is determined by three parameters; the electron spin relaxation time (T_{1e}), the mean residence lifetime (τ_m), and the rotation correlation time (τ_R).

$$\frac{1}{\tau_{ci}} = \frac{1}{T_{1e}} + \frac{1}{\tau_m} + \frac{1}{\tau_R} \quad \text{i=1, 2} \qquad \textbf{equation 6}$$

High relaxivity CAs will normally vary the τ_R of the above equation. The outer-sphere relaxation is not well understood and it is difficult to control then the better understood inner-sphere relaxation. The ideal case is when the Larmor frequency is equal to the total correlation time, which is why the relaxivity of the CA changes with the magnetic field.

Hydration number

When using CAs, one of the most important properties is the number of water molecules that is in direct contact with the metal (**Figure 8.2**). This number is represented by the letter q.

From the **equation 4**, q is directly proportional to the relaxation time. When q is increased, the relaxation time is decreased, generating a higher intensity image on the MR image. Current clinically used CAs have q = 1, where the chelator occupies eight of the possible nine binding sites of the Gd(III) ion. The association constants of these molecules are very high (~21-25), preventing the dissociation of the Gd(III) metal.[201] It is not simple to increase q because as one increases the number of bound waters, the association constant decreases.[200] Because Gd(III) is toxic, one must keep a high stability constant and this has constrained the use of contrast agents to q = 1.[202] Raymond's group at the University of California, Berkeley has developed some of the most important q = 2 ligands for MRI CAs that maintain a high stability constant classified under the name HOPO CAs.[161, 192, 203-208]

Water exchange rate

The water exchange rate is very important to the relaxivity and research is currently involved with optimization of τ_m.[209-212] Essentially, if the bound water molecules lifetime is too short, the paramagnetic ion does not have time to relax the proton fully.[161] Woods et al. completed much of the work associated with the water exchange rate and DOTA derivatives.[213-215] If the lifetime is too long, there is not enough water cycling through the metal ion and the relaxivity decreased. The optimal time is based upon the magnetic field strength and in current scanners this time is ~10 ns.[7, 158] The clinically used CAs have τ_m ~200 ns and are far from optimal.[216]

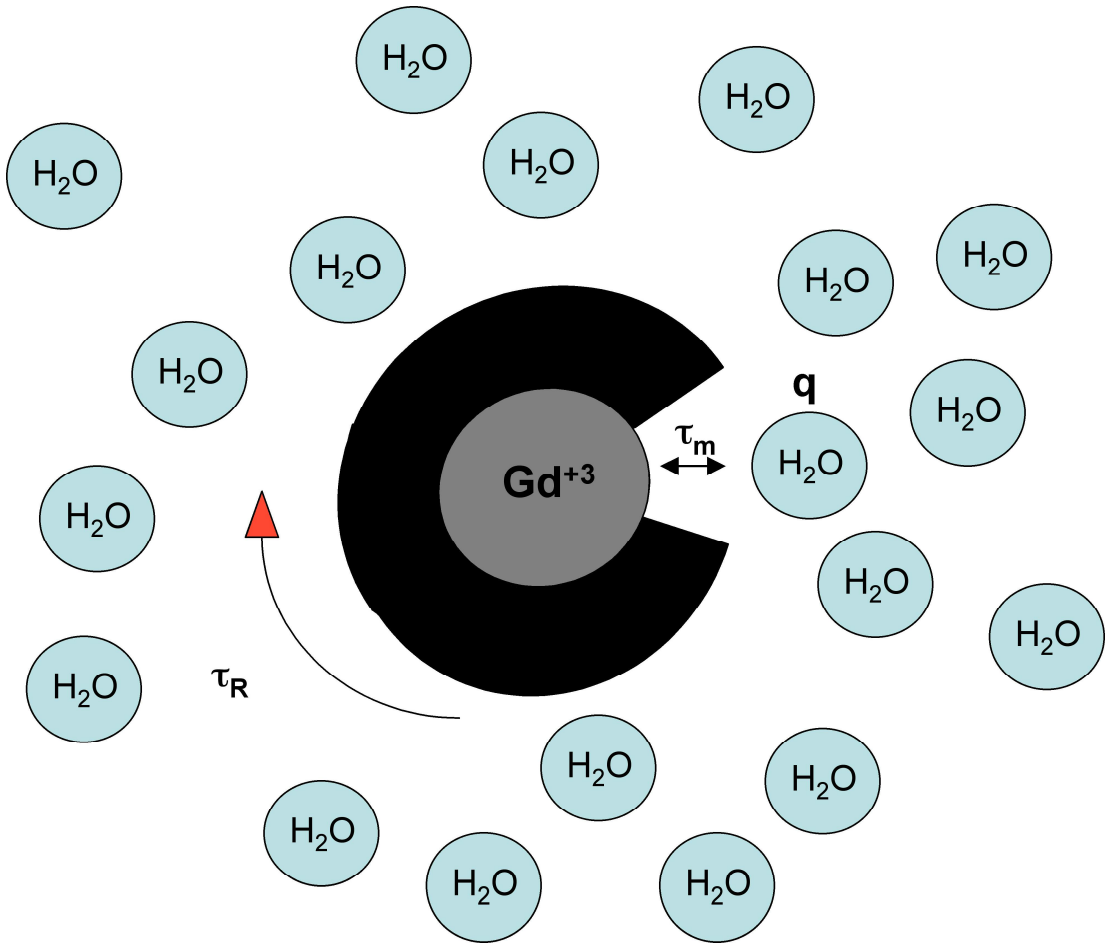

Figure 8.2 Cartoon depicting the variables involved with relaxivity. τ_r : rotational correlation time (optimize based upon the electronic relaxation time, $\tau_r << T_{1e}$); τ_m : water exchange rate (optimize normally ~10 ns); q : hydration number (optimize with the dissociation constant, normally 1-2)

Rotational correlation time

The most important factor in determining relaxivity in small molecular CAs is the rotational correlation time.[184] Currently used CAs have a τ_R in the 0.1 ns range, ideally one would like to have it • 10 ns.[158] This τ_R is close to that of proteins and large molecules and much research has been done into attaching these CAs to large proteins, either covalently or noncovalently[159, 217-219] to increase the rotation correlation time and research has been conducted on

using hydrogen bonds to increase the rotational correlation time.[220] These strategies are called the receptor induced magnetization enhancement (RIME).[48, 221]

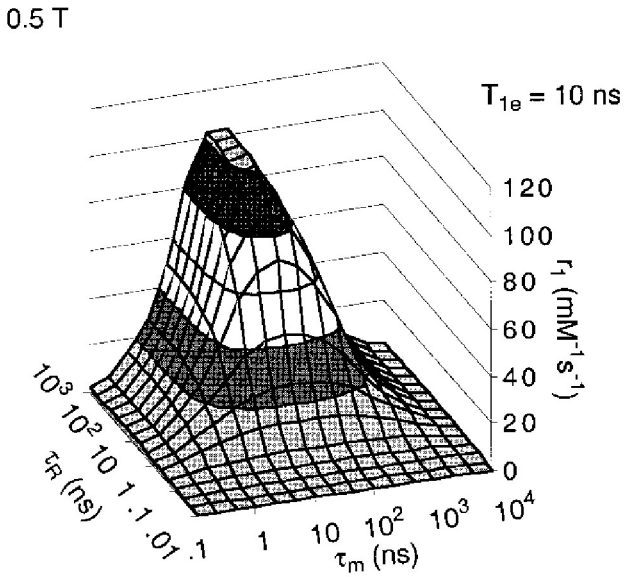

Figure 8.3 Graph depicting the theoretical maximum relaxivity possible when optimizing both τ_R and τ_m.[7]

Simultaneous manipulation of q, τ_R, and τm will provide the best relaxivity contrast agent. If only it was that easy…

References

1. Mansson, S.; Bjornerud, A., *The Chemistry of Contrast Agents in Medical Magnetic Resonance Imaging*. John Wiley and Sons: New York, 2001; p 1-44.

2. Thunus, L.; Lejeune, R., Overview of Transition Metals and Lanthanide Complexes as Diagnostic Tools. *Coordination Chemistry Reviews* **1999,** 184, 125-155.

3. Reichert, D. E.; Lewis, J. S.; Anderson, C. J., Metal Complexes as Diagnostic Tools. *Coordination Chemistry Reviews* **1999,** 184, 3-66.

4. Mansfiel.P; Grannell, P. K., Nmr Diffraction in Solids. *Journal of Physics C-Solid State Physics* **1973,** 6, (22), L422-L426.

5. Lauterbu.Pc, Image Formation by Induced Local Interactions - Examples Employing Nuclear Magnetic-Resonance. *Nature* **1973,** 242, (5394), 190-191.

6. Aime, S.; Botta, M.; Fasano, M.; Terreno, E., Prototropic and Water-Exchange Processes in Aqueous Solutions of Gd(III) Chelates. *Accounts of Chemical Research* **1999,** 32, (11), 941-949.

7. Caravan, P.; Ellison, J. J.; McMurry, T. J.; Lauffer, R. B., Gadolinium(III) Chelates as MRI Contrast Agents: Structure, Dynamics, and Applications. *Chemical Reviews (Washington, D. C.)* **1999,** 99, (9), 2293-2352.

8. Aime, S.; Botta, M.; Fasano, M.; Terreno, E., Lanthanide(III) chelates for NMR biomedical applications. *Chemical Society Reviews* **1998,** 27, (1), 19-29.

9. Louie, A. Y.; Duimstra, J. A.; Meade, T. J., *Brain Mapping, The Methods*. Elsevier Science: San Diego, 2002.

10. Weishaupt, D.; Kochli, V. D.; marincek, B., *How does MRI work?* 3 ed.; Springer Verlag: New York, Berlin, Paris, 2003.

11. Reichert, D. E.; Lewis, J.; Anderson, C. J., Metal Complexes as Diagnostic Tools. *Coordination Chemistry Reviews* **1999,** 184, 3-66.

12. Toth, E.; Helm, L.; Merbach, A. E., *The Chemistry of Contrast Agents in Medical Magnetic Resonance Imaging*. 1 ed.; John Wiley and Sons: New York, 2001; p 45-120.

13. Caravan, P.; Astashkin, A. V.; Raitsimring, A. M., The Gadolinium(III)-Water Hydrogen Distance in MRI Contrast Agents. *Inorganic Chemistry* **2003,** 42, (13), 3972-3974.

14. Bertini, I. L., C., *NMR of Paramagnetic Molecules in Biological Systems*. Benjamin/Cummings: Menlo Park, CA, 1986.

15. Banci, L.; Bertini, I.; Luchinat, C., *Nuclear and Electronic Relaxation: The Magnetic Nucleus-Unpaired Electron Coupling in Solution*. New York, 1991.

16. Kumar, K.; Chang, C. A.; Francesconi, L. C.; Dischino, D. D.; Malley, M. F.; Gougoutas, J. Z.; Tweedle, M. F., Synthesis, Stability, and Structure of Gadolinium(III) and Yttrium(III) Macrocyclic Poly(amino carboxylates). *Inorganic Chemistry* **1994,** 33, (16), 3567-75.

17. Dischino, D. D.; Delaney, E. J.; Emswiler, J. E.; Gaughan, G. T.; Prasad, J. S.; Srivastava, S. K.; Tweedle, M. F., Synthesis of nonionic gadolinium chelates useful as contrast agents for magnetic resonance imaging: 1,4,7-tris(carboxymethyl)-10-substituted-1,4,7,10-tetraazacyclododecanes and their corresponding gadolinium chelates. *Inorganic Chemistry* **1991,** 30, (6), 1265-9.

18. Wang, X.; Jin, T.; Comblin, V.; Lopez-Mut, A.; Merciny, E.; Desreux, J. F., A kinetic investigation of the lanthanide DOTA chelates. Stability and rates of formation and of dissociation of a macrocyclic gadolinium(III) polyaza polycarboxylic MRI contrast agent. *Inorganic Chemistry* **1992,** 31, (6), 1095-9.

19. Aime, S.; Calabi, L.; Cavallotti, C.; Gianolio, E.; Giovenzana, G. B.; Losi, P.; Maiocchi, A.; Palmisano, G.; Sisti, M., [Gd-AAZTA](-): A new structural entry for an improved generation of MRI contrast agents. *Inorganic Chemistry* **2004,** 43, (24), 7588-7590.

20. Gries, H., Extracellular MRI contrast agents based on gadolinium. *Topics in Current Chemistry* **2002,** 221, (Contrast Agents I), 1-24.

21. Li, C.; Winnard, P. T.; Takagi, T.; Artemov, D.; Bhujwalla, Z. M., Multimodal image-guided enzyme/prodrug cancer therapy. *Journal of the American Chemical Society* **2006,** 128, (47), 15072-15073.

22. Zheng, Q.; Dai, H. Q.; Merritt, M. E.; Malloy, C.; Pan, C. Y.; Li, W. H., A new class of macrocyclic lanthanide complexes for cell labeling and magnetic resonance imaging applications. *Journal Of The American Chemical Society* **2005,** 127, (46), 16178-16188.

23. Vuu, K.; Xie, J. W.; McDonald, M. A.; Bernardo, M.; Hunter, F.; Zhang, Y. T.; Li, K.; Bednarski, M.; Guccione, S., Gadolinium-rhodamine nanoparticles for cell labeling and tracking via magnetic resonance and optical imaging. *Bioconjugate Chemistry* **2005,** 16, (4), 995-999.

24. Crich, S. G.; Biancone, L.; Cantaluppi, V.; Esposito, D. D. G.; Russo, S.; Camussi, G.; Aime, S., Improved route for the visualization of stem cells labeled with a Gd-/Eu-chelate as dual (MRI and fluorescence) agent. *Magnetic Resonance in Medicine* **2004,** 51, (5), 938-944.

25. Poduslo, J. F.; Wengenack, T.; Curran, G. V.; Macura, S.; Borowski, B.; Jack, C.; Wisniewski, T.; Sigurdsson, E., Molecular targeting of Alzheimer's amyloid plaques for contrast-enhanced magnetic resonance imaging. *Neurobiology of Aging* **2002,** 23, (1), S422-S422.

26. Poduslo, J. F.; Curran, G. L.; Peterson, J. A.; McCormick, D. J.; Fauq, A. H.; Khan, M. A.; Wengenack, T. M., Design and chemical synthesis of a magnetic resonance contrast agent with enhanced in vitro binding, high blood-brain barrier permeability, and in vivo targeting to Alzheimer's disease amyloid plaques. *Biochemistry* **2004,** 43, (20), 6064-6075.

27. Allen, M. J.; MacRenaris, K. W.; Venkatasubramanian, P. N.; Meade, T. J., Cellular delivery of MRI contrast agents. *Chemistry & Biology* **2004,** 11, (3), 301-307.

28. Allen, M. J.; Meade, T. J., Synthesis and visualization of a membrane-permeable MRI contrast agent. *Journal of Biological Inorganic Chemistry* **2003,** 8, (7), 746-750.

29. Jacques, V.; Desreux, J. F., New classes of MRI contrast agents. *Topics in Current Chemistry* **2002,** 221, (Contrast Agents I), 123-164.

30. Louie, A. Y.; Huber, M. M.; Ahrens, E. T.; Rothbacher, U.; Moats, R.; Jacobs, R. E.; Fraser, S. E.; Meade, T. J., In vivo visualization of gene expression using magnetic resonance imaging. *Nature Biotechnology* **2000,** 18, (3), 321-325.

31. Jacobs, R. E.; Ahrens, E. T.; Meade, T. J.; Fraser, S. E., Looking deeper into vertebrate development. *Trends in Cell Biology* **1999,** 9, (2), 73-6.

32. Frullano, L.; Tejerina, B.; Meade, T. J., Synthesis and characterization of a doxorubicin-Gd(III) contrast agent conjugate: A new approach toward prodrug-procontrast complexes. *Inorganic Chemistry* **2006,** 45, (21), 8489-8491.

33. Li, W.-h.; Fraser, S. E.; Meade, T. J., A Calcium-Sensitive Magnetic Resonance Imaging Contrast Agent. *Journal of the American Chemical Society* **1999,** 121, (6), 1413-1414.

34. Li, W.-h.; Parigi, G.; Fragai, M.; Luchinat, C.; Meade, T. J., Mechanistic Studies of a Calcium-Dependent MRI Contrast Agent. *Inorganic Chemistry* **2002,** 41, (15), 4018-4024.

35. Hanaoka, K.; Kikuchi, K.; Urano, Y.; Nagano, T., Selective sensing of zinc ions with a novel magnetic resonance imaging contrast agent. *Journal of the Chemical Society, Perkin Transactions 2* **2001**, (9), 1840-1843.

36. Que, E. L.; Chang, C. J., A Smart Magnetic Resonance Contrast Agent for Selective Copper Sensing. *Journal of the American Chemical Society* **2006,** 128, (50).

37. Zhang, S.; Wu, K.; Sherry, A. D., A novel pH-sensitive MRI contrast agent. *Angewandte Chemie, International Edition* **1999,** 38, (21), 3192-3194.

38. Mikawa, M.; Miwa, N.; Brautigam, M.; Akaike, T.; Maruyama, A., A pH-sensitive contrast agent for functional magnetic resonance imaging (MRI). *Chemistry Letters* **1998,** 7, 693-694.

39. Aime, S.; Castelli, D. D.; Terreno, E., Novel pH-reporter MRI contrast agents. *Angewandte Chemie, International Edition* **2002,** 41, (22), 4334-4336.

40. Lowe, M. P.; Parker, D.; Reany, O.; Aime, S.; Botta, M.; Castellano, G.; Gianolio, E.; Pagliarin, R., pH-Dependent Modulation of Relaxivity and Luminescence in Macrocyclic Gadolinium and Europium Complexes Based on Reversible Intramolecular Sulfonamide Ligation. *Journal of the American Chemical Society* **2001,** 123, (31), 7601-7609.

41. Woods, M.; Kiefer, G. E.; Bott, S.; Castillo-Muzquiz, A.; Eshelbrenner, C.; Michaudet, L.; McMillan, K.; Mudigunda, S. D. K.; Grin, D.; Tircso, G.; Zhang, S. R.; Zhao, P.; Sherry, A. D., Synthesis, relaxometric and photophysical properties of a new pH-Responsive MRI contrast agent: The effect of other ligating groups on dissociation of a p-nitrophenolic pendant arm. *Journal of the American Chemical Society* **2004,** 126, (30), 9248-9256.

42. Toth, E.; Bolskar, R. D.; Borel, A.; Gonzalez, G.; Helm, L.; Merbach, A. E.; Sitharaman, B.; Wilson, L. J., Water-soluble gadofullerenes: Toward high-relaxivity, pH-responsive MRI contrast agents. *Journal of the American Chemical Society* **2005,** 127, (2), 799-805.

43. Thulborn, K. R.; Waterton, J. C.; Matthews, P. M.; Radda, G. K., Oxygenation dependence of the transverse relaxation time of water protons in whole blood at high field. *Biochimica et Biophysica Acta* **1982,** 714, (2), 265-70.

44. Ogawa, S.; Tank, D. W.; Menon, R.; Ellermann, J. M.; Kim, S. G.; Merkle, H.; Ugurbil, K., Intrinsic signal changes accompanying sensory stimulation: functional brain mapping with magnetic resonance imaging. *Proceedings of the National Academy of Sciences of the United States of America* **1992,** 89, (13), 5951-5.

45. Burai, L.; Scopelliti, R.; Toth, E., EuII-cryptate with optimal water exchange and electronic relaxation: a synthon for potential pO2 responsive macromolecular MRI contrast agents. *Chemical Communications (Cambridge, England)* **2002**, (20), 2366-7.

46. Aime, S.; Botta, M.; Gianolio, E.; Terreno, E., A p(O2)-responsive MRI contrast agent based on the redox switch of manganese(II/III)-porphyrin complexes. *Angewandte Chemie, International Edition* **2000,** 39, (4), 747-750.

47. Hines, J. V.; Ammar, G. M.; Buss, J.; Schmalbrock, P., Paramagnetic oligonucleotides: contrast agents for magnetic resonance imaging with proton relaxation enhancement effects. *Bioconjugate Chemistry* **1999,** 10, (2), 155-8.

48. Nivorozhkin, A. L.; Kolodziej, A. F.; Caravan, P.; Greenfield, M. T.; Lauffer, R. B.; McMurry, T. J., Enzyme-activated Gd3+ magnetic resonance imaging contrast agents with a prominent receptor-induced magnetization enhancement. *Angewandte Chemie, International Edition* **2001,** 40, (15), 2903-2906.

49. De Leon-Rodriguez, L. M.; Ortiz, A.; Weiner, A. L.; Zhang, S. R.; Kovacs, Z.; Kodadek, T.; Sherry, A. D., Magnetic resonance imaging detects a specific peptide-protein binding event. *Journal of The American Chemical Society* **2002,** 124, (14), 3514-3515.

50. Josephson, L.; Perez, J. M.; Weissleder, R., Magnetic nanosensors for the detection of oligonucleotide sequences. *Angewandte Chemie-International Edition* **2001,** 40, (17), 3204-+.

51. Genove, G.; DeMarco, U.; Xu, H. Y.; Goins, W. F.; Ahrens, E. T., A new transgene reporter for in vivo magnetic resonance imaging. *Nature Medicine* **2005,** 11, (4), 450-454.

52. Aime, S.; Botta, M.; Cravotto, G.; Frullano, L.; Giovenzana, G. B.; Crich, S. G.; Palmisano, G.; Sisti, M., Gadolinium(III) complexes of dota-derived N-sulfonylacetamides (H-4(dota-NHSO2R)=10-{2-[(R)sulfonylamino]-2-oxoethyl}-1,4,7,10-tetraaza cyclododecane-1,4,7-triacetic acid): A new class of relaxation agents for magnetic resonance imaging applications. *Helvetica Chimica Acta* **2005,** 88, (3), 588-603.

53. Aime, S.; Delli Castelli, D.; Fedeli, F.; Terreno, E., A paramagnetic MRI-CEST agent responsive to lactate concentration. *Journal of the American Chemical Society* **2002,** 124, (32), 9364-5.

54. Zhang, S.; Merritt, M.; Woessner, D. E.; Lenkinski, R. E.; Sherry, A. D., PARACEST Agents: Modulating MRI Contrast via Water Proton Exchange. *Accounts of Chemical Research* **2003,** 36, (10), 783-790.

55. Zhang, S.; Michaudet, L.; Burgess, S.; Sherry, A. D., The amide protons of an ytterbium(III) dota tetraamide complex act as efficient antennae for transfer of magnetization to bulk water. *Angewandte Chemie, International Edition* **2002,** 41, (11), 1919-1921.

56. Zhang, S.; Winter, P.; Wu, K.; Sherry, A. D., A Novel Europium(III)-Based MRI Contrast Agent. *Journal of the American Chemical Society* **2001,** 123, (7), 1517-1518.

57. Black, J., *Biological performance of materials*. Marcel Decker, Inc.: New York, 1999.

58. Stupp, S. I.; Donners, J.; Li, L. S.; Mata, A., Expanding frontiers in biomaterials. *Mrs Bulletin* **2005,** 30, (11), 864-873.

59. Ghods, A. J.; Savaj, S., Iranian model of paid and regulated living-unrelated kidney donation. *Clinical Journal of the American Society of Nephrology* **2006,** 1, (6), 1136-1145.

60. *2004 Annual Report of the U.S. Organ Procurement and Transplantation Network and the Scientific Registry of Transplant Recipients: Transplant Data 1994-2003*.

61. Ratner, B. D., *Biomaterials Science: An Introduction to Materials in Medicine*. Elsevier Academic Press: San Diego, 2004.

62. Anderson, D. G.; Burdick, J. A.; Langer, R., Materials science - Smart biomaterials. *Science* **2004,** 305, (5692), 1923-1924.

63. Ratner, B. D.; Bryant, S. J., Bioaterials: Where we have been and where we are going. *Annual Review of Biomedical Engineering* **2004**, (6), 41-75.

64. Duchenyne, P.; Qiu, Q., Bioactive ceramics: The Effect of surface reactivity on bone formation and bone cell function. *Biomaterials* **1999**, (20), 2287-2303.

65. http://www.drmcdougall.com/misc/2006nl/sept/angio.htm.

66. Alexis, F.; Venkatraman, S.; Rath, S. K.; Gan, L. H., Some insight into hydrolytic scission mechanisms in bioerodible polyesters. *Journal of Applied Polymer Science* **2006,** 102, (4), 3111-3117.

67. Shin, H.; Jo, S.; Mikos, A. G., Biomimetic materials for tissue engineering. *Biomaterials* **2003,** 24, (24), 4353-4364.

68. Lee, K. Y.; Mooney, D. J., Hydrogels for tissue engineering. *Chemical Reviews* **2001,** 101, (7), 1869-1879.

69. Boontheekul, T.; Mooney, D. J., Protein-based signaling systems in tissue engineering. *Current Opinion in Biotechnology* **2003,** 14, (5), 559-565.

70. Hirano, Y.; Mooney, D. J., Peptide and protein presenting materials for tissue engineering. *Advanced Materials* **2004,** 16, (1), 17-25.

71. Hamley, I. W., Nanotechnology with soft materials. *Angewandte Chemie-International Edition* **2003,** 42, (15), 1692-1712.

72. Whitesides, G. M.; Mathias, J. P.; Seto, C. T., Molecular Self-Assembly and Nanochemistry - a Chemical Strategy for the Synthesis of Nanostructures. *Science* **1991,** 254, (5036), 1312-1319.

73. Lehn, J. M., Toward self-organization and complex matter. *Science* **2002,** 295, (5564), 2400-2403.

74. Paull, R.; Wolfe, J.; Hebert, P.; Sinkula, M., Investing in nanotechnology. *Nature Biotechnology* **2003,** 21, (10), 1144-1147.

75. Tirrell, M.; Kokkoli, E.; Biesalski, M., The role of surface science in bioengineered materials. *Surface Science* **2002,** 500, (1-3), 61-83.

76. Tew, G. N.; Pralle, M. U.; Stupp, S. I., Supramolecular materials with electroactive chemical functions. *Angewandte Chemie-International Edition* **2000,** 39, (3), 517-+.

77. Zubarev, E. R.; Pralle, M. U.; Li, L. M.; Stupp, S. I., Conversion of supramolecular clusters to macromolecular objects. *Science* **1999,** 283, (5401), 523-526.

78. Stupp, S. I.; LeBonheur, V.; Walker, K.; Li, L. S.; Huggins, K. E.; Keser, M.; Amstutz, A., Supramolecular materials: Self-organized nanostructures. *Science* **1997,** 276, (5311), 384-389.

79. Zubarev, E. R.; Pralle, M. U.; Sone, E. D.; Stupp, S. I., Self-assembly of dendron rodcoil molecules into nanoribbons. *Journal of the American Chemical Society* **2001,** 123, (17), 4105-4106.

80. Hartgerink, J. D.; Zubarev, E. R.; Stupp, S. I., Supramolecular one-dimensional objects. *Current Opinion in Solid State & Materials Science* **2001,** 5, (4), 355-361.

81. Hartgerink, J. D.; Beniash, E.; Stupp, S. I., Self-assembly and mineralization of peptide-amphiphile nanofibers. *Science (Washington, DC, United States)* **2001,** 294, (5547), 1684-1688.

82. Hartgerink, J. D.; Beniash, E.; Stupp, S. I., Peptide-amphiphile nanofibers: a versatile scaffold for the preparation of self-assembling materials. *Proceedings of the National Academy of Sciences of the United States of America* **2002,** 99, (8), 5133-5138.

83. Stupp, S. I.; Son, S.; Li, L. S.; Lin, H. C.; Keser, M., Bulk Synthesis of 2-Dimensional Polymers - the Molecular Recognition Approach. *Journal of the American Chemical Society* **1995,** 117, (19), 5212-5227.

84. Stupp, S. I.; Son, S.; Lin, H. C.; Li, L. S., Synthesis of 2-Dimensional Polymers. *Science* **1993,** 259, (5091), 59-63.

85. Kokkoli, E.; Mardilovich, A.; Wedekind, A.; Rexeisen, E. L.; Garg, A.; Craig, J. A., Self-assembly and applications of biomimetic and bioactive peptide-amphiphiles. *Soft Matter* **2006,** 2, (12), 1015-1024.

86. Claussen, R. C.; Rabatic, B. M.; Stupp, S. I., Aqueous self-assembly of unsymmetric peptide bolaamphiphiles into nanofibers with hydrophilic cores and surfaces. *Journal of the American Chemical Society* **2003,** 125, (42), 12680-12681.

87. Silva, G. A.; Czeisler, C.; Niece, K. L.; Beniash, E.; Harrington, D. A.; Kessler, J. A.; Stupp, S. I., Selective Differentiation of Neural Progenitor Cells by High-Epitope Density Nanofibers. *Science* **2004,** 303, 1352-1355.

88. Rajangam, K.; Behanna, H. A.; Hui, M. J.; Han, X. Q.; Hulvat, J. F.; Lomasney, J. W.; Stupp, S. I., Heparin binding nanostructures to promote growth of blood vessels. *Nano Letters* **2006,** 6, (9), 2086-2090.

89. Jones, R. A. L., *Soft Condensed Matter*. Oxford University Press: New York City, 2002.

90. Read, M. W.; Escobedo, J. O.; Willis, D. M.; Beck, P. A.; Strongin, R. M., Convenient Iterative Synthesis of an Octameric Tetracarboxylate-Functionalized Oligophenylene Rod with Divergent End Groups. *Organic Letters* **2000,** 2, (20), 3201-3204.

91. Liess, P.; Hensel, V.; Schlueter, A. D., Oligophenylene rods. A repetitive approach. *Liebigs Annalen* **1996**, (7), 1037-1040.

92. Zhu, L.; Duquette, J.; Zhang, M., An Improved Preparation of Arylboronates: Application in One-Pot Suzuki Biaryl Synthesis. *Journal of Organic Chemistry* **2003,** 68, (9), 3729-3732.

93. Ishiyama, T.; Murata, M.; Miyaura, N., Palladium(0)-Catalyzed Cross-Coupling Reaction of Alkoxydiboron with Haloarenes: A Direct Procedure for Arylboronic Esters. *Journal of Organic Chemistry* **1995,** 60, (23), 7508-10.

94. Harris, D. C., *Quantitative Chemical Analysis*. Fifth ed.; W. H. Freeman and Company: New York, 1999.

95. Yu, Y. C.; Berndt, P.; Tirrell, M.; Fields, G. B., Self-assembling amphiphiles for construction of protein molecular architecture. *Journal of the American Chemical Society* **1996,** 118, (50), 12515-12520.

96. von Maltzahn, G.; Vauthey, S.; Santoso, S.; Zhang, S. U., Positively charged surfactant-like peptides self-assemble into nanostructures. *Langmuir* **2003,** 19, (10), 4332-4337.

97. Paramonov, S. E.; Jun, H. W.; Hartgerink, J. D., Self-assembly of peptide-amphiphile nanofibers: The roles of hydrogen bonding and amphiphilic packing. *Journal of the American Chemical Society* **2006,** 128, (22), 7291-7298.

98. Bull, S. R.; Guler, M. O.; Bras, R. E.; Meade, T. J.; Stupp, S. I., Self-Assembled Peptide Amphiphile Nanofibers Conjugated to MRI Contrast Agents. *Nanoletters* **2005,** 5, (1), 1-4.

99. Lehn, J. M., Supramolecular Chemistry - Scope and Perspectives Molecules, Supermolecules, and Molecular Devices. *Angewandte Chemie-International Edition in English* **1988,** 27, (1), 89-112.

100. Alberts, B.; Bray, D.; Lewis, J.; Raff, M.; Roberts, K.; Watson, J. D., *Molecular Biology of The Cell*. 3 ed.; Garland Publishing: New York, 1994.

101. Hunter, C. A.; Tomas, S., Accurate length control of supramolecular oligomerization: Vernier assemblies. *Journal of the American Chemical Society* **2006,** 128, (27), 8975-8979.

102. Klug, A., The tobacco mosaic virus particle: structure and assembly. *Philosophical Transactions of the Royal Society of London Series B-Biological Sciences* **1999,** 354, (1383), 531-535.

103. Schlick, T. L.; Ding, Z. B.; Kovacs, E. W.; Francis, M. B., Dual-surface modification of the tobacco mosaic virus. *Journal of the American Chemical Society* **2005,** 127, (11), 3718-3723.

104. Stupp, S. I., Biomaterials for regenerative medicine. *Mrs Bulletin* **2005,** 30, (7), 546-553.

105. Stendahl, J. C.; Rao, M. S.; Guler, M. O.; Stupp, S. I., Intermolecular forces in the self-assembly of peptide amphiphile nanofibers. *Advanced Functional Materials* **2006,** 16, (4), 499-508.

106. Bae, J.; Choi, J. H.; Yoo, Y. S.; Oh, N. K.; Kim, B. S.; Lee, M., Helical nanofibers from aqueous self-assembly of an oligo(p-phenylene)-based molecular dumbbell. *Journal of the American Chemical Society* **2005,** 127, (27), 9668-9669.

107. Gin, M. S.; Yokozawa, T.; Prince, R. B.; Moore, J. S., Helical Bias in Solvophobically Folded Oligo(Phenylene Ethynylene)s. *Journal of the American Chemical Society* **1999,** 121, (11), 2643-2644.

108. Xue, C. H.; Luo, F. T., Rapid syntheses of oligo(p-phenyleneethynylene)s via iterative convergent approach. *Tetrahedron* **2004,** 60, (30), 6285-6294.

109. Bull, S. R.; Guler, M. O.; Bras, R. E.; Venkatasubramanian, P. N.; Stupp, S. I.; Meade, T. J., Magnetic resonance imaging of self-assembled biomaterial scaffolds. *Bioconjugate Chemistry* **2005,** 16, (6), 1343-1348.

110. Moore, J. S.; Stupp, S. I., Room-Temperature Polyesterification. *Macromolecules* **1990,** 23, (1), 65-70.

111. Victor R. Fuchs, H. C. S., Physicians' Views of the Relative Importance of Thirty medical Innovations. *Health Affairs* **2001,** 20, (5), 30-43.

112. Meade, T. J.; Taylor, A. K.; Bull, S. R., New magnetic resonance contrast agents as biochemical reporters. *Current Opinion in Neurobiology* **2003,** 13, (5), 597-602.

113. Brucher, E., Kinetic stabilities of gadolinium(III) chelates used as MRI contrast agents. *Topics in Current Chemistry* **2002,** 221, (Contrast Agents I), 103-122.

114. Aime, S.; Dastru, W.; Crich, S. G.; Gianolio, E.; Mainero, V., Innovative magnetic resonance imaging diagnostic agents based on paramagnetic Gd(III) complexes. *Biopolymers* **2003,** 66, (6), 419-428.

115. Aime, S.; Botta, M.; Crich, S. G.; Giovenzana, G.; Palmisano, G.; Sisti, M., Novel paramagnetic macromolecular complexes derived from the linkage of a macrocyclic GD(III) complex to polyamino acids through a squaric acid moiety. [Erratum to document cited in CA130:245597]. *Bioconjugate Chemistry* **1999,** 10, (4), 701.

116. Hoegemann-Savellano, D.; Bos, E.; Blondet, C.; Sato, F.; Abe, T.; Josephson, L.; Weissleder, R.; Gaudet, J.; Sgroi, D.; Peters, P. J.; Basilion, J. P., The transferrin receptor: a

potential molecular imaging marker for human cancer. *Neoplasia (Wilton, CT, United States)* **2003,** 5, (6), 495-506.

117. Ladd, D. L.; Hollister, R.; Peng, X.; Wei, D.; Wu, G.; Delecki, D.; Snow, R. A.; Toner, J. L.; Kellar, K.; Eck, J.; Desai, V. C.; Raymond, G.; Kinter, L. B.; Desser, T. S.; Rubin, D. L., Polymeric Gadolinium Chelate Magnetic Resonance Imaging Contrast Agents: Design, Synthesis, and Properties. *Bioconjugate Chemistry* **1999,** 10, (3), 361-370.

118. Hueber, M. M.; Staubli, A. B.; Kustedjo, K.; Gray, M. H. B.; Shih, J.; Fraser, S. E.; Jacobs, R. E.; Meade, T. J., Fluorescently Detectable Magnetic Resonance Imaging Agents. *Bioconjugate Chemistry* **1998,** 9, (2), 242-249.

119. Hernandez, G.; Tweedle, M. F.; Bryant, R. G., Proton Magnetic-Relaxation Dispersion in Aqueous Glycerol Solutions of Gd(Dtpa)2- and Gd(Dota). *Inorganic Chemistry* **1990,** 29, (25), 5109-5113.

120. Kimpe, K.; Parac-Vogt, T. N.; Laurent, S.; Pierart, C.; Vander Elst, L.; Muller, R. N.; Binnemans, K., Potential MRI contrast agents based on micellar incorporation of amphiphilic bis(alkylamide) derivatives of [(Gd-DTPA)(H2O)](2-). *European Journal Of Inorganic Chemistry* **2003**, (16), 3021-3027.

121. Nicolle Gaelle, M.; Toth, E.; Eisenwiener, K.-P.; Macke Helmut, R.; Merbach Andre, E., From monomers to micelles: investigation of the parameters influencing proton relaxivity. *Journal of Biological Inorganic Chemistry* **2002,** 7, (7-8), 757-69.

122. Antonella Accardo, D. T., Paola Roscigno, Eliana Gianolio, Luigi Paduano, Gerardino D'Errico, Carlo Pedone, Giancarlo Morelli, Physicochemical Properties of Mixed Micellar Aggregates Containing CCK Peptides and Gd Compleses Designed as Tumor Specific Contrast Agents in MRI. *Journal of the American Chemical Society* **2004,** 126, 3097-3107.

123. Morawski, A. M.; Winter, P. M.; Crowder, K. C.; Caruthers, S. D.; Fuhrhop, R. W.; Scott, M. J.; Robertson, J. D.; Abendschein, D. R.; Lanza, G. M.; Wickline, S. A., Targeted nanoparticles for quantitative imaging of sparse molecular epitopes with MRI. *Magnetic Resonance in Medicine* **2004,** 51, (3), 480-486.

124. Morawski, A.; Lanza, G.; Wickline, S., Targeted contrast agents for magnetic resonance imaging and ultrasound. *Current Opinion in Biotechnology* **2005,** 16, 89-92.

125. Perez, J. M.; Simeone, F. J.; Tsourkas, A.; Josephson, L.; Weissleder, R., Peroxidase Substrate Nanosensors for MR Imaging. *Nano Letters* **2004,** 4, (1), 119-122.

126. Andre, J. P.; Toth, E.; Fischer, H.; Seelig, A.; Macke, H. R.; Merbach, A. E., High relaxivity for monomeric Gd(DOTA)-based MRI contrast agents, thanks to micellar self-organization. *Chemistry--A European Journal* **1999,** 5, (10), 2977-2983.

127. Torchilin, V. P., PEG-based micelles as carriers of contrast agents for different imaging modalities. *Advanced Drug Delivery Reviews* **2002,** 54, (2), 235-252.

128. Kumar, K.; Tweedle, M. F., Macrocyclic Polyaminocarboxylate Complexes of Ianthanides as Magnetic-Resonance-Imaging Contrast Agents. *Pure and Applied Chemistry* **1993,** 65, (3), 515-520.

129. Greenfield, N.; Fasman, G. D., Computed Circular Dichroism Spectra for Evaluation of Protein Conformation. *Biochemistry* **1969,** 8, (10), 4108-4116.

130. Flacke, S.; Fischer, S.; Scott, M. J.; Fuhrhop, R. J.; Allen, J. S.; McLean, M.; Winter, P.; Sicard, G. A.; Gaffney, P. J.; Wickline, S. A.; Lanza, G. M., Novel MRI contrast agent for molecular imaging of fibrin implications for detecting vulnerable plaques. *Circulation* **2001,** 104, (11), 1280-1285.

131. Aletras, A.; Barlos, K.; Gatos, D.; Koutsogianni, S.; Mamos, P., Preparation of the very acid-sensitive Fmoc-Lys(Mtt)-OH. Application in the synthesis of side-chain to side-chain cyclic peptides and oligolysine cores suitable for the solid-phase assembly of MAPs and TASPs. *International journal of peptide and protein research* **1995,** 45, (5), 488-96.

132. De Leon-Rodriguez, L. M.; Kovacs, Z.; Dieckmann, G. R.; Sherry, A. D., Solid-phase synthesis of DOTA-peptides. *Chemistry--A European Journal* **2004,** 10, (5), 1149-1155.

133. Xiong, J. P.; Stehle, T.; Diefenbach, B.; Zhang, R. G.; Dunker, R.; Scott, D. L.; Joachimiak, A.; Goodman, S. L.; Arnaout, M. A., Crystal structure of the extracellular segment of integrin alpha V beta 3. *Science* **2001,** 294, (5541), 339-345.

134. Loncin, M. F.; Desreux, J. F.; Merciny, E., Coordination of lanthanides by two polyamino polycarboxylic macrocycles: formation of highly stable lanthanide complexes. *Inorganic Chemistry* **1986,** 25, (15), 2646-8.

135. Lu, Z.-R.; Wang, X.; Parker, D. L.; Goodrich, K. C.; Buswell, H. R., Poly(L-glutamic acid) Gd(III)-DOTA Conjugate with a Degradable Spacer for Magnetic Resonance Imaging. *Bioconjugate Chemistry* **2003,** 14, (4), 715-719.

136. Lu, Z. R.; Parker, D. L.; Goodrich, K. C.; Wang, X. H.; Dalle, J. G.; Buswell, H. R., Extracellular biodegradable macromolecular gadolinium(III) complexes for MRI. *Magnetic Resonance in Medicine* **2004,** 51, (1), 27-34.

137. Zhang, S., Fabrication of novel biomaterials through molecular self-assembly. *Nature Biotechnology* **2003,** 21, (10), 1171-1178.

138. Langer, R.; Tirrell, D. A., Designing materials for biology and medicine. *Nature* **2004,** 428, (6982), 487-492.

139. Kisiday, J.; Jin, M.; Kurz, B.; Hung, H.; Semino, C.; Zhang, S.; Grodzinsky, A. J., Self-assembling peptide hydrogel fosters chondrocyte extracellular matrix production and cell division: Implications for cartilage tissue repair. *Proceedings of the National Academy of Sciences of the United States of America* **2002,** 99, (15), 9996-10001.

140. Holmes, T. C., Novel peptide-based biomaterial scaffolds for tissue engineering. *Trends in Biotechnology* **2002,** 20, (1), 16-21.

141. Bhorade, R.; Weissleder, R.; Nakakoshi, T.; Moore, A.; Tung, C.-H., Macrocyclic Chelators with Paramagnetic Cations Are Internalized into Mammalian Cells via a HIV-Tat Derived Membrane Translocation Peptide. *Bioconjugate Chemistry* **2000,** 11, (3), 301-305.

142. Niece, K. L.; Hartgerink, J. D.; Donners, J.; Stupp, S. I., Self-assembly combining two bioactive peptide-amphiphile molecules into nanofibers by electrostatic attraction. *Journal of the American Chemical Society* **2003,** 125, (24), 7146-7147.

143. Behanna, H. A.; Donners, J.; Gordon, A. C.; Stupp, S. I., Coassembly of amphiphiles with opposite peptide polarities into nanofibers. *Journal Of The American Chemical Society* **2005,** 127, (4), 1193-1200.

144. Guler, M. O.; Soukasene, S.; Hulvat, J. F.; Stupp, S. I., Presentation and recognition of biotin on nanofibers formed by branched peptide amphiphiles. *Nano Letters* **2005,** 5, (2), 249-252.

145. Weissleder, R.; Poss, K.; Wilkinson, R.; Zhou, C.; Bogdanov, A., Quantitation of Slow Drug-Release from an Implantable and Degradable Gentamicin Conjugate by in-Vivo Magnetic-Resonance-Imaging. *Antimicrobial Agents and Chemotherapy* **1995,** 39, (4), 839-845.

146. Kohn, J., New approaches to biomaterials design. *Nature Materials* **2004,** 3, (11), 745-747.

147. Mader, K.; Cremmilleux, Y.; Domb, A. J.; Dunn, J. F.; Swartz, H. M., In vitro in vivo comparison of drug release and polymer erosion from biodegradable P(FAD-SA) polyanhydrides - A noninvasive approach by the combined use of electron paramagnetic resonance spectroscopy and nuclear magnetic resonance imaging. *Pharmaceutical Research* **1997,** 14, (6), 820-826.

148. Mader, K.; Bacic, G.; Domb, A.; Elmalak, O.; Langer, R.; Swartz, H. M., Noninvasive in vivo monitoring of drug release and polymer erosion from biodegradable polymers by EPR spectroscopy and NMR imaging. *Journal of Pharmaceutical Sciences* **1997,** 86, (1), 126-134.

149. Melia, C. D.; Rajabi-Siahboomi, A. R.; Bowtell, R. W., Magnetic resonance imaging of controlled release pharmaceutical dosage forms. *Pharmaceutical Science & Technology Today* **1998,** 1, (1), 32-39.

150. Aime, S.; Botta, M.; Garino, E.; Crich, S. G.; Giovenzana, G.; Pagliarin, R.; Palmisano, G.; Sisti, M., Non-covalent conjugates between cationic polyamino acids and GdIII chelates: a route for seeking accumulation of MRI-contrast agents at tumor targeting sites. *Chemistry--A European Journal* **2000,** 6, (14), 2609-2617.

151. Stroman, P. W.; Dorvil, J. C.; Marois, Y.; Poddevin, N.; Guidoin, R., In vivo time course studies of the tissue responses to resorbable polylactic acid implants by means of MRI. *Magnetic Resonance in Medicine* **1999,** 42, (1), 210-214.

152. Traore, A. S.; Woerly, S.; Doan, V. D.; Marois, Y.; Guidoin, R., In vivo magnetic resonance imaging and relaxometry study of a porous hydrogel implanted in the trapezius muscle of rabbits. *Tissue Engineering* **2000,** 6, (3), 265-278.

153. Guidoin, R.; Langevin, F.; Basle, M. F.; Alarcone, C.; Legrand, A. P.; Zhang, Z.; Basse-Cathalinat, B.; Franconi, J. M.; Douville, Y.; Baquey, C., Can magnetic resonance imaging be the key technique to visualize and investigate endovascular biomaterials? *Artificial Cells Blood Substitutes and Immobilization Biotechnology* **2004,** 32, (1), 105-127.

154. Pihlajamaki, H.; Kinnunen, J.; Bostman, O., In vivo monitoring of the degradation process of bioresorbable polymeric implants using magnetic resonance imaging. *Biomaterials* **1997,** 18, (19), 1311-1315.

155. Pierschbacher, M. D.; Ruoslahti, E., Cell Attachment Activity of Fibronectin Can Be Duplicated by Small Synthetic Fragments of the Molecule. *Nature* **1984,** 309, (5963), 30-33.

156. Costa, J.; Toth, E.; Helm, L.; Merbach, A. E., Dinuclear, bishydrated Gd-III polyaminocarboxylates with a rigid xylene core display remarkable proton relaxivities. *Inorganic Chemistry* **2005,** 44, (13), 4747-4755.

157. Toth, E.; Helm, L.; Merbach, A. E., Relaxivity of MRI contrast agents. *Topics in Current Chemistry* **2002,** 221, (Contrast Agents I), 61-101.

158. Lauffer, R. B., Paramagnetic metal complexes as water proton relaxation agents for NMR imaging: theory and design. *Chemical Reviews (Washington, DC, United States)* **1987,** 87, (5), 901-27.

159. Aime, S.; Gianolio, E.; Longo, D.; Pagliarin, R.; Lovazzano, C.; Sisti, M., New insights for pursuing high relaxivity MRI agents from modelling the binding interaction of Gd-III chelates to HSA. *Chembiochem* **2005,** 6, (5), 818.

160. Aime, S.; Frullano, L.; Crich, S. G., Compartmentalization of a gadolinium complex in the apoferritin cavity: A route to obtain high relaxivity contrast agents for magnetic resonance imaging. *Angewandte Chemie-International Edition* **2002,** 41, (6), 1017-+.

161. Thompson, M. K.; Doble, D. M. J.; Tso, L. S.; Barra, S.; Botta, M.; Aime, S.; Raymond, K. N., Hetero-tripodal hydroxypyridonate gadolinium complexes: Syntheses, relaxometric properties, water exchange dynamics, and human serum albumin binding. *Inorganic Chemistry* **2004,** 43, (26), 8577-8586.

162. Allen, M. J.; Raines, R. T.; Kiessling, L. L., Contrast agents for magnetic resonance imaging synthesized with ring-opening metathesis polymerization. *Journal of the American Chemical Society* **2006,** 128, (20), 6534-6535.

163. Kiessling, F.; Heilmann, M.; Lammers, T.; Ulbrich, K.; Subr, V.; Peschke, P.; Waengler, B.; Mier, W.; Schrenk, H. H.; Bock, M.; Schad, L.; Semmler, W., Synthesis and characterization

of HE-24.8: A polymeric contrast agent for magnetic resonance angiography. *Bioconjugate Chemistry* **2006,** 17, (1), 42-51.

164. Kobayashi, H.; Brechbiel, M. W., Dendrimer-based nanosized MRI contrast agents. *Current Pharmaceutical Biotechnology* **2004,** 5, (6), 539-549.

165. Pierre, V. C.; Botta, M.; Raymond, K. N., Dendrimeric gadolinium chelate with fast water exchange and high relaxivity at high magnetic field strength. *Journal of the American Chemical Society* **2005,** 127, (2), 504-505.

166. Allen, M.; Bulte, J. W. M.; Liepold, L.; Basu, G.; Zywicke, H. A.; Frank, J. A.; Young, M.; Douglas, T., Paramagnetic viral nanoparticles as potential high-relaxivity magnetic resonance contrast agents. *Magnetic Resonance In Medicine* **2005,** 54, (4), 807-812.

167. Langereis, S.; de Lussanet, Q. G.; van Genderen, M. H. P.; Backes, W. H.; Meijer, E. W., Multivalent contrast agents based on gadolinium-diethylenetriaminepentaacetic acid-terminated poly(propylene imine) dendrimers for magnetic resonance imaging. *Macromolecules* **2004,** 37, (9), 3084-3091.

168. Langereis, S.; de Lussanet, Q.; van Genderen, M.; Meijer, E.; Beets-Tan, R.; Griffioen, A.; van Engelshoven, J.; Backes, W., Evaluation of Gd(III)DTPA-terminated poly(propylene imine) dendrimers as contrast agents for MR imaging. *NMR in Biomedicine* **2006,** 19, 133-141.

169. Rudovsky, J.; Hermann, P.; Botta, M.; Aime, S.; Lukes, I., Dendrimeric Gd(III) complex of a monophosphinated DOTA analogue: optimizing relaxivity by reducing internal motion. *Chemical Communications* **2005**, (18), 2390-2392.

170. Rudovsky, J.; Botta, M.; Hermann, P.; Hardcastle, K. I.; Lukes, I.; Aime, S., PAMAM dendrimeric conjugates with a Gd-DOTA phosphinate derivative and their adducts with polyaminoacids: The interplay of global motion, internal rotation, and fast water exchange. *Bioconjugate Chemistry* **2006,** 17, (4), 975-987.

171. Fulton, D. A.; O'Halloran, M.; Parker, D.; Senanayake, K.; Botta, M.; Aime, S., Efficient relaxivity enhancement in dendritic gadolinium complexes: effective motional coupling in medium molecular weight conjugates. *Chemical Communications* **2005**, (4), 474-476.

172. Uzgiris, E., The role of molecular conformation on tumor uptake of polymeric contrast agents. *Investigative Radiology* **2004,** 39, (3), 131-137.

173. Boger, D. L., *Modern Organic Synthesis*. TSRI Press: La Jolla, 1999.

174. Caravan, P., Strategies for increasing the sensitivity of gadolinium based MRI contrast agents. *Chemical Society Reviews* **2006,** 35, 512-523.

175. Tieke, B.; Lieser, G.; Wegner, G., Polymerization of Diacetylenes in Multilayers. *Journal of Polymer Science Part a-Polymer Chemistry* **1979,** 17, (6), 1631-1644.

176. Cantow, H. J., *Polydiacetylenes*. Springer-Verlag: Berlin, 1984.

177. Dunand, F. A.; Toth, E.; Hollister, R.; Merbach, A. E., Lipari-Szabo approach as a tool for the analysis of macromolecular gadolinium(III)-based MRI contrast agents illustrated by the [Gd(EGTA-BA-(CH2)(12))](n)(n+) polymer. *Journal of Biological Inorganic Chemistry* **2001,** 6, (3), 247-255.

178. Yang, S. F.; Leong, K. F.; Du, Z. H.; Chua, C. K., The design of scaffolds for use in tissue engineering. Part 1. Traditional factors. *Tissue Engineering* **2001,** 7, (6), 679-689.

179. Discher, D. E.; Janmey, P.; Wang, Y. L., Tissue cells feel and respond to the stiffness of their substrate. *Science* **2005,** 310, (5751), 1139-1143.

180. Liu, W.; Chen, C., Engineering biomaterials to control cell function. *Materials Today* **2005,** 8, 28-35.

181. Neves, A. A.; Medcalf, N.; Smith, M.; Brindle, K. M., Evaluation of engineered meniscal cartilage constructs based on different scaffold geometries using magnetic resonance imaging and spectroscopy. *Tissue Engineering* **2006,** 12, (1), 53-62.

182. Cheery, S., In vivo molecular and genomic imaging: new challenges for imaging physics. *Physics in Medicine and Biology* **2004,** 49, R13-R48.

183. Huber, M. M.; Staubli, A. B.; Kustedjo, K.; Gray, M. H. B.; Shih, J.; Fraser, S. E.; Jacobs, R. E.; Meade, T. J., Fluorescently detectable magnetic resonance imaging agents. *Bioconjugate Chemistry* **1998,** 9, (2), 242-249.

184. Clarkson, R. B., Blood-pool MRI contrast agents: properties and characterization. *Topics in Current Chemistry* **2002,** 221, (Contrast Agents I), 201-235.

185. Uzgiris, E. E.; Cline, H.; Moasser, B.; Grimmond, B.; Amaratunga, M.; Smith, J. F.; Goddard, G., Conformation and structure of polymeric contrast agents for medical imaging. *Biomacromolecules* **2004,** 5, (1), 54-61.

186. Sirlin, C.; Vera, D.; Corbell, J.; Caballero, M.; Buxton, R.; Mattrey, R., Gadolinium-DTPA-dextran: a macromolecular MR blood pool contrast agent. *Academic Radiology* **2004,** 11, 1361-169.

187. Nakamura, E.; Makino, K.; Okano, T.; Yamamoto, T.; Yokoyama, M., A polymeric micelle MRI contrast agent with changeable relaxivity. *Journal of Controlled Release* **2006,** 114, (3), 325-333.

188. Preda, A.; van Vliet, M.; Krestin, G. P.; Brasch, R. C.; van Dijke, C. F., Magnetic resonance macromolecular agents for monitoring tumor microvessels and angiogenesis inhibition. *Investigative Radiology* **2006,** 41, (3), 325-331.

189. Wen, X. X.; Jackson, E. F.; Price, R. E.; Kim, E. E.; Wu, Q. P.; Wallace, S.; Charnsangavej, C.; Gelovani, J. G.; Li, C., Synthesis and characterization of poly(L-glutamic acid) gadolinium chelate: A new biodegradable MRI contrast agent. *Bioconjugate Chemistry* **2004,** 15, (6), 1408-1415.

190. Corot, C.; Port, M.; Raynal, I.; Dencausse, A.; Schaefer, M.; Rousseaux, O.; Simonot, C.; Devoldere, L.; Lin, J.; Foulon, M.; Bourrinet, P.; Bonnemain, B.; Meyer, D., Physical, chemical, and biological evaluations of P760: A new gadolinium complex characterized by a low rate of interstitial diffusion. *Journal of Magnetic Resonance Imaging* **2000,** 11, (2), 182-191.

191. Jebasingh, B.; Alexander, V., Synthesis and relaxivity studies of a tetranuclear gadolinium(III) complex of DO3A as a contrast-enhancing agent for MRI. *Inorganic Chemistry* **2005,** 44, (25), 9434-9443.

192. Doble, D. M. J.; Botta, M.; Wang, J.; Aime, S.; Barge, A.; Raymond, K. N., Optimization of the relaxivity of MRI contrast agents: Effect of poly(ethylene glycol) chains on the water-exchange rates of Gd-III complexes. *Journal Of The American Chemical Society* **2001,** 123, (43), 10758-10759.

193. Vander Eulst, L.; Port, M.; Raynal, I.; Simonot, C.; Muller, R. N., Physicochemical characterization of P760, a new macromolecular contrast agent with high relaxivity. *European Journal of Inorganic Chemistry* **2003**, (13), 2495-2501.

194. Ruloff, R.; van Koten, G.; Merbach, A. E., Novel heteroditopic chelate for self-assembled gadolinium(iii) complex with high relaxivity. *Chemical Communications (Cambridge, United Kingdom)* **2004**, (7), 842-843.

195. Strijkers, G.; Mulder, W.; van Heeswijk, R.; Frederik, P.; Bomans, P.; Magusin, P.; Nicolay, K., Relaxivity of liposomal paramagnetic MRI contrast agents. *Magma* **2005,** 18, 186-192.

196. Barbash, I. M.; Leor, J.; Feinberg, M. S.; Tessone, A.; Aboulafia-Etzion, S.; Orenstein, A.; Ruiz-Cabello, J.; Cohen, J. S.; Mardor, Y., Interventional magnetic resonance imaging for guiding gene and cell transfer in the heart. *Heart* **2004,** 90, (1), 87-91.

197. Won, J.; Barron, A., A new cloning method for the preparation of long repetitive polypeptides without a sequence requirement. *Macromolecules* **2002,** 35, 8281-8287.

198. Anelli, P. L.; Lattuada, L.; Gabellini, M.; Recanati, P., DOTA Tris(phenylmethyl) Ester: A New Useful Synthon for the Synthesis of DOTA Monoamides Containing Acid-Labile Bonds. *Bioconjugate Chemistry* **2001,** 12, (6), 1081-1084.

199. Aime, S.; Ascenzi, P.; Comoglio, E.; Fasano, M.; Paoletti, S., Molecular Recognition of R- and T-States of Human Adult Hemoglobin by a Paramagnetic Gd(III) Complex by Means of the Measurement of Solvent Water Proton Relaxation Rate. *Journal of the American Chemical Society* **1995,** 117, (36), 9365-6.

200. Reichert, D. E.; Hancock, R. D.; Welch, M. J., Molecular Mechanics Investigation of Gadolinium(III) Complexes. *Inorganic Chemistry* **1996,** 35, (24), 7013-7020.

201. Laurent, S.; Vander, L.; Copoix, F.; Muller, R. N., Stability of MRI paramagnetic contrast media: a proton relaxometric protocol for transmetalation assessment. *Investigative Radiology* **2001,** 36, (2), 115-122.

202. Thompson, K. H.; Orvig, C., Boon and Bane of Metal Ions in Medicine. *Science (Washington, DC, United States)* **2003,** 300, (5621), 936-939.

203. Johnson, A. R.; O'Sullivan, B.; Raymond, K. N., Synthesis of a Ligand Based upon a New Entry into the 3-Hydroxy-N-alkyl-2(1H)-pyridinone Ring System and Thermodynamic Evaluation of Its Gadolinium Complex. *Inorganic Chemistry* **2000,** 39, (12), 2652-2660.

204. Thompson, M. K.; Botta, M.; Nicolle, G.; Helm, L.; Aime, S.; Merbach, A. E.; Raymond, K. N., A Highly Stable Gadolinium Complex with a Fast, Associative Mechanism of Water Exchange. *Journal of the American Chemical Society* **2003,** 125, (47), 14274-14275.

205. Doble, D. M. J.; Melchior, M.; O'Sullivan, B.; Siering, C.; Xu, J.; Pierre, V. C.; Raymond, K. N., Toward Optimized High-Relaxivity MRI Agents: The Effect of Ligand Basicity on the Thermodynamic Stability of Hexadentate Hydroxypyridonate/Catecholate Gadolinium(III) Complexes. *Inorganic Chemistry* **2003,** 42, (16), 4930-4937.

206. Xu, J.; Churchill, D. G.; Botta, M.; Raymond, K. N., Gadolinium(III) 1,2-hydroxypyridonate-based complexes: Toward MRI contrast agents of high relaxivity. *Inorganic Chemistry* **2004,** 43, (18), 5492-5494.

207. Raymond, K. N.; Pierre, V. C., Next generation, high relaxivity gadolinium MRI agents. *Bioconjugate Chemistry* **2005,** 16, (1), 3-8.

208. Puerta, D. T.; Botta, M.; Jocher, C. J.; Werner, E. J.; Avedano, S.; Raymond, K. N.; Cohen, S. M., Tris(pyrone) chelates of Gd(III) as high solubility MRI-CA. *Journal Of The American Chemical Society* **2006,** 128, (7), 2222-2223.

209. Caravan, P.; Amedio, J. C.; Dunham, S. U.; Greenfield, M. T.; Cloutier, N. J.; McDermid, S. A.; Spiller, M.; Zech, S. G.; Looby, R. J.; Raitsimring, A. M.; McMurry, T. J.; Lauffer, R. B., When are two waters worse than one? Doubling the hydration number of a Gd-DTPA derivative decreases relaxivity. *Chemistry-A European Journal* **2005,** 11, (20), 5866-5874.

210. Andre, J. P.; Brucher, E.; Kiraly, R.; Carvalho, R. A.; Macke, H.; Geraldes, C., H(5)dotasa (=(alpha RS)-alpha-(carboxymethyl)-1,4,7,10-tetraazacyclododecane-1,4,7,10-tetraa cetic acid), an asymmetrical derivative of H(4)dota (=1,4,7,10-tetraazacyclododecane-1,4,7,10-tetraacetic acid) substituted at one acetate pendant arm: H-1-NMR and potentiometric studies of the ligand and its lanthanide(III) complexes. *Helvetica Chimica Acta* **2005,** 88, (3), 633-646.

211. Messeri, D.; Lowe, M. P.; Parker, D.; Botta, M., A stable, high relaxivity, diaqua gadolinium complex that suppresses anion and protein binding. *Chemical Communications* **2001**, (24), 2742-2743.

212. Polasek, M.; Rudovsky, J.; Hermann, P.; Lukes, I.; Vander Else, L.; Muller, R. N., Lanthanide(III) complexes of a pyridine N-oxide analogue of DOTA: exclusive M isomer

formation induced by a six-membered chelate ring. *Chemical Communications* **2004**, (22), 2602-2603.

213. Woods, M.; Aime, S.; Botta, M.; Howard, J. A. K.; Moloney, J. M.; Navet, M.; Parker, D.; Port, M.; Rousseaux, O., Correlation of Water Exchange Rate with Isomeric Composition in Diastereoisomeric Gadolinium Complexes of Tetra(carboxyethyl)dota and Related Macrocyclic Ligands. *Journal of the American Chemical Society* **2000,** 122, (40), 9781-9792.

214. Woods, M.; Kovacs, Z.; Zhang, S.; Sherry, A. D., Towards the rational design of magnetic resonance imaging contrast agents: isolation of the two coordination isomers of lanthanide DOTA-type complexes. *Angewandte Chemie, International Edition* **2003,** 42, (47), 5889-5892.

215. Woods, M.; Botta, M.; Avedano, S.; Wang, J.; Sherry, A. D., Towards the rational design of MRI contrast agents: a practical approach to the synthesis of gadolinium complexes that exhibit optimal water exchange. *Dalton Transactions* **2005**, (24), 3829-3837.

216. Frullano, L.; Rohovec, J.; Peters, J. A.; Geraldes, C. F. G. C., Structures of MRI contrast agents in solution. *Topics in Current Chemistry* **2002,** 221, (Contrast Agents I), 25-60.

217. Zhang, Z. D.; Greenfield, M. T.; Spiller, M.; McMurry, T. J.; Lauffer, R. B.; Caravan, P., Multilocus binding increases the relaxivity of protein-bound MRI contrast agents. *Angewandte Chemie-International Edition* **2005,** 44, (41), 6766-6769.

218. Aime, S.; Botta, M.; Fasano, M.; Crich, S. G.; Terreno, E., Gd(III) complexes as contrast agents for magnetic resonance imaging: A proton relaxation enhancement study of the interaction with human serum albumin. *Journal Of Biological Inorganic Chemistry* **1996,** 1, (4), 312-319.

219. Aime, S.; Barge, A.; Botta, M.; Casnati, A.; Fragai, M.; Luchinat, C.; Ungaro, R., A calix[4]arene Gd-III complex endowed with high stability, relaxivity, and binding affinity to serum albumin. *Angewandte Chemie-International Edition* **2001,** 40, (24), 4737-+.

220. Toth, E.; Connac, F.; Helm, L.; Adzamli, K.; Merbach, A. E., O-17-NMR, EPR and NMRD characterization of [Gd(DTPA-BMEA)(H2O)]: A neutral MRI contrast agent. *European Journal Of Inorganic Chemistry* **1998**, (12), 2017-2021.

221. Lauffer, R. B., Targeted Relaxation Enhancement Agents for MRI. *Magnetic Resonance in Medicine* **1991,** 22, (2), 339-342.

Vita

Steve Bull was born in Grand Junction Colorado in 1978 to Elaine and Malcolm Bull. He spent his beginning years there with his three sisters (Lara, Missy and Diana) and his brother (Todd). He attended elementary school in CO before moving to TX for junior high school and then VA for high school. In high school he became the captain of the soccer team where the team placed second in the state tournament. He was also part of an Odyssey of the Mind team that was invited to the world finals.

After graduation from Frank W. Cox High School (1997) he attended the University of North Carolina at Chapel Hill. His junior year in college, he studied abroad at Ehime Diagaku in Matsuyama Japan. There he studied language and culture by traveling extensively. Upon his return, he decided to major in chemistry and spent the next two years finishing class work and gaining experience in the lab of Prof. Holden Thorp. Under Prof. Thorp's graduate student, Tony Leone, Steve completed his honors research and graduated in 2002.

In September of 2002 he began his graduate work in the department of Chemistry at Northwestern University. He became a joint student in the research groups of Samuel Stupp and Thomas Meade. He was awarded an NIH Biotechnology Training Grant and was chosen to attend the Lindau Meeting of Nobel Laureates where he met both Sir Peter Mansfield and Paul Lauterbur (nobel prize winners in MRI). Steve also performed an internship under Prof. Alicia Löffler at the Kellogg School of Management authoring a report on the future of the biomedical industry for the NYSE. After completing his degree, Steve will join the consulting firm of LEK to pursue a career in strategy consulting.

Steve Bull
178 Prairie Ave.
Wilmette, IL 60091
stevebull8@mac.com

Education:

2006	Finance, Biotechnology classes, Kellogg School of Management
2002-7	Ph.D., Department of Chemistry, Northwestern University (3.6 GPA)
1996-2	BS biochemistry with honors, University of North Carolina at Chapel Hill (3.6 GPA)
1999-0	Year abroad at Ehime Diagaku (Matsuyama, Japan)

Research Experience:

2005-6	Research Assistant, Professor Alicia Löffler (Kellogg School of Management)
2002-7	Ph.D. candidate under Samuel I. Stupp and Thomas J. Meade (Northwestern)
2002	Research Assistant, Professor Michael Wasielewski (Northwestern)
2001-2	Research Assistant, Professor Holden Thorp (UNC Chapel Hill)

Teaching experience:

2004-5	General chemistry tutor for the African American student affairs at NWU
2002-3	Organic chemistry teaching assistant
2002-7	General chemistry private tutor
1999-0	English conversation instructor (Matsuyama Japan)

Honors/Activities:

2005	Internship for the NYSE in collaboration with Kellogg School of Management (Alicia Löffler), analyst report on the biomedical industry
2005	Phi Lamda Upsilon (PLU) travel grant recipient
2005	Most-Accessed Articles January-June, 2005 (#6, Nanoletters)
2005-6	President of the Graduate Student Association (Northwestern)
2005	Selected on behalf of D.O.E. (Dept. of Energy) for the Lindau Meeting of Nobel Laureates and Students
2005-6	Stupp group lab manager
2004-7	Member of Phi Lamba Upsilon chemistry fraternity
2004-6	NIH Biotechnology Training Fellow
2004-	Founder and president of Galileo Investment Club

Publications:

Leone, A. M.; Tibodeau, J. D.; **Bull, S. R**.; Feldberg, S. W.; Thorp, H. H.; Murray, R. W.; "Ion Atmoshphere Relaxation and Percolative Electron Transfer in Co Bipyridine DNA Molton Salts," *JACS*, 2003, (125), pg. 6784-6790.

Meade, T. J.; **Bull S. R**.; Taylor, A. K.; "New magnetic resonance contrast agents as biochemical reporters," *Curr. Opin. Neurobiol.*, 2003, (13), pg. 597-602.

Bull, S. R.; Guler, M. O.; Bras, R. E.; Meade, T. J.; Stupp, S. I.; "Self-Assembled Peptide Amphiphile Nanofibers Conjugated to MRI Contrast Agents," *Nano Letters*, 2005, (5), pg. 1-4.

Bull, S.R.; Guler, M. O.; Bras, R. E.; Palamadia, N. V.; Stupp, S. I.; Meade, T. J.; "Magnetic Resonance Imaging of Self-Assembled Biomaterial Scaffolds," *Bioconjugate Chemistry*, 2005, vol 16, (6), 1343-1348

Invention Disclosures:

Bull, S. R.; Meade, T. J.; Stupp, S. I.; "MRI Contrast Agents Conjugated to Self-Assembling Peptide Amphiphiles" (2004) Intellectual Property Application

Bull, S. R.; Guler, M. O.; Meade, T. J.; Stupp, S. I.; "F^{19} Traceable Self-Assembling Peptide Amphiphiles" (2004) Intellectual Property Application

Bull, S. R.; Taylor, A. K.; Meade, T. J.; "Enhanced Relaxivities of MRI Contrast Agents Through Creation of Self-Assembled Conjugates" (2004) Intellectual Property Application

Bull, S. R.; Taylor, A. K.; Meade, T. J.; "Q Modulation of MRI Contrast Agents Through Hydrogen Bonding" (2004) Intellectual Property Application

Bull, S. R.; Haynes, R. H.; Barron, A.; Meade, T. J.; "High Relaxivity Contrast Agents Using Peptoidal Backbones" (2006) Intellectual Property Application

Barron, A.; Meade, T. J.; Karfeld, L. S.; **Bull, S. R.**; "High Relaxivity Contrast Agents Using Protein Polymer Backbones" (2006) Intellectual Property Application

Presentations:

12/15/04 "MR active, self-assembling nanofibers" Northwestern University, Evanston IL (oral)

1/24/05 "Imaging of MR active, self-assembling nanofibers" Northwestern University, Evanston IL (oral)

3/08/05 "MR active, self-assembling nanofibers" to the NSF/MEXT US-Japan Young Scientists Symposium on BioNanotechnology (oral)

05/05/05 "Imaging of MR active, self-assembling nanofibers" Industrial Associates meeting, Northwestern University, Evanston IL (poster)

09/08/05 "Magnetic Resonance Active Self-Assembling Biomaterials" the Society for Molecular Imaging, Cologne Germany (poster)

09/27/05 "Magnetic Resonance Active Self-Assembling Biomaterials" Imaging in 2020, Jackson Hole WY (poster)

04/11/06 "Magnetic Resonance Active Self-Assembling Biomaterials" Bio2006, Chicago IL (poster)

04/14/07 "Peptide Amphiphiles and their use in Regenerative Medicine" Yonsei University Symposium (oral)